MAGNETOM Flash

The Magazine of MR

Issue Number 2/2008
RSNA Edition

SIEMENS

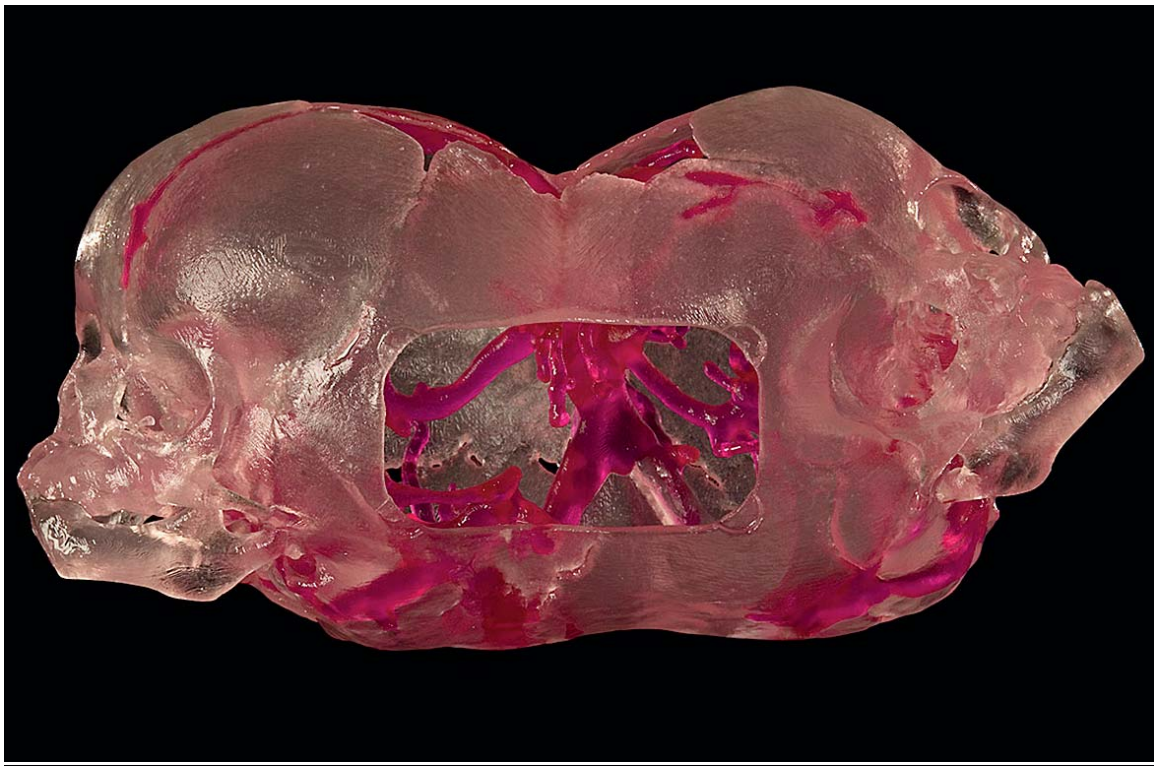

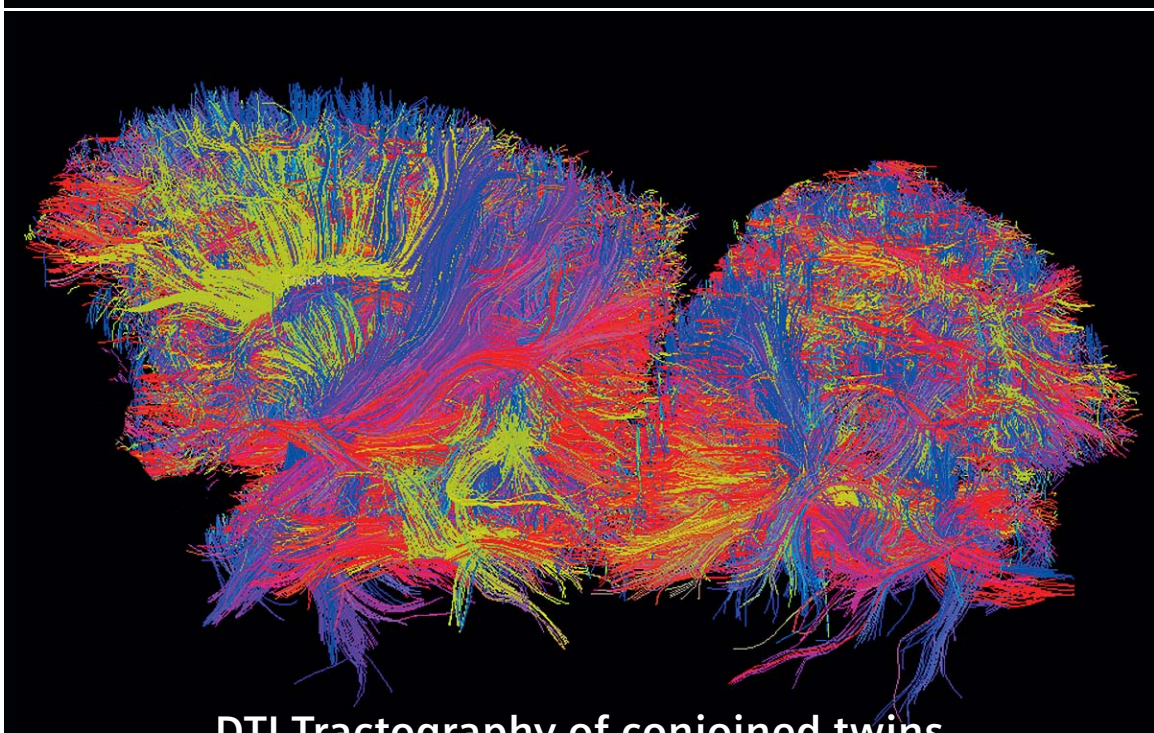

DTI Tractography of conjoined twins

39

A. Nejat Bengi, M.D.

Matthias Lichy, M.D.

Dear MAGNETOM user,

The articles and case reports in this issue of MAGNETOM Flash are proof of the broad spectrum of examinations that are supported or even enabled by Tim – the Total imaging matrix. From diffusion-weighted imaging throughout the whole body to examinations of our smallest patients as presented in the case reports from the Royal Children's Hospital, Melbourne, Australia.

The case of the conjoined twins clearly demonstrates that the combination of the Body Matrix coil with sequence developments such as 3D imaging, contrast enhanced dynamic imaging techniques with high temporal resolution such as *syngo* TWIST and functional imaging such as *syngo* DTI really does make a difference.

Back in 2002, when Dr. Ali Nejat Bengi began as Editor-in-Chief of the MAGNETOM Flash magazine, none of this would have been possible. Dr Bengi succeeded in giving the Flash a very clinical orientation, focusing on relevant information. As the mastermind behind the MAGNETOM World he organized the first MAGNETOM World Summit, developed the MAGNETOM World Internet site and set up the 90-day-free-of-charge trial license program, amongst other ventures. He constantly sought ways to link MAGNETOM users worldwide and to enable users with common interests to meet, learn and exchange valuable information that would improve their clinical and financial outcomes. After 6 years Dr. Bengi has left the MR Marketing group to tackle new tasks in the United States. We can happily report, however, that there will still be some overlap between his new goals and the ethos behind MAGNETOM Flash. We therefore wish to express our great appreciation for all he has helped us achieve and to wish him well in his future position.

To ensure that the Flash does not lose its clinical focus, the position of Editor-in-Chief will be taken by Dr. Matthias Lichy, currently Radiologist at Tübingen University in Germany. He will also help to ensure that the MAGNETOM World Internet Site, Trial Licenses and Summits will continue to flourish. We are looking forward to welcoming Dr. Lichy on the Editorial Board!

Regards,

Antje Hellwich
Associate Editor

The Editorial Team

We appreciate your comments.
Please contact us at magnetomworld.med@siemens.com

Antje Hellwich
Associate Editor

Dagmar Thomsik-Schröpfer,
Ph.D., MR Marketing-Products,
Erlangen, Germany

Okan Ekinci, M.D.
Segment Manager
Cardiovascular MRI
Erlangen, Germany

Heike Weh,
Clinical Data Manager,
Erlangen, Germany

Bernhard Baden,
Clinical Data Manager,
Erlangen, Germany

Peter Kreisler, Ph.D.
Collaborations & Applications,
Erlangen, Germany

Wellesley Were
MR Business Development
Manager
Australia and New Zealand

Milind Dhamankar, M.D.
Sr. Director, MR Product
Marketing, Malvern, USA

Michelle Kessler, US
Installed Base Manager,
Malvern, PA, USA

Gary R. McNeal, MS (BME)
Advanced Application Specialist,
Cardiovascular MR Imaging
Hoffman Estates, USA

Dr. Sunil Kumar S.L.
Senior Manager Applications,
Canada

Content

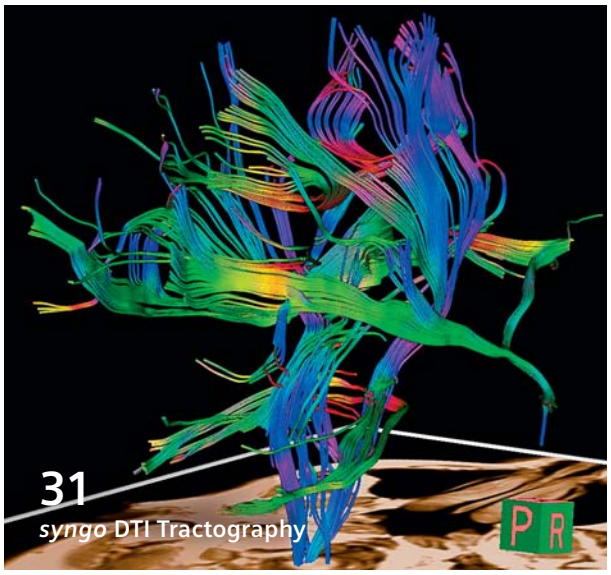

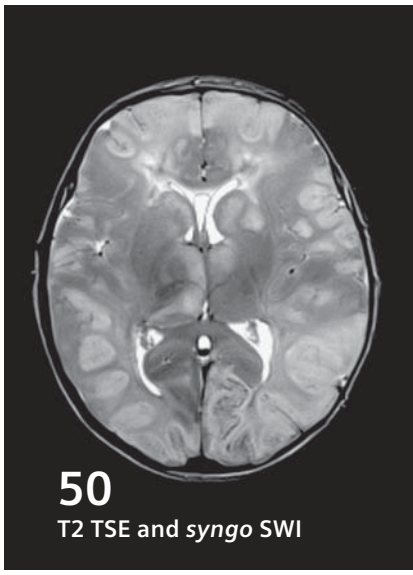

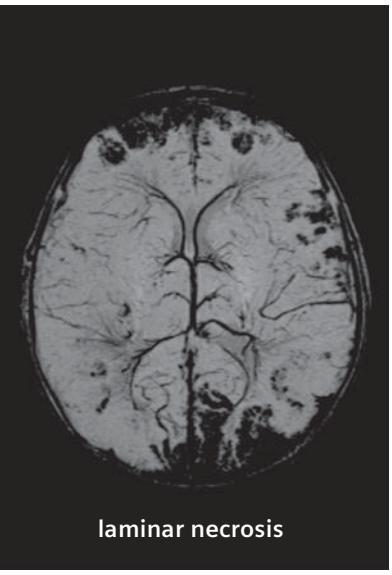
laminar necrosis

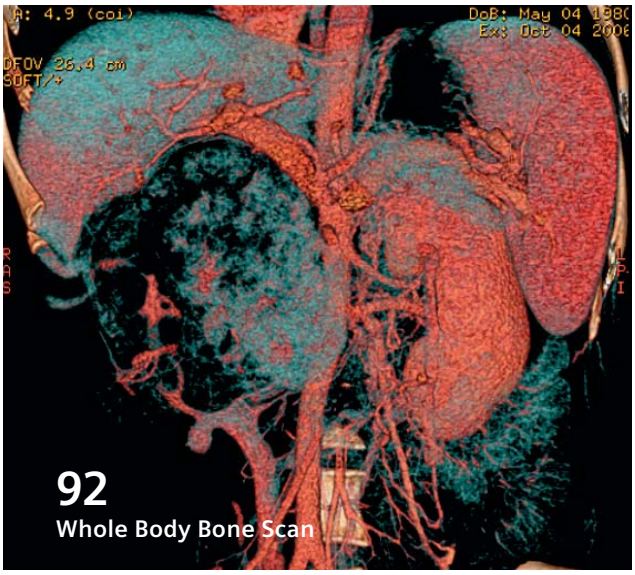

92
Whole Body Bone Scan

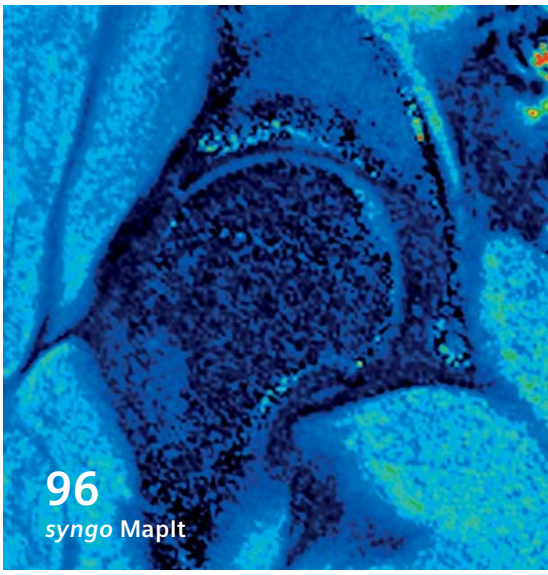
96
syngo MapIt

Detection and Characterization of Focal Liver Lesions using Respiratory-Triggered Diffusion-Weighted MR Imaging (DWI)

Konstantin Holzapfel; Melanie Bruegel; Matthias Eiber; Ernst J. Rummeny; Jochen Gaa

Department of Radiology, Technical University Munich, Germany

Diffusion-weighted MR imaging (DWI), theoretically described as far back as the 1950s and 1960s by Carr/Purcell and Stejskal/Tanner [1, 2], has become an established method in neuroradiology since the introduction of the intravoxel incoherent motion technique by Le Bihan and coworkers in 1988 [3]. Due to a number of technical challenges, the use of DWI was initially confined to the brain with its low incidence of movement artifacts and the high homogeneity and signal-to-noise ratio (SNR) of brain tissue. Physiological motion artifacts (e.g. motility of the bowel, cardiac pulsation, respiratory motions) and the heterogeneous composition of many extracranial organs had precluded the application of DWI in body imaging until a series of technologic advances such as the development of echo-planar imaging (EPI), high-gradient amplitudes, multichannel coils and parallel imaging techniques enabled the acquisition of high quality diffusion-weighted images of the body. Over the last few years, DWI has become increasingly used in extracranial organs to detect and characterize tumors for the functional evaluation of different organs and for response evaluation in oncology (for review see [4, 5]).

The term 'diffusion' defines the random thermally induced motion of water molecules in biologic tissues ('Brownian motion'). The addition of motion probing gradient (MPG) pulses to MR sequences allows quantifying the combined effects of capillary perfusion ('pseudodiffusion') and diffusion in vivo by means of the apparent diffusion coefficient (ADC). For DWI, diffusion gradients are applied before and after the 180°-pulse of a single-shot spin-echo echoplanar imaging (SSEPI) sequence, for example. The b-value represents the diffusion factor [s/mm^2] and represents amplitude and duration of the diffusion gradients. The ADC [mm^2/s] describes the slope of the curve of signal intensity vs. b-value, and is calculated using the following formula: $ADC = (\ln SI_1/SI_2)/(b_2-b_1)$ where b_1 and b_2 are motion-probing gradient factors (diffusion factors) of sequences S_1 and S_2, and SI_1 and SI_2 are signal intensities in these sequences.

Liver DWI protocol used in our institution [6]

At the Department of Radiology of the Technical University of Munich we use a SSEPI sequence at a 1.5T scanner (MAGNETOM Avanto) for DWI. MR imaging is performed with two six-channel body phased array coils anterior and two spine clusters (three channels each) posterior. As image quality of respiratory-triggered sequences has been shown to be superior to breath-hold sequences, we obtain diffusion-weighted images applying respiratory-triggering using prospective acquisition correction (PACE). A single-shot EPI readout is preceded by a diffusion-sensitizing block consisting of two 180° radiofrequency pulses and four motion probing gradient (MPG) pulses in order to reduce the influence of eddy currents compared to the conventional Stejskal-Tanner preparation. The technical parameters are as follows: echo time: 69 ms; echo train length: 58; echo spacing: 0.69; receiver bandwidth: 1,736 Hz/pixel; spectral fat saturation; field of view: 263 × 350 mm; matrix: 144 × 192; number of signal averages: 3; section thickness: 5 mm; intersection gap: 0.5 mm; 30–45 transverse sections acquired; ≈ 4–6 min acquisition time, b-values of 50, 300 and 600 s/mm^2. Integrated parallel imaging techniques (iPAT) by means of generalized autocalibrating partially parallel acquisitions (GRAPPA) with a twofold acceleration factor is used to shorten the echo train length.

Detection of focal liver lesions using DWI

Over the last few years several studies have investigated the use of DWI in the detection of focal liver lesions (FLL). DWI was superior to T2-weighted sequences [7–10] and to superparamagnetic iron oxide (SPIO)-enhanced MR imaging in the detection of focal liver lesions [11]. The detection of small FLLs in particular seems to be significantly improved by DWI [7, 9, 10] (Fig. 1). High SNRs and high lesion-to-liver signal intensity ratios are seen especially at low b values alleviating the depiction of focal liver lesions. In addition, the 'black blood effect' of diffusion-weighted images makes it easier to distinguish small FLLs from hepatic vessels. Furthermore, DWI seems to improve the perceptibility of FLLs, especially of hepatocellular car-

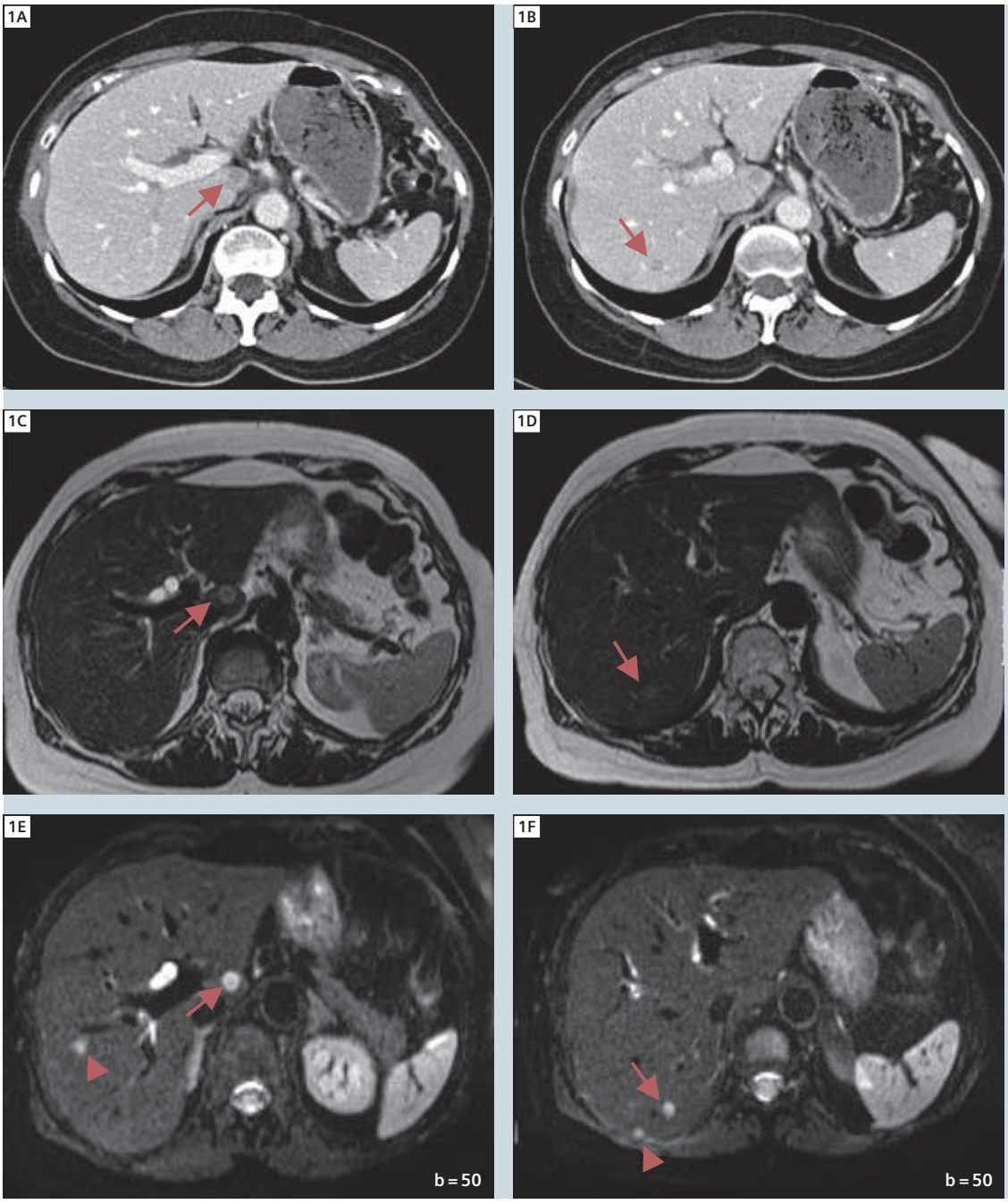

1 Detection of focal liver lesions using DWI. Multi-slice CT (MSCT, A, B), T2-weighted TSE (C, D) and diffusion-weighted SSEPI MR images (E, F) of a patient with breast cancer. On MSCT and T2-weighted MR images one liver metastasis can be seen on each image (arrows). However, on diffusion-weighted images on each slice an additional metastasis can be identified that cannot be seen on MSCT and T2-weighted MR images (arrowheads).

cinomas (HCCs) in patients with liver cirrhosis as that the heterogeneity and increased signal intensity of the cirrhotic liver parenchyma as a result of nodular regeneration, fibrosis, and scarring appears to be less pronounced on DWI compared to T2-weighted images [7]. However, in one study DWI was inferior to Manganese dipyridoxyl-diphosphate (MnDPDP)-enhanced MRI in the detection of FLLs [12] and the potential benefit of DWI in association or compared with conventional gadolinium-enhanced liver MR imaging remains to be investigated [7].

Characterization of focal liver lesions using DWI

Differences in cellularity between benign and malignant liver lesions resulting in different diffusion properties of water protons within these lesions are reflected by different ADC values measured by DWI. Typically, benign liver lesions like cysts or hemangiomas that are hypocellular compared to liver parenchyma allow relatively unhindered diffusion of water protons resulting in high ADC values (e.g. ~ 2 × 10–3 mm^2/s in hemangiomas, ~ 3 × 10–3 mm^2/s in cysts) compared to low ADC values in commonly hypercellular malignant liver lesions such as metastases or HCCs (e.g. 1.1 – 1.3 × 10–3 mm^2/s in HCCs and 1.1 – 1.4 × 10–3 mm^2/s in metastases) where diffusion of water protons is

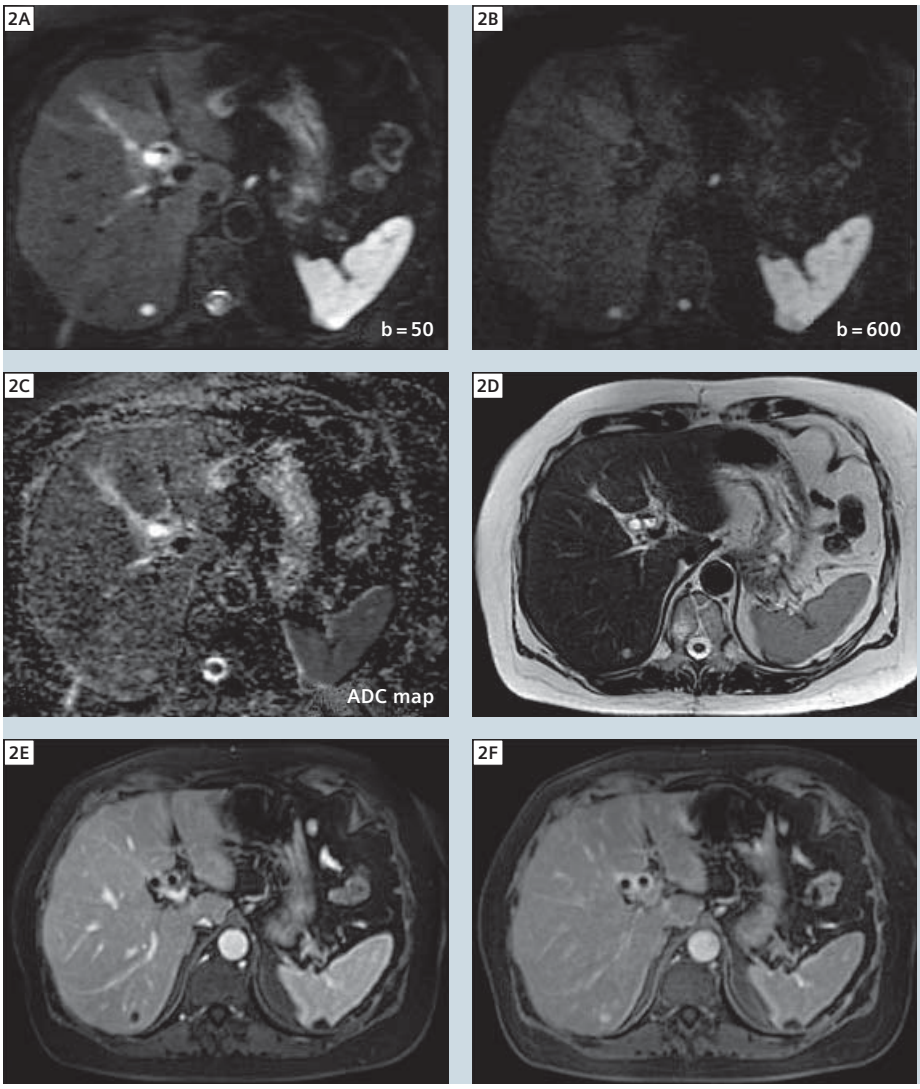

2 Characterization of focal liver lesions by DWI. Diffusion-weighted SSEPI (A–C), T2-weighted TSE (D) and Gd-enhanced T1-weighted MR images (3D Volume Interpolated Breathhold Examination [VIBE] with fat saturation, E, F) in a patient with pancreatic cancer. A small focal liver lesion in segment 7 is hyperintense on the b-50 image (A), shows signal loss at a high b-value (B) and thus, a moderately high ADC value (1.96 × 10–3 mm^2/s, c) typically seen in hemangiomas. The lesion is hyperintense on the T2-weighted image (D) and shows centripetal enhancement on dynamic post-contrast images (E, F), features typical for hemangiomas.

more restricted [6] (Figs. 2, 3). Thus, several studies have identified significantly lower ADC values in malignant compared to benign FLLs [6, 7, 13]. A feasible threshold ADC for differentiating benign from malignant FLLs would be 1.5 – 1.7 × 10–3 mm^2/s [6]. As in the brain, secondary to highly viscous pus containing proteinaceous fluid and necrotic cells, hepatic abscesses show extremely low ADC values in most cases and therefore are an exception to this rule [14, 15]. However, the differentiation between benign solid FLLs like focal nodular hyperplasia (FNHs) and adenomas from malignant lesions often is impossible by DWI as there is considerable overlap of ADC values between both groups. Furthermore, although mean ADC values of hemangiomas and metastases are significantly different, characterizing a single liver lesion by means of the ADC value prospectively can be difficult. Thus, in our opinion, DWI should be used as a complementary method in the characterization of FLLs.

DWI for response evaluation of treated liver tumors

The value of DWI in the detection and prediction of tumor response to chemotherapy, radiation therapy, or other modalities is increasingly studied. Effective anticancer treatment results in lysis of tumor cells, loss of cell membrane integrity, increased extracellular space, and, consequently, an increase in water diffusion reflected by a rising ADC value [5]. Promising animal studies report a significant rise in ADC values in patients with HCC who respond to transcatheter arterial chemoembolization [16]. In addition, amongst patients with colorectal hepatic metastases, an increase in ADC was observed in those with at least a partial response to treatment, while no ADC increase was observed in non-responders [17]. Furthermore, in the same study, metastases with low baseline ADC values have been shown to respond better to chemotherapy than tumors that exhibit high pre-treatment ADC values [17]. One possible explanation is that tumors with high pre-treatment ADC values are likely to be more necrotic than those with low values. Necrotic tumors frequently are hypoxic, acidotic, and poorly perfused, leading to diminished sensitivity to chemotherapy and to radiation therapy [5].

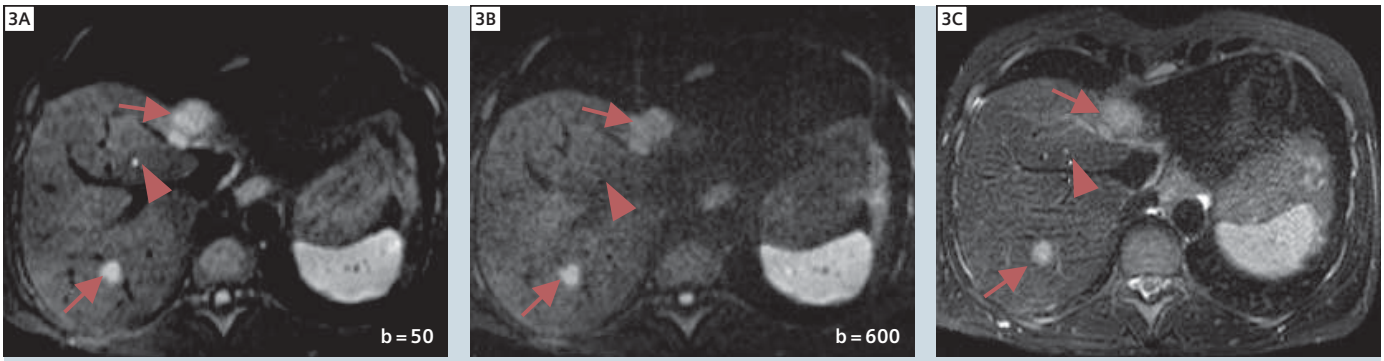

3 Characterization of focal liver lesions by DWI. Diffusion-weighted SSEPI (A, B) and fat-saturated T2-weighted TSE MR images (C) in a patient with rectal cancer. Two metastases (arrows) are hyperintense both on the b-50 (A) and b-600 image (B) resulting in low ADC values (1.18 and 1.27 × 10–3 mm²/s, respectively) typically seen in malignant liver lesions. A small cyst (arrowhead) is hyperintense on the b-50 image (A) but shows considerable signal loss on the b-600 image (B) resulting in a high ADC value (2.79 × 10–3 mm²/s). Note that on the T2-weighted image the small cyst can hardly be differentiated from a small metastasis (C).

Conclusion

In summary, DWI is a valuable tool in the detection of FLLs, especially with regard to small lesions. In the characterization of FLLs, DWI is of use as an additional, complementary method being interpreted in conjunction with other MR sequences. Finally, DWI seems to have great potential in the response evaluation of treated liver tumors: This has to be investigated in further studies.

Contact
Konstantin Holzapfel, M.D.
Technical University Munich
Dept. of Radiology
holzapfel@roe.med.tum.de

References

1 Carr HY, Purcell EM (1954) Effects of diffusion on free precession in nuclear magnetic resonance experiments. Phys Rev 94:630–638.
2 Stejskal EO, Tanner JE (1965) Spin diffusion measurements: spin echoes in the presence of a time-dependent field gradient. J Chem Phys 42:288–292.
3 Le Bihan D, Breton E, Lallemand D, Aubin ML, Vignaud J, Laval-Jeantet M (1988) Separation of diffusion and perfusion in intravoxel incoherent motion MR imaging. Radiology 168:497–505.
4 Thoeny HC, De Keyzer F (2007) Extracranial applications of diffusion-weighted magnetic resonance imaging. Eur Radiol 17:1385–1393.
5 Koh DM, Collins DJ (2007) Diffusion-weighted MRI in the body: applications and challenges in oncology. AJR Am J Roentgenol 188:1622–1635.
6 Bruegel M, Holzapfel K, Gaa J, Woertler K, Waldt S, Kiefer B, Stemmer A, Ganter C, Rummeny EJ (2008) Characterization of focal liver lesions by ADC measurements using a respiratory triggered diffusion-weighted single-shot echo-planar MR imaging technique. Eur Radiol 18:477–485.
7 Parikh T, Drew SJ, Lee VS, Wong S, Hecht EM, Babb JS, Taouli B (2008) Focal liver lesion detection and characterization with diffusion-weighted MR imaging: comparison with standard breath-hold T2-weighted imaging. Radiology 246:812–822.
8 Zech CJ, Herrmann KA, Dietrich O, Horger W, Reiser MF, Schoenberg SO (2008) Black-blood diffusion-weighted EPI acquisition of the liver with parallel imaging: comparison with a standard T2-weighted sequence for detection of focal liver lesions.Invest Radiol 43:261–266.
9 Coenegrachts K, Delanote J, Ter Beek L, Haspeslagh M, Bipat S, Stoker J, Van Kerkhove F, Steyaert L, Rigauts H, Casselman JW (2007) Improved focal liver lesion detection: comparison of single-shot diffusion-weighted echoplanar and single-shot T2 weighted turbo spin echo techniques. Br J Radiol 80:524–531.
10 Bruegel M, Gaa J, Waldt S, Woertler K, Holzapfel K, Kiefer B, Rummeny EJ (2008) Diagnosis of hepatic metastases: comparison of respiration-triggered diffusion-weighted echo-planar MRI and five T2-weighted turbo spin-echo sequences. AJR Am J Roentgenol (in press).
11 Nasu K, Kuroki Y, Nawano S, Kuroki S, Tsukamoto T, Yamamoto S, Motoori K, Ueda T (2006) Hepatic metastases: diffusion-weighted sensitivity-encoding versus SPIO-enhanced MR imaging. Radiology 239:122–130.
12 Koh DM, Brown G, Riddell AM, Scurr E, Collins DJ, Allen SD, Chau I, Cunningham D, deSouza NM, Leach MO, Husband JE (2008) Detection of colorectal hepatic metastases using MnDPDP MR imaging and diffusion-weighted imaging (DWI) alone and in combination. Eur Radiol 18:903–910.
13 Taouli B, Vilgrain V, Dumont E, Daire JL, Fan B, Menu Y (2003) Evaluation of liver diffusion isotropy and characterization of focal hepatic lesions with two single-shot echo-planar MR imaging sequences: prospective study in 66 patients. Radiology 226:71–78.
14 Chan JH, Tsui EY, Luk SH, Fung AS, Yuen MK, Szeto ML, Cheung YK, Wong KP (2001) Diffusion-weighted MR imaging of the liver: distinguishing hepatic abscess from cystic or necrotic tumor. Abdom Imaging 26:161–165.
15 Holzapfel K, Rummeny E, Gaa J (2007) Diffusion-weighted MR imaging of hepatic abscesses: possibility of different apparent diffusion coefficient (ADC)-values in early and mature abscess formation. Abdom Imaging 32:538–539.
16 Chen CY, Li CW, Kuo YT, Jaw TS, Wu DK, Jao JC, Hsu JS, Liu GC (2006) Early response of hepatocellular carcinoma to transcatheter arterial chemoembolization: choline levels and MR diffusion constants--initial experience. Radiology 239:448–456.
17 Koh DM, Scurr E, Collins D, Kanber B, Norman A, Leach MO, Husband JE (2007) Predicting response of colorectal hepatic metastasis: value of pretreatment apparent diffusion coefficients. AJR Am J Roentgenol 188:1001–1008.

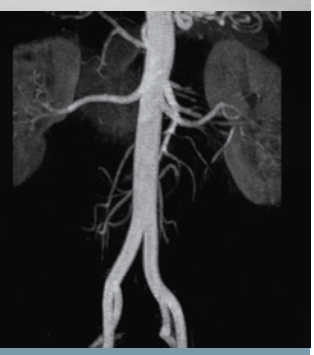

What if one size fits them all?

MAGNETOM Espree – the first open bore MRI for any patient.

With the shortest 1.5T magnet in the industry and its 70 cm inner diameter, MAGNETOM® Espree provides 1.5T high-field power with the highest level of patient comfort. Powered by Tim® (Total imaging matrix) technology, MAGNETOM Espree provides a new level of flexibility, accuracy, and speed. The combination of ultimate patient comfort and superb image quality will attract new referrals and will maximize your patient throughput.
www.siemens.com/healthcare +49 69 797 6420

Answers for life.

SIEMENS

MR-Z1098-1-7600

Revisiting Liver Imaging with VIBE

Eric Hatfield, M.D.[1]; Agus Priatna, Ph.D.[2]; Samuel Chang, M.D.[1]; Wilhelm Horger[3]; Stephan Kannengiesser, Ph.D.[3]; Vamsi Narra, M.D.[1]

[1]Mallinckrodt Institute of Radiology, Washington University School of Medicine, St Louis, Missouri, USA
[2]R&D Collaborations, Siemens Medical Solutions, St Louis, Missouri, USA
[3]PLM AW Oncology, Siemens Healthcare, Erlangen, Germany

Introduction

Volume Interpolated Breath-hold Examination (VIBE) [1] offers three-dimensional multiphase image acquisition before and following contrast administration on a breath-hold time scale. The dynamic behavior of liver lesions and structures during the precontrast, arterial, portal venous, early equilibrium and 5-minute-delayed equilibrium phases of enhancement allows more accurate characterization than static pre- and postcontrast analysis. VIBE is specifically designed for this task, and is a central pulse sequence in the MR evaluation of the liver.
However, routine clinical constraints present significant challenges in the acquisition of optimal diagnostic images. Delicate diagnostic decisions require fine image detail and appropriate anatomic coverage, but very ill patients preclude extended breath-holding, limiting matrix size and resolution. Short acquisition times are thus critical for both patient comfort and diagnostic success. The VIBE sequence can overcome these challenges and maintain image quality despite clinical realities.
The VIBE protocol we use at Mallinckrodt Institute of Radiology/ Washington University School of Medicine in St. Louis provides the flexibility to ensure robust, high quality images in diverse clinical situations, on both open bore imaging systems such as the Siemens 1.5 Tesla MAGNETOM Espree and standard bore systems such as the 1.5 Tesla MAGNETOM Symphony, A Tim System.

Method

Patients were scanned with a standard liver protocol on an open 70 cm bore diameter 1.5 Tesla MAGNETOM Espree system, or a standard 60 cm bore 1.5 Tesla MAGNETOM Symphony, A Tim system with Quantum gradient system. Imaging was performed with the standard 6-channel Body Matrix coil of the Total imaging matrix (Tim). In addition to dynamic pre- and postcontrast VIBE, the liver imaging protocol included in-phase/opposed-phase T1 gradient echo, T2 HASTE, multiple breath-hold T2 STIR Turbo Spin Echo, and diffusion-weighted imaging (*syngo* DWI).
Dynamic pre- and postcontrast enhanced VIBE was acquired with a variety of sequence parameter combinations.

These included 256 or 320 base resolutions,
TE = 1.9–2.4 msec,
TR = 4.3–5.0 msec,
FOV = 300–380 mm,
phase FOV = 80–90%,
partition thickness = 3–4 mm,
slices per slab = 56–72,
slice resolution = 64–67%,
flip angle = 10°–12°,
symmetric or reversed asymmetric echo*,
slice and phase partial Fourier = 6/8 or 7/8,
bandwidth = 360–490 Hz/pixel,
and iPAT parallel imaging with acceleration factor = 2.
Quick FatSat was used for fat suppression.

Clinical cases

The following cases demonstrate the advances and high quality images available with the above parameters on the product and works-in-progress* VIBE sequences.

Case 1

This 59-year-old female was evaluated for a liver lesion with VIBE using a reduced 10° flip angle and Quick FatSat. Figure 1 demonstrates a T1 hypointense mass with progressive discontinuous centripetal enhancement characteristic of a giant cavernous hemangioma [2]. The central non-enhancing portion of the lesion likely represents a fluid cavity in the setting of degeneration. Excellent tissue contrast provides superb evaluation of lesion behavior pre- and post-contrast. Homogeneous fat suppression further enhances image contrast. These images were acquired at 256 base resolution with a bandwidth of 490 Hz/pixel, FOV of 350 mm, partition thickness of 4 mm, and symmetric echo with TE/TR of 1.9/4.3 msec, respectively.

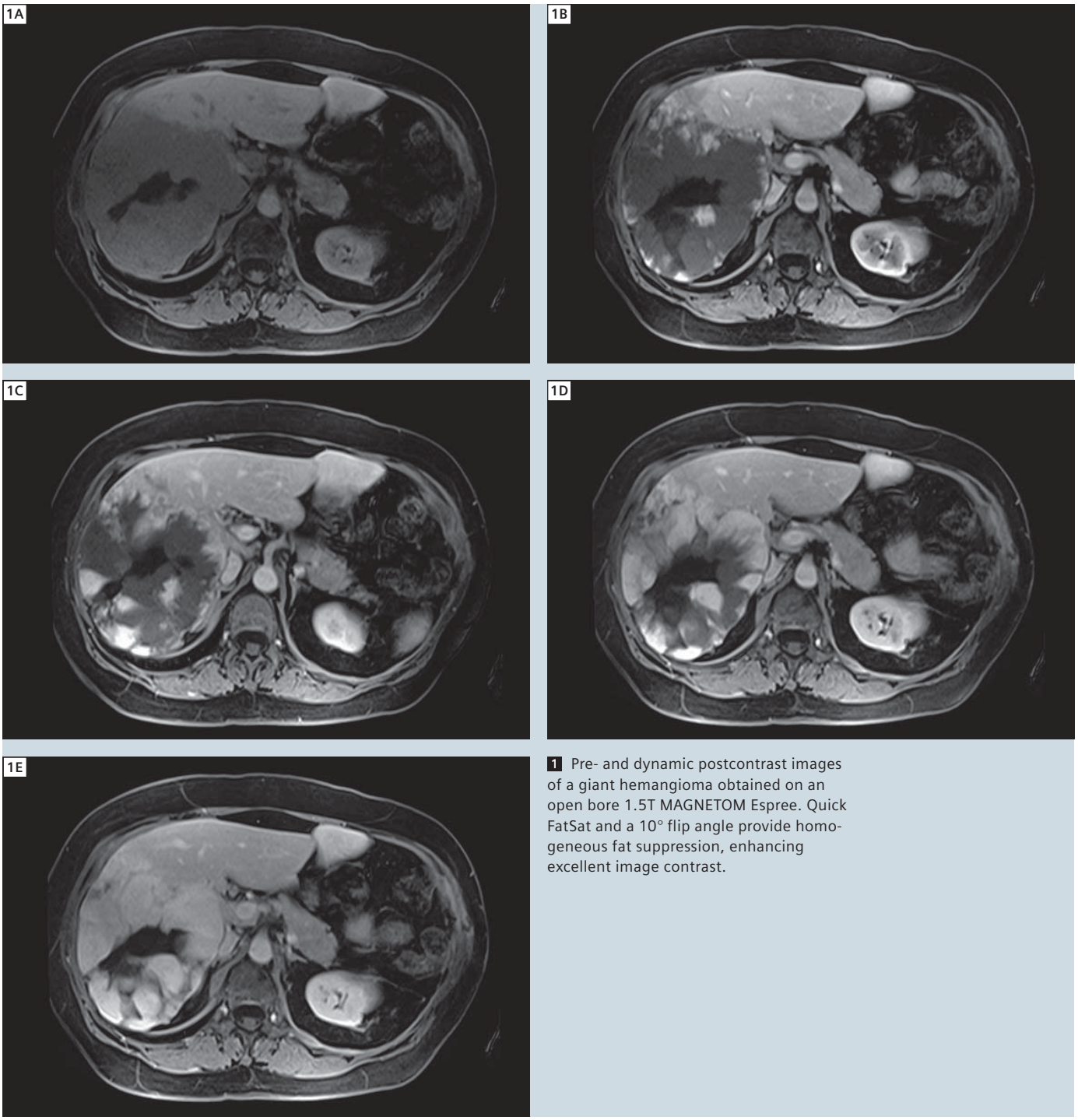

1 Pre- and dynamic postcontrast images of a giant hemangioma obtained on an open bore 1.5T MAGNETOM Espree. Quick FatSat and a 10° flip angle provide homogeneous fat suppression, enhancing excellent image contrast.

Case 2

This 44-year-old female with cirrhosis was evaluated with VIBE with an increased base resolution of 320 (Fig. 2). High quality images are required to define the somewhat subtle differences in parenchymal signal and architecture between the background cirrhotic parenchyma and the large central regenerating nodule [3] that might otherwise have been mistaken for a mass. Improvement in resolution is apparent, and signal-to-noise and tissue contrast are maintained. This acquisition required a standard 22 second breathhold. In addition to 320 base resolution, these images were acquired with a bandwidth of 390 Hz/pixel, FOV of 350 mm, flip angle of 10°, partition thickness of 3.5 mm, Quick FatSat and symmetric echo with TE/TR of 2.4/5.0 msec, respectively.

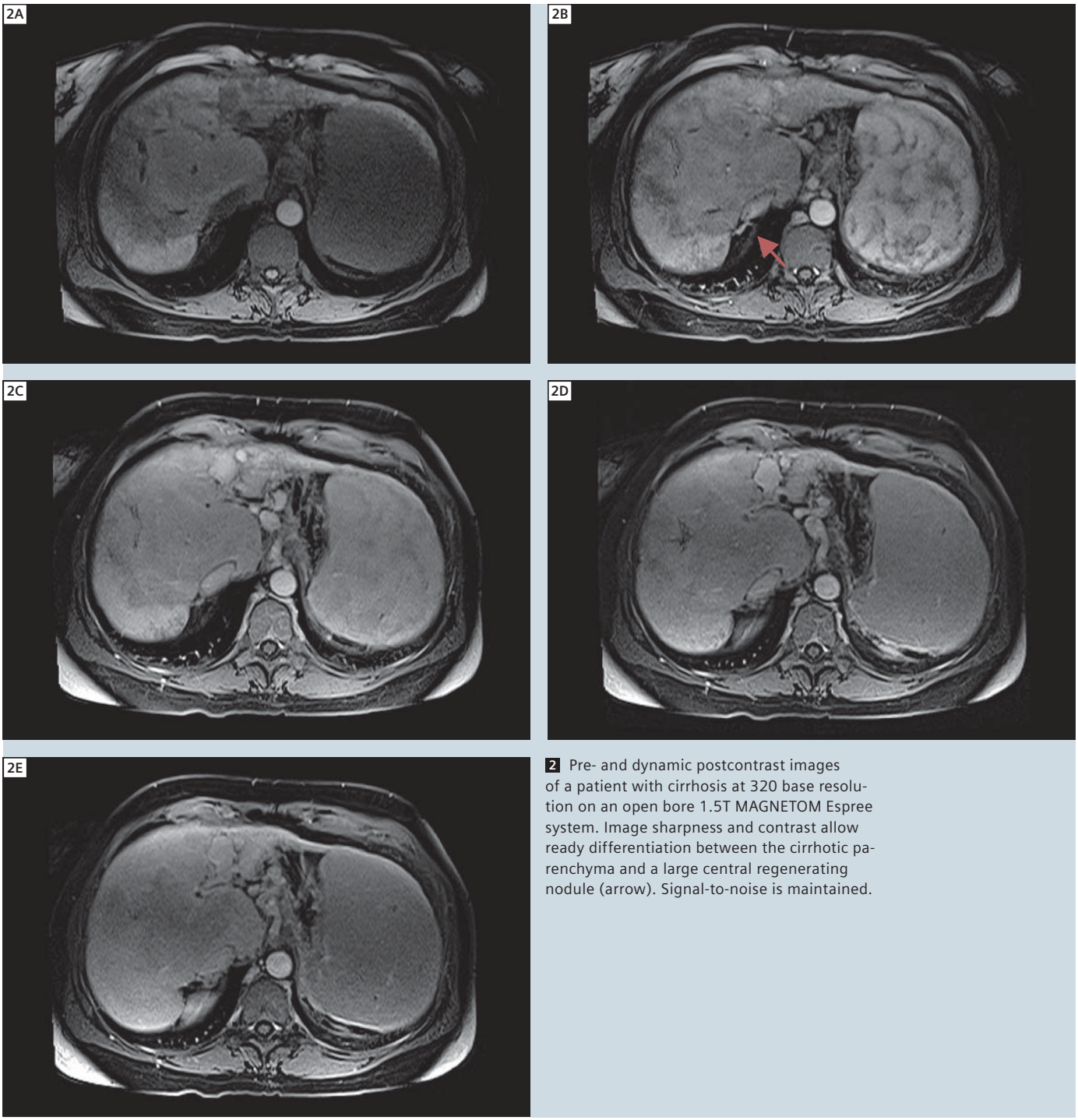

2 Pre- and dynamic postcontrast images of a patient with cirrhosis at 320 base resolution on an open bore 1.5T MAGNETOM Espree system. Image sharpness and contrast allow ready differentiation between the cirrhotic parenchyma and a large central regenerating nodule (arrow). Signal-to-noise is maintained.

Case 3

This 50-year-old male with cirrhosis was evaluated with VIBE at 320 base resolution and reversed asymmetric echo acquisition* (Fig. 3). Despite acquisition in the delayed phase of enhancement, excellent contrast and resolution allow the demonstration of numerous enhancing fibrotic bands throughout the cirrhotic parenchyma. The two hypointense foci within the left lobe represent large siderotic nodules [4]. Reversed asymmetric echo acquisition*, allowing shorter TR, and 7/8 partial phase Fourier result in an acquisition time of 16 seconds, sufficient for successful breath holding in this ill patient. In addition to 320 base resolution, reversed asymmetric echo*, and 7/8 partial phase Fourier, these images were acquired with a bandwidth of 360 Hz/pixel, flip angle of 10°, FOV of 320 mm, partition thickness of 3 mm, 64 slices per slab, Quick FatSat and opposed phase TE.

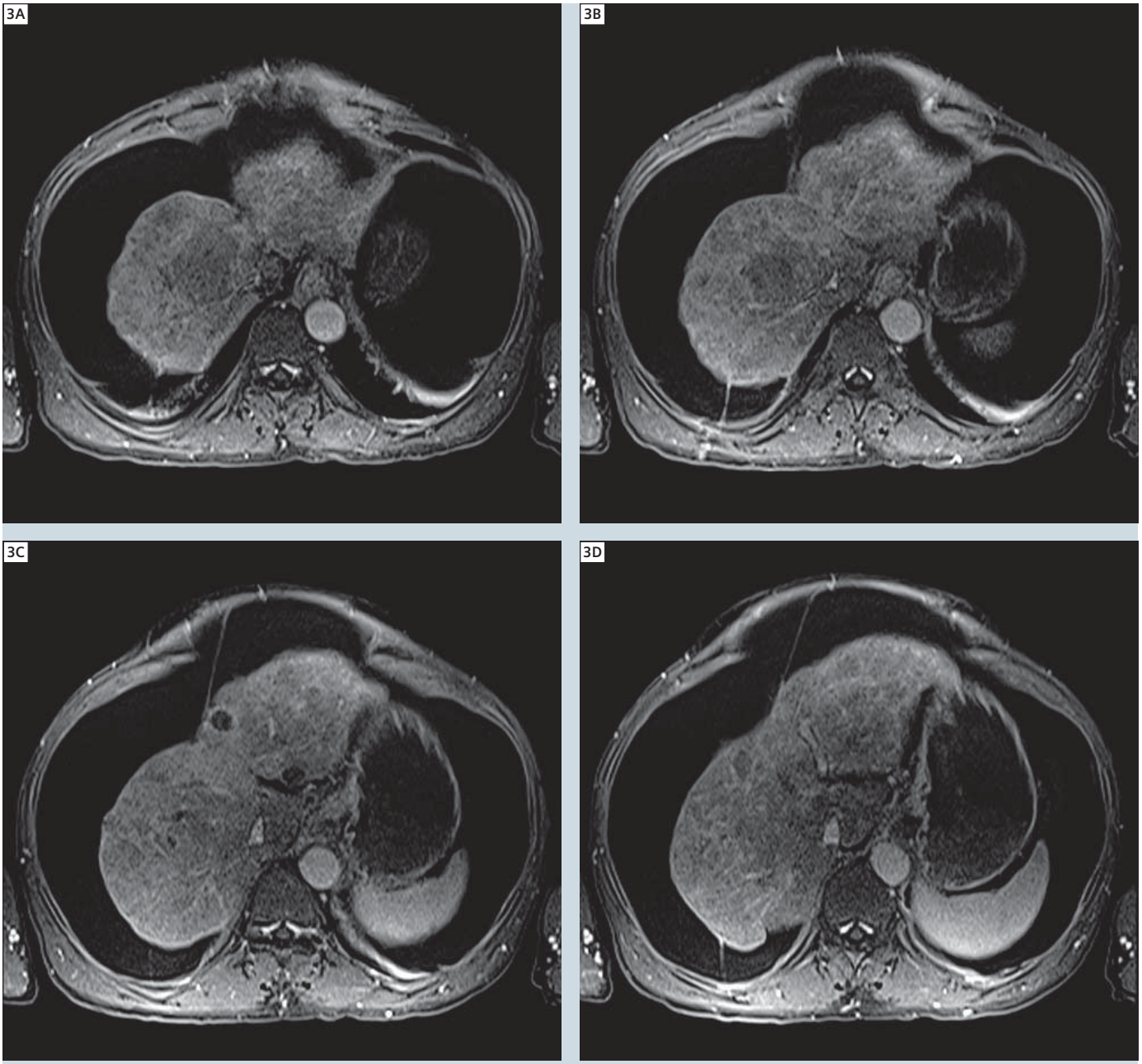

3 Postcontrast delayed equilibrium images of a patient with cirrhosis at 320 base resolution on a 1.5T MAGNETOM Symphony, A TIM system. 7/8 phase partial Fourier and reversed asymmetric echo* shorten acquisition time to 16 seconds. Excellent sharpness and contrast are maintained.

Case 4

This 18-year-old female was evaluated with VIBE with enhanced 320 base resolution, but an acquisition time of only 13 seconds (Fig. 4). This allows a successful and comfortable breath-hold for almost any patient. Partial phase Fourier of 6/8 with phase correction* provides the additional time savings, while preserving gains in resolution and preventing artifacts. The images of figure 5 were acquired in the delayed phase of enhancement, but tissue contrast is maintained. In addition to the above parameters, these images were acquired with a bandwidth of 360 Hz/pixel, flip angle of 10°, partition thickness of 3.5 mm, 60 slices per slab, reversed asymmetric echo acquisition*, Quick FatSat and opposed phase TE.

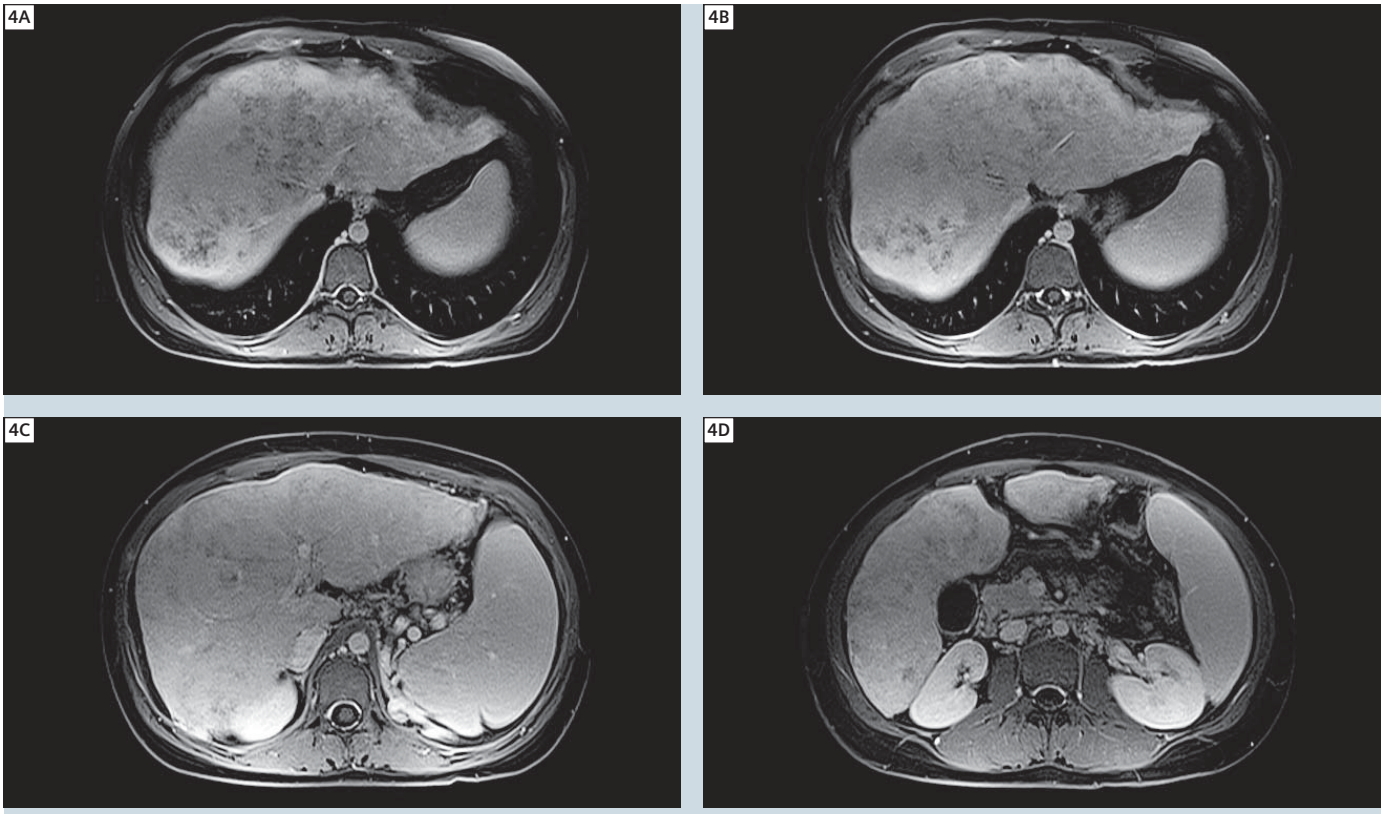

4 Postcontrast delayed equilibrium images of a patient with cirrhosis at 320 base resolution on a 1.5T MAGNETOM Symphony, A Tim System. 6/8 phase partial Fourier with phase correction* and reversed asymmetric echo* shorten acquisition time to 13 seconds. Excellent sharpness and contrast are maintained without artifacts.

Conclusion

VIBE provides state-of-the-art dynamic contrast enhanced imaging of the liver. It allows improved and robust fat suppression, image sharpness, tissue contrast, anatomic coverage, and shortened acquisition times even in challenging clinical scenarios. Image quality is maintained on the open 70 cm bore diameter 1.5T MAGNETOM Espree system and the standard 60 cm bore diameter 1.5T MAGNETOM Symphony, A Tim system.

References

1 Rofsky NM, Lee VS, et al. Abdominal MR Imaging with a Volume Interpolated Breath-hold Examination. Radiology. 1999 Sept; 212(3):876–84.
2 Danet IM, Semelka RC, et al. Giant Hemangioma of the liver: MR imaging characteristic in 24 patients. Magnetic Resonance Imaging 2003 Feb; 21(2): 95–101.
3 Vitellas KM, Tzalonikou MT, et al. Cirrhosis: spectrum of findings on unenhanced and dynamic gadolinium-enhanced MR imaging. Abdominal Imaging. 2001 Nov–Dec;26(6):601–15.
4 Krinksy GA, Lee VS, et al. Siderotic nodules at MR imaging: regenerative or dysplastic? J Comput Assist Tomogr. 2000 Sept–Oct;24(5):773–6.

* WIP – Works in progress. The information about this product is preliminary. The product is under development and its future availability in the U.S. cannot be ensured.

Contact
Vamsi Narra, M.D.
Mallinckrodt Institute of Radiology
Washington University School of Medicine
St. Louis, Missouri
USA
narrav@mri.wustl.edu

Spectral Adiabatic Inversion Recovery (SPAIR) MR imaging of the Abdomen

Thomas C. Lauenstein

Department of Diagnostic and Interventional Radiology and Neuroradiology, University Hospital Essen, Germany

Background

Magnetic resonance imaging (MRI) has become a major imaging tool for the depiction and characterization of abdominal disease. Standard abdominal MRI protocols encompass different forms of T1-weighted (T1w) and T2-weighted (T2w) data acquisition. These sequences can be collected in less than 20 seconds, which typically is within the patients' ability to suspend respiration. Hence, artifacts due to physiological motion including respiration and bowel motion can be reduced, if not avoided. While most T1-weighted imaging techniques of the abdomen include gradient echo (GRE) sequences, T2-weighted imaging is based on the collection of single shot fast spin echo (SSFSE) data. The latter sequences in conjunction with fat saturation play a key role for the interpretation of different abdominal processes as liver lesions can be most accurately delineated and specified [1]. Furthermore, T2-weighted imaging with fat saturation is crucial for the depiction of edema and/or free fluid. This is particularly helpful for the depiction of inflammatory processes of the bowel, e.g. in patients with Crohn's disease [2, 3], appendicitis [4, 5] or diverticulitis [6–8]. Finally, T2-weighted data may be particularly useful in the setting of pregnant patients*. As the intravenous administration of gadolinium based contrast agents is contraindicated in this patient group, T1-weighted imaging is restricted and only provides limited information. Hence, T2-weighted imaging with fat saturation has been found to be the key sequence in pregnant* women with suspected abdominal inflammation or tumor disease [9–12]. Different techniques for fat saturation in MRI can be used. The most common form in abdominal imaging is the use of a 180° excitation pre-pulse, which suppresses the signal specific tissue depending on the inversion time applied. The inversion time (TI) is set according to the T1 of fat in order to selectively null the fat signal (TI = 150-170 ms). In the most common implementation, the inversion pulse is applied with a wide frequency bandwidth to include both fat and water spins. A potential drawback to this approach is that the water signal will not be fully recovered during data acquisition, and the overall water signal-to-noise ratio (SNR) will be diminished. This can negatively impact the contrast-to-noise ratio (CNR) of lesions surrounded by tissue, such as tumors within the liver.

Technical considerations for SPAIR

The inversion recovery (IR) technique can be modified by using chemical selective or spectral pre-saturation attenuated inversion-recovery pre-pulses. SPAIR (Spectral Adiabatic Inversion Recovery) is a powerful technique for fat suppression which offers different advantages over conventional fat suppression techniques. The technique is insensitive to B1 inhomogenities and only fat spins are suppressed/inverted. SPAIR uses a spectrally selective adiabatic inversion pulse to invert the fat spins in the imaging volume. After the adiabatic pulse a large spoiler is utilized in order to destroy any transverse magnetization. The fat spins will now decay according to the T1 relaxation rate and after a certain characteristic time (TI null) the longitudinal magnetization will be zero. At this time point the excitation pulse of the SSFSE T2-weighted module is applied. As the fat spins have zero longitudinal magnetization at this point they will not contribute to the MR signal.

Clinical applications

Homogeneity and degree of fat suppression

The implementation of SPAIR fat suppression techniques will result in a more profound and homogenous fat saturation compared to conventional fat suppression techniques. In a recent study, SNR of mesenteric and retroperitoneal fat was measured for both IR and SPAIR fat suppression in conjunction with T2-weighted SSFSE imaging in order to determine the degree of fat suppression [13]. The study showed that improved fat suppression was found when SPAIR-SSFSE was applied (Fig. 1).

Depiction of anatomical structures

An advantage of SPAIR compared to conventional IR techniques is demonstrated by the improvement in CNR of the hepatic lesions. The better liver lesion contrast on SPAIR-SSFSE images is consistent with the predicted benefits of applying a frequency-sensitive inversion pulse. This leaves the maximum possible water signal intact as only the fat spins are inverted. Two types of focal liver lesions have been evaluated [13]: hemangiomas with a relatively high CNR and metastases with a relatively low CNR. The CNR was found significantly increased for both families of lesions when using SPAIR compared to IR SSFSE (Figs. 2 and 3).
Furthermore, delineation of bowel wall structures is markedly improved on SPAIR SSFSE (Fig. 4). This improvement is due to two different factors that dif-

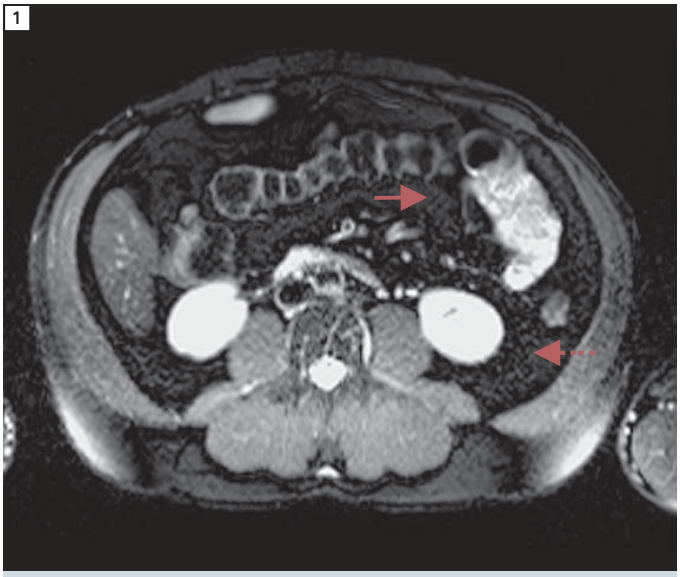

1 Homogeneous fat saturation in the retroperitoneum (dashed arrow) and the mesenteries (arrow) with the SPAIR technique.

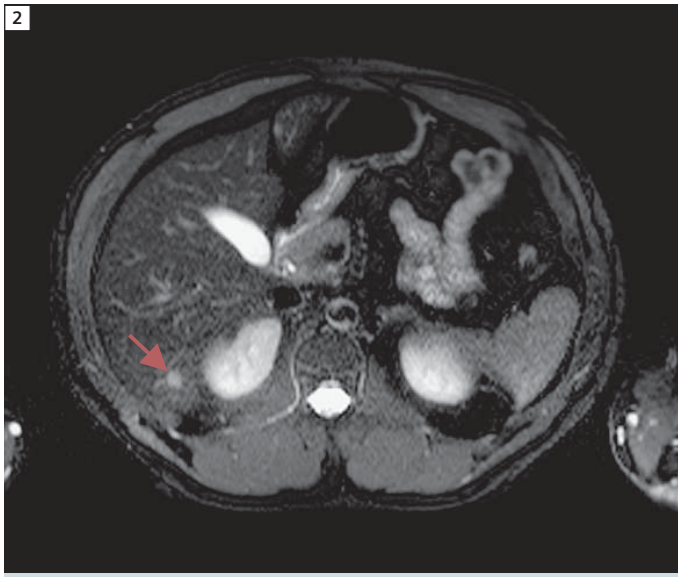

2 Patient with liver metastases (arrow) of colorectal cancer. The lesion is evident and provides high CNR values on SPAIR T2-weighted imaging.

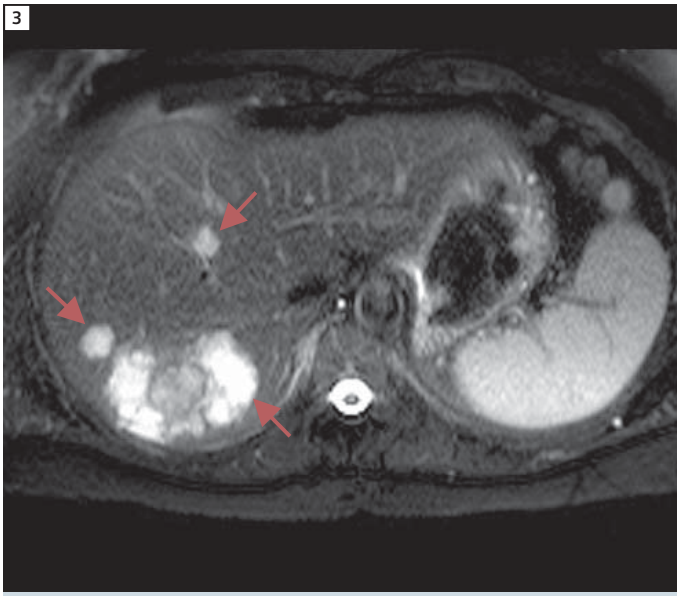

3 Patient with several hemangiomas (arrows). SPAIR T2-weighted MRI.

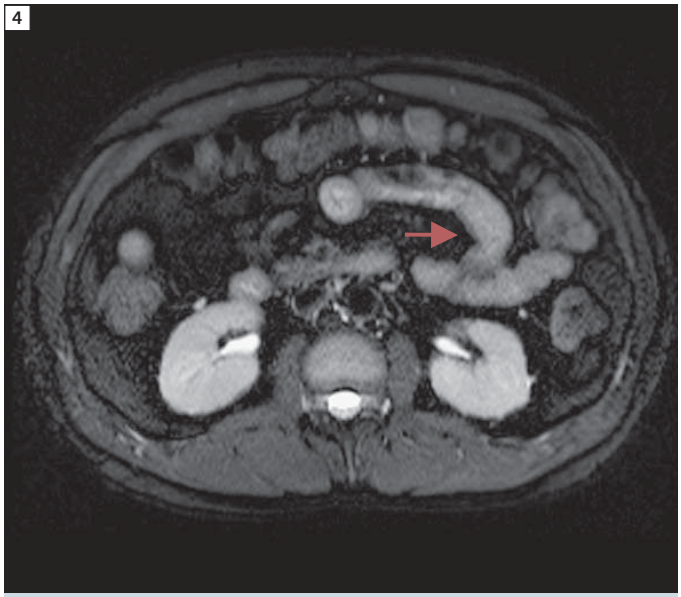

4 Conspicuous bowel loops (arrow) using the SPAIR technique.

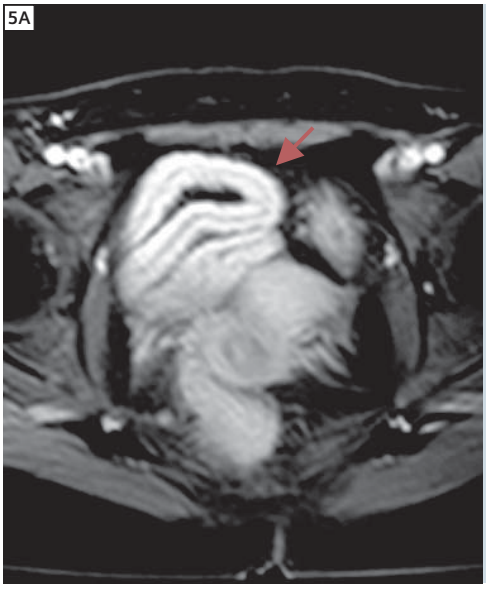

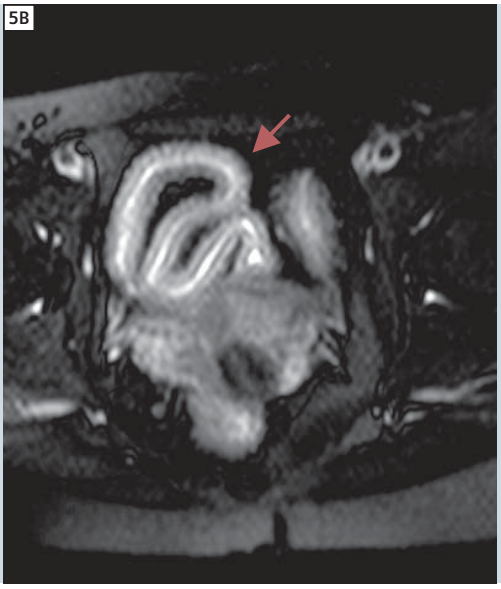

5 Patient with active colitis. There is increased contrast enhancement after iv gadolinium administration shown on T1-weighted GRE imaging (5A; arrow). A high T2 signal of the bowel wall can be depicted on T2-weighted SPAIR images (5B; arrow), which is consistent with active inflammatory disease due to edematous changes.

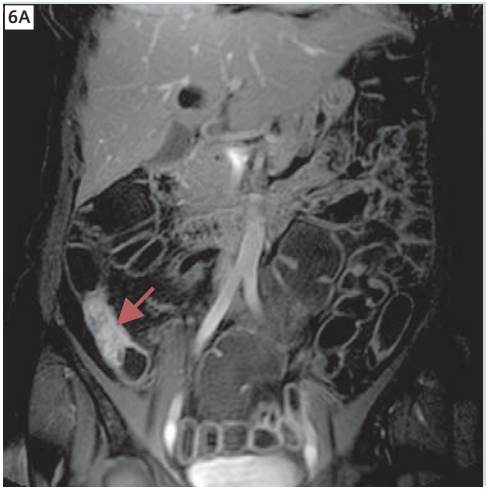

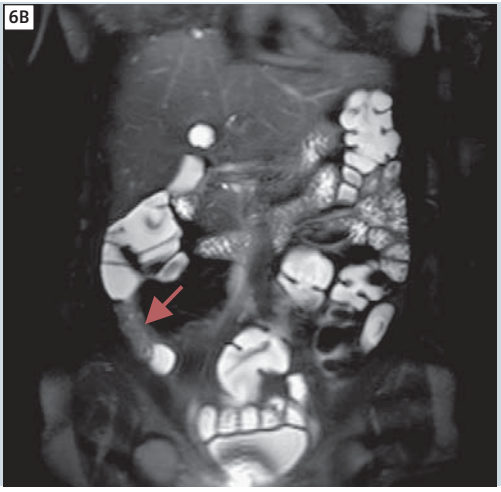

6 Patient with mildly active inflammatory changes of the ascending colon (arrow). T1-weighted contrast-enhanced MRI reveals increased contrast uptake of the inflamed bowel segment and thickening of the bowel wall (6A). The T2 signal on the SPAIR image is only slightly elevated (6B).

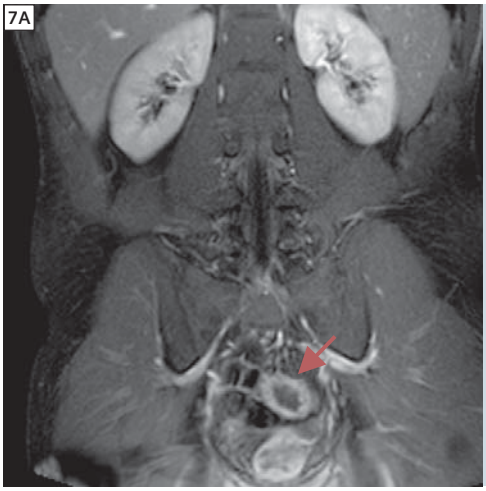

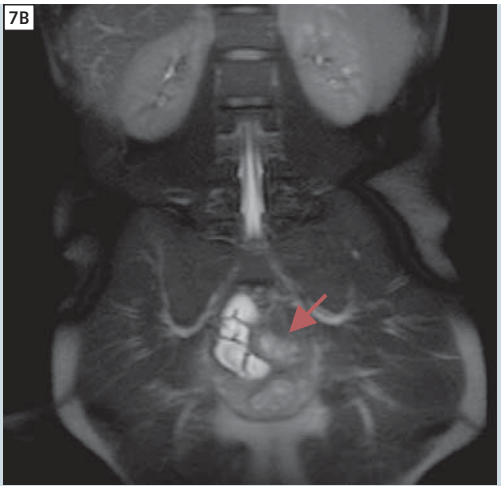

7 Patient with non-active / fibrotic inflammation of the sigmoid colon (arrow). Similar to the active forms of inflammatory bowel disease (IBD) there is increased contrast enhancement on T1-weighted MRI (7A). However, there is lack of edema, and thus the T2 signal is not elevated on the SPAIR image (7B).

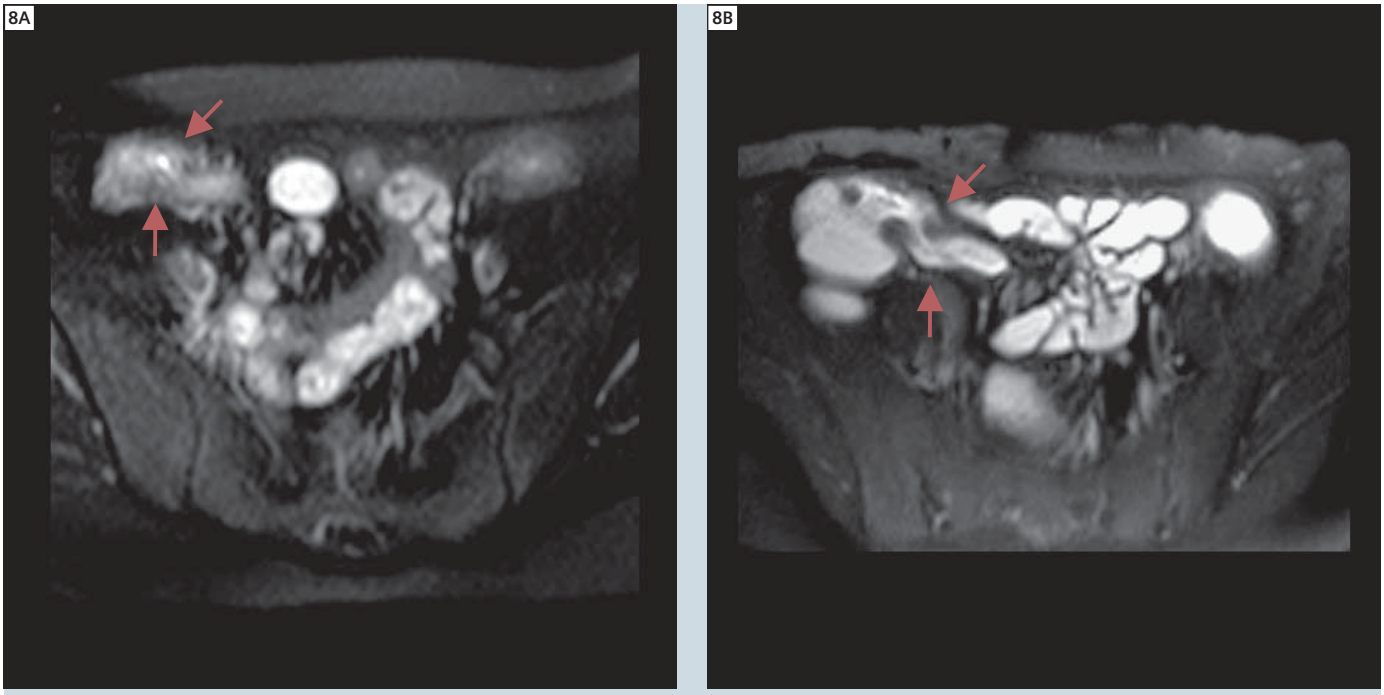

8 SPAIR T2-weighted SSFSE MRI can be used as a stand-alone sequence for therapeutic monitoring. This patient presented with sign of active inflammation in the terminal ileum and highly elevated T2 signal on SPAIR imaging (8A). One week after the initiation of anti-inflammatory medication the T2 signal dropped as a correlation of therapeutic response (8B).

ferentiate SPAIR SSFSE: one factor is the relatively greater sensitivity to motion of standard IR SSFSE. In addition, bowel wall visualization should benefit from the increased SNR of water-containing structures on SPAIR SSFSE.

Inflammatory abdominal processes

Evaluation of disease activity in patients with inflammatory bowel disease (IBD) is often a challenging clinical situation. While active inflammation is treated with systemic corticosteroids or other immuno-modulator drugs, surgical therapeutic options are chosen for chronic disease. This discrepancy in therapy strategies underlines the need for an accurate categorization and differentiation between active and chronic disease. Attempts of classifying IBD in the past were based on different variables that were either time-consuming (e.g. MR based perfusion analyses), invasive (colonoscopy / biopsy) or inaccurate (CDAI). Hence, a relatively fast, simple and non-invasive technique is desired in appraising the level of inflammatory activity and also in following up these patients for treatment response.

SPAIR T2-weighted SSFSE sequences and gadolinium enhanced T1-weighted sequences are complementary techniques in patients with IBD [14]. Gadolinium-enhanced T1-weighted data is helpful to detect IBD independent of its activity state with a high sensitivity. However, accuracy of T1-weighted imaging to differentiate between active and non-active disease is only moderate. Enhancement patterns of T1-weighted imaging are unspecific: both bowel segments with active and chronic inflammation show an increased contrast enhancement [15]. Hyperintensity on T2-weighted images, however, is related to increased edema and inflammatory fluid components within or adjacent to the bowel wall, whereas T1-weighted hyperintensity may be attributed to a hypervascularity (in active disease) or a delayed wash-out (in fibrotic /chronic disease).

Examples of contrast-enhanced T1-weighted GRE images and SPAIR T2-weighted SSFSE images are shown in figures 5–7 for highly active, intermediate active and non-active IBD. Once the diagnosis of IBD is established, SPAIR T2-weighted SSFSE imaging can be used as a stand-alone sequence for therapy monitoring (Fig. 8). Furthermore, this method is also very helpful not only for the assessment of IBD including Crohn's

* The safety of imaging fetuses/infants has not been established.

disease and Ulcerative colitis, but also for diverticulitis (Fig. 9) and the depiction of fistulae (Fig. 10).

Conclusion

There are overall benefits of SPAIR SSFSE that can be measured on clinical abdominal MR images regarding fat saturation, particularly in fat adjacent to bowel and for improving overall image contrast even between non-fatty soft tissues, such as can be demonstrated with liver masses. Furthermore, SPAIR SSFSE is a crucial tool for the depiction of inflammatory processes in the abdomen, particularly IBD. By means of SPAIR T2-weighted SSFSE a differentiation between active and non-active inflammatory processes can be easily established.

Contact
Thomas C. Lauenstein, M.D.
University Hospital Essen
Dept. of Diagnostic and Interventional Radiology and Neuroradiology
Hufelandstr. 55
45122 Essen, Germany
thomas.lauenstein@uni-due.de

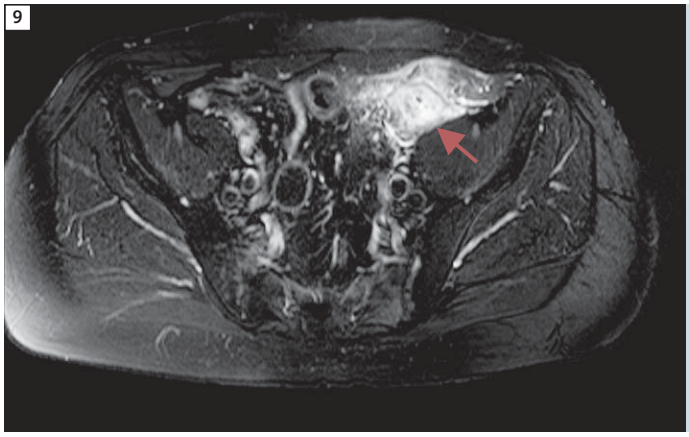

9 Patient with active diverticulitis. There is increased T2-weighted signal in and adjacent to the wall of the sigmoid colon (arrow) in keeping due to edema.

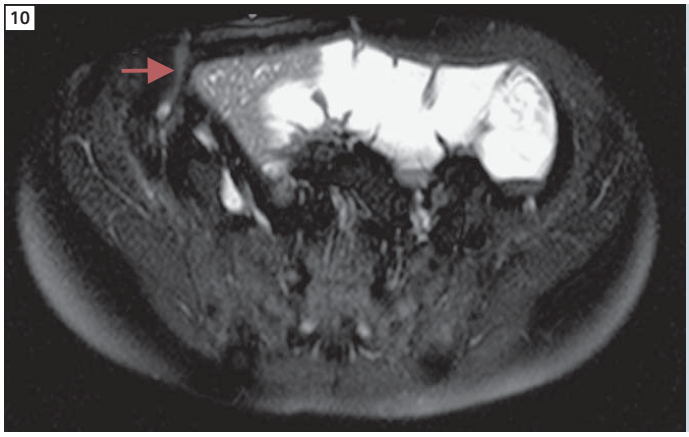

10 T2-weighted SPAIR imaging can easily display not only an inflammatory process itself, but also complications such as a fluid-filled fistula – between bowel and cutis – (arrow).

References

1 Gaa J, Hatabu H, Jenkins RL, Finn JP, Edelman RR. Liver masses: replacement of conventional T2-weighted spin-echo MR imaging with breath-hold MR imaging. Radiology 1996;200: 459–464.
2 Florie J, Wasser MN, Arts-Cieslik K, Akkerman EM, Siersema PD, Stoker J. Dynamic contrast-enhanced MRI of the bowel wall for assessment of disease activity in Crohn's disease. AJR Am J Roentgenol 2006;186:1384–1392.
3 Maccioni F, Bruni A, Viscido A, et al. MR imaging in patients with Crohn disease: value of T2- versus T1-weighted gadolinium-enhanced MR sequences with use of an oral superparamagnetic contrast agent. Radiology 2006;238:517–530.
4 Martin DR, Danrad R, Herrmann K, Semelka RC, Hussain SM. Magnetic resonance imaging of the gastrointestinal tract. Top Magn Reson Imaging 2005;16:77–98.
5 Nitta N, Takahashi M, Furukawa A, Murata K, Mori M, Fukushima M. MR imaging of the normal appendix and acute appendicitis. J Magn Reson Imaging 2005;21:156–165.
6 Cobben LP, Groot I, Blickman JG, Puylaert JB. Right colonic diverticulitis: MR appearance. Abdom Imaging 2003;28:794–798.
7 Heverhagen JT, Ishaque N, Zielke A, et al. Feasibility of MRI in the diagnosis of acute diverticulitis: initial results. Magma 2001;12:4–9.
8 Heverhagen JT, Zielke A, Ishaque N, Bohrer T, El-Sheik M, Klose KJ. Acute colonic diverticulitis: visualization in magnetic resonance imaging. Magn Reson Imaging 2001;19:1275–1277.
9 Birchard KR, Brown MA, Hyslop WB, Firat Z, Semelka RC. MRI of acute abdominal and pelvic pain in pregnant patients. AJR Am J Roentgenol 2005;184:452–458.
10 Brown MA, Birchard KR, Semelka RC. Magnetic resonance evaluation of pregnant patients with acute abdominal pain. Semin Ultrasound CT MR 2005;26:206–211.
11 Cobben LP, Groot I, Haans L, Blickman JG, Puylaert J. MRI for clinically suspected appendicitis during pregnancy. AJR Am J Roentgenol 2004;183:671–675.
12 Tang Y, Yamashita Y, Takahashi M. Ultrafast T2-weighted imaging of the abdomen and pelvis: use of single shot fast spin-echo imaging. J Magn Reson Imaging 1998;8:384–390.
13 Lauenstein TC, Sharma P, Hughed T, Heberlein K, Tudorascu D, Martin DR. Evaluation of optimized inversion-recovery fat-suppression techniques for T2-weighted abdominal MR Imaging. J Magn Reson Imaging 2008:27:1448–1454.
14 Maccioni F, Bruni A, Viscido A, et al. MR imaging in patients with Crohn disease: value of T2- versus T1-weighted gadolinium-enhanced MR sequences with use of an oral superparamagnetic contrast agent. Radiology 2006;238:517–530.
15 Udayasankar UK, Lauenstein TC, Martin DR. Role of Spectral Presaturation Attenuated Inversion-Recovery (SPAIR) T2 Fat-suppressed MR Imaging in Active Inflammatory Bowel Disease. RSNA 2007.

Diffusion-Weighted MR Imaging in Brain Tumor

L. Celso Hygino da Cruz Jr.; Emerson L. Gasparetto; Roberto C. Domingues; Romeu C. Domingues

CDPI e Multi-Imagem Ressonância Magnética, Rio de Janeiro – RJ, Brazil

Introduction

Primary neoplasms of the central nervous system (CNS) have a prevalence of between 15,000 and 17,000 new cases annually in the United States and are estimated to cause the deaths of 13,000 patients. Gliomas are the leading cause of primary CNS tumors, accounting for 40–50% of cases and 2–3% of all cancers[4]. Despite new treatment techniques, patients' survival still remains very low, varying between 16 and 53 weeks.
It is generally accepted that conventional magnetic resonance imaging (MRI) tends to underestimate the extent of the tumor, which can in turn lead to a suboptimal treatment. New functional magnetic resonance imaging sequences, such as diffusion tensor imaging (DTI) and diffusion-weighted imaging (DWI), have been widely used to evaluate such tumors.

Diffusion-weighted MR image

Diffusion-weighted imaging is based on the random or Brownian motion of water molecules in relation to their thermal energy.
DWI has been used to assess brain tumors and while it has had limited success as a definitive prognostic tool, its proponents suggest that in certain settings it can increase both the sensitivity and specificity of MR imaging.
One example of a specific arena in which DWI may be helpful is in distinguishing between brain abscesses and necrotic and cystic neoplasms on MRI. This differentiation is still a challenge on both clinical and radiological setting. The abscesses have a high signal on DWI and a reduced Apparent Diffusion Coefficient (ADC) within the cavity. This restricted diffusion is thought to be related to the characteristic of the pus in the cavity; this may in turn lead to reduced water mobility, lower ADC, and bright signal on DWI. By contrast, necrotic and cystic tumors display a low signal on DWI (similar to the CSF in the ventricles) with an increased ADC as well as isointense or hypointense DWI signal intensity in the lesion margins.

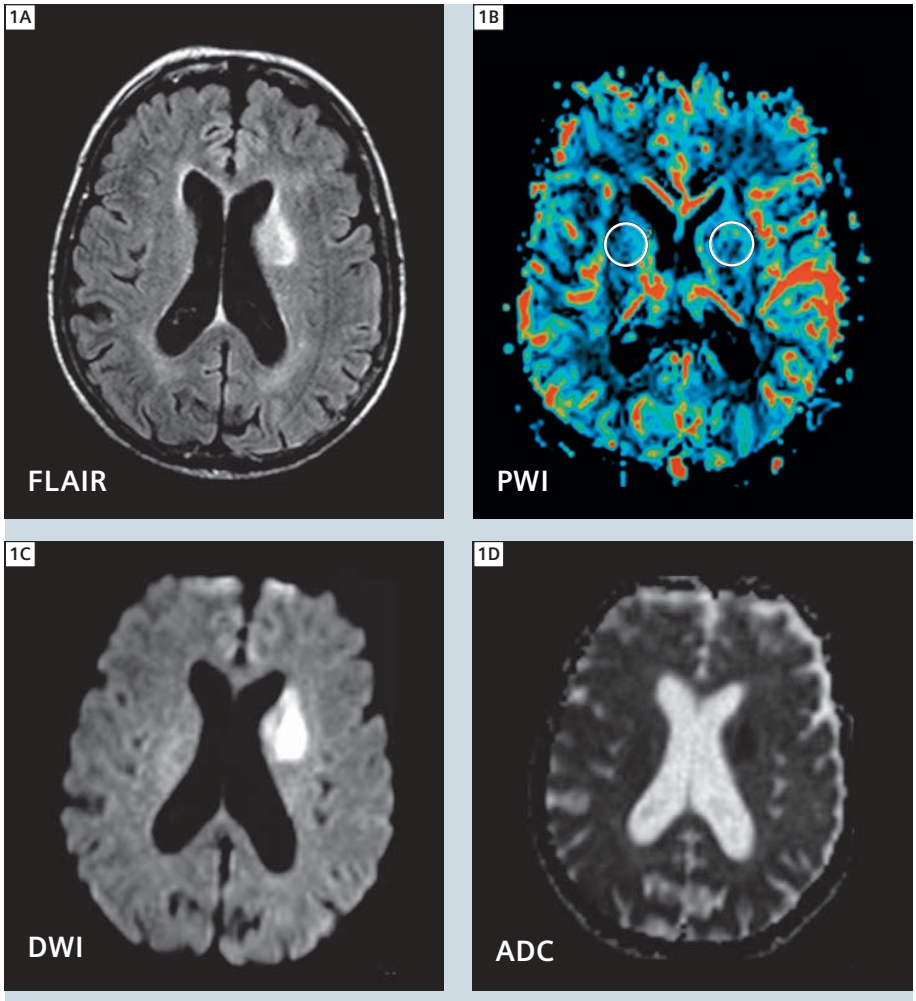

1 72-year-old female presented with mental and language disturbance, since 20 days. Enhancing lesion, low perfusion, restricted diffusion on DWI and ADC.
Diagnosis: Lymphoma

DWI is also an effective way of differentiating an arachnoid cyst from epidermoid tumors. Both lesions present similar signal intensity characteristic of cerebrospinal fluid (CSF) on T1 and T2 sequences. On DWI, epidermoid tumors are hyperintense – for they are solidly composed – whereas arachnoid cysts are hypointense, demonstrating high diffusivity. The ADC values of epidermoid tumors are similar to those of the brain parenchyma, whilst ADC values of arachnoid cysts are similar to those of CSF.
In certain settings diffusion-weighted imaging can increase both the sensitivity and specificity of MR imaging in the evaluation of brain tumors by providing information about tumor cellularity, which may in turn improve prediction of tumor grade. The mechanism in which DWI may help in the tumor grading is based on the fact that free water molecule diffusivity is restricted by cellularity increase in high-grade lesions. The reduction in extracellular space caused by tumor cellularity causes a relative reduction in the apparent diffusion coefficient (ADC) values. Perhaps most helpfully, high grade tumors have in some studies been found to have low ADC values, suggesting a correlation between ADC values and tumor cellularity. In some studies, however, ADC values found in high- and low-grade gliomas have overlapped somewhat. It is well known that the brain tumors, specially the gliomas, are heterogeneous. Usually within a same neoplasm grade, mostly high-grade, different histologic features of grades II–IV are presented. This limitation may also be explained by the fact that it is not only the tumor cellularity that is responsible for reducing the diffusibility.
Lymphoma, a highly cellular tumor, has hyperintensity on DWI and reduced ADC values. While meningiomas also have a restricted diffusion, displaying low ADC values, they rarely present difficulty in diagnosis. DWI can be somewhat helpful in distinguishing medulloblastoma from other pediatric brain tumors, as it seems to display restricted diffusion presumably because of the densely packed tumor cells and high nuclear-to-cytoplasm ratio. The solid enhancing portion of cerebellar haemangioblastomas demon-

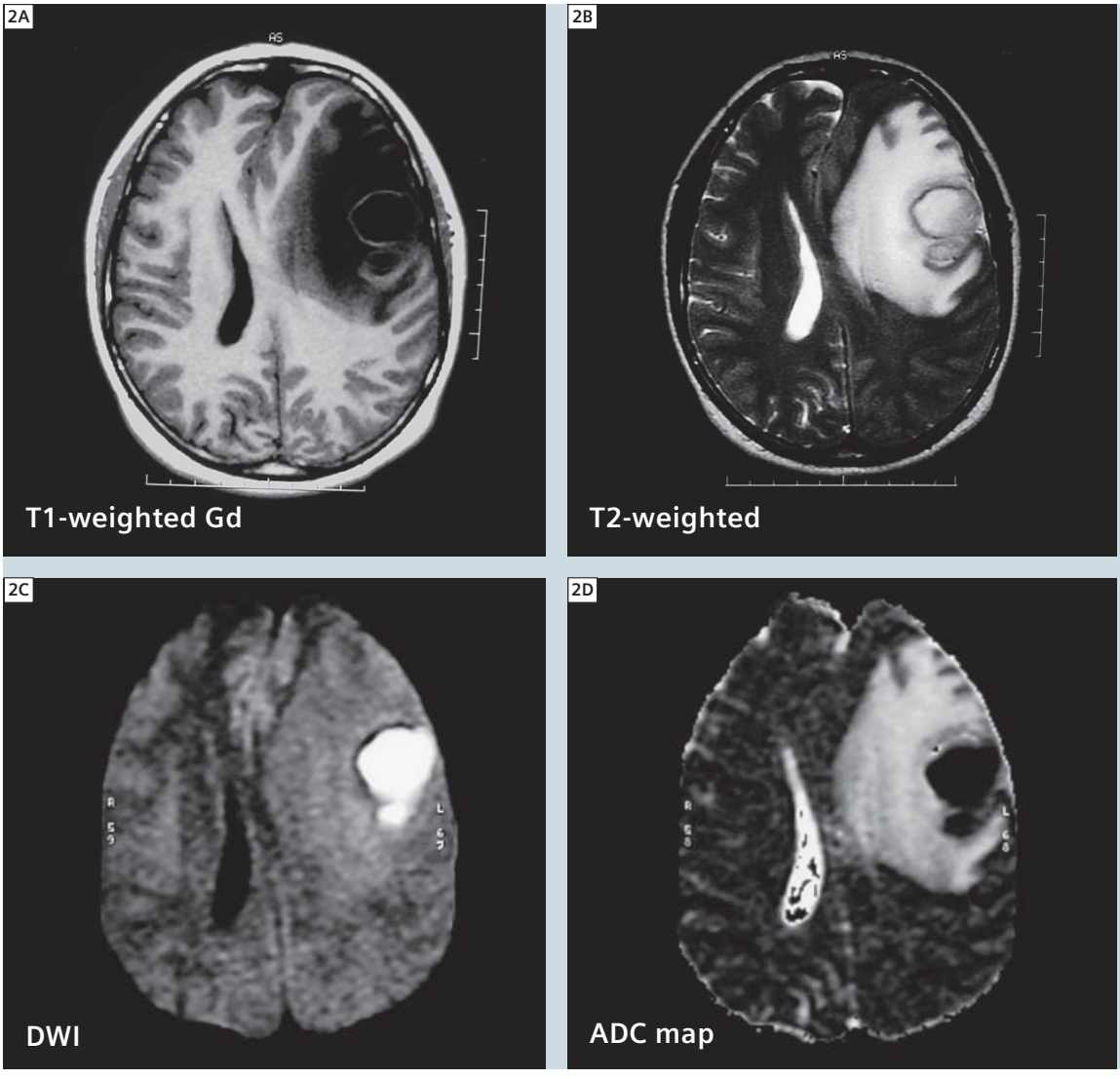

2 A bilobulated ring enhancing necrotic lesion, surrounded by vasogenic edema, demonstrating restricted diffusion within the lesion. **Diagnosis:** Abscess

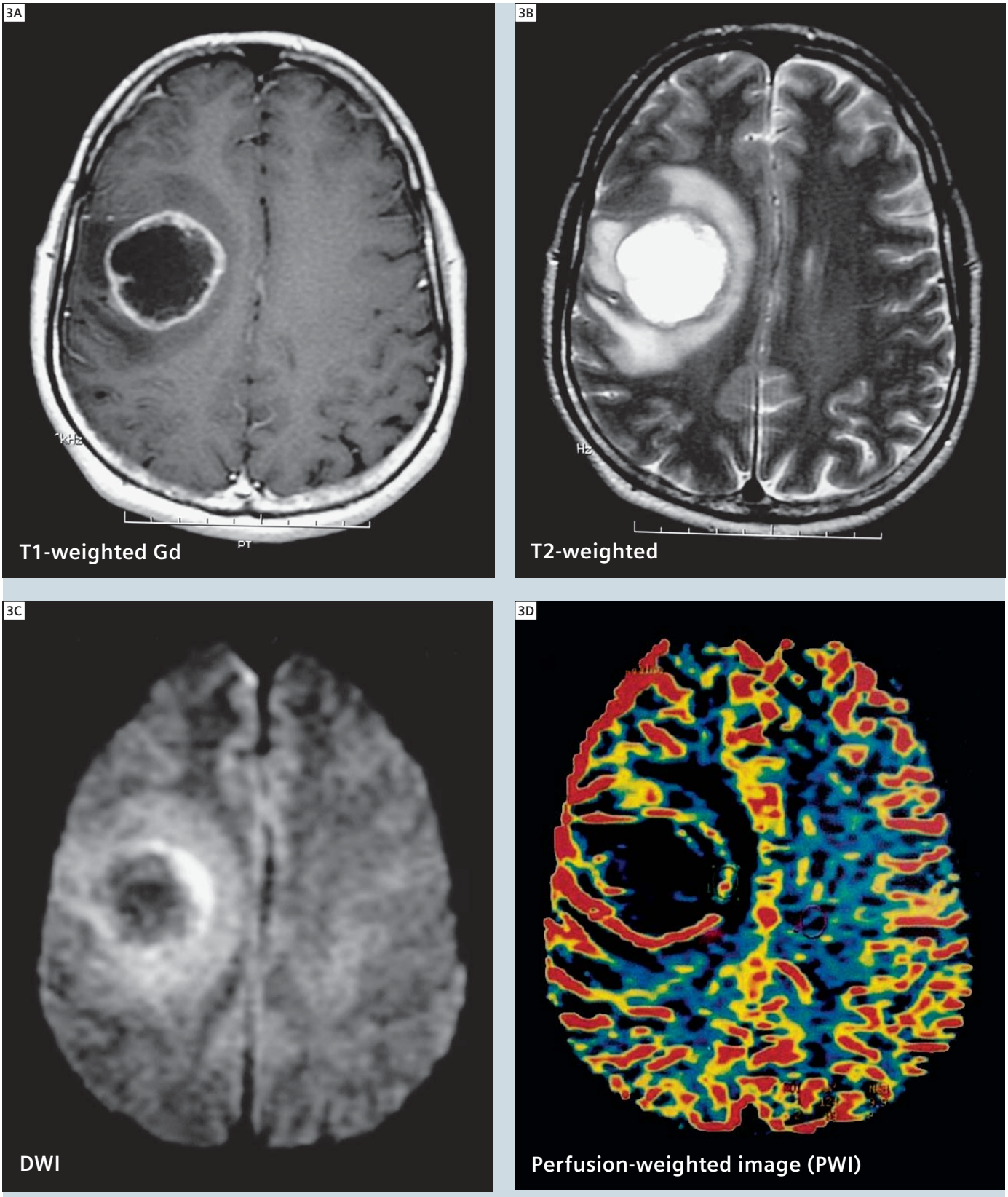

3 An expansive ring enhancing cystic/necrotic lesion, surrounded by vasogenic edema/infiltrative lesion, demonstrating restricted diffusion and high perfusion in its borders and unrestricted diffusion within the lesion.
Diagnosis: Glioblastoma Multiforme (GBM)

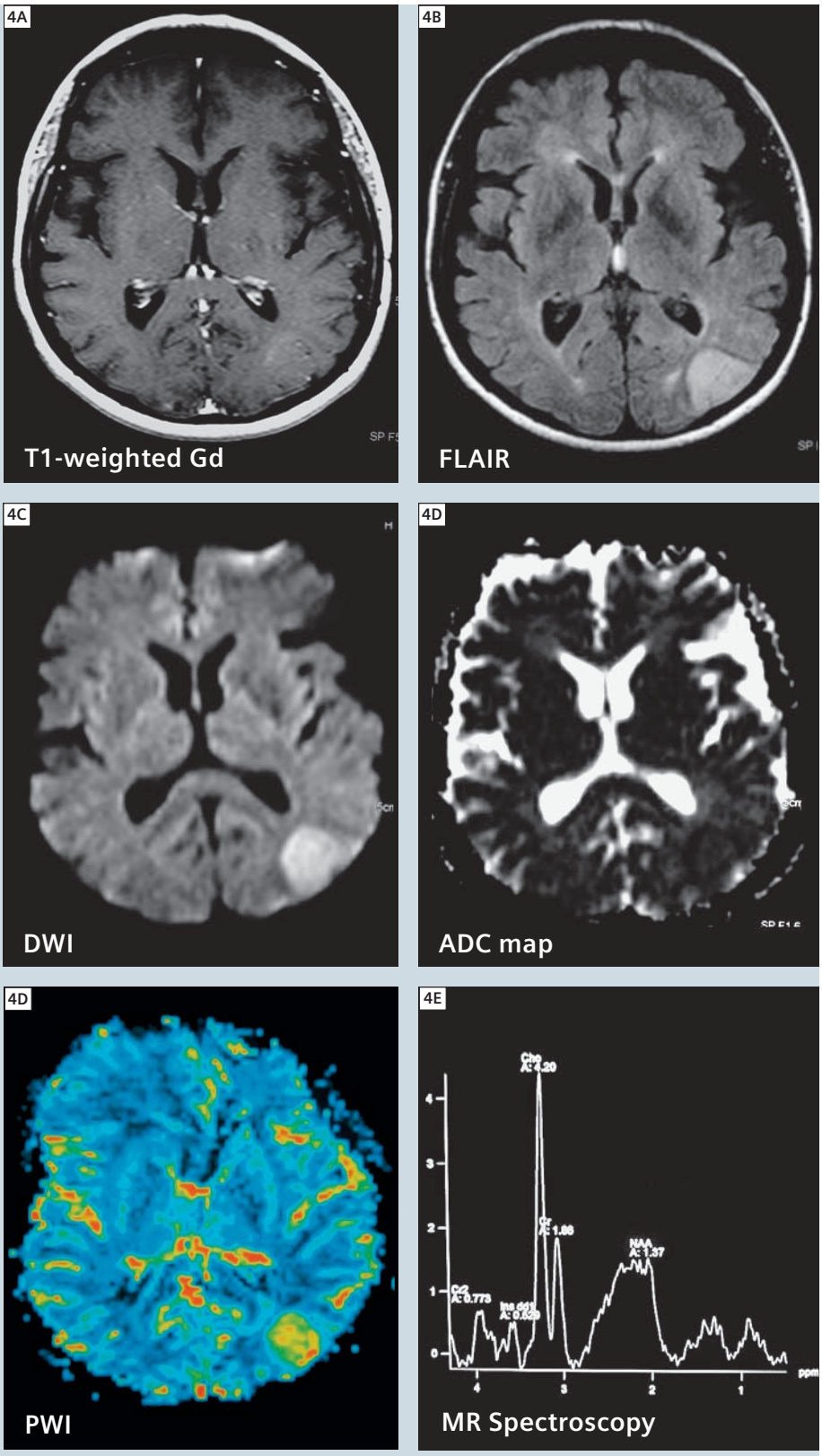

4 A non-enhancing cortical lesion, with high perfusion and restricted diffusion. MR-spectroscopy demonstrates a very high choline peak and low NAA.
Diagnosis: Anaplastic astrocytoma

strates high diffusibility, due to its rich vascular spaces.

Diffusion-Tensor MR image

The movement of water occurs in all three directions, and is assumed to behave in a manner physicists can describe using a Gaussian approximation. When water molecules diffuse equally in all directions, this is termed isotropic diffusion. In the white matter, however, free water molecules diffuse anisotropically, that is to say the water diffusion is not equal in all three orthogonal directions. The fractional anisotropy (FA) measures the fraction of the total magnitude of diffusion anisotropy. In addition to assessment of the diffusion in a single voxel, DTI has been used to attempt to map the white matter fiber tracts. A color-coded map of fiber orientation can also be determined by DTI. A different color has been attributed to represent a different fiber orientation along the three orthogonal spatial axes.

The precise determination of the margins of the tumor is of the utmost importance to the management of brain tumors. The goal of a surgical approach to the brain neoplasm is the complete resection of the tumor, coupled with minimum neurological deficit.

Since it is generally accepted that conventional MR imaging underestimates the real extent of the brain tumor, given its ability to verify neoplastic cells that infiltrate peritumoral areas of abnormal T2-weighted signal intensity, many practitioners are uncomfortable using only conventional MRI approaches. While this remains to be proven, it does appear from straightforward inspection that DTI is able to illustrate the relationship of a tumor with the nearby main fiber tracts. Because of this, many have begun to suggest that DTI might be used to aid in surgical planning and possibly aid radiotherapy planning, as well as to monitor the tumor recurrence and the response to the treatment.

Based on these findings, DTI seems to be of great value in the detection of FA values, variation in pure vasogenic edema and the combination of vasogenic edema

Continued on page 28

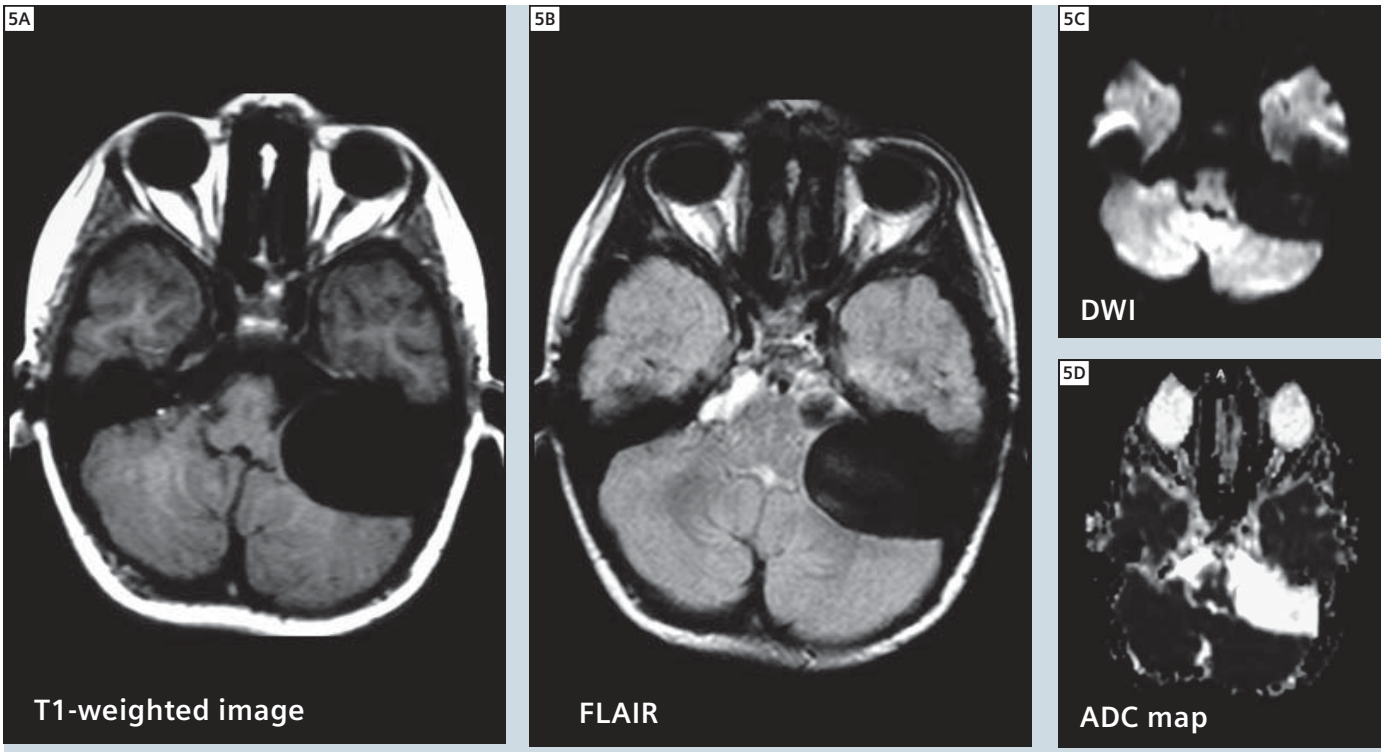

5 An expansive lesion in the left aspect of the posterior fossa, demonstrating similar signal intensity to CSF and high diffusibility.
Diagnosis: Arachnoid cyst

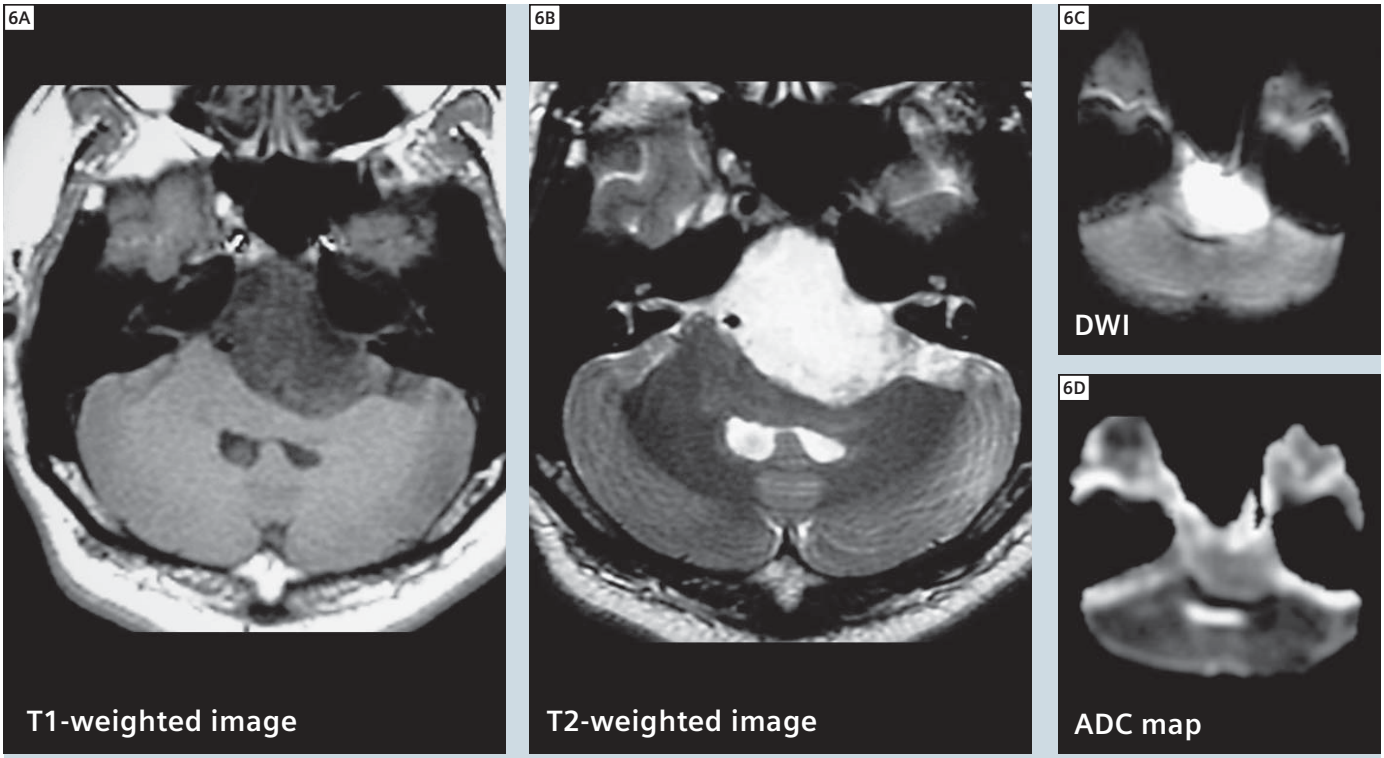

6 An expansive lesion in the left aspect of the posterior fossa, demonstrating similar signal intensity to CSF and high signal intensity on diffusion-weighted imaging (DWI). **Diagnosis:** Epidermoid

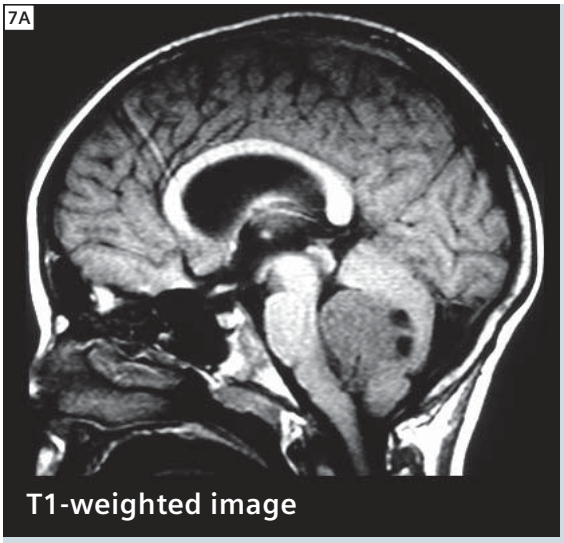

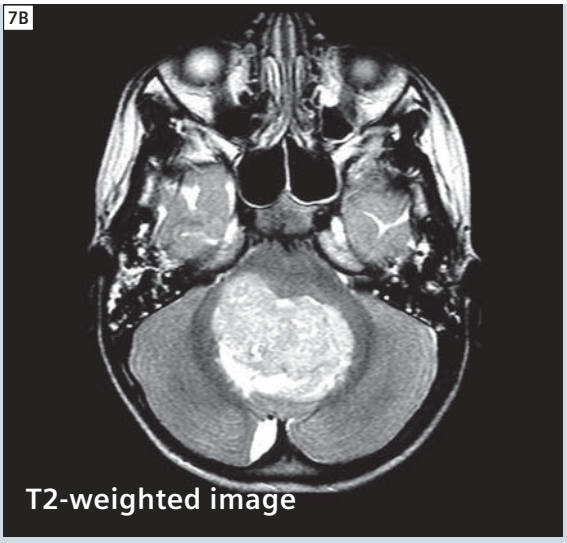

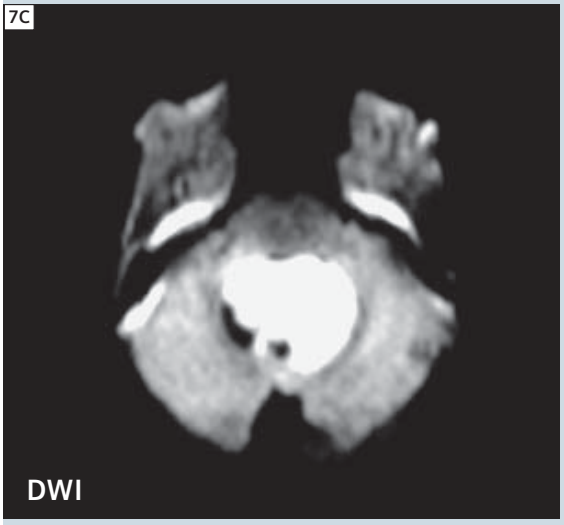

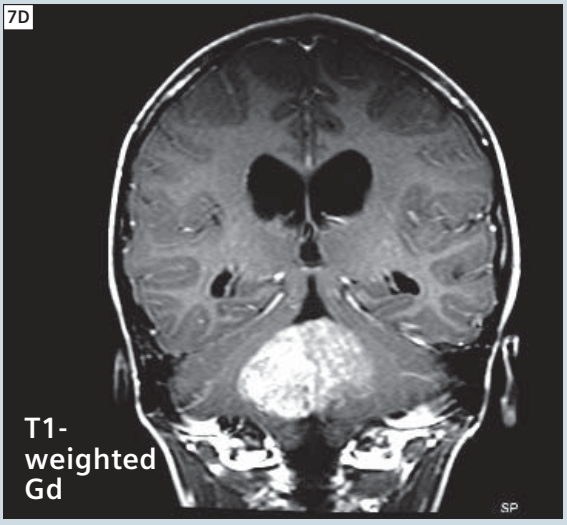

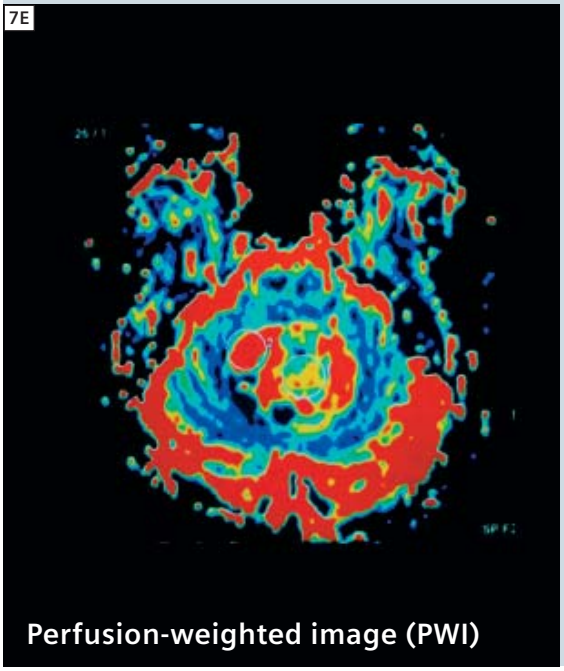

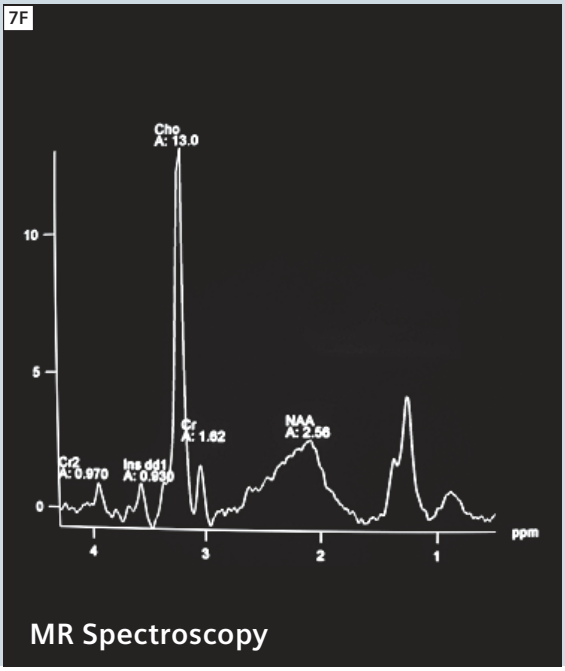

7 An expansive intraventricular enhancing lesion in the fourth ventricle, demonstrating restricted diffusion, hyperperfusion and a very high Choline peak, low NAA and lipids/lactate peak.
Diagnosis: Medulloblastoma

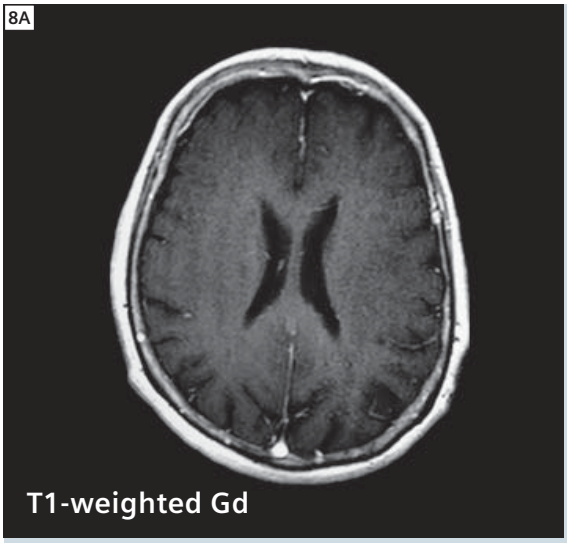

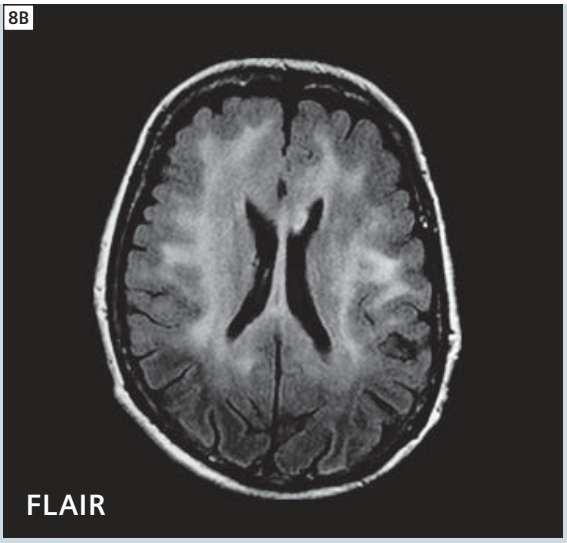

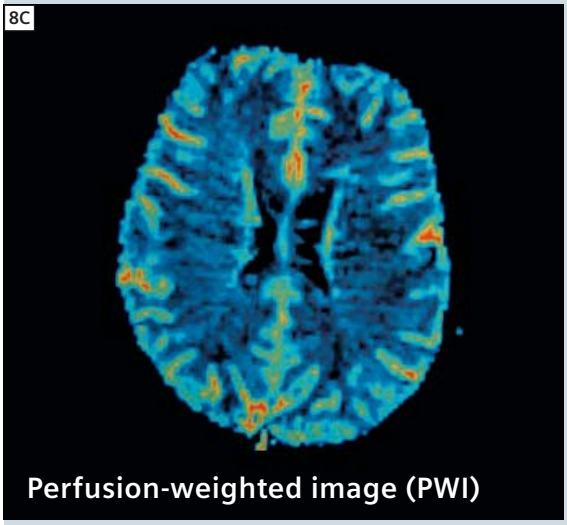

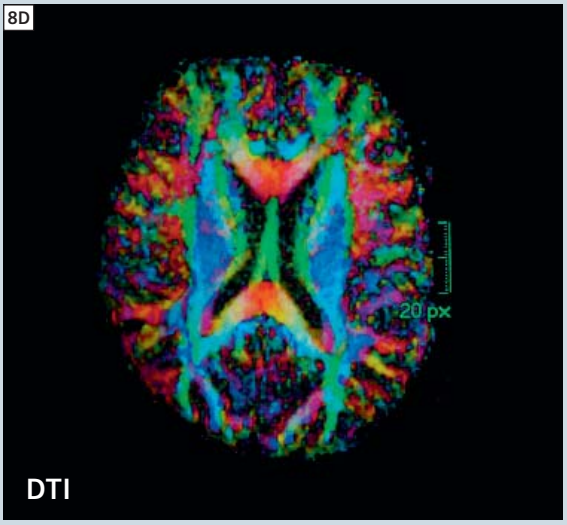

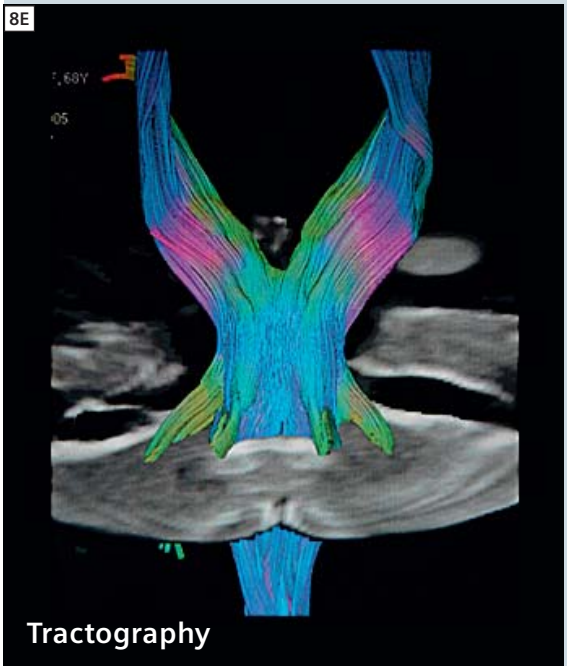

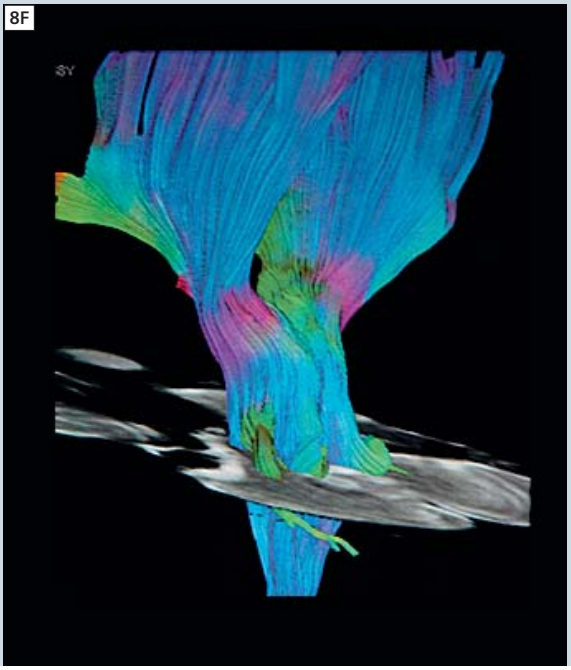

8 An infiltrative, non-enhancing white matter lesion, without hyperperfusion. Diffusion Tensor Imaging (DTI) demonstrates a reduction in FA values, preserving the direction of the main fiber tracts. **Diagnosis:** Gliomatosis cerebri

and extracellular matrix destruction. In conclusion, DTI may be able to distinguish high-grade gliomas from low-grade gliomas and metastatic lesions.

Pre-surgical planning

DTI appears to be the only non-invasive method of obtaining information about the fiber tracts and is able to suggest them three-dimensionally, though the validity of these suggestions remains to be carefully studied. Frequently, the involvement of the white matter tracts can be clearly identified in brain tumor patients by using both anisotropic maps (FA maps are the most widely used) and tractography. Based on DTI findings, resulting from studies of brain tumor patients, the white matter involvement by a tumor can be arranged into five different categories:

- Displaced: maintained normal anisotropy relative to the contralateral tract in the corresponding location, but situated in an abnormal T2-weighted signal intensity area or presented an abnormal orientation.
- Invaded: slightly reduced anisotropy without displacement of white matter architecture, remaining identifiable on orientation maps.
- Infiltrated: reduced anisotropy but remaining identifiable on orientation maps.
- Disrupted: marked reduced anisotropy and unidentifiable on oriented maps.
- Edematous: maintained normal anisotropy and normally oriented but located in an abnormal T2-weighted signal intensity area.

In short, DTI is gaining enthusiasm as a pre-operative MRI method of evaluating brain tumors closely related to eloquent regions. DTI appears to be particularly advantageous for certain types of surgical planning, optimizing the surgical evaluation of brain tumors near white matter tracts. Formal studies that demonstrate that DTI can successfully prevent post-operative complications have yet to be carried out but preliminary data appear promising.

Intracranial neoplasms may involve both the functional cortex and the corresponding white matter tracts. The preoperative identification of eloquent areas through noninvasive methods, such as blood-oxygen-level-dependent (BOLD) functional MR imaging (fMRI) and DTI tractography, offers some advantages.

Increasingly, investigators are beginning to combine fMRI with DTI: this might allow us to precisely map an entire functional circuit. Even though fMRI locates eloquent cortical areas, the determination of the course and integrity of the fiber tracts remains essential to the surgical planning.

Limitations

While initial reports suggest advantages of DWI and DTI in the evaluation of patients with brain tumors, these reports are largely single-center, uncontrolled, preliminary findings. Therefore these results must be cautiously interpreted. Furthermore, there remain substantial technical hurdles, even though the rapid evolution of MRI systems is making ever more powerful approaches possible. Such improvements are particularly welcome given the limited signal-to-noise ratio of diffusion overall. Nevertheless, these initial data are promising.

Summary

Diffusion imaging appears to have the potential to add important information to pre-surgical planning. While experience is limited, DTI appears to provide useful local information about the structures near the tumor, and this appears to be useful in planning. In the future, DTI may provide an improved way to monitor intraoperative surgical procedures as well as their complications. Furthermore, the evaluation of the response of treatment to chemotherapy and to radiation therapy might also be possible. While diffusion imaging has some limitations, its active investigation and further study are clearly warranted.

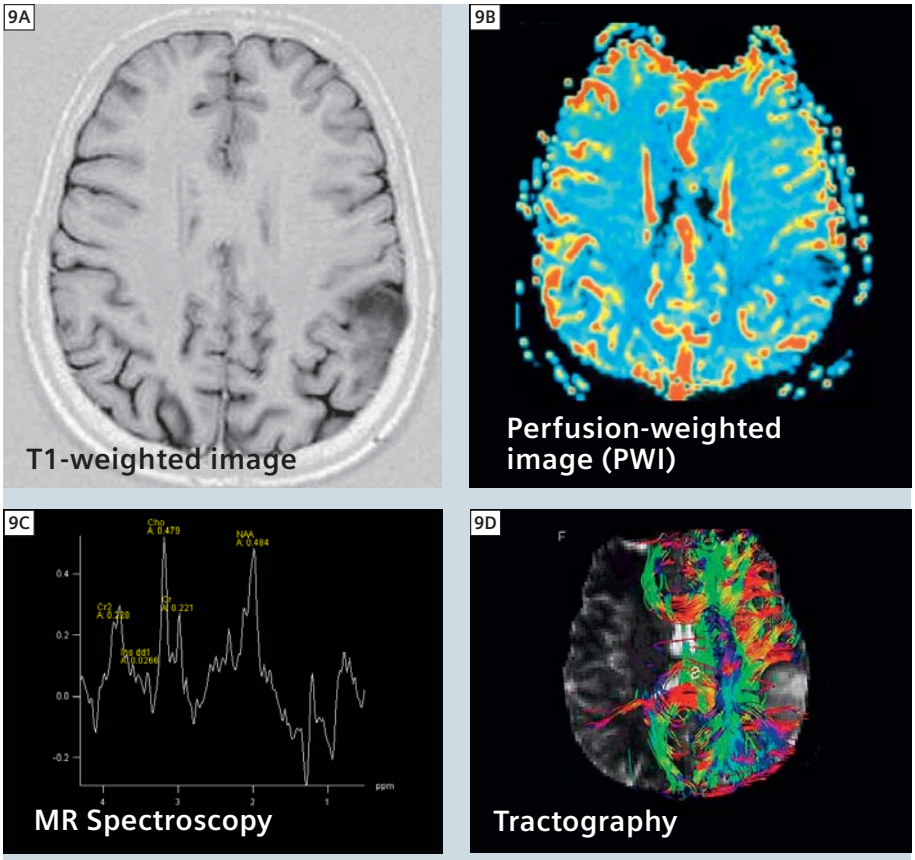

9 An expansive cortical lesion, with hypoperfusion. MR-spectroscopy demonstrates a high Choline peak and low NAA. The lesion seems to dislocate the main adjacent fiber tracts.
Diagnosis: Low grade Glioma

References

1 Berens ME, Rutka JT, Rosenblum ML. Brain tumor epidemiology, growth, and invasion. Neurosurg Clin North Am 1990; 1:1–18.

2 Jemal A, Thomas A, Murray T, et al. Cancer statistics2002.CA2002;52(1):23–47.

3 Felix R, Schorner W, Laniado M, et al. Brain tumors: MR imaging with gadolin-DPTA. Radiology 1985; 156:681–688.

4 Knopp EA, Cha S, Johnson G, et al. Glial Neoplams: Dynamic Contrast-enhanced T2*-weighted MR imaging. Radiology 1999; 211:791–798.

5 Brunberg JA, Chenevert TL, McKeever PE, Ross DA, Junck LR, Muraszko KM, et al. In vivo MR determination of water diffusion coefficients and diffusion anisotropy: Correlation with structural alteration in gliomas of the cerebral hemispheres. AJNR Am J Neuroradiol 1995;16:361–371.

6 Mori S, Frederiksen K, Van Zijl PCM, Stieltjes B, Kraut MA,Slaiyappan M, et al. Brain White Matter Anatomy of Tumor Patients Evaluated With Diffusion Tensor Imaging. Ann Neurol 2002; 51:377–380.

7 Price SJ, Burnet NG, Donovan T, Green HAL, Pena A, Antoun NM , et al . Diffusion Tensor Imaging of Brain Tumors at 3T: A potential tool for assessing white matter tract invasion. Clinical Radiology 2003; 58:455–462.

8 Schulder M, Maldjian JA, Liu WC, Holodny AI, Kalnin AT, Mun IK, et al. Functional image-guided surgery of intracranial tumors located in or near the sensorimotor cortex. J Neurosurg 1998; 89:412–418.

9 Holodny AI, Ollenschlager M. Diffusion imaging in brain tumor. Neuroimaging Clin N Am 2002; 12:107–124.

10 Barboriak DP. Imaging of brain tumors with diffusion-weighted and diffusion tensor MR imaging. Magn Reson Imaging Clin N Am 2003;11:379–401.

11 Tsuruda JS, Chew WM, Moseley ME, Norman D. Diffusion-weighted MR imaging of the brain : value of differentiating between extra-axial cysts and epidermoid tumors. Am J Neuroradiol 1990; 155:1049–1065.

12 Chen S, Ikawa F, Kurisu K, Arita K, Takaba J, Kanou Y. Quantitative MR evaluation of intracranial epidermoid tumors by fast fluid-attenuated inversion recovery imaging and echo-planar diffusion-weighted imaging. Am J Neuroradiol 2001; 22(6):1089–1096.

13 Laing AD, Mitchell PJ, Wallace D. Diffusion-weighted magnetic resonance imaging of intracranial epidermoid tumors . Aust Radiol 1999; 43:16–19.

14 Guo AC, Provenzale JM, Cruz Jr LCH, Petrella JR. Cerebral abscesses: investigation using apparent diffusion coefficient maps. Neuroradiology 2001;43:370–374, 2001.

15 Chang SC, Lai PH, Chen WL,Weng HH, Ho JT, Wang JS. Diffusion-weighted MRI features of brain abscess and cystic or necrotic brain tumors: comparison with conventional MRI. Clin Imaging 2002; 26(4):227–236.

16 Tien RD, Feldesberg GJ, Friedman H, Brown M, MacFall J. MR imaging of high-grade cerebral gliomas: Value of diffusion-weighted echo-planar pulse sequence. AJR Am J Roentgenol 1994;162:671–677.

17 Krabbe K, Gideon P, Wang P, Hansen U, Thomsen C, Madsen F. MR diffusion imaging of human intracranial tumours. Neuroradiology 1997; 39:483–489.

18 Le Bihan D, Douek P, Argyropoulou M, Turner R, Patronas N, Fulham M . Diffusion and perfusion magnetic resonance imaging in brain tumors. Top Mang Reson Imaging 1993; 5:25–31.

19 Tsuruda JS, Chew WM, Moseley ME, Norman D. Diffusion-Weighted MR imaging of extraaxial tumors. Magn Reson Med 1991; 19:316–320.

20 Cruz, Jr LCH; Sorensen AG. Diffusion tensor magnetic resonance imaging of brain tumors. Neurosurg Clin N Am 16(2005)115–134.

21 Cruz, Jr LCH; Sorensen AG. Diffusion tensor magnetic resonance imaging of brain tumors. Magn Reson Clin N Am 2006 May 14(2);183–202.

22 Stadnik TW, Chaskis C, Michotte A, Shabana WM, van Rompaey K, Luypaert R, et al. Diffusion-weighted MR imaging of intrcerebral masses: Comparison with conventional MR imaging and histologic findings. AJNR Am J Neuroradiol 2001; 22:969–976.

23 Guo AC, Cummings TJ, Dash RC, Provenzale JM. Lymphomas and high-grade astrocytomas: comparison of water diffusibility and histologic characteristics. Radiology 2002; 224(1):177–183.

24 Kono K, Inoue Y, Nakayama K, Shakudo M, Morino M, Ohata K, et al. The Role of Diffusion-Weighted Imaging in Patients with Brain Tumors. AJNR Am J Neuroradiol 2001; 22:1081–1088.

25 Koetsenas AL, Roth TC, Manness WK, Faeber EN. Abnormal diffusion-weighted MRI in medulloblastoma: Does it reflect small cell histology? Pediatric Radiol 1999;29:524–526.

26. Quadrery FA, Okamoto K. Diffusion-weighted MRI of haemangioblastomas and other cerebellar tumours. Neuroradiology 2003;45(4): 212–219.

27 Goebell E, Paustenbach S, Vaeterlein O, Ding X, Heese O, Fiehler J, Kucinski T, Hagel C, Westphal M, Zeumer H. Radiology 2006;239:217–222. Low-Grade and Anaplastic Gliomas: Differences in Architecture Evaluated with Diffusion-Tensor MR Imaging.

28 Inoue T, Ogasawara K, Beppu T, Ogawa A, Kabasawa H. Diffusion tensor imaging for preoperative evaluation of tumor grade in gliomas. Clin Neurol Neurosurg 2005;107:174–180.

29 Jellinson BJ, Field AS, Medow J, et al. Diffusion Tensor Imaging of Cerebral White Matter: A Pictorial Review of Physics, Fiber Tract Anatomy, and Tumor Imaging Patterns. AJNR Am J Neuroradiol 2004; 23:356–369.

30 Sha S, Bastin ME, Whittle IR, Wardlaw JM. Diffusion Tensor MR Imaging of High-grade cerebral gliomas. AJNR Am J Neuroradiol 2002; 23:520–527.

31 Witwer BP, Moftakhar R, Hasan KM, Deshmukh P, Haughton V, Field A, et al. Diffusion-tensor imaging of white matter tracts in patients with cerebral neoplasm. J Neurosurg 2002; 97:568–575.

32 Weishmann UC, Symms MR, Parker GJM, Clark CA, Lemieux L, Barker GJ, et al. Diffusion tensor imaging demonstrates deviation of fibers in normal appearing white matter adjacent to a brain tumour. J Neurol Neurosurg Psychiatry 2000; 68:501–503.

33 Holodny AI, Schwartz TH, Ollenschleger M, Liu WC, Schulder M. Tumor involvement of the corticospinal tract: diffusion magnetic resonance tractography with intraoperative correlation. J Neurosurg 2001; 95(6): 1082.

34 Holodny AI, Ollenschleger M, Liu WC, Schulder M, Kalnin AJ. Identification of the corticospinal tracts achieved using blood-oxygen-level-dependent and diffusion functional MR imaging in patients with brain tumors.

35 Krings T, Reiges MH, Thiex R, Gilsbach JM, Thron A. Functional and diffusion-weighted magnetic resonance images of space-occupying lesions affecting the motor system: imaging the motor cortex and pyramidal tracts. J Neurosurg 2001; 95(5):816–824.

36 Guye M, Parker GJM, Symms M, Boulby P, Wheeler-Kingshott CAM, Salek-Haddadi A, et al. Combined functional MRI and tractography to demonstrate the connectivity of the human primary motor cortex in vivo. Neuroimage 2003; 19:1349–1360.

Contact
L. Celso Hygino da Cruz Jr.
CDPI e Multi-Imagem
Ressonância Magnética
Rio de Janeiro, Brazil
celsohygino@hotmail.com

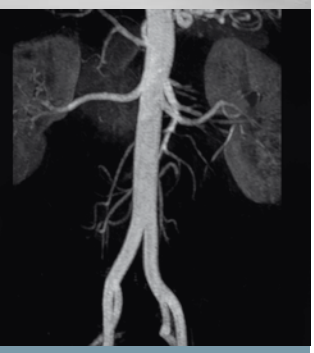

What if one size fits them all?

MAGNETOM Espree – the first open bore MRI for any patient.

With the shortest 1.5T magnet in the industry and its 70 cm inner diameter, MAGNETOM® Espree provides 1.5T high-field power with the highest level of patient comfort. Powered by Tim® (Total imaging matrix) technology, MAGNETOM Espree provides a new level of flexibility, accuracy, and speed. The combination of ultimate patient comfort and superb image quality will attract new referrals and will maximize your patient throughput.
www.siemens.com/healthcare +49 69 797 6420

Answers for life.

SIEMENS

MR-Z1097-1-7600

Clinical Neurological Imaging on an Open Bore MRI System (MAGNETOM Espree)

Robert M. Cargile, M.D.[1]; Agus Priatna, Ph.D.[2]; Stefan Huwer[3]; Tammie L.S. Benzinger, M.D., Ph.D.[1]

[1]Mallinckrodt Institute of Radiology, Washington University School of Medicine, St. Louis, MO, USA
[2]R&D Collaborations, Siemens Medical Solutions, St. Louis, MO, USA
[3]Siemens Healthcare, MR PLM AW Advanced Neuro, Erlangen, Germany

Introduction

An open bore MRI has the practical advantage of accommodating large or claustrophobic patients. Unfortunately, until the advent of the 1.5T MAGNETOM Espree, "open" was often synonymous with inferior image quality. However, in addition to the large 70 centimeter bore, the Espree system offers advanced coil combinations using the Total imaging matrix (Tim) and isocenter imaging technology. Together, these features allow for performance of advanced neuroimaging protocols in new clinical populations.
This article demonstrates neuroimaging applications routinely obtained in our clinical practice at Mallinckrodt Institute of Radiology, Washington University School of Medicine in St. Louis. The open bore Espree delivers excellent image quality, expanding the utility of MRI to meet diagnostic challenges increasingly encountered in clinical neuroimaging.

Methods

Image acquisitions were performed with a 1.5 Tesla MAGNETOM Espree scanner using the 12-channel head coil and spine coils of the Total imaging matrix. Our standard neurological examination on the Espree system includes common cross-platform protocols such as MPRAGE, FLAIR, T2 TSE, DSC Perfusion, and Spectroscopy. The Espree also enables advanced imaging sequences, including T2 BLADE [1], Susceptibility-Weighted Imaging (SWI) [2], and Diffusion Tensor Imaging (DTI) [3], for which we use the following protocols:

T2 BLADE protocol: TE = 102 msec, TR = 4000 msec, FOV = 240 mm, pFOV = 100%, slice thickness = 5 mm, base resolution = 384 (results in spatial resolution = 0.6 x 0.6 x 5.0 mm), average = 1, concatenations = 2, flip angle = 150°, BLADE coverage = 111%, echo spacing = 6.64 msec, turbo factor = 35, echo train per slice = 20, motion correction = ON, bandwidth = 362 Hx/pixel, acquisition time: 2:50 min.

SWI protocol: TE = 40 msec, TR = 50 msec, FOV = 240, pFOV = 100%, slice thickness = 2 mm, slices per slab = 72, base resolution = 256, phase resolution = 79%, slice resolution = 75% (results in spatial resolution = 1.2 x 0.9 x 2.0 mm), average = 1, flip angle = 15, PAT acceleration factor = 2, bandwidth = 80 Hz/pixel, spatial resolution = 1.2 x 0.9 x 2.0 mm, acquisition time 3:34 min.

DTI protocol: TE = 107 msec, TR = 3500 msec, FOV = 240 mm, pFOV = 100%, slice thickness = 5 mm, base resolution = 128, phase resolution = 100% (results in spatial resolution = 1.9 x 1.9 x 5 mm), averages = 3, Fatsat, phase partial Fourier = 6/8, PAT acceleration factor = 2, echo spacing = 0.92 msec, EPI factor = 128, BW = 1220 Hz/pixel, b-values = 0, 1000 sec/mm2, 12 diffusion directions. Average ADC map, trace-weighted map, FA map, and tensor data were created Inline. Acquisition time: 2:08 min.

Post-processing was performed with the Neuro 3D application package. The package has the capability of processing directional color encoded fractional anisotropy map (blue = SI direction, green = AP direction, and red = RL direction), tensor map, aligned tensor and anatomy data, aligned tensor and fractional anisotropy data, and tractography.

Clinical cases

The following examples demonstrate brain stem pathology which is difficult to image on a non-Tim system due to the position of the lesion and unavailability of coil combination. For brainstem cases examined on the MAGNETOM Espree system, the head coil and cervical spine elements were combined using the Total imaging matrix to better visualize the lesions. Tumor cases are also routinely examined on the Espree system. An example is also included in this article.

→ **Visit www.siemens.com/magnetom-world** to read T. Benzinger's "Clinical Applications of Diffusion Tensor Imaging" published in MAGNETOM Flash 37, p. 74–86.

Patient 1

77-year-old man undergoing evaluation for stroke had a normal MRI (Fig. 1). The study exhibits tracts of the normal brain acquired with the 1.5T Espree system. DTI tractography processed with the Neuro 3D software resolves ponto-cerebellar fibers and the pyramidal decussation with great corresponding anatomic detail [4]. The DTI dataset is acquired in less than 3 minutes, and replaces the standard 3 direction DWI data for clinical stroke imaging on this scanner.

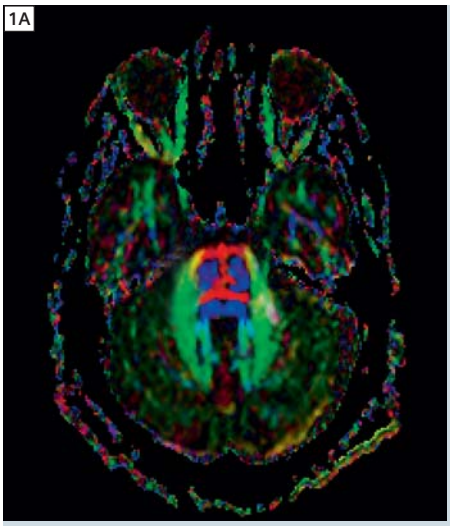

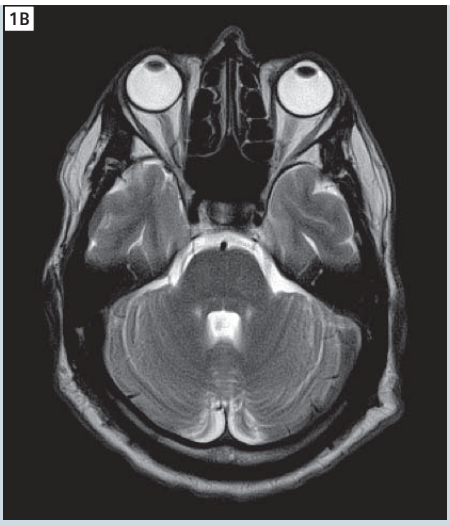

1 Normal brain MRI acquired on an open bore 1.5T MAGNETOM Espree using 12-channel head coil and spine coils of the Total imaging matrix:
A: Color fractional anisotropy of the normal pontine white matter.
B: Axial T2 BLADE demonstrates the corresponding pontine anatomy.
C: Normal DTI tractography showing the red pontine fiber shown in A (white arrow) and pyramidal decussation (red arrow). These images were generated from a 2 minute scan.

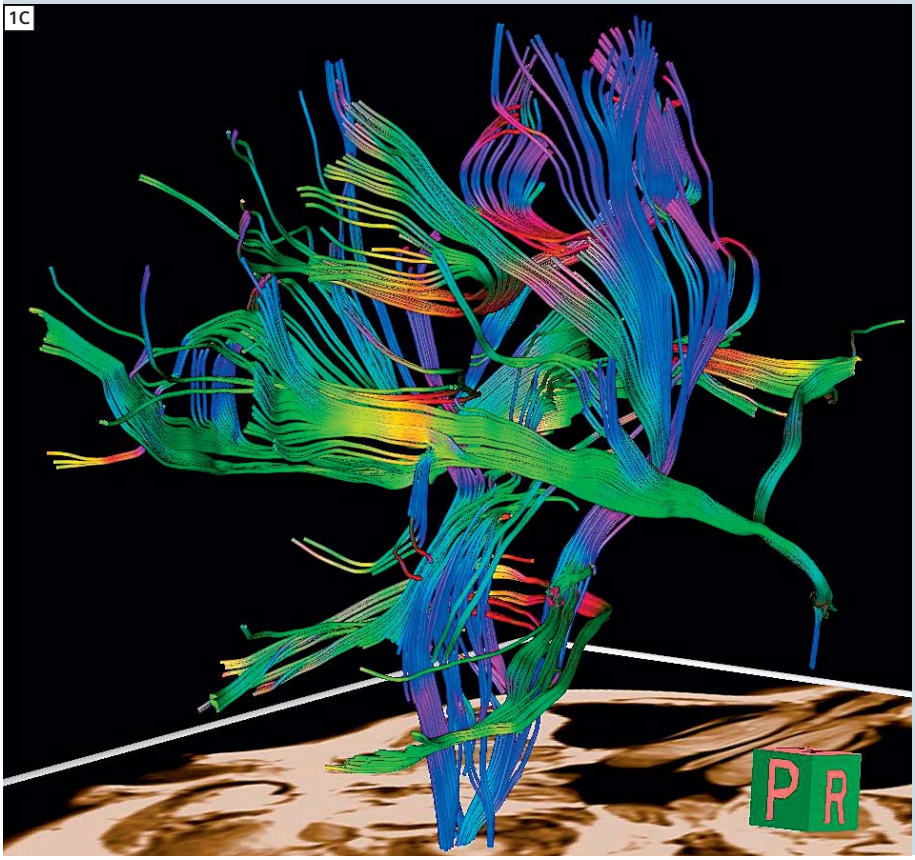

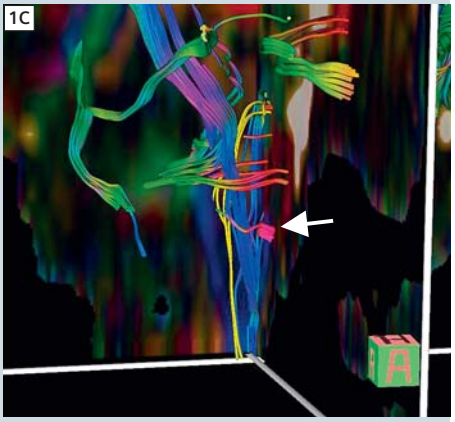

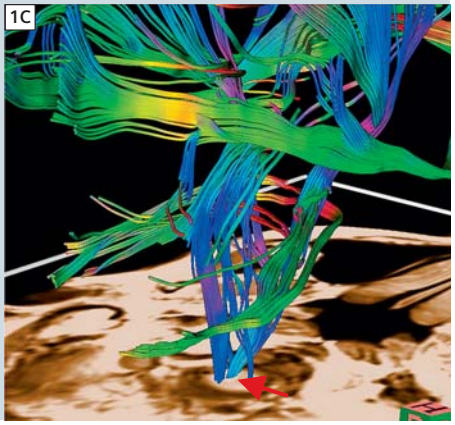

Patient 2

This 39-year-old obese woman presented for evaluation of dysphagia and left upper and lower extremity paresthesias. The brain MRI demonstrates a non-enhancing T2 hyperintense brainstem mass extending from the medulla into the cervical cord. Spectroscopy reveals a decreased NAA to choline signal ratio within this lesion. There is no diffusion restriction or T2* abnormality, but diffusion tractography is useful in demonstrating the spatial distortion by the expansile mass without infiltration of the longitudinal brainstem white matter tracts (Fig. 2).

Continued on page 34

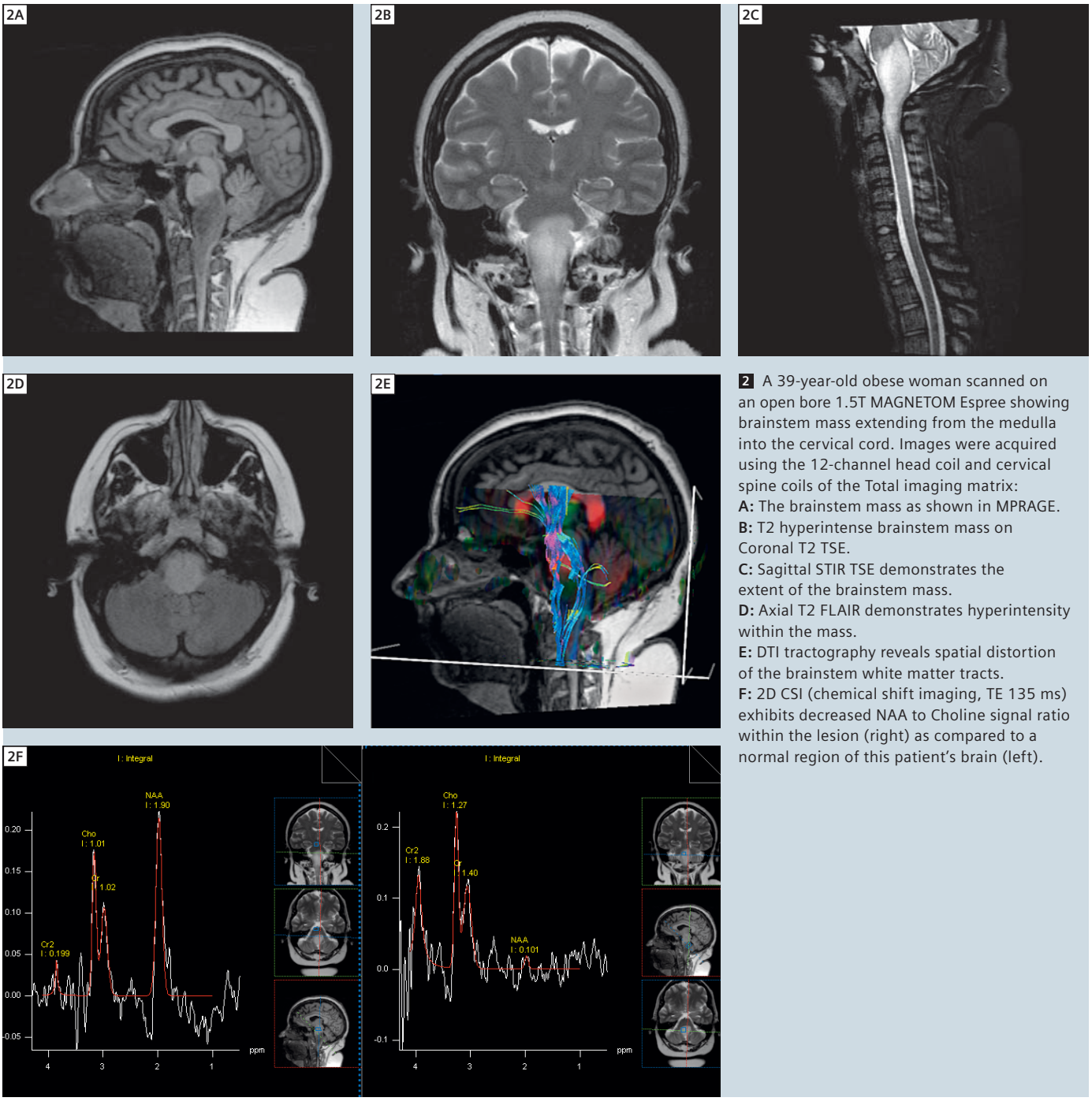

2 A 39-year-old obese woman scanned on an open bore 1.5T MAGNETOM Espree showing brainstem mass extending from the medulla into the cervical cord. Images were acquired using the 12-channel head coil and cervical spine coils of the Total imaging matrix:
A: The brainstem mass as shown in MPRAGE.
B: T2 hyperintense brainstem mass on Coronal T2 TSE.
C: Sagittal STIR TSE demonstrates the extent of the brainstem mass.
D: Axial T2 FLAIR demonstrates hyperintensity within the mass.
E: DTI tractography reveals spatial distortion of the brainstem white matter tracts.
F: 2D CSI (chemical shift imaging, TE 135 ms) exhibits decreased NAA to Choline signal ratio within the lesion (right) as compared to a normal region of this patient's brain (left).

Following radiotherapy and four cycles of Temodar, the MRI study is repeated on the same equipment. There is no interval change (Fig. 3).

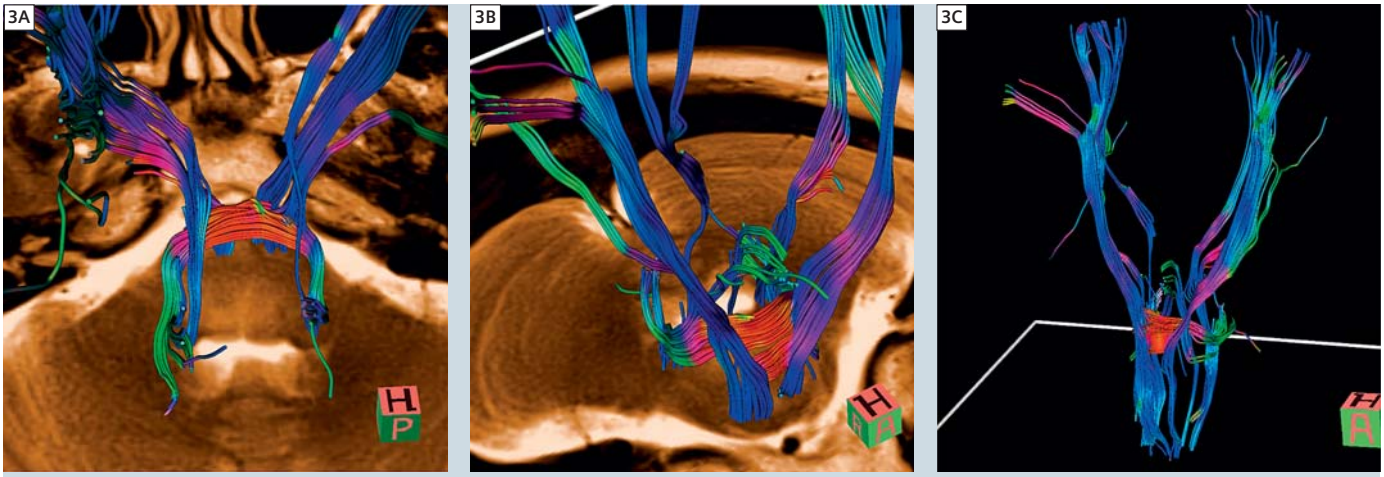

3 An MRI study was repeated on the same patient as Figure 2 on the 1.5T MAGNETOM Espree following radiotherapy and four cycles of Temodar. DTI tractography nicely demonstrates the radial displacement of major pontine white matter tracts. Pontocerebellar fibers (red) are intact.

Patient 3

This 52-year-old man with a 12 months history of diplopia, dizziness and progressive left facial weakness presented to an outside facility where an MRI revealed a non-enhancing brainstem mass. A more detailed study on the Espree system demonstrates a mass arising in the posterior pons from midbrain to medulla with extension into the left middle cerebellar peduncle. Spectroscopy demonstrates decreased NAA and elevated choline signal within the lesion (Fig. 4).

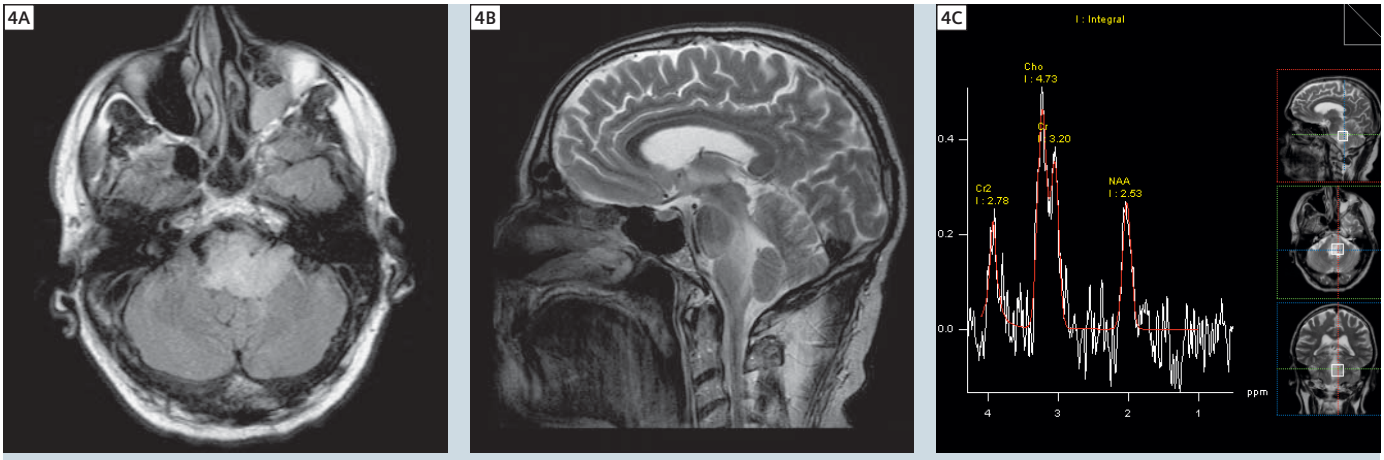

4 A 52-year-old man admitted with diplopia, dizziness and hemifacial weakness was scanned with 1.5T MAGNETOM Espree, revealing a non-enhancing brainstem mass. Images were acquired using the head and cervical spine coils of the Total imaging matrix:
A: Axial T2 FLAIR shows the brainstem mass extending into the left brachium pontis.
B: Sagittal T2 TSE demonstrates T2 hyperintensity of the pontine mass extending from midbrain to medulla.
C: Single voxel spectroscopy reveals decreased NAA and elevated Choline signals within the mass.

Patient 4

This 30-year-old man was evaluated for six weeks of progressive nausea and headache. He was found to have an area of irregular, infiltrative T2 hyperintensity in the pons. T1 TSE sequence post contrast demonstrates regions of mild enhancement. Although the absolute value of choline is not elevated by spectroscopy, the signal ratio of NAA to choline is depressed. These imaging characteristics favor a glial neoplasm, which was confirmed by open biopsy of a spinal drop metastasis (Fig. 5).

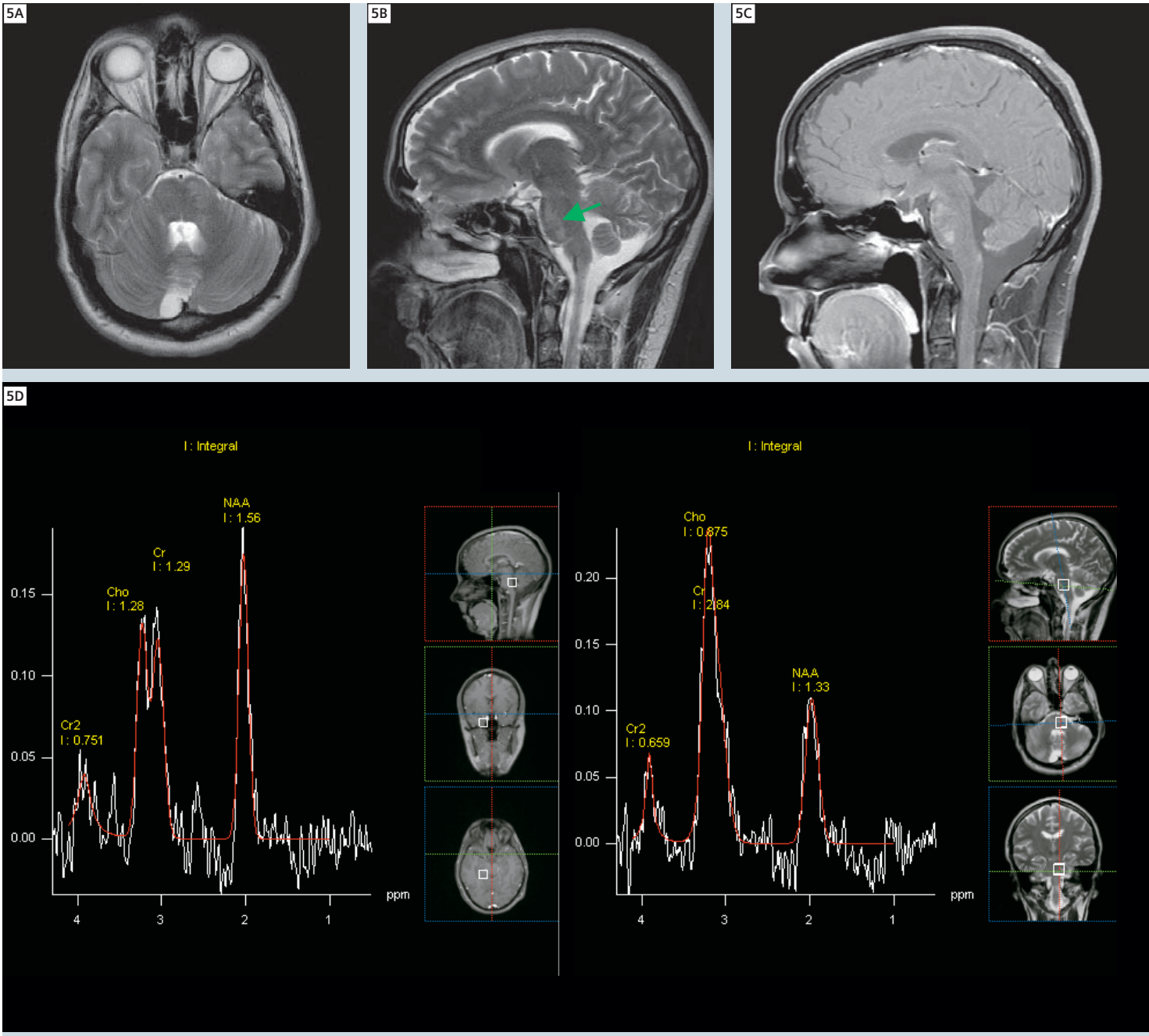

5 A 30-year-old man examined on the 1.5T MAGNETOM Espree with a diagnosis of malignant glial neoplasm of the brainstem. Images were acquired by selecting the head and cervical spine coils of the Total imaging matrix:
A: Axial T2 BLADE and **(B)** Sagittal T2 TSE demonstrate the T2 hyperintensity of the mass.
C: T1 TSE post contrast shows enhancement of the mass.
D: Single voxel spectroscopy reveals the reduced NAA to choline ratio within the lesion (right) as compared to this patient's normal tissue (left).

Patient 5

This 55-year-old man presented with a several week history of right-sided numbness, unsteadiness, and a mild comprehensive and expressive aphasia. Biopsy of a left thalamic glioblastoma multiforme resulted in parenchymal hemorrhage, necessitating open evacuation (Fig. 6). T1 TSE sequence post contrast exhibits avid enhancement at the margins of a centrally necrotic left thalamic mass. The medial portion of the tumor shows increased perfusion. DTI tractography demonstrates anterior deviation of the posterior limb of the left internal capsule (directionally encoded in blue), but the longitudinal fiber tracts remain intact. The transthalamic white matter tracts (yellow for clarity) are displaced radially with abrupt termination. Note inferolateral deviation of the optic radiations [5].

Conclusion

In addition to standard neuroimaging sequences, advanced applications such as spectroscopy, *syngo* BLADE, *syngo* SWI, and *syngo* DTI have produced excellent imaging results on the 1.5T MAGNETOM Espree system at Mallinckrodt Institute of Radiology, Washington University School of Medicine in St. Louis. The Espree scanner enables excellent clinical neurological diagnostics under the most difficult circumstances, including obese and claustrophobic patients as well as difficult imaging anatomy, such as brain stem masses. With the advances of Tim technology, the practicality of an open bore system no longer demands compromises in image quality.

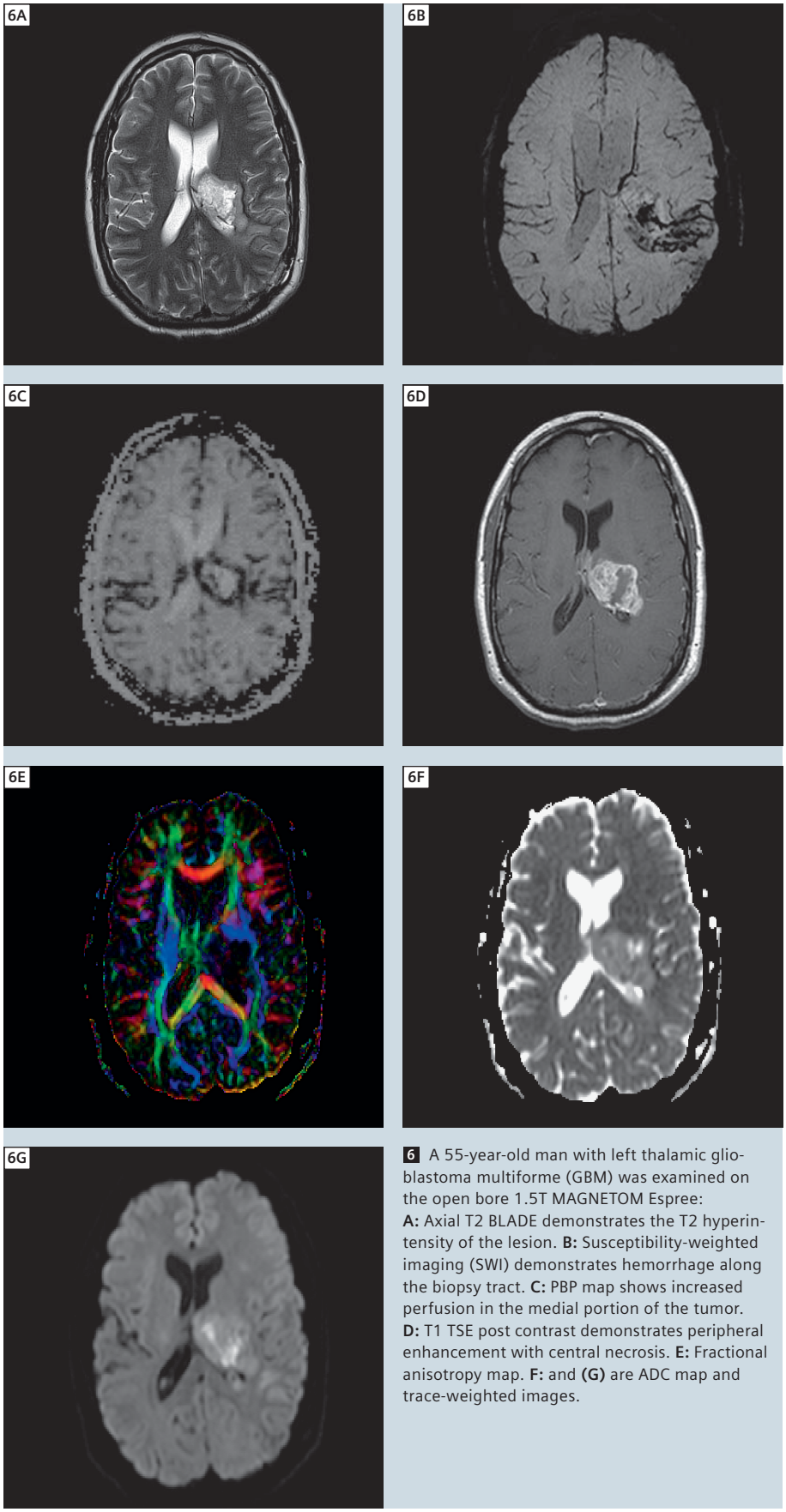

6 A 55-year-old man with left thalamic glioblastoma multiforme (GBM) was examined on the open bore 1.5T MAGNETOM Espree: **A:** Axial T2 BLADE demonstrates the T2 hyperintensity of the lesion. **B:** Susceptibility-weighted imaging (SWI) demonstrates hemorrhage along the biopsy tract. **C:** PBP map shows increased perfusion in the medial portion of the tumor. **D:** T1 TSE post contrast demonstrates peripheral enhancement with central necrosis. **E:** Fractional anisotropy map. **F:** and **(G)** are ADC map and trace-weighted images.

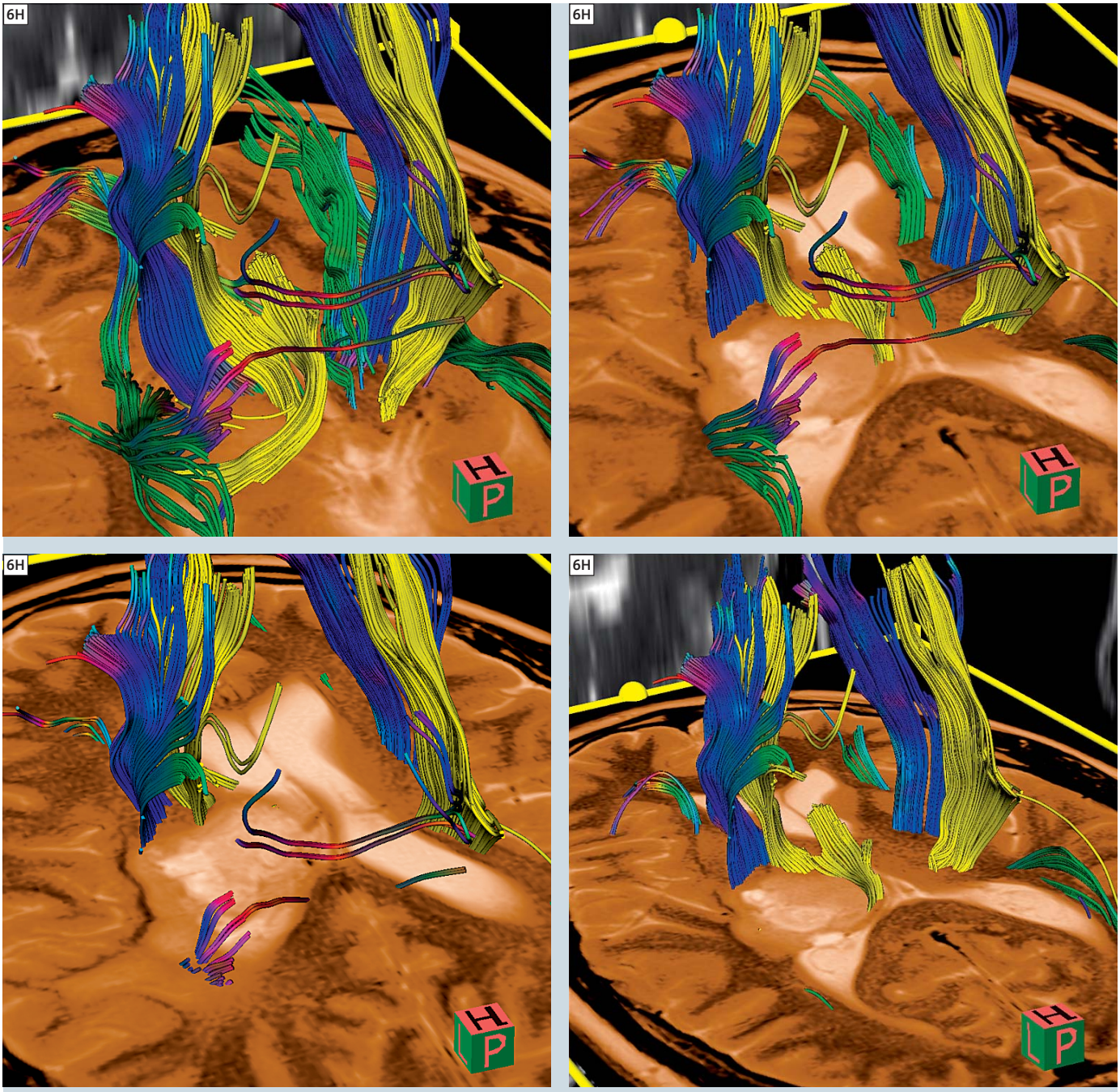

6H DTI Tractography demonstrates anterior deviation of the intact posterior limb of the left internal capsule (directionally encoded in blue). The optic radiations of the left hemispere (directionally encoded in green) are displaced inferolaterally. Transthalamic white matter (yellow for clarity) is displaced radially and disrupted at the rostral margin of the tumor.

References

1 Forbes KP, Pipe JG, et al. Propeller MRI : Clinical testing of a novel technique for quantification and compensation of head motion. J Magn Reson Imag. 2001 Sept;14(3):215–22.

2 Haacke EM. Susceptibility Weighted Imaging (SWI). Med Phys. 2006;16(4):237.

3 Stejskal EO, Tanner JE. Spin diffusion measurements: spin echoes in the presence of a time-dependent field gradient. J Chem Phys 1965;42:288–292.

4 Mukherjee P, et al. Diffusion tensor imaging and fiber tractography:Technical considerations. AJNR 2008 May; 29:843–52.

5 Jellison BJ, Field SF, et al. Diffusion tensor imaging of cerebral white matter: A pictorial review of physics, fiber tract anatomy, and tumor imaging patterns. AJNR 2004 March;25:356–369.

Contact
Tammie Benzinger, M.D., Ph.D.
Mallinckrodt Institute of Radiology
Washington University School of Medicine
St. Louis, Missouri
USA
benzingert@mir.wustl.edu

32-Channel Head Coil Imaging at 3T Case Reports from Scott and White Clinic and Hospital

Val M. Runge, M.D.

Robert and Alma Moreton Centennial Chair in Radiology, Texas A&M University Health Science Center, Temple, Texas, USA

Advanced head coil design with 3T imaging substantially improves the available signal-to-noise ratio (SNR), making possible a substantial reduction in scan time, the use of advanced parallel imaging, high spatial resolution imaging (reduced voxel size in 3D acquisitions, whether for imaging of the brain itself or the vasculature) and implementation of innovative imaging techniques. The use of higher parallel imaging factors in conventional diffusion-weighted echo planar imaging (EPI), together with the implementation of a turbo spin echo (TSE) based BLADE diffusion-weighted scan is illustrated in patients with acute infarction (the latter free of bulk susceptibility artifact and geometric image distortion). With T1-weighted imaging, the 32-channel coil design permits a factor of two reduction in scan time for 2D imaging, and enables the use of a T1-weighted TurboFLASH BLADE technique for motion robust imaging and, alternatively, an ultra-high resolution 3D T1-weighted FLASH scan for more cooperative patients. High resolution, short scan time, 3D T2-weighted scans can also be acquired.

Case 1

Patient history

This 46-year-old woman presented with relatively sudden onset of left upper extremity/hand weakness. Speech was minimally slurred.

Image findings

Two scans are illustrated, both acquired with the 32-channel coil, in a patient with enhancing (active) multiple sclerosis plaques. The first scan was obtained with a short TE T1-weighted 2D FLASH sequence, with voxel dimensions of 0.9 x 0.9 x 4 mm^3, which is substantially degraded (by image blurring) due to patient motion despite the very short scan time (0:56 min) made possible by use of the 32-channel coil. The second scan was obtained with a T1-weighted *syngo* BLADE TurboFLASH sequence, with equivalent voxel dimension, acquired in 2:45 min. Note the marked improvement in image quality on the BLADE scan, with elimination of the blurring noted in the first scan due to patient motion.

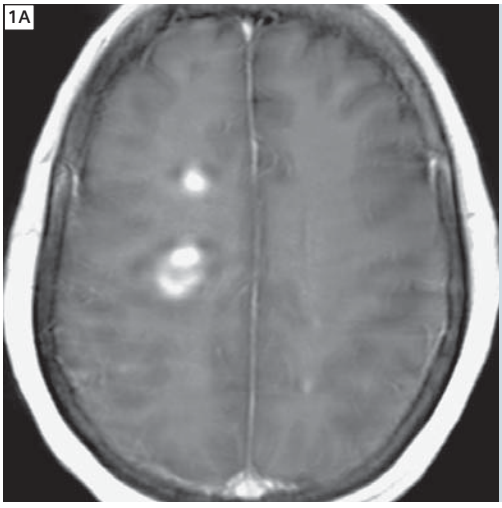

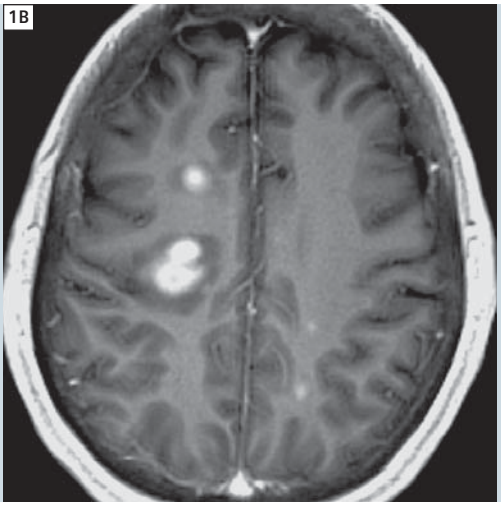

1A, B Post-contrast T1-weighted scans, acquired with slice thickness 4 mm, both using the 32-channel head coil and using 2D FLASH and 3D TurboFLASH respectively.
A: fl2d, TR 250 ms, TE 2.4 ms, FOV 192 x 220 mm^2, matrix 448 x 512 interpolated, bandwidth 320 Hz/pixel, flip angle 70°, 1 acquisition, TA 56 sec.
B: *syngo* BLADE t1w TurboFLASH*, TI 1166 ms, TR 3200 ms, TE 2.8 ms, FOV 230 mm, matrix 256 x 256, bandwidth 280 Hz/pixel, 1 acquisition, TA 48* 3 sec.

Case 2

Patient history

This 56-year-old man presented with right facial pain (trigeminal distribution) and was subsequently found to have a right posterior fossa arteriovenous malformation. He underwent embolization by interventional radiology, with resultant marked decrease in size of the lesion and resolution of his facial pain. Imaging following this treatment revealed a marked decrease in size of the lesion, with the residual nidus measuring less than 2 cm.

Image findings

In Fig. 2, post-contrast T1-weighted scans are compared using the (A) 12 and (B) 32-channel coils. Image quality is equivalent, despite a two-fold reduction in scan time for (B) as opposed to (A), permitted by the use of the 32-channel coil. The low signal intensity noted within the cerebellum reflects predominantly the embolized portion of this lesion.

In Fig. 3A 0.9 x 0.9 x 0.9 mm^3 voxel size, 2:12 min acquisition time, 3D T2-weighted SPACE scan is illustrated, acquired with the 32-channel coil. This partially embolized, posterior fossa, arteriovenous malformation is well visualized, with high image quality on reformatted images in the (A) sagittal, (B) coronal, and (C) axial planes.

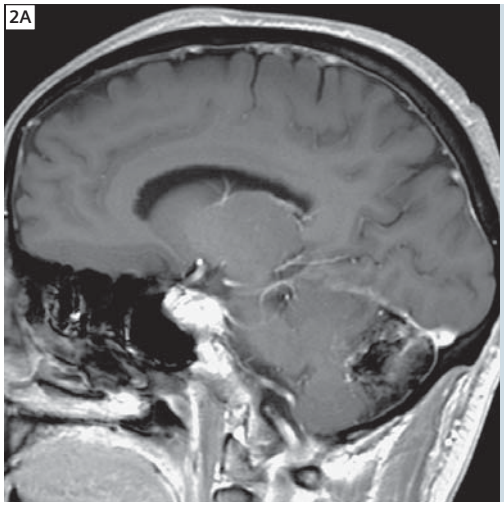

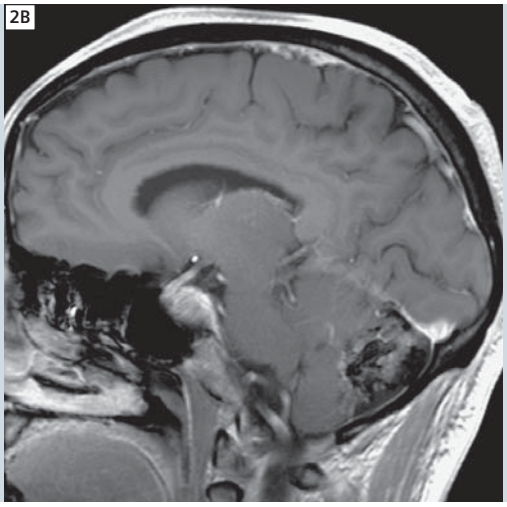

2A, B T1-weighted fl2d, TR 250 ms, TE 2.5 ms, FOV 220 mm, matrix 512 x 512 interpolated, slice thickness 4 mm, bandwidth 320 Hz/pixel, flip angle 70°. Comparing results obtained with **(A)** the 12-channel head coil using 2 averages (TA 2:08 min) to that obtained with **(B)** the 32-channel head coil using 1 average (TA 1:04 min).

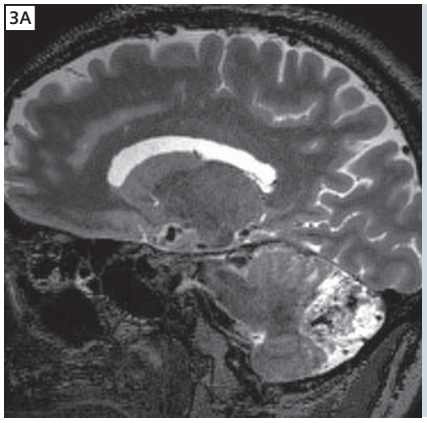

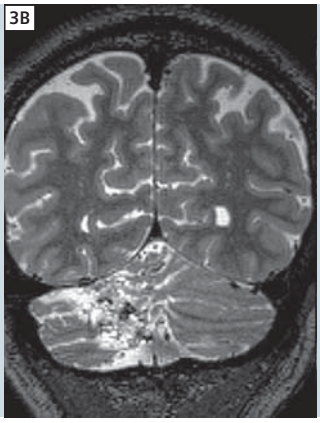

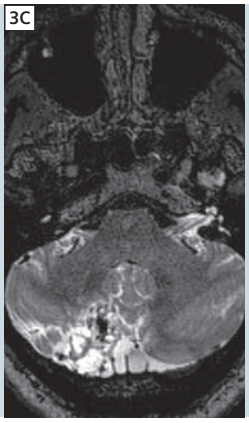

3A, B, C T2-weighted SPACE, TR 3200 ms, TE 546 ms, 0.9 x 0.9 x 0.9 mm^3 voxel dimension, bandwidth 745 Hz/pixel, PAT 4, TA 2:12 min.

Case 3

Patient history

This 58-year-old woman presented to the hospital following three episodes of tingling/paresthesias involving her lips and right side of the body. She was noted during her hospital stay to have labile hypertension. Imaging revealed an early subacute left thalamic infarct.

Image findings

Bulk susceptibility artifact (white arrow) is reduced by increasing the PAT factor to 4 in (B) as compared to 2 in (A). Despite the increase in PAT factor, scan quality (specifically SNR) is maintained, due to the use of the 32-channel coil in (B) as opposed to the 12-channel coil in (A). Note the elimination of the bulk susceptibility artifact (seen in A, arrow, in this instance originating from the frontal sinus) using the BLADE TSE diffusion-weighted approach (C). This sequence has inherently lower SNR, with the 32-channel coil making this scan approach clinically viable. Note also the reduced T2* effect, in this instance due to normal hemosiderin content in the globus pallidus, with the BLADE TSE scan as opposed to the echo planar scan (green arrow). Hemorrhage will have less of a deleterious effect on BLADE TSE diffusion-weighted scans, a finding confirmed in early clinical experience.

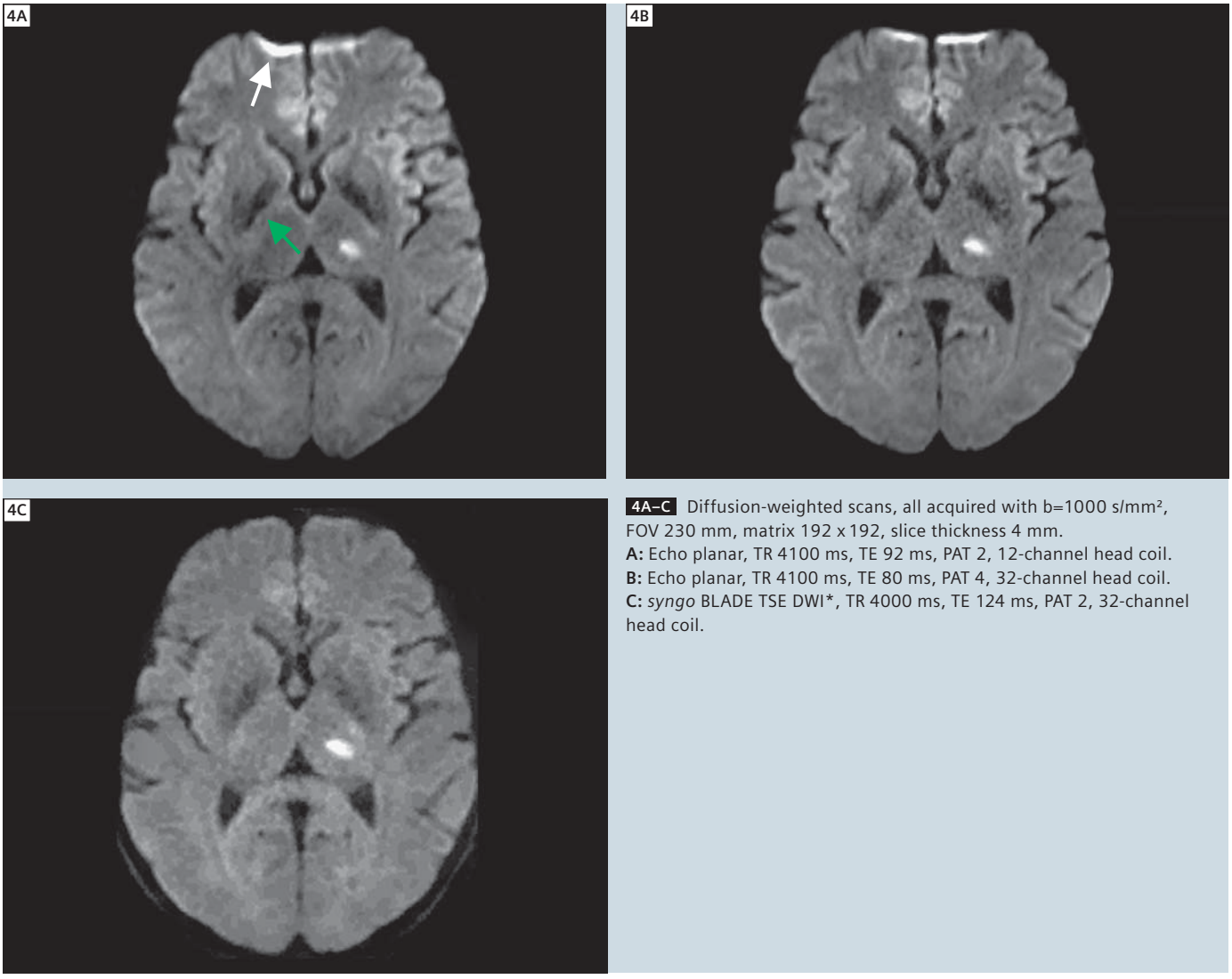

4A–C Diffusion-weighted scans, all acquired with b=1000 s/mm², FOV 230 mm, matrix 192 x 192, slice thickness 4 mm.
A: Echo planar, TR 4100 ms, TE 92 ms, PAT 2, 12-channel head coil.
B: Echo planar, TR 4100 ms, TE 80 ms, PAT 4, 32-channel head coil.
C: *syngo* BLADE TSE DWI*, TR 4000 ms, TE 124 ms, PAT 2, 32-channel head coil.

Case 4

Patient history

This 65-year-old man with stage IV pancreatic cancer presented for evaluation three days following a transient episode of aphasia, with right hand weakness that has since persisted. The leading diagnosis is embolic infarction from non-bacterial thrombotic endocarditis, with the primary risk factor being the known mucin-producing adenocarcinoma.

Image findings

Multiple punctate early subacute infarcts are illustrated. In (A), echo planar diffusion-weighted imaging was performed using the 12-channel coil and a PAT factor of 2. The capability of the 32-channel coil for higher PAT factors (without increasing the number of scan averages, and so prolonging scan time), and thus less bulk susceptibility artifact, in all planes is illustrated in figures B–D with PAT 4 scans in the axial, sagittal, and coronal planes.

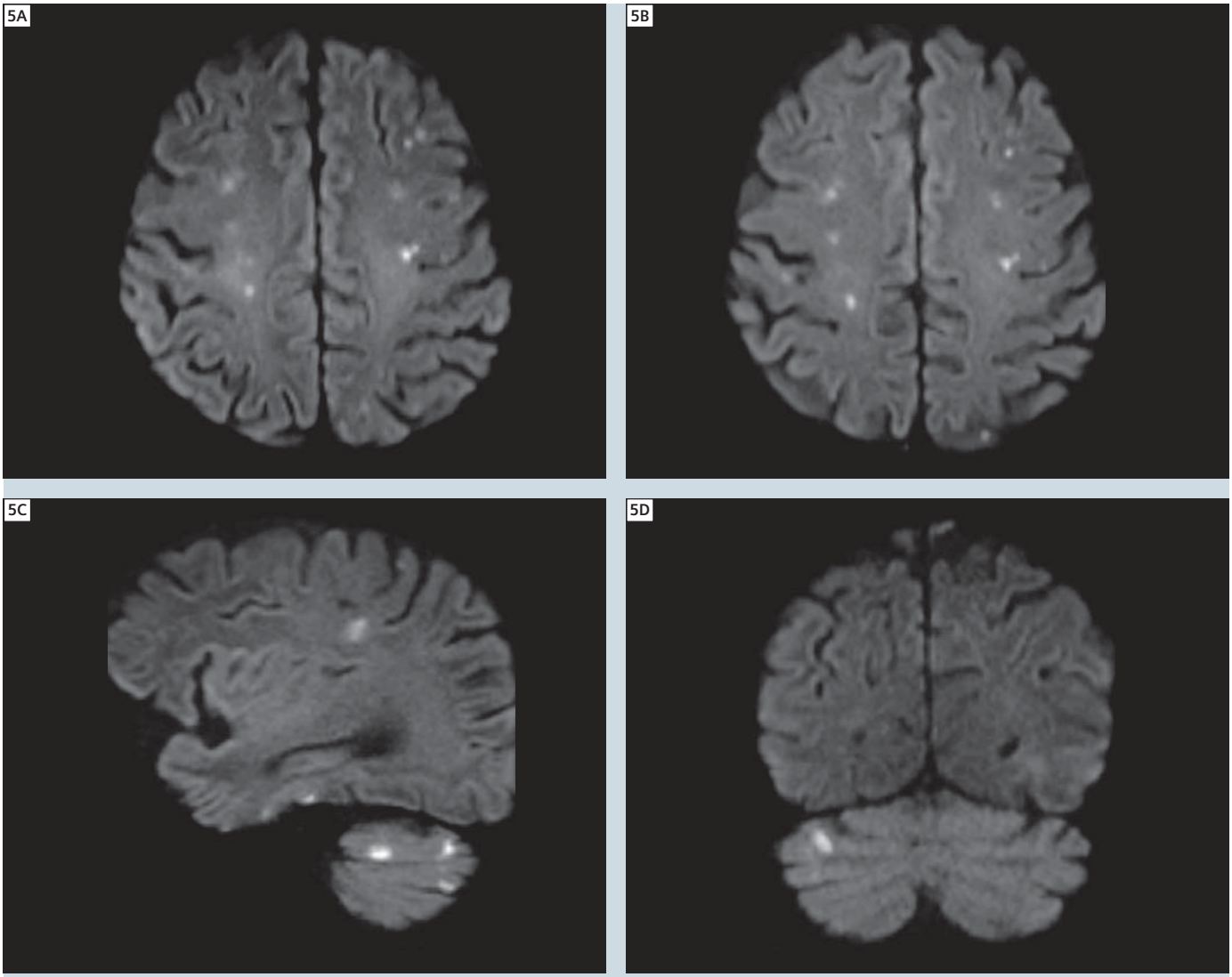

5A–D Echo planar diffusion-weighted scans, all acquired with b=1000 s/mm², FOV 230 mm, matrix 192 x 192, slice thickness 4 mm.
A: TR 4100 ms, TE 92 ms, bandwidth 1240 Hz/pixel, PAT 2, 12-channel head coil.
C–D: TR 4100 ms, TE 80 ms, BW 1240 Hz/pixel, PAT 4, 32-channel head coil.

Case 5

Patient history

This 60-year-old woman has metastatic breast cancer, and has been treated with multiple chemotherapeutic regimens. She received whole brain radiation for brain metastases eleven months prior to the current MRI.

Image findings

Short TE 2D T1-weighted FLASH scans are presented, comparing a scan acquired (A) with the 12-channel coil in a 1:52 min scan time to that acquired (B) with the 32-channel coil in a 0:56 min scan time. Image quality is equivalent for depiction of the large enhancing parenchymal brain metastasis, as well as two smaller metastases. (C, D) FLAIR and T2-weighted 2D axial *syngo* BLADE scans are also illustrated, both acquired with the 32-channel coil. An iPAT (integrated Parallel Acquisition Technique) factor of 2 was used for both scans, with these scans typically performed when using the 12-channel coil without iPAT, leading to a two-fold reduction in scan time. In this instance, the scan times were 1:03*2 and 0:28* 2 min, with both scans providing whole brain coverage using a 4 mm slice thickness.

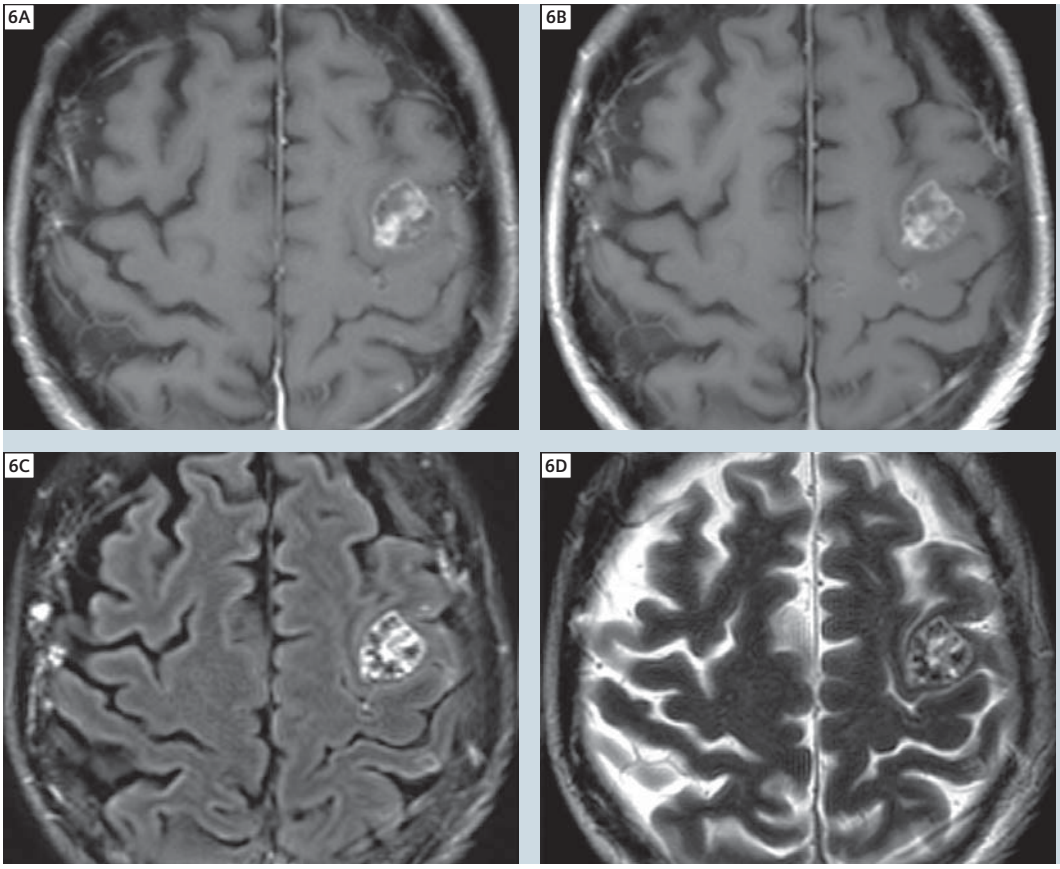

6A, B T1-weighted fl2d, TR 250 ms, TE 2.5 ms, FOV 193 x 220 mm², matrix 448 x 512 interpolated, slice thickness 4 mm, bandwidth 320 Hz/pixel, flip angle 70°. Comparing results obtained with (A) the 12-channel head coil using 2 averages (TA 1:52 min) to that obtained with (B) the 32-channel head coil using 1 average (TA 0:56 min).
C, D: 32-channel FLAIR axial imaging with *syngo* BLADE and T2-weighted TSE with *syngo* BLADE illustrating a reduction in scan time by half when compared to conventional imaging with the 12-channel coil.
C: FLAIR BLADE, TI 2500 ms, TR 9000 ms, TE 118 ms, FOV 220 mm, matrix 256 x 256, slice thickness 4 mm, bandwidth 290 Hz/pixel, ETL 33, PAT 2, TA 1:03*2.
D: T2-weighted BLADE, TR 3500 ms, TE 118 ms, FOV 220 mm, matrix 320 x 320, slice thickness 4 mm, bandwidth 290 Hz/pixel, PAT 2, TA 0:28*2.

*Work in progress (WIP). The information about this product is preliminary. The product is under development and not commercially a vailable in the U.S., and its future availability cannot be ensured.

Contact
Val M. Runge, M.D.
Scott and White Clinic and Hospital
Texas A&M University Health Science Center
Temple, TX, USA
val.runge@mac.com

→ **Visit www.siemens.com/magnetom-world** for the technical aspects of the 32-channel coil: "Highly Parallel Detection for MRI" by Lawrence L. Wald and Graham Wiggins. MAGNETOM Flash 38 (1/2008) page 34-44.

Case Report: Cortical Dysplasia

Michael Kean; Micheal Ditchfield, M.D.

Children's MRI Centre, Royal Children's Hospital, Parkville, Victoria, Australia

Patient history

12-year-old girl presented after inconclusive scan at an outside institution. The patient was scheduled for a standard Epilepsy scan on our 1.5T MAGNETOM Avanto using a standard Head Matrix coil. The patient was then referred to the 3T MAGNETOM Trio and examined using the 32-channel Head Matrix coil.

Sequence details

The images obtained are from a 1.5T MAGNETOM Avanto with software version *syngo* MR 13 (MPRAGE 0.7 mm isotropic voxels) and from a 3T MAGNETOM Trio with software version *syngo* MR B15 (MPRAGE 0.7 mm isotropic, 0.9 mm isotropic voxels using Water Excitation (WE), DarkFluid 3D SPACE and lipid suppressed 135 ms TE single voxel MR spectroscopy – MRS)

Image findings

The patient presented with migraines and 1.5T MR demonstrated a left frontal lesion possibly a cortical dysplasia or developmental tumor (DNET).
3T MR demonstrates a focally thickened cortical ribbon with blurring of the grey/white matter interface. The MR appearances are that of a cortical malformation.

Discussion

The images obtained using the 1.5T MAGNETOM Avanto clearly show the lesion but the increased signal-to-noise ratio (SNR) of the 32-channel Head Matrix coil and 3T (MPRAGE and 3D SPACE) provide the radiologist with a level of anatomical detail that enables a diagnosis with a higher degree of sensitivity and specificity.

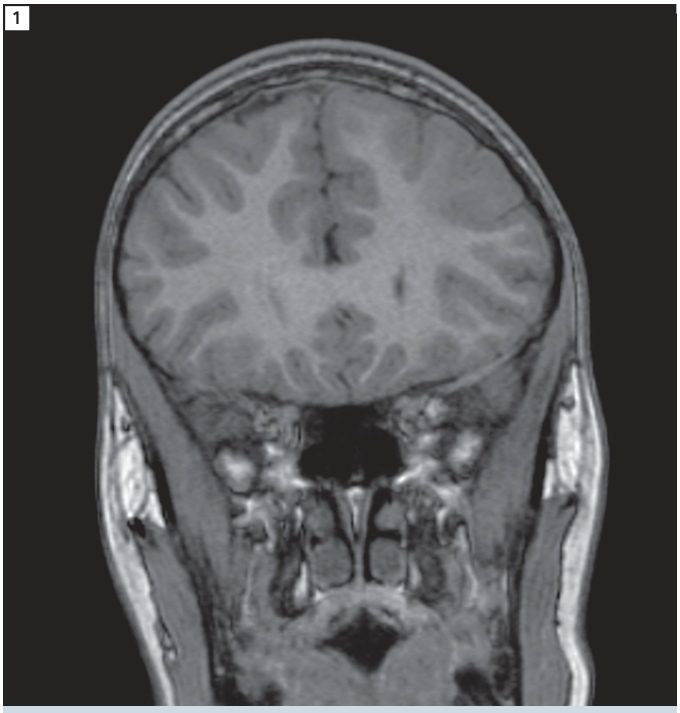

1 MPRAGE image with 0.7 mm isotropic voxel, acquired using a 1.5T MAGNETOM Avanto system, demonstrating the left frontal lesion.

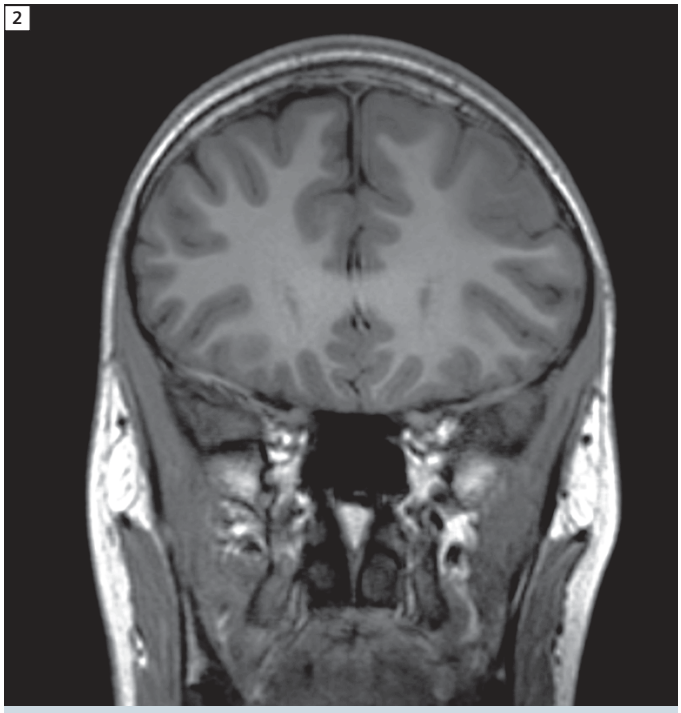

2 Corresponding MPRAGE image acquired using a 3T MAGNETOM Trio and the 32-channel Head Matrix coil. The focally thickened cortical ribbon and the blurring of the grey/white matter interface are clearly visible.

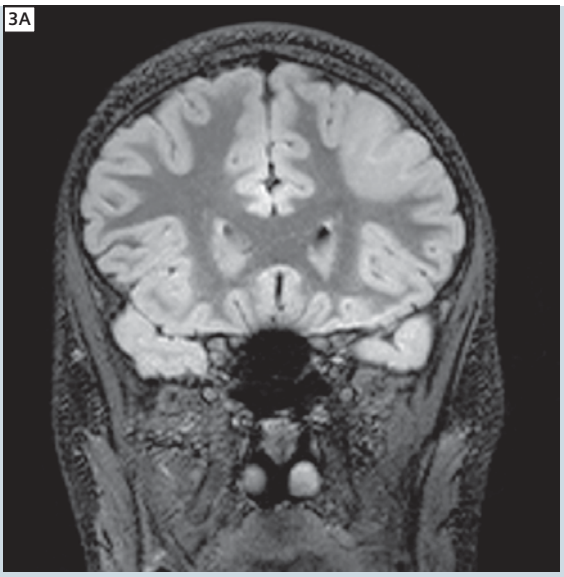

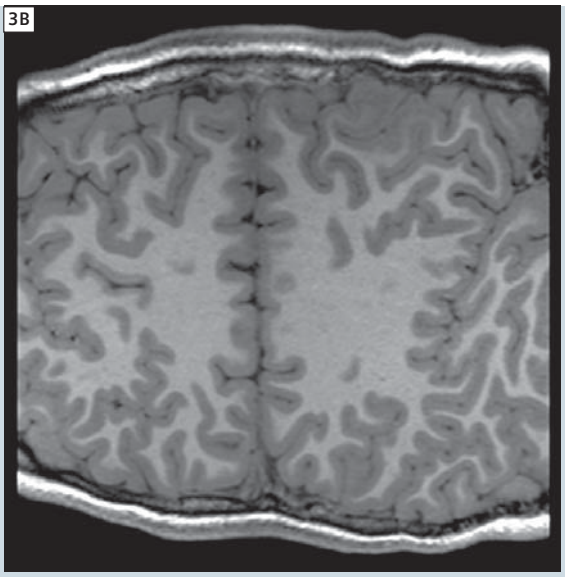

3 The acquisition of a highly resolved 3D dataset also enables the radiologist to perform a detailed retrospective interactive multiplanar evaluation of the whole brain.
In figures 3A–D the reformatted DarkFluid 3D SPACE images are shown, displaying the disorganization of the left frontal cortical layer in detail.

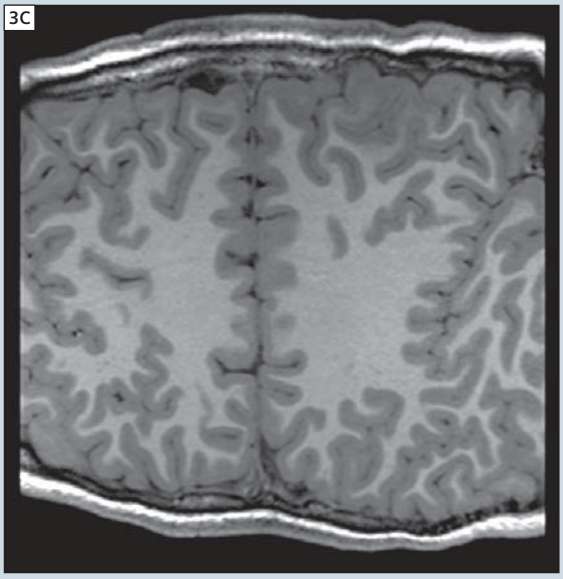

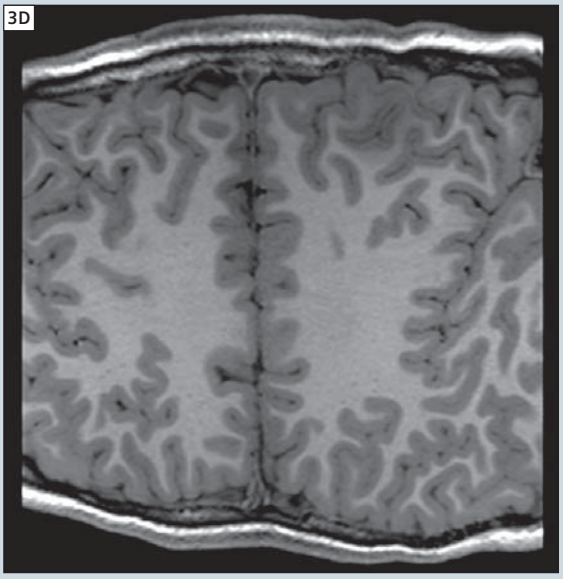

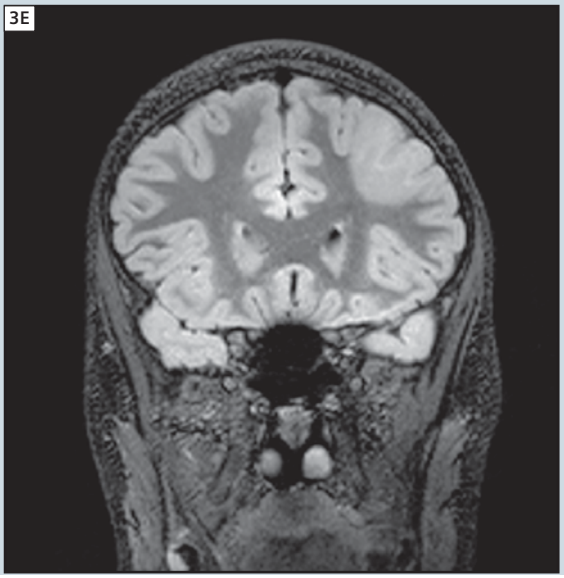

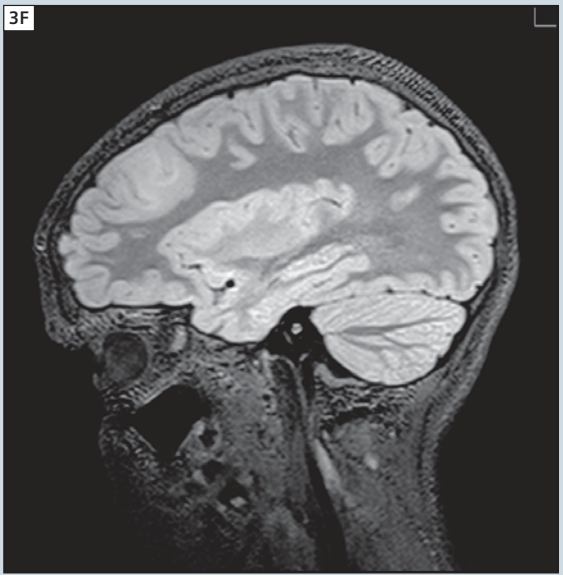

3E standardized coronal and 3F sagittal reformation of the acquired T2-weighted *syngo* SPACE images.

Case Report: Cortical Dysplasia

Michael Kean; Michael Ditchfield, M.D.

Children's MRI Centre, Royal Children's Hospital, Parkville, Victoria, Australia

Patient history

10-year-old girl presented after inconclusive scan at an outside institution. The patient has a history of Epilepsy, developmental regression and autistic behavior. The patient was referred to the 3T MAGNETOM Trio and examined using the 32-channel Head Matrix coil utilizing our current high resolution Epilepsy protocol.

Sequence details

The images are from 3T MAGNETOM Trio with software version *syngo* MR B15 (MPRAGE 0.7 mm isotropic, 0.9 mm isotropic voxels using Water Excitation (WE), DarkFluid 3D SPACE, high resolution 2.5 mm coronal Turbo Spin Echo (TSE) T2 and lipid suppressed 135 ms TE single voxel MR Spectroscopy – MRS)

Image findings

There is a cortically based lesion within the left frontal lobe containing cystic and solid components that do not enhance with contrast. There is a "tail" of increased signal that extends from the lesion to the anterior horn of the lateral ventricle. The MRS confirms appearance of a focal trans mantle cortical dysplasia.

Discussion

The high signal-to-noise ratio (SNR) afforded by the use of the 32-channel Head Matrix coil and 3T permits the technologist to run high-resolution isotropic 3D acquisitions in scan times that are conducive to high patient compliance. The reformatted images (MPRAGE 0.7 mm and 3D SPACE 0.9 mm) combined with the high-resolution T2 provide the radiologist with a level of anatomical detail that provides a diagnosis with a higher degree of sensitivity and specificity. The ability to use these 3D data sets to perform curvilinear reformations improves pre-surgical localization. The lipid suppression characteristics of the MRS enable lesions close to the outer table of the skull to be evaluated.

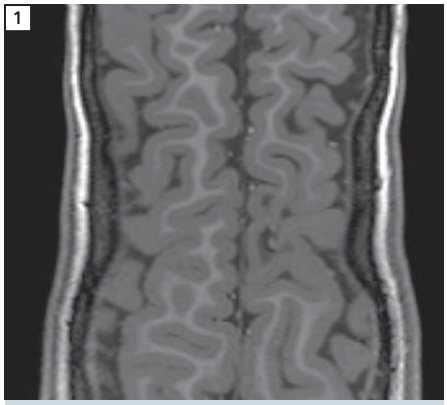

1 The reformatted image from 0.7 mm isotropic voxel MPRAGE proves to increase the diagnostic specificity.

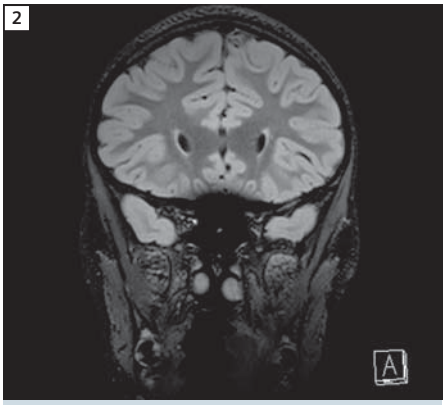

2 DarkFluid 3D SPACE shows the left frontal lobe lesion containing solid and cystic components.

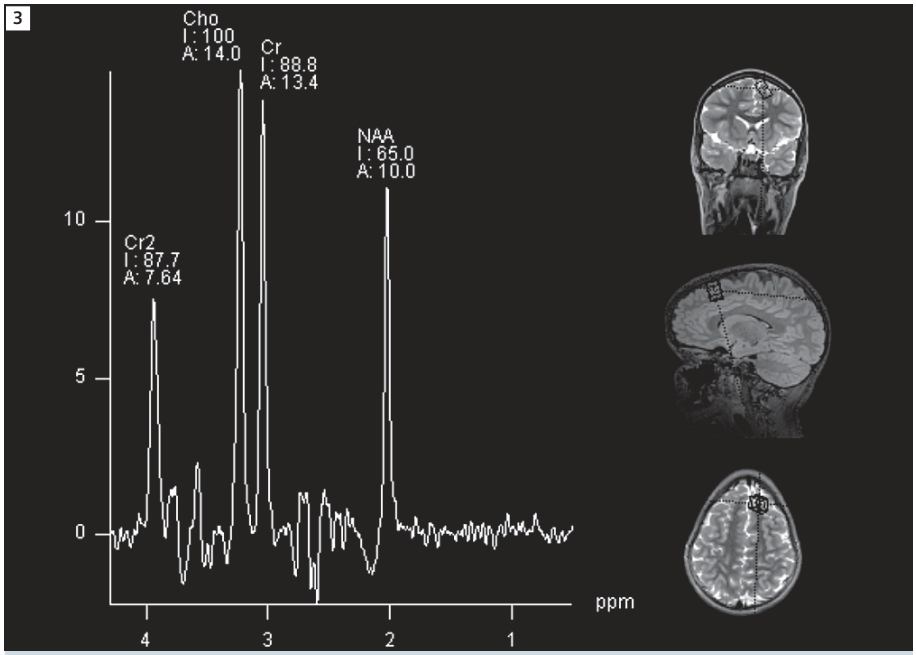

3 Lipid suppressed 135 ms single voxel MR spectrum from the lesion of the left frontal lobe supports the diagnosis of a focal trans mantle cortical dysplasia.

Case Report: Left PCA Fusiform Aneurysm

Michael Kean; Michael Ditchfield, M.D.

Children's MRI Centre, Royal Children's Hospital, Parkville, Victoria, Australia

Patient history

Patient presented for yearly follow-up of a 6 mm diameter Fusiform Aneurysm of the left PCA. Previous imaging has been done using a 1.5 Tesla system.

Sequence details

The following images were acquired on our 3T MAGNETOM Trio, A Tim System using the 32-channel head coil: multiplanar T1-weighted, T2-weighted, susceptibility-weighted (SWI) imaging and 3D MOTSA MR Angiography (MRA). "Balanced" transverse imaging using SPAIR was performed to demonstrate any thrombus within the aneurysmal dilation. TR 2250 ms, TE 12 ms, spatial resolution 0.4 mm x 0.4 mm x 2.5 mm, SPAIR, FOV 160 mm, Matrix 256 x 320, Bandwidth 130 Hz/Pixel, PAT factor 2. 3D Time of Flight MRA spatial resolution 0.5 x 0.3 x 0.6 mm, FOV 200 mm, Phase FOV 80.7, TR 25 ms, TE 4.63 ms, Flip angle 15°, Matrix 704 x 60%, Phase resolution 60%, Slice Resolution 66%, PAT factor 2, TONE Ramp 70%.

Image findings

Known left PCA aneurysm approximately 6 mm in diameter demonstrates no interval change. Signal void on fat suppressed "balanced" images demonstrates no evidence of calcification or hemorrhage. No further aneurysms are demonstrated.

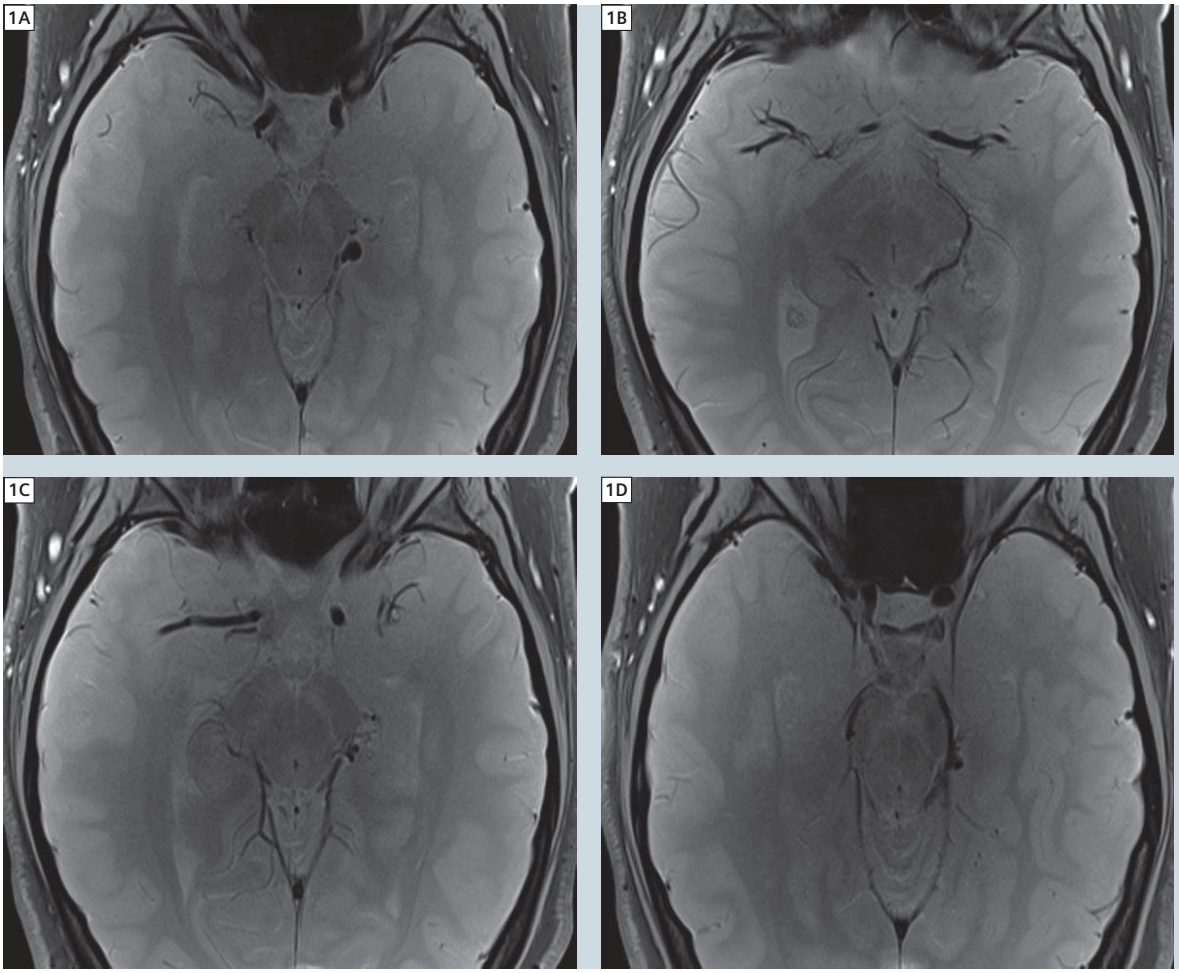

1 The T2-weighted transversal Turbo Spin Echo images, acquired with MAGNETOM Trio, A Tim system, using the 32-channel Head Matrix coil, show the 6 mm sized aneurysm of the left PCA.

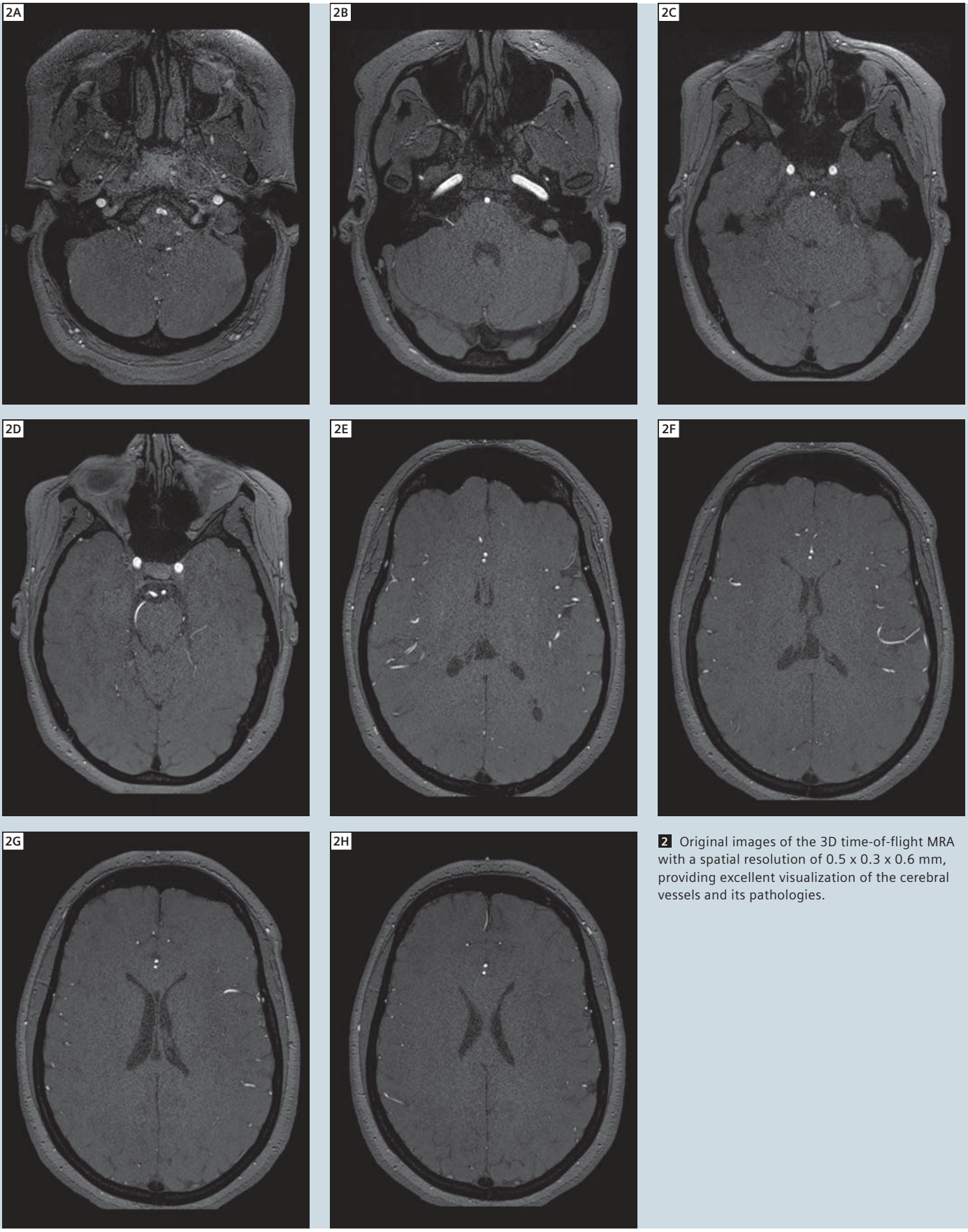

2 Original images of the 3D time-of-flight MRA with a spatial resolution of 0.5 x 0.3 x 0.6 mm, providing excellent visualization of the cerebral vessels and its pathologies.

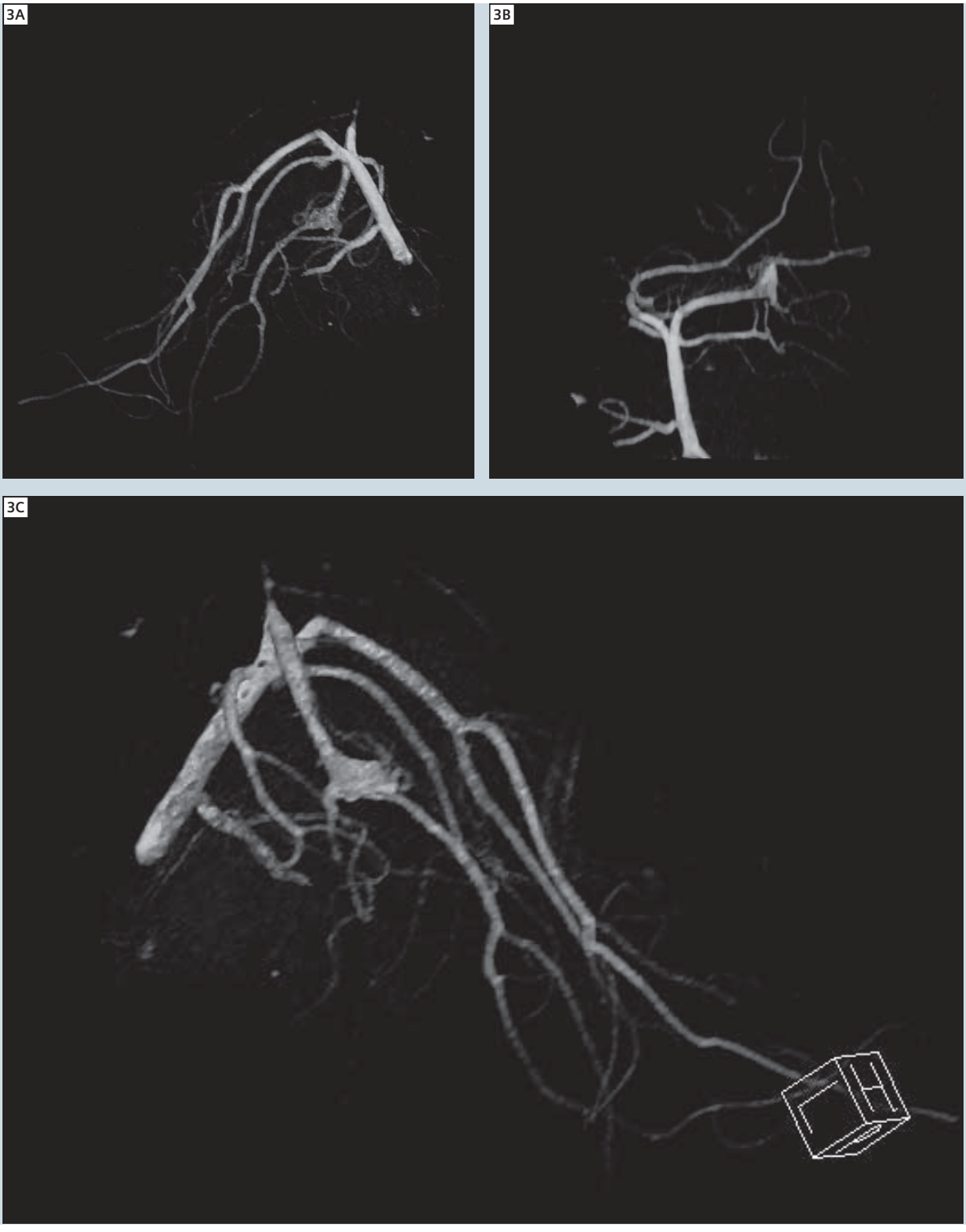

3 Based on 3D time-of-flight MR angiography, a maximum intensity projection (MIP) was calculated for improved evaluation of the extend, configuration and localization of the small sized aneurysm of the left PCA.

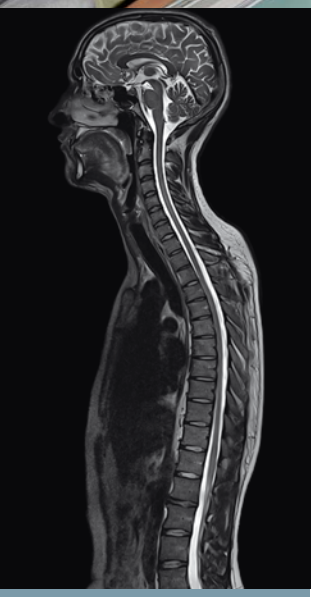

How can we reduce exam times by 50% for higher patient comfort?

Siemens Tim technology enables multi-organ exams in one single patient setup.

By combining coils in any way, Tim® (Total imaging matrix) technology helps you to reduce your examination times by up to 50%. Around the world, Tim has become a standard in MRI. With its unmatched 32 independent RF channels and up to 102 seamlessly integrated Matrix coil elements, Tim is providing you incredible flexibility, accuracy, and speed for high-quality patient care. **www.siemens.com/healthcare +49 69 797 6420**

Answers for life.

SIEMENS

MR-Z1093-2-7600

Case Report: Neonatal* Laminar Cortical Necrosis

Michael Kean; Michael Ditchfield, M.D.

Children's MRI Centre, Royal Children's Hospital, Parkville, Victoria, Australia

Patient history

The patient was transferred from the Pediatric Intensive Care Unit, severe group B strep with shock. The patient was acidotic and seizing. The clinical question concerned cerebral injury.

Sequence details

Standard neonatal hypoxic ischemic injury series including transverse and coronal T2-weighted images, diffusion-weighted imaging (DWI) with SPAIR, susceptibility-weighted images (SWI), 3D MPRAGE T1 and Water Excitation (WE) 3D MPRAGE post contrast.

Parameters:

SWI (TR/TE 28/20, TA 5:48 min, SL 9.6 mm, FoV 124 x 180, matrix 172 x 384). T2 TSE Restore with *syngo* BLADE (TR/TE 5170/145, TA 2:56 min, SL 2.5 mm, FoV 135 x 135, matrix 256 x 256). The images were acquired on a 3T MAGNETOM Trio, A Tim System with software version *syngo* MR 15B using the transmit/receive extremity coil.

Image findings

Images show extensive bilateral hemorrhagic laminar necrosis and bilateral basal ganglia foci of focal cerebritis or ischemia.

Discussion

Standard neonatal T2-weighted imaging utilizes *syngo* BLADE motion correction to permit increased signal-to-noise without scan time penalty. Whole head T2-weighted imaging utilizing *syngo* BLADE enables 2.5 mm high-resolution slices to be acquired in 3 minutes. SWI images are acquired using 1.2 mm slices with high in-plane resolution of 0.6 mm.

* The safety of imaging fetuses/infants has not been established.

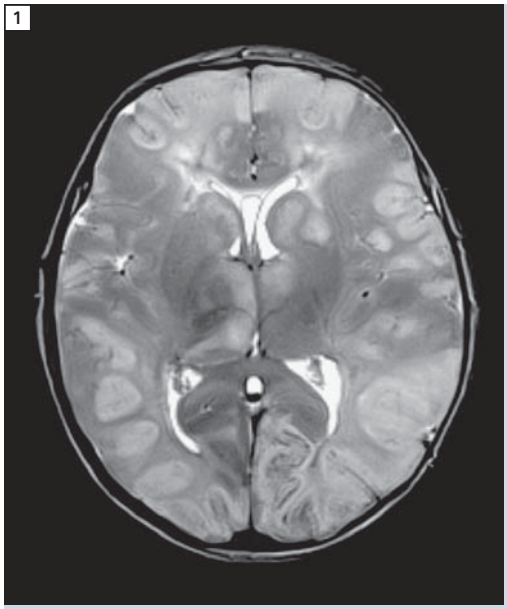

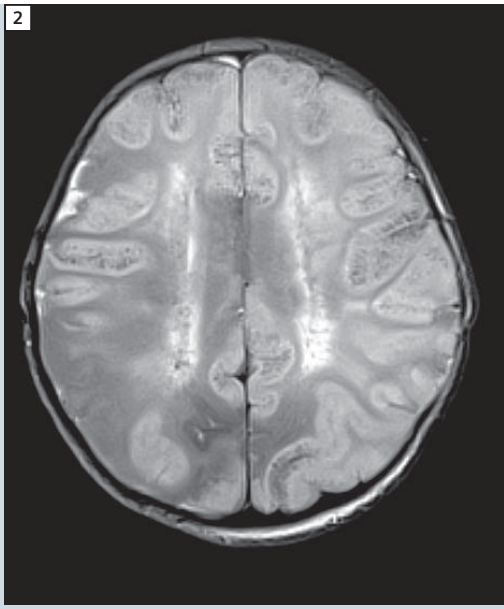

1 **2** In these exemplary chosen transversal T2-weighted Turbo Spin Echo images, the extensive bilateral laminar necrosis and the presence of basal ganglia foci are clearly visible.

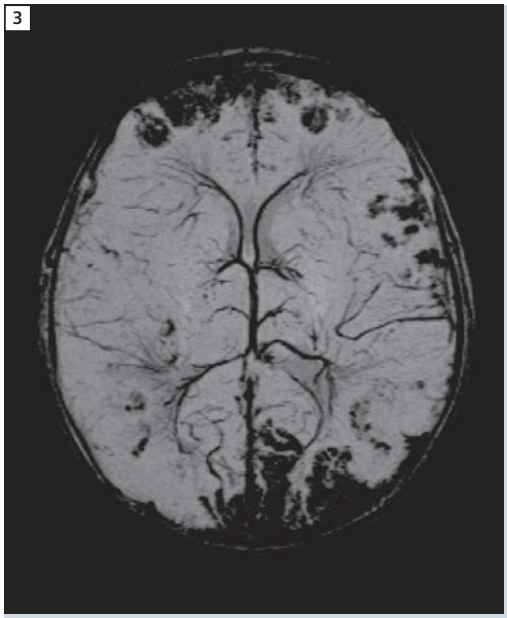

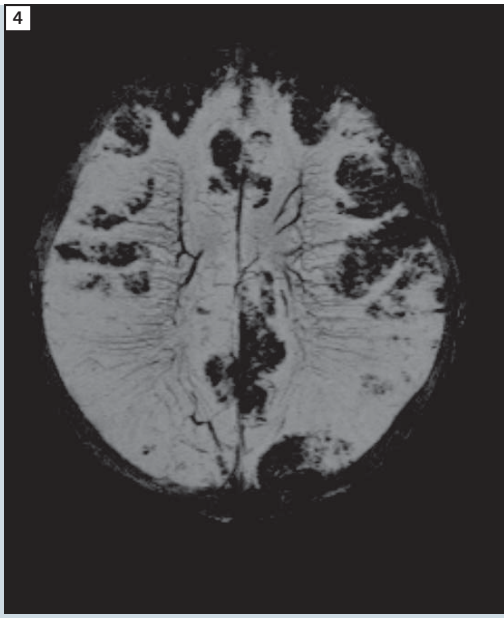

3 **4** Corresponding susceptibility-weighted images (*syngo* SWI) clearly visualize the extensive hemorrhage.

Case Report: Cervical Spine Trauma

Michael Kean; Michael Ditchfield, M.D.

Children's MRI Centre, Royal Children's Hospital, Parkville, Victoria, Australia

Patient history

4-year-old female patient was involved in a high-speed vehicle accident. At the scene the girl was distressed, bradycardic and not moving limbs. She was transferred to the Pediatric Trauma Centre and MR imaging requested for prognostic information regarding treatment.

Sequence details

All images have been acquired at our MAGNETOM Trio, A Tim System using the Spine Matrix coil.
Sagittal Turbo Spin Echo (TSE) images with TR 4300 ms, TE 107 ms, BW = 240 Hz/Px, Turbo Factor 25, slice thickness 2.5 mm, FOV 230 mm, matrix 346 x 384.
Transverse images with TR 2000 ms, TE 12 ms, Turbo Factor 5, BW = 132 Hz/Pixel, slice thickness 3.5 mm, FOV 160 mm, using SPAIR.

Image findings

Images show a transection of the cervical cord at the level of C5–C6 with approximately 6 mm of separation.

Contact
Michael Kean
Children's MR Centre
Royal Children's Hospital
Melbourne, Australia
michael.kean@rch.org.au

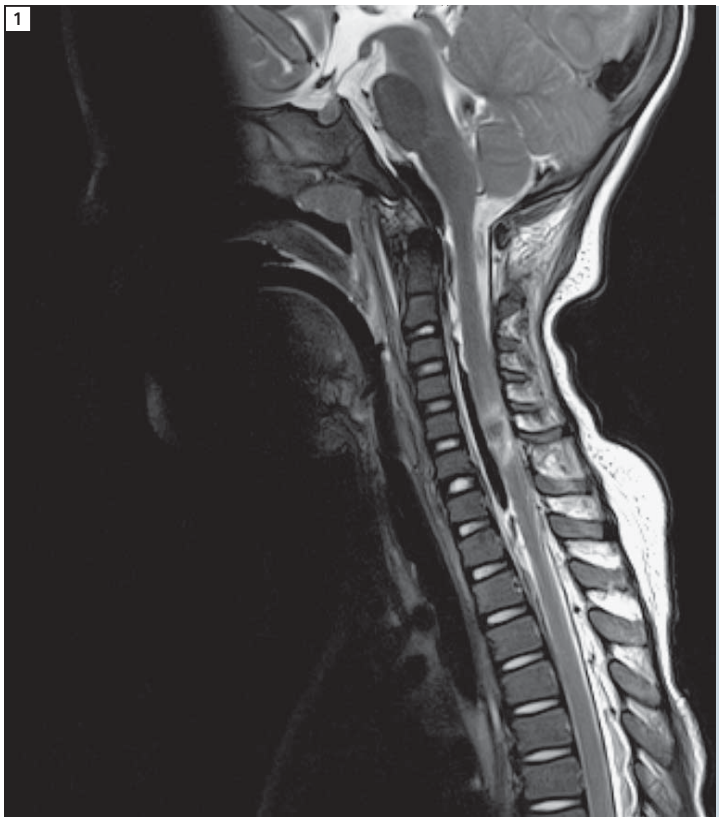

1 The sagittal T2-weighted Turbo Spin Echo image demonstrates a traumatic transection of the spinal cord at the level of C5–C6.

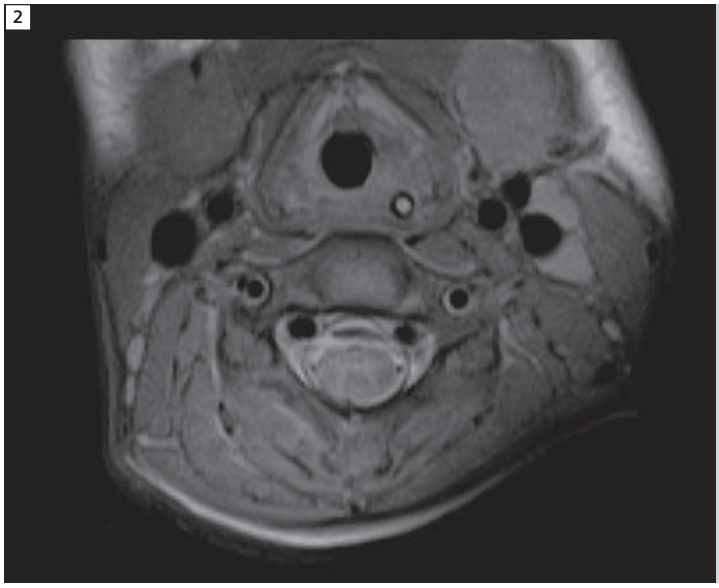

2 The corresponding transversal image supports the diagnoses of the separation of the cervical cord.

Case Report: Conjoined Twins Evaluation Using *syngo* TWIST and *syngo* Diffusion Tensor Imaging

Michael Kean; Michael Ditchfield, M.D.; Wirginia Maixner, M.D.

Children's MRI Centre, Royal Children's Hospital, Parkville, Victoria, Australia

Patient history

11-month-old* craniopagus conjoint twins were referred for evaluation of venous anatomy to plan separation surgery. Repeated MR examinations were undertaken to plan the surgery and MR venography using *syngo* TWIST enabled surgeons to study the results of embolization and surgical venous occlusion.

Sequence details

The patients were placed in a partial left decubitus position on the scan table of our MGNETOM Trio, A Tim System. The decubitus position was necessary due to congestive cardiac failure brought about by twin–twin circulation. The Body Matrix coil was used as it provided a balance between signal-to-noise ratio (SNR), the availability of integrated Parallel Acquisition Techniques (iPAT) and the volume of interest.

3D MPRAGE (TR 1900 ms, TE 2.6 ms, TI 900 ms, Flip angle 9°, FOV 270 mm, PAT factor 2, 320 x 90 %, 60 % phase oversampling) isotropic 0.9 mm resolution was initially performed to aide with pre-

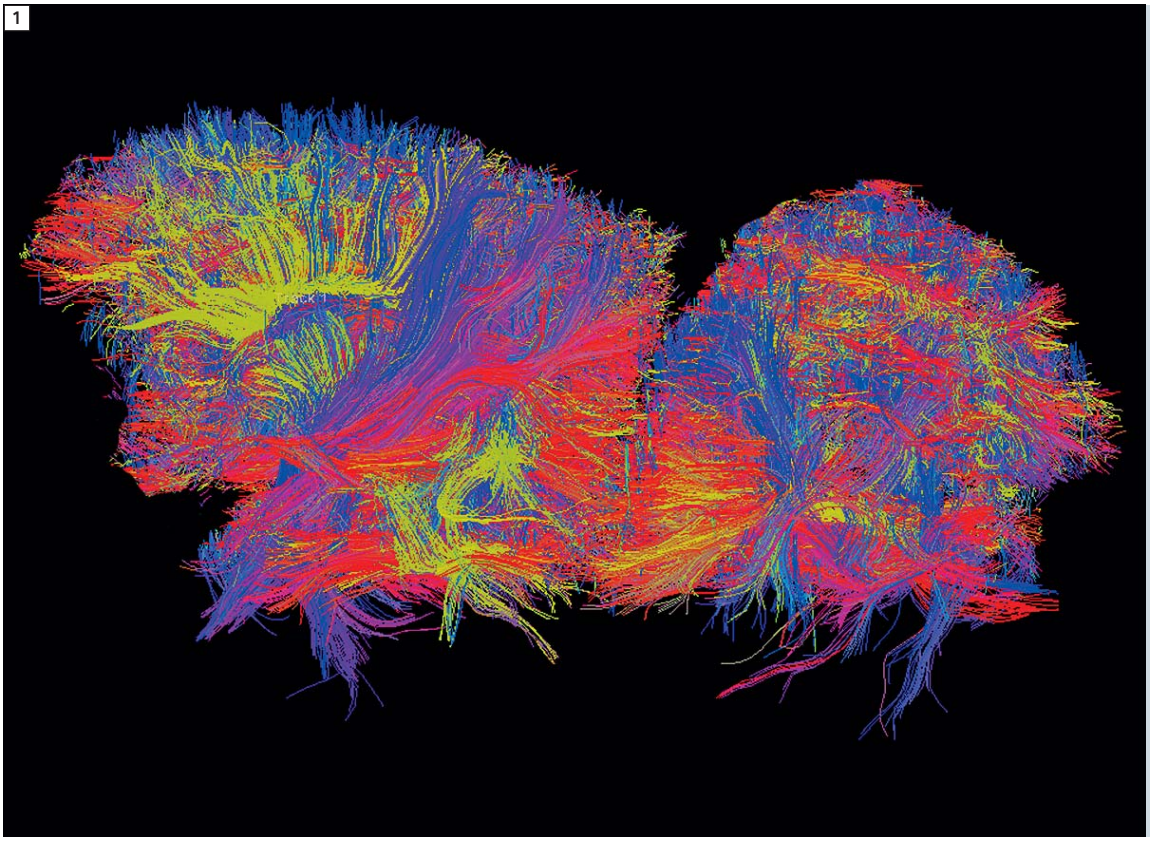

1 *syngo* DTI allows to study the structural integrity of the cerebral nerve tracts of the conjoined twins in each dimension (resulting spatial resolution: 2.2 x 2.2 x 2.0 mm).

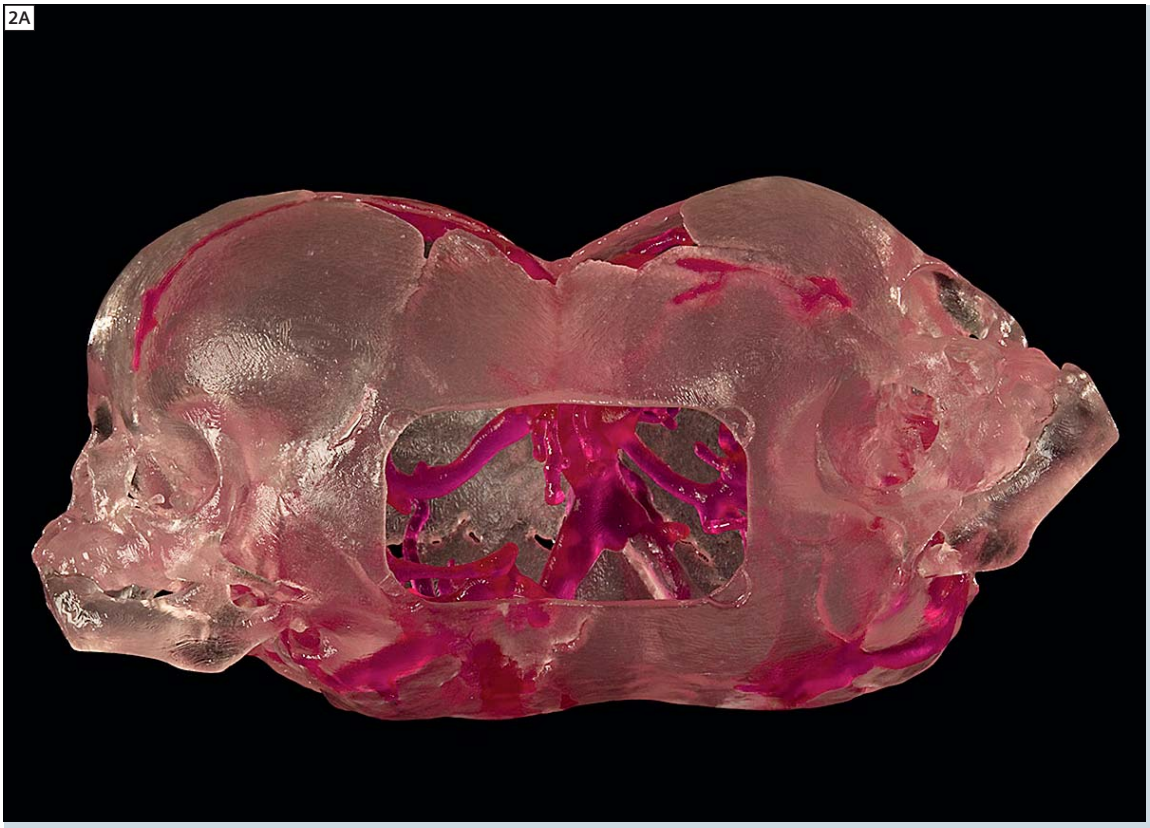

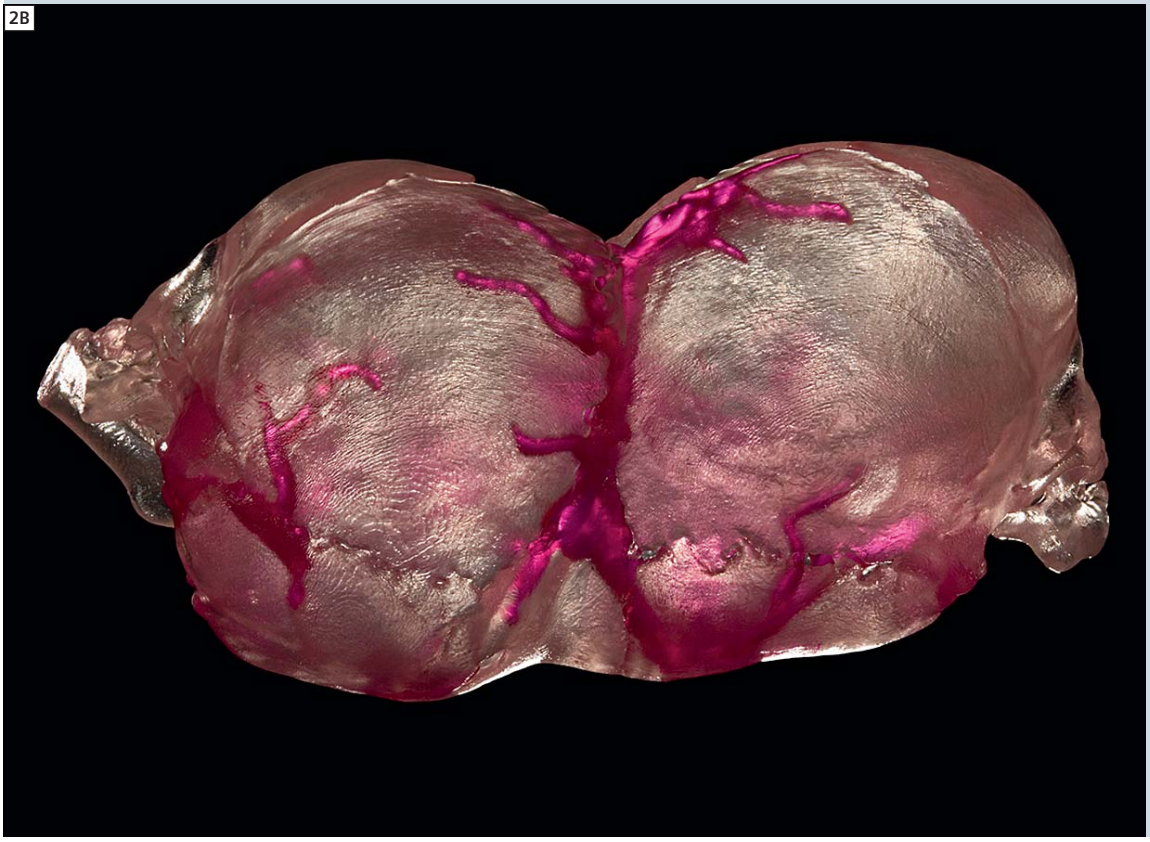

2 1:1 3D plastic model to provide an anatomical depiction of the venous sinus and the sculls of the twins.

scribing T2-weighted imaging planes. The 3D data was loaded into the 3D card and true anatomical planes (axial, coronal and sagittal) were identified and image stamps saved that were then imported into the Exam card. These image stamps were used to copy the image position to define the imaging planes for the anatomical acquisitions. T2-weighted Turbo Spin Echo (TSE) data sets were obtained in three planes (TR 5000 ms, TE 144 ms, 2 Acquisitions, spatial resolution 0.6 x 0.5 x 3.5 mm. *syngo* DTI acquisition was performed using TR 10460 ms, TE 90 ms, B = 1000,

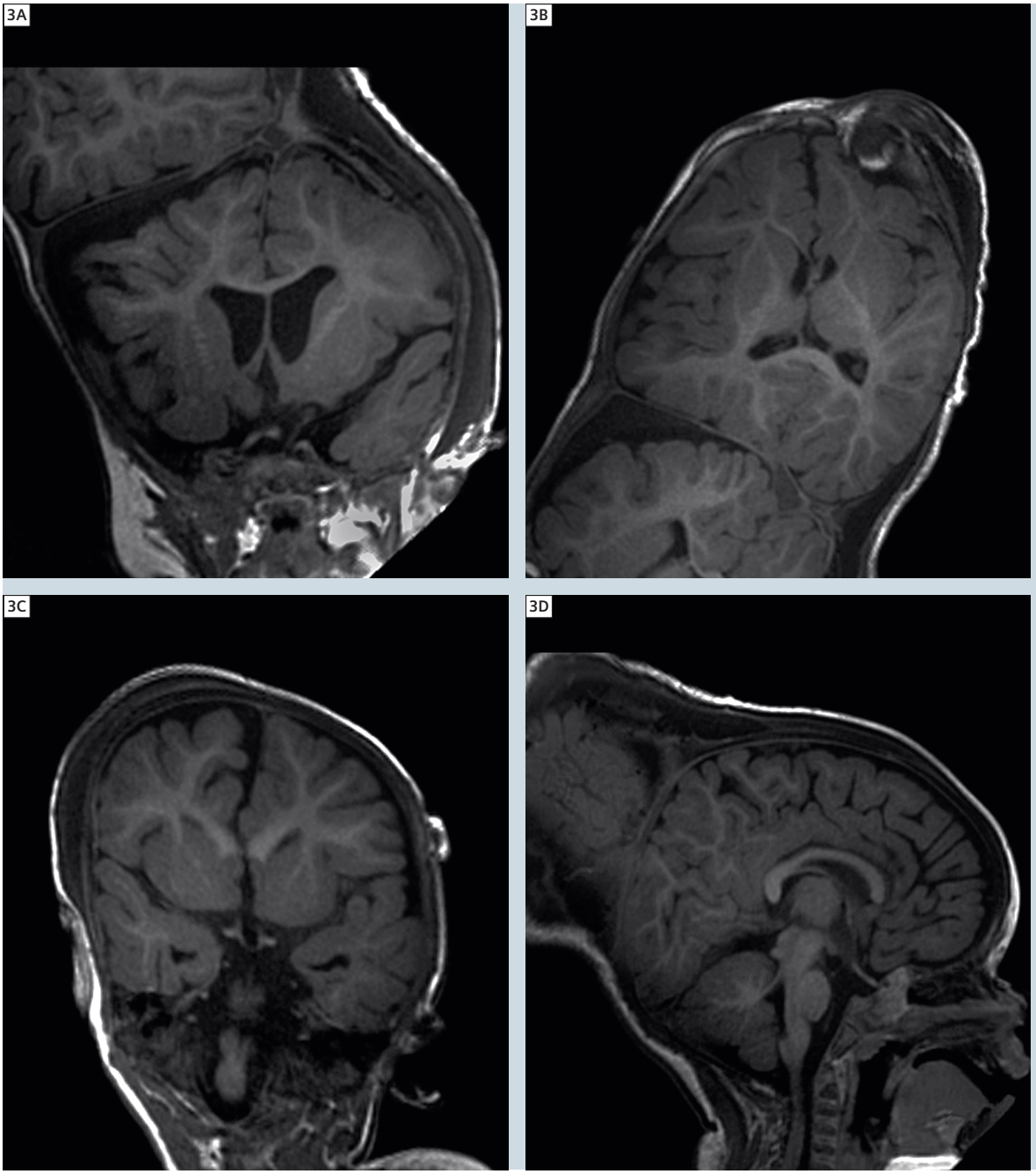

3 To aid with sequence planning in this complex case and to identify the true anatomical planes for both twins, a 3D MPRAGE measurement was performed initially and loaded into the 3D task card. The true anatomical planes could then easily be identified and used for further planning of 2D MR imaging.

spatial resolution of 2.2 x 2.2 x 2 mm, 60 directions, PAT factor 2, FOV 280 mm, 80 slices.
syngo TWIST imaging to evaluate the twin-twin venous connection was performed. Each twin was injected separately. TR 2.56 ms , TE 0.95 ms, spatial resolution 1.2 x 0.8 x 1.2 mm (FOV 320, 384 x 70%), slice resolution 64%, PAT factor 4, 20 measurements, virtual temporal resolution 2.29 sec, *syngo* TWIST sampling central A = 33% peripheral B 50%. TWIST images show clearly the communicating vein between the twins. These images proved to be

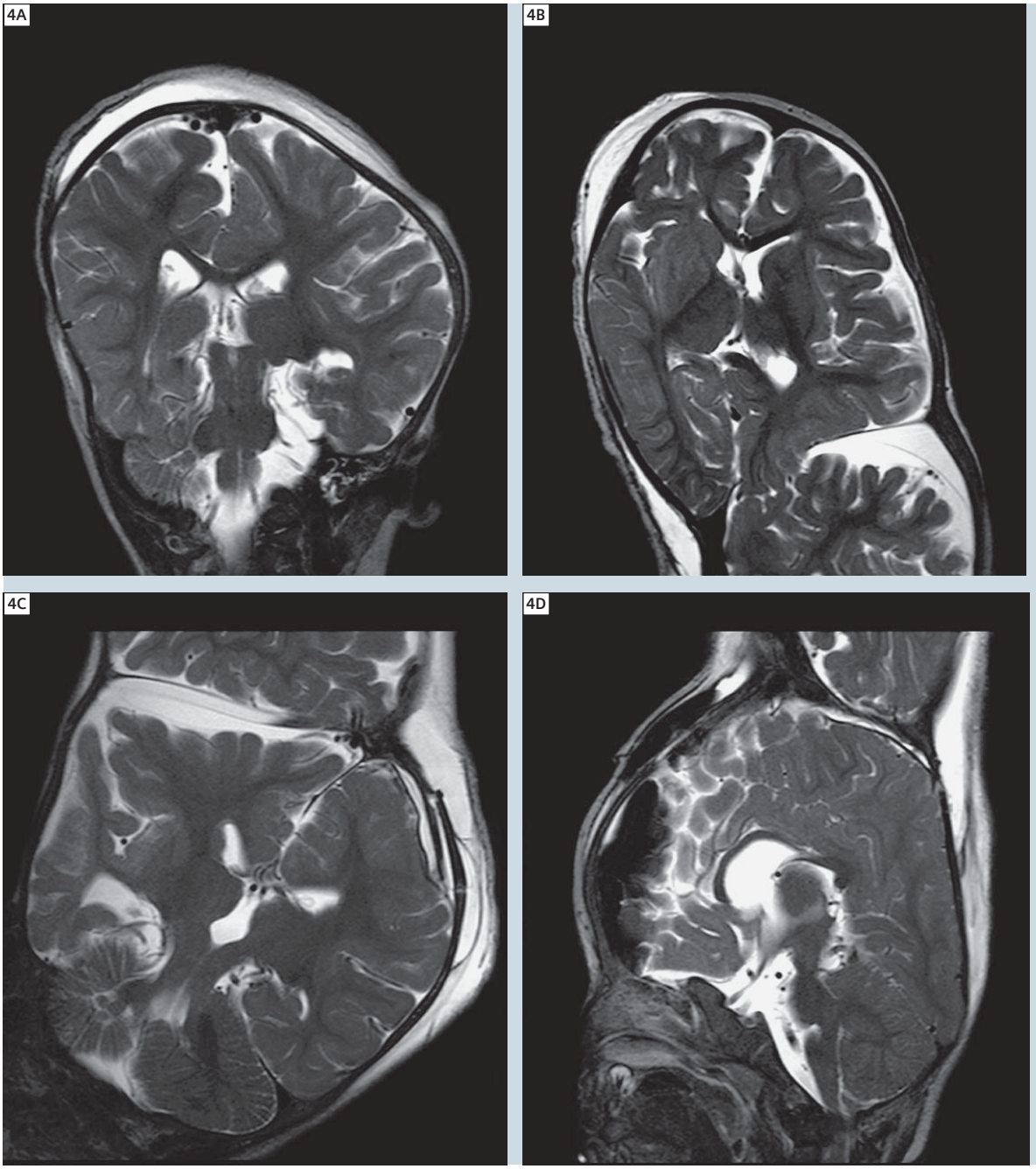

4 *syngo* SPACE was used to generate a high resolution data set with high T2 contrast. In combination with the 3D task card, an interactive and detailed image analysis can be performed retrospectively, improving the overall diagnostic accuracy.

useful in guiding the partial embolization and the following ligation process.

Comments

The use of *syngo* TWIST aided the surgical planning (4D InSpace) because it could be viewed as individual 3D volumes or as a dynamic 4D model. Data was used to generate a 3D physical model to plan subsequent surgeries. The neuroradiologists and neurosurgeon found the TWIST acquisitions more beneficial in planning surgery.

* The safety of imaging fetuses/infants has not been established.

Contact
Michael Kean
Children's MR Centre
Royal Children's Hospital
Melbourne, Australia
michael.kean@rch.org.au

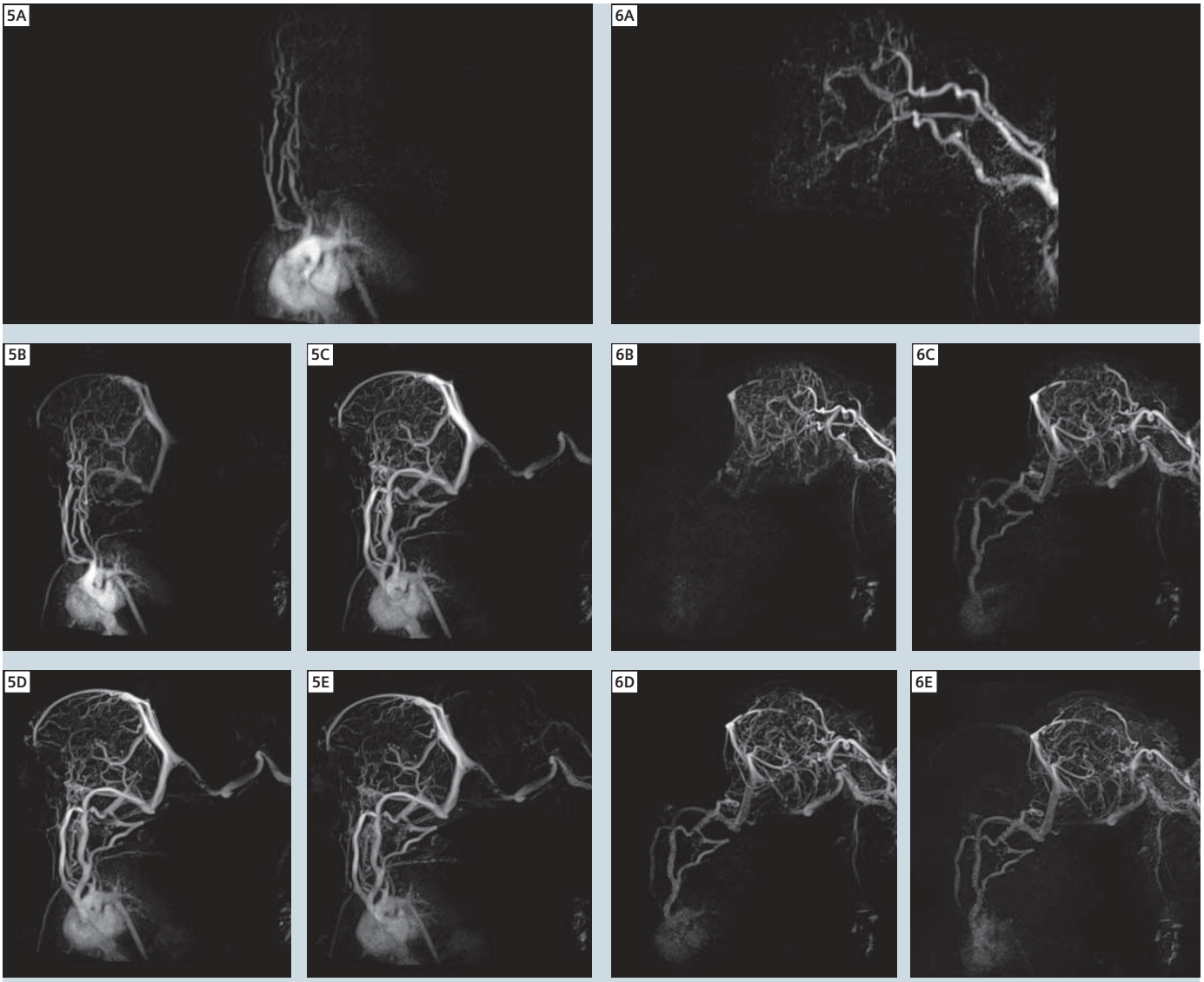

5 **6** *syngo* TWIST was used to evaluate vessel anatomy and especially to visualize the twin-twin venous connection; contrast media was injected in each twin separately. With a virtual temporal resolution of 2.29 sec and a resulting spatial resolution of 1.2 x 0.8 x 1.2 mm, *syngo* TWIST could provide detailed information about the anatomical and functional relationship of the venous connection between the twins (5A–E twin I, 6A–E twin II).

Case Report: Tuberculosis 4-Channel Flex Coil

Michael Kean; Michael Ditchfield, M.D.

Children's MRI Centre, Royal Children's Hospital, Parkville, Victoria, Australia

Patient history

5-year-old patient, a recent refugee from Africa, presented with restriction of movement and swelling. The plain radiograph demonstrated ill defined extensive lytic permeative lesion in the proximal third of radius. The MR was requested to further define the anatomical boundaries and to determine whether the pathology demonstrated was infective or a tumor.

Sequence details

The patient was positioned supine on the MR table or our 3T MAGNETOM Trio, A Tim System with the small 4-channel flex coil wrapped around the proximal forearm. Multiplanar Turbo Spin Echo images were acquired using SPAIR. Post-contrast imaging was obtained using water excitation VIBE.

Image findings

The appearances are suggestive of an indolent infection such as tuberculosis.

Comments

The use of SPAIR enabled consistent fat-suppression throughout the area of interest. The field-of-view (FOV) coverage of the small 4-channel flex coil was sufficient to cover the extent of the pathology. The high signal-to-noise ratio (SNR) characteristics of the coil enabled high spatial resolution (in-plane and through plane) in acceptable scan times.

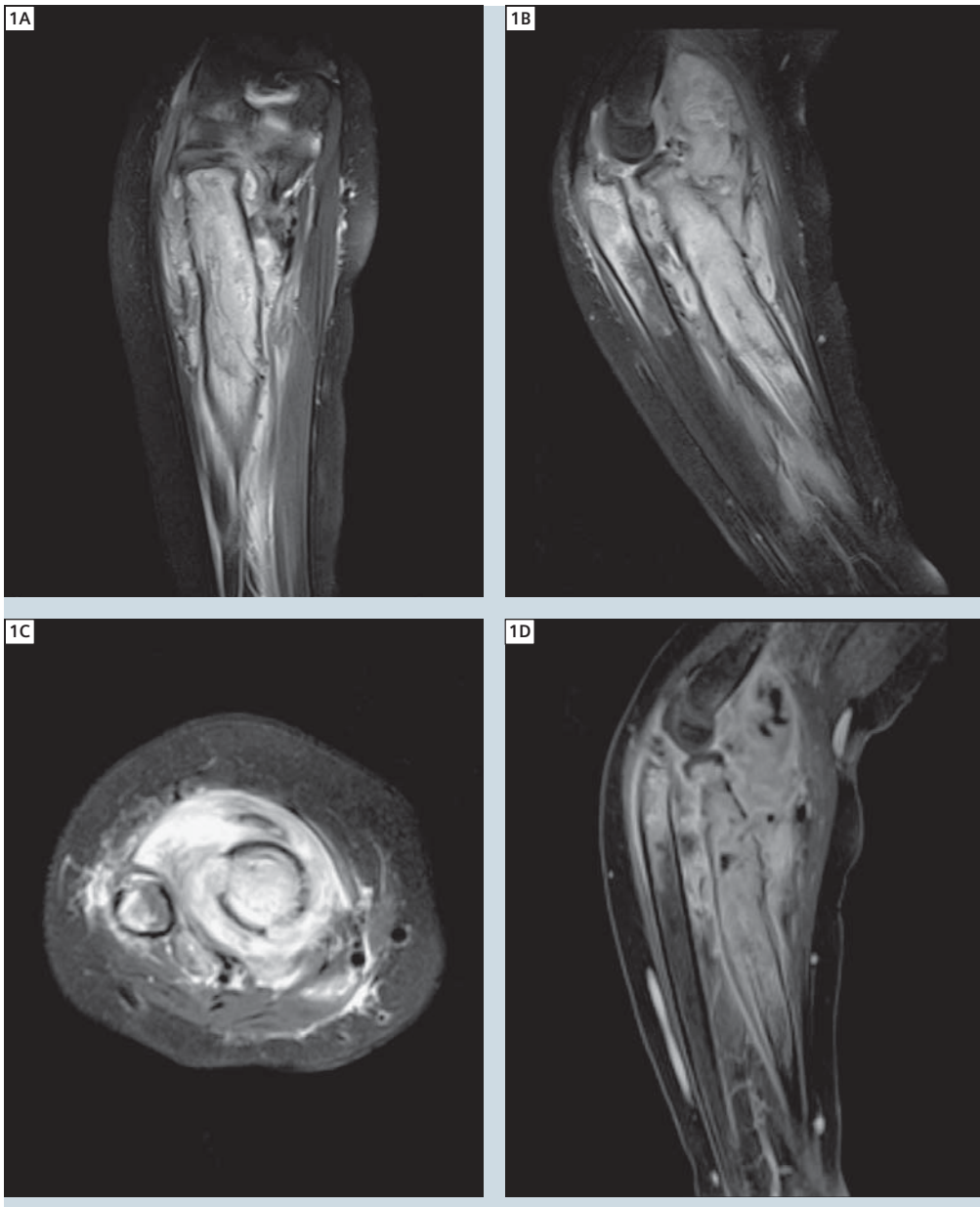

1 Multiplanar SPAIR images (Fig. 1A, coronal and Fig. 1B, sagittal) and fat-suppressed T1-weighted VIBE images after contrast (Fig. 1C, transversal and Fig. 1D, sagittal) are shown. All images have been acquired using the 4-channel flex coil, providing high signal-to-noise ratio and therefore detailed anatomical information about the pathology. The extend of the lytic involvement of the radius is well delineated. Note the excellent fat saturation in this anatomically difficult area.

Case Report: Abdominal Neuroblastoma

Michael Kean; Michael Ditchfield, M.D.

Children's MRI Centre, Royal Children's Hospital, Parkville, Victoria, Australia

Patient history

3-year-old* girl with a history of Neuroblastoma presented with urinary retention and constipation. Suspicion of spinal cord compression.

Sequence details

Transverse Turbo Spin Echo (TSE) sequence with *syngo* BLADE motion correction. TR 4000 ms, TE 99 ms, BW = 360 Hz/Pixel, Turbo Factor 35, slice thickness 5 mm, FOV 250 mm, Matrix 256 x 256. Images were acquired on our 1.5T MAGNETOM Avanto using the Body Matrix coil.

Image findings

Confirmation of intraspinal disease progression through neural foramin to form an extradural mass. There is impingement of the distal spinal nerve roots but no spinal cord compression. The MR clearly depicts greater disease extent than represented on the previous CT scan.

Comments

syngo BLADE was used to offset the motion of abdominal contents due to respiration. The images did not use any form of navigator based respiratory compensation.

Contact
Michael Kean
Children's MR Centre
Royal Children's Hospital
Melbourne, Australia
michael.kean@rch.org.au

* The safety of imaging fetuses/infants has not been established.

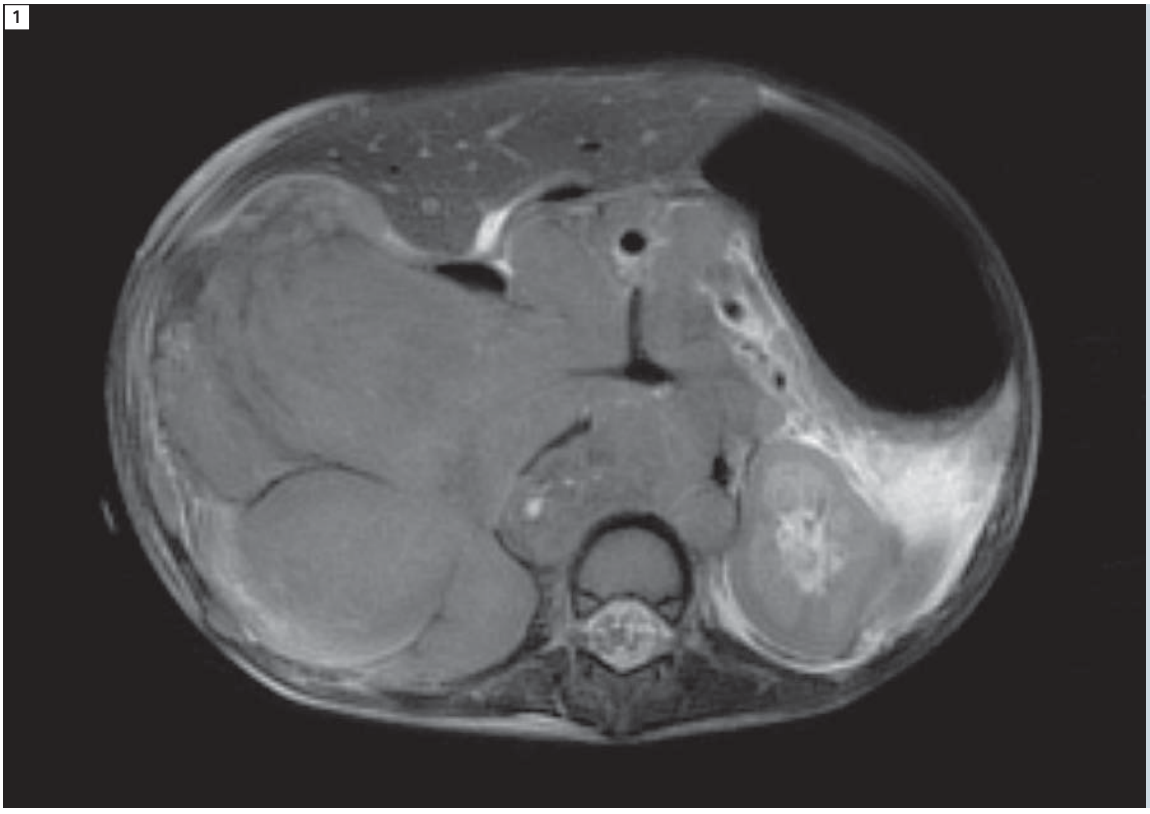

1 Transverse T2-weighted Turbo Spin Echo sequence with *syngo* BLADE motion correction was used in this case of a 3-year-old girl. This image was acquired while free breathing and without navigator based respiratory compensation, clearly demonstrating the potential of *syngo* BLADE in reducing motion artifacts. In this exemplary chosen transversal slice it is demonstrated that the extent of the abdominal neuroblastoma is well delineated and all relevant anatomical structures are visualized in detail.

Case Report: Thoracic Neuroblastoma

Michael Kean; Michael Ditchfield, M.D.

Children's MRI Centre, Royal Children's Hospital, Parkville, Victoria, Australia

Patient history

2-year-old* boy presented with fever and limp. Nuclear Medicine Bone Scan showed increased uptake in the left Ileum. Inflammatory markers continued to increase despite IV antibiotic treatment. Suspicion of Ewings Sarcoma, Abscess, Cellulitis.

Sequence details

Targeted T2-weighted FS imaging of the pelvis was performed on our 3T MAGNETOM Trio, A Tim System, using the Spine and Body Matrix coils. The images demonstrated abnormal widespread bone marrow signal intensity suggestive of a more complex pathology. STIR whole-body imaging was performed.

Image findings

Coronal whole-body STIR imaging demonstrated extensive marrow involvement in the pelvis, upper and lower extremities and L3 vertebral body. Targeted transverse T2-weighted imaging was performed on a large lobulated anterior mediastinal mass. The findings were consistent with a primary thoracic neuroblastoma with extensive marrow deposits and local lymph node involvement.

* The safety of imaging fetuses/infants has not been established.

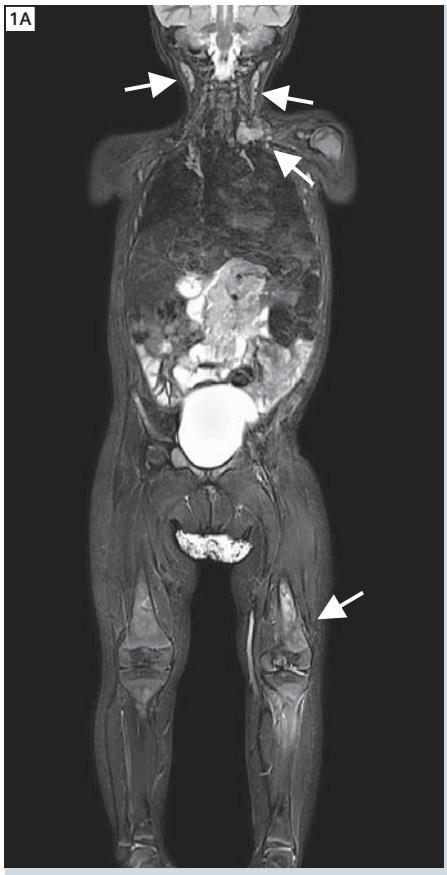

1A T2-weighted TIRM images of the pelvis with spectral fat suppression, demonstrating the abnormal widespread bone marrow signal intensity. Also, a large anterior mediastinal tumor was found in this 2-year-old* boy.

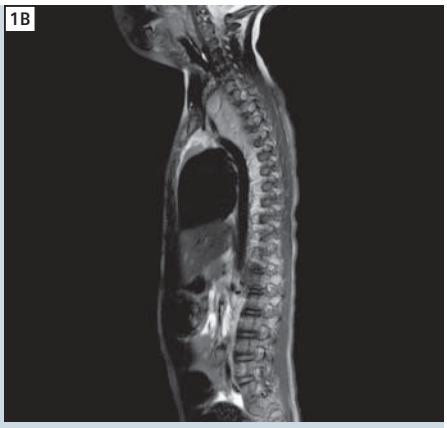

1B The craniocaudal extend of this large tumor mass is well visualized on the sagittal T2-weighted whole-spine image.

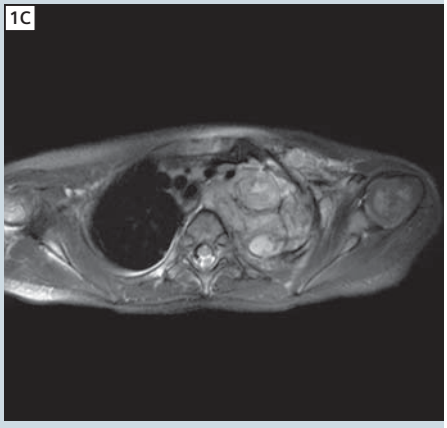

1C Demonstrates the expansive spread of the thoracic lesion. Histopathology revealed a neuroblastoma.

The Flexibility of the 4-Channel Flex Coil

Heike Wein; Nina Kaarmann

Siemens Healthcare, Erlangen, Germany

4-channel Flex coils come in two sizes (Fig. 1). Both are very flexible, with superior signal-to-noise ratio, and can be used almost universally. Furthermore, *syngo* BLADE motion correction functions extremely well with Flex coils, producing optimum results.
The smaller version of the coil can be used for small to medium-sized shoulders (e.g. of children), the elbow (Fig. 2), the wrist (Fig. 3), and for smaller feet or the forefoot (also refer to the use of Flex coils in pediatric imaging as shown in the case studies by Michael Kean on page 57 ff).

The larger coil is suitable for use on the hips, knee (Fig. 4), or ankle. If a Body Matrix coil is positioned on the liver and the large Flex coil on the pelvis, the entire abdomen can be covered.
Here is an example for displaying the entire foot – from the tip of the toes to the ankle – using a fast protocol.
The patient is positioned on his side. The Spine coil is used from below, and the large Flex coil is positioned on top of the foot. The foot is then immobilized with sandbags (Fig. 5). If the foot is positioned properly, parallel imaging can be used in heel – toe direction and in Spine coil – Flex coil direction, that is, axial/transverse and sagittal.

→ **Visit www.siemens.com/magnetom-world** to download this protocol as Phoenix image.

1 CP Flex coil large and small.

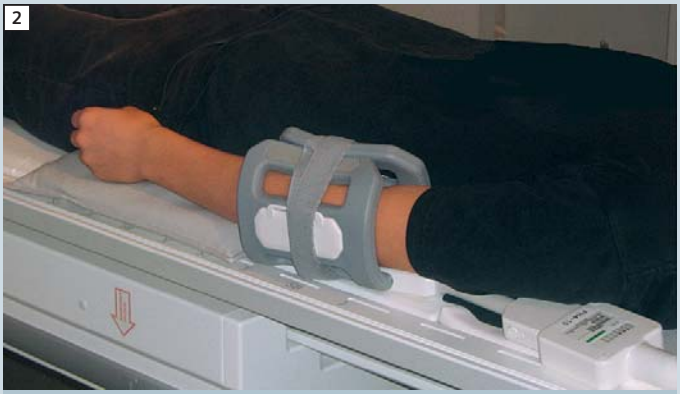

2 Small Flex coil for elbow imaging.

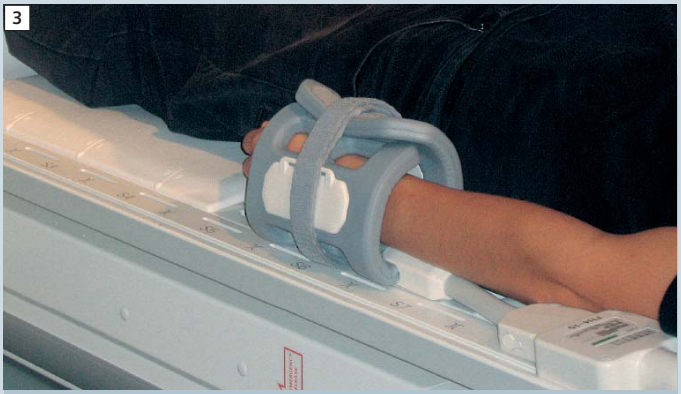

3 Small Flex coil for wrist imaging.

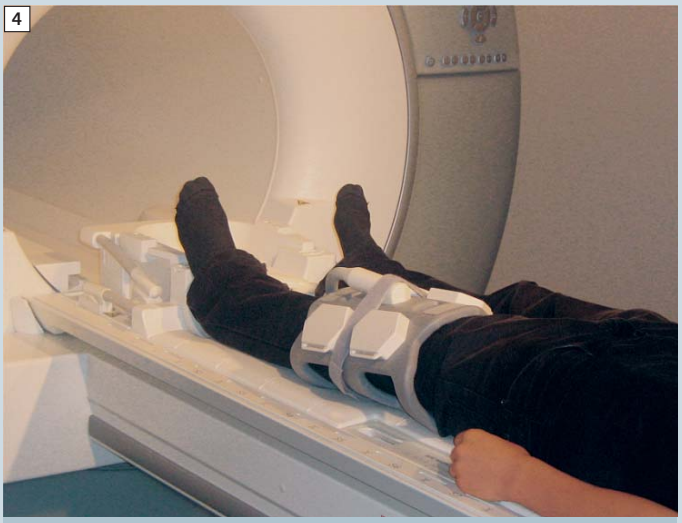

4 Large Flex coil for knee imaging.

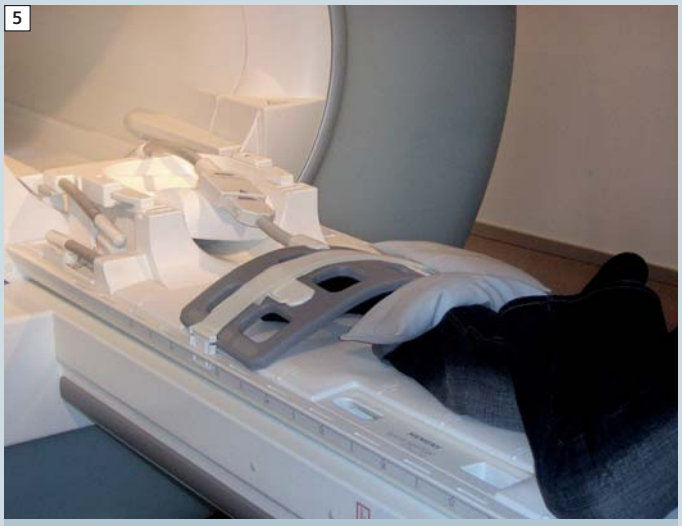

5 Patient positioning for fast whole foot imaging.

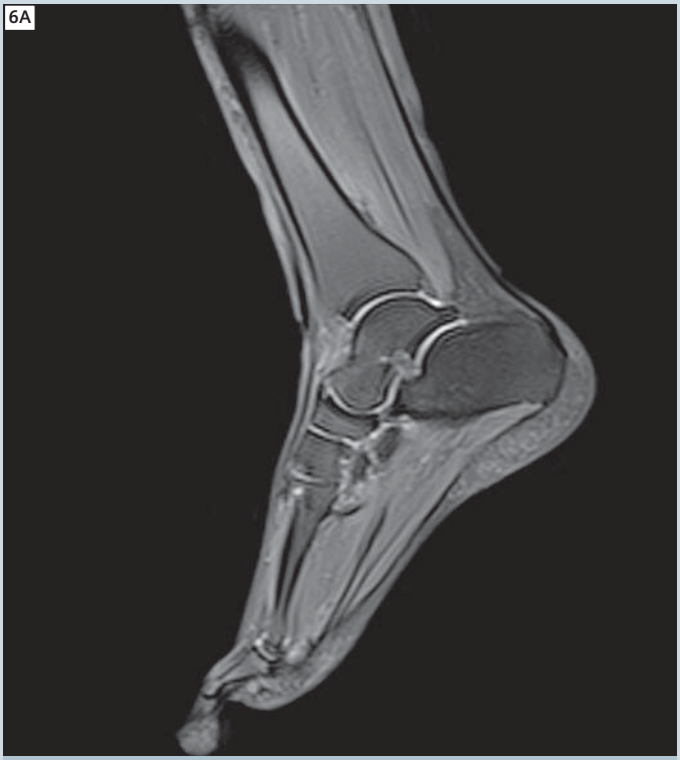

6A 3T MAGNETOM Verio, PD Turbo Spin Echo (TSE) using spine and large Flex coil. TR 3000, TE 47, TA 42 sec, SL 3 mm, slices 19, FOV 330 x 330 mm, matrix 205 x 256, GRAPPA 2.

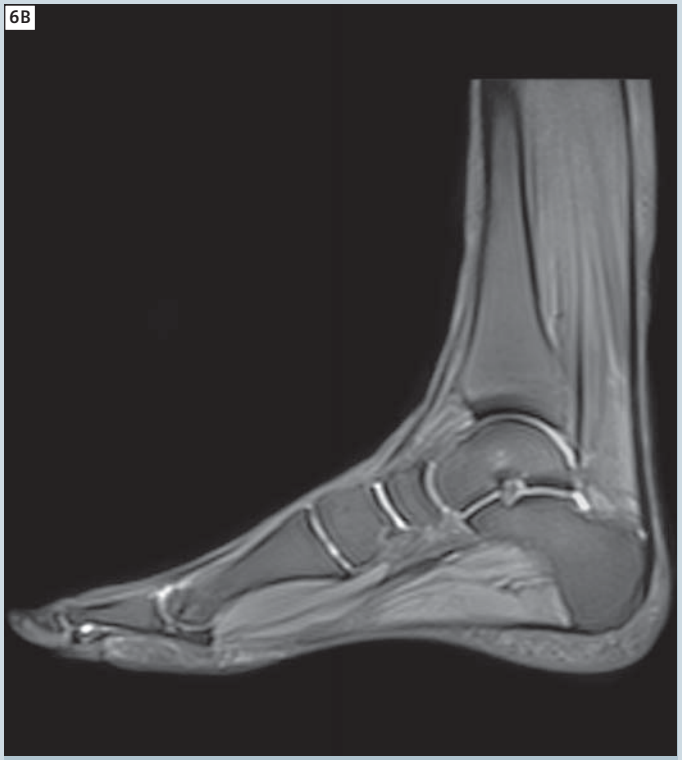

6B 3T MAGNETOM Verio, PD Turbo Spin Echo (TSE) using the Foot Ankle Coil. TR 3000, TE 47, TA 42 sec, SL 3 mm, slices 19, FOV 330 x 330 mm, matrix 205 x 256, GRAPPA 2.

Contact
Nina Kaarmann
Siemens AG – Healthcare Sector
MR Marketing, Green Team
Karl-Schall-Str. 6
D-91052 Erlangen, Germany
+49 (0)9131-84-5547
nina.kaarmann@siemens.com

Let's TWIST again: Temporal and Spatial High-Resolution 3D MR-Angiography of the Hand

Anton S. Quinsten[1]; Stefan Maderwald[1,2]; Katja Seng[1]; Birayet Uçan[1]; Harald H. Quick[1,2]

[1]*Institute for Diagnostic and Interventional Radiology and Neuroradiology, Essen University Hospital, Essen, Germany*
[2]*Erwin L. Hahn Institute for Magnetic Resonance Imaging, University of Duisburg-Essen, Germany*

Compared to conventional contrast-enhanced MR angiography (MRA), which provides a spatial high-resolution three-dimensional (3D) MRA data set of the vascular target region, MRA with TWIST (time-resolved angiography with stochastic trajectories) with its high temporal resolution offers an additional dynamic component. It presents a broad range of advantages for all vascular diagnostic questions where blood flow dynamics play a role. For example, an angiographic 3D display with high temporal resolution is a prerequisite for evaluating arterio-venous malformation (AVM), as well as venous malformations (DVM) in the brain, aortic dissections or vascular shunts. Data acquisition with the *syngo* TWIST sequence creates a series of high-resolution 3D MRA data sets that together contain this dynamic information. Additionally, the acquisition of multiple measurements in rapid succession renders the aspect of contrast agent timing less critical. For the reasons indicated above, *syngo* TWIST examinations are gaining in clinical relevance. From a technical perspective, one challenge to this examination is the relatively high storage capacity required for data acquisition and subsequent reconstruction, whereby data reconstruction of all dynamic 3D MRA data sets requires several minutes. From a medical perspective, the challenge lies in the relatively large number of images to be acquired and diagnosed. For this reason, the data to be reconstructed (source images, subtractions, maximum intensity projections (MIP), etc.) should be clarified beforehand with the physician.
In the following, we report on the use of time-resolved TWIST-MRA of the hand and present a possible examination sequence. We begin, however, by taking a brief look at the theory behind TWIST data acquisition.

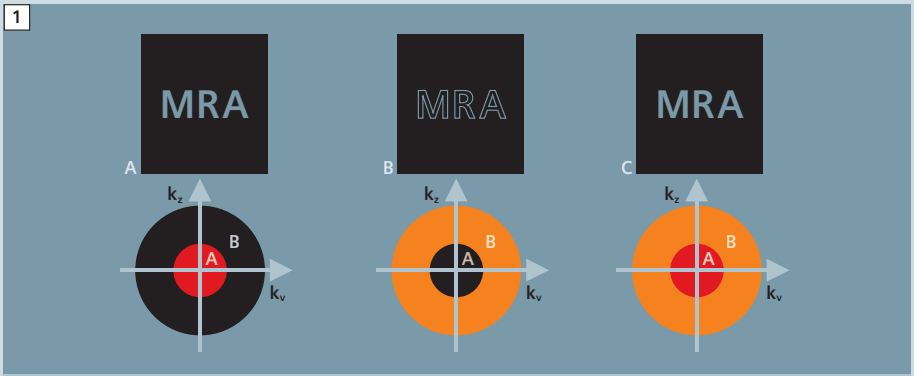

1 Reconstruction of a 3D data record: (A) only the inner k-space (Region A, core) was reconstructed. Contrast is available, but the sharp structures/edges and detailed information are missing in the reconstructed image. (B) Only the outer k-space (Region B, mantle) was reconstructed. Sharp edges (high spatial frequencies) are visible, but contrast is missing from the reconstructed image. (C) The full k-space (Region A + Region B) was reconstructed. It takes the reconstruction of Regions A+B to produce a sharp, contrast-enhanced image.

Theory of *syngo* TWIST data acquisition

Before an image can be reconstructed in MRT, the acquired data have to be stored in a specific order in a raw data matrix, the so-called k-space. Generally, the central k-space (Region A) contains the information that delivers image contrast after reconstruction. In contrast, the peripheral portion of the k-space (Region B) contains the information that delivers image details after reconstruction. Only both k-space regions together deliver a sharp, full-contrast image or a sharp, contrast-enhanced 3D MRA data set after reconstruction (Fig. 1). By varying the percentage sizes of Regions A and B, the examining physician can largely vary the contrast or resolution of a TWIST data set. During TWIST acquisition, the previously determined size of Region A is always filled completely. It is in this area that one expects the greatest changes in contrast due to the inflow of contrast agent. Region B is also completely covered in a single measurement, but it is sampled with a reduced sampling density . As a result, multiple passes through B are required to obtain the data from Region B with full density. However, missing points in k-space can be supplemented from previous or future measurements of Region B to calculate a complete 3D MRA data set at any time.

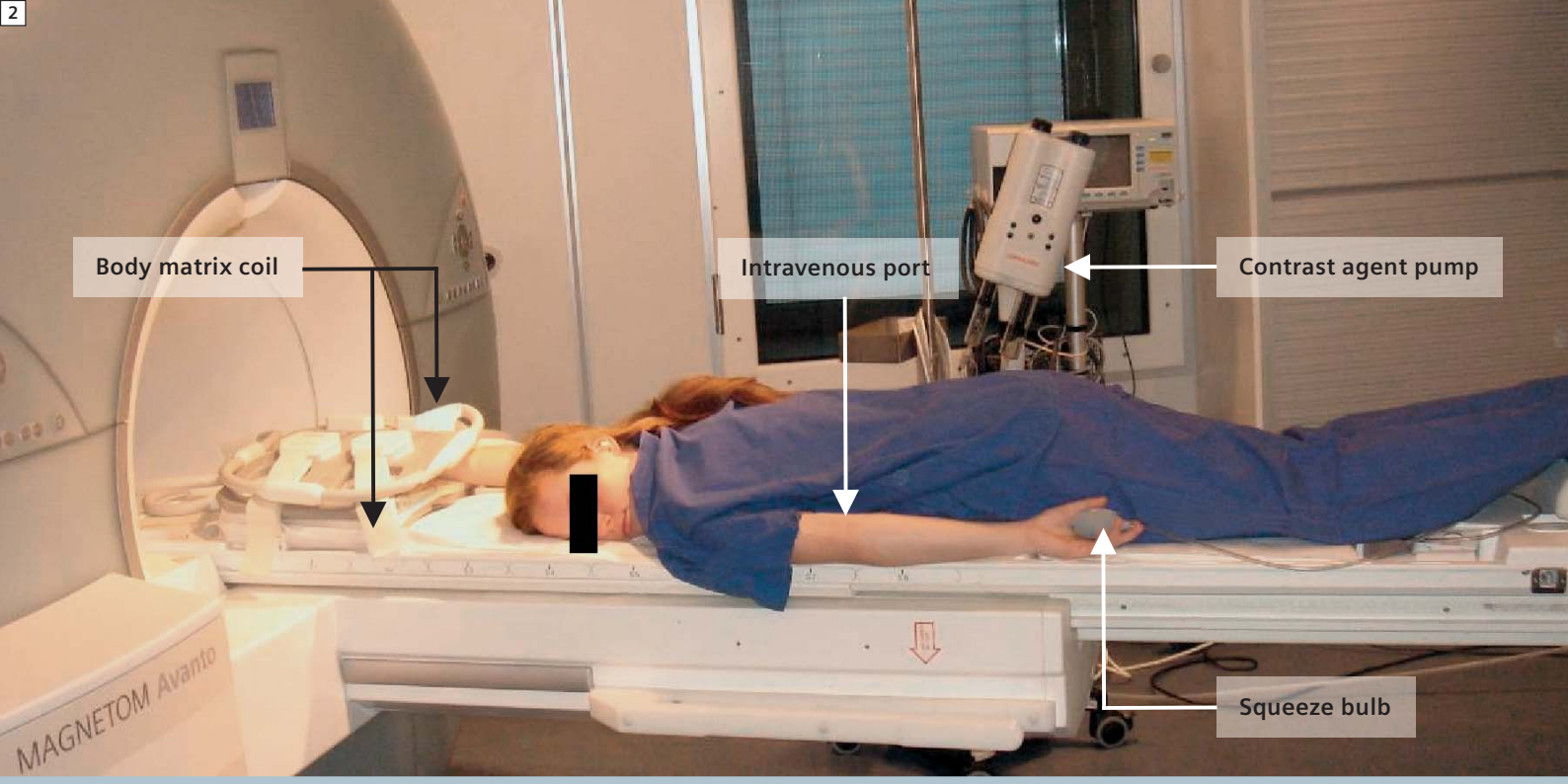

2 Patient positioned on tabletop of a 1.5T Siemens MAGNETOM Avanto system.

The most frequent clinical indications for TWIST MRA of the hand

There are numerous clinical indications for dynamic MR angiographic examinations. Examples include:

- General vascular pathologies
- Vascular malformations
- Hemangioma
- Arterio-venous (AV) fistulas
- Vascular insufficiency
- Raynaud syndrome
- Scleroderma
- Rheumatism
- Tumorous diseases
- Surgical planning e.g., to clarify if surgery is possible

Patient preparation and positioning

As with all MRT examinations, the patient should first read the internal hospital questionnaire regarding possible contra-indications, and then complete and sign a consent form for the examination. Based on this information, the radiologist meets with the patient to answer any questions and discuss possible risks associated with the examination, such as contrast agent side effects. A current creatinine and glomerular filtration rate (GFR) value should be available for the patient. If it is not in the normal range or if the patient is intolerant to contrast agents, special precautionary measures are required, such as corresponding premedication or targeted hydration (oral or infusion) before and after contrast agent administration. After the patient puts on MR-suitable hospital clothing, an intravenous port is set up in the arm not being examined (at least 22 gauge). It now has to be ensured that the patient has removed all metal objects (e.g., glasses, watch, coins, etc.) before entering the examination room. These represent primarily a potential hazard, but could also interfere with the examination (metal artifacts) or be damaged. This entire procedure ensures that the patient is fully informed and agrees to the examination, and that all potential risks have been minimized, so that the MRT examination can now be performed safely.

In the examination room, the patient receives hearing protection (for this examination, earplugs are preferable to headphones) and is placed in the prone position (Fig. 2). The arm to be examined is extended forward (the legendary "Superman pose") and "sandwiched" between two Body Matrix coils. The other arm is positioned along the body pointed toward the back, and is equipped with the squeeze bulb. Using positioning cushions, sandbags, and if necessary vacuum cushions, a comfortable position is ensured for the patient, while his finger or hand to be examined is immobilized. It is necessary to ensure that the area to be examined is placed in the isocenter of the coil to the fullest extent possible, and remains as far as possible in an unbent position. Through this optimal positioning, smaller fields of view (FOVs) can be used (improving spatial resolution) for example, and fewer slices are necessary (increasing temporal resolution). The optimized position (extended finger, straight back of the hand) ensures the optimal diagnostic course of the vessels. From a technical view, these simple measures optimize temporal and spatial resolution. From a medical perspective, they optimize the examination results.

Before the actual examination can begin, and while the contrast agent pump is being connected, the patient should be reminded again regarding motion artifacts and asked to lie still during the entire examination and to not move his fingers or hand.

Performing the examination

The complete *syngo* TWIST MRA examination of the hand generally takes less than 5 minutes (excluding patient positioning and data reconstruction). First, fast "three-plane localizers" are taken to localize the region of interest (ROI). Ideally, the TWIST data should be acquired in coronal orientation. The *syngo* TWIST measurement is started simultaneously with the contrast agent injection. The TWIST sequence acquires 29 consecutive T1-weighted data sets where A = 20% and B = 10%, as well as with GRAPPA (iPAT R = 2). The protocol parameters are: TR/TE = 2.92 ms / 1.2 ms, FA = 25°, FOV = 260 mm x 162.5 mm, slices = 36, bandwidth = 650 Hz/Px, with an acquisition matrix of 384 x 240 pixels. This

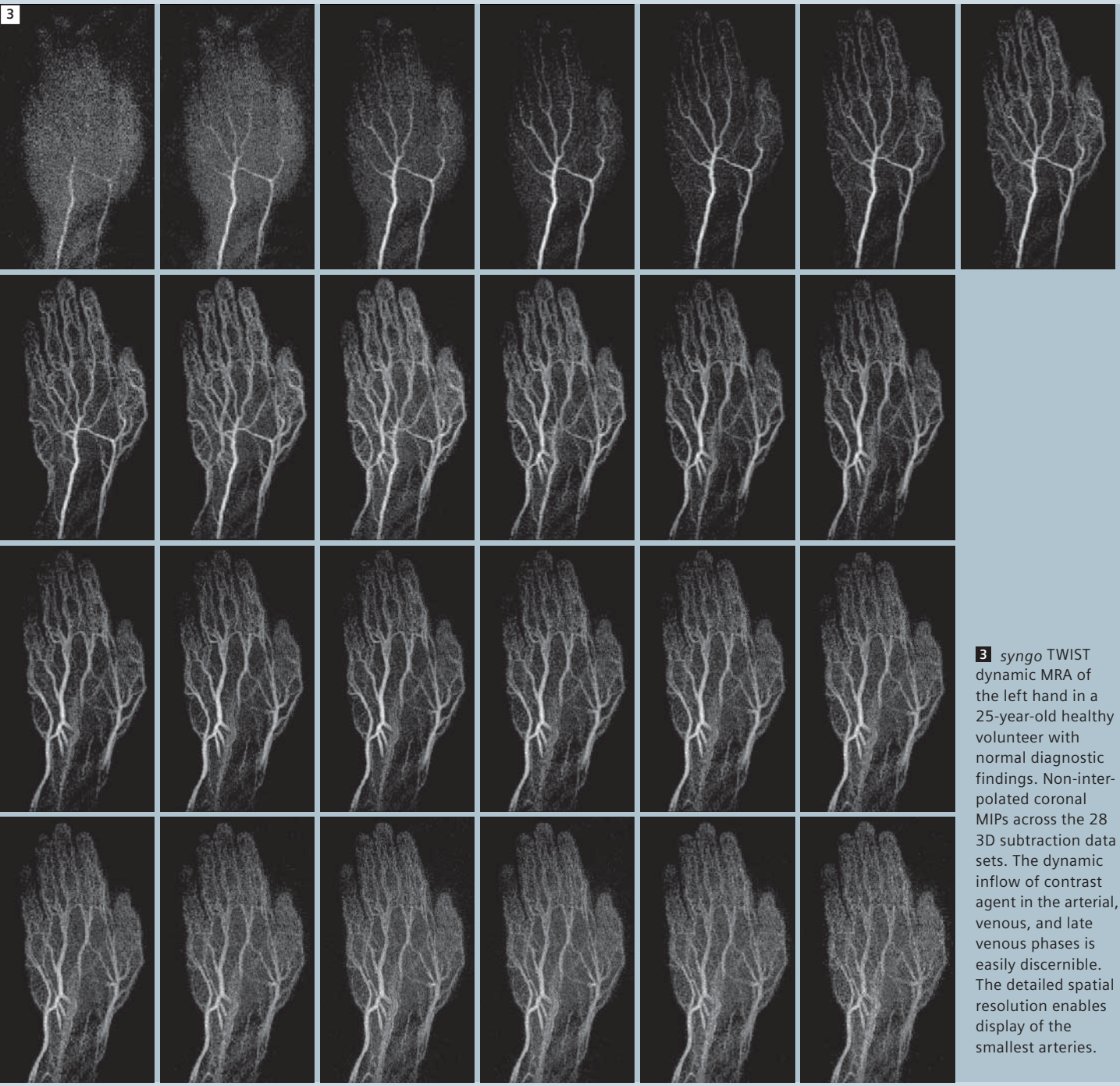

3 *syngo* TWIST dynamic MRA of the left hand in a 25-year-old healthy volunteer with normal diagnostic findings. Non-interpolated coronal MIPs across the 28 3D subtraction data sets. The dynamic inflow of contrast agent in the arterial, venous, and late venous phases is easily discernible. The detailed spatial resolution enables display of the smallest arteries.

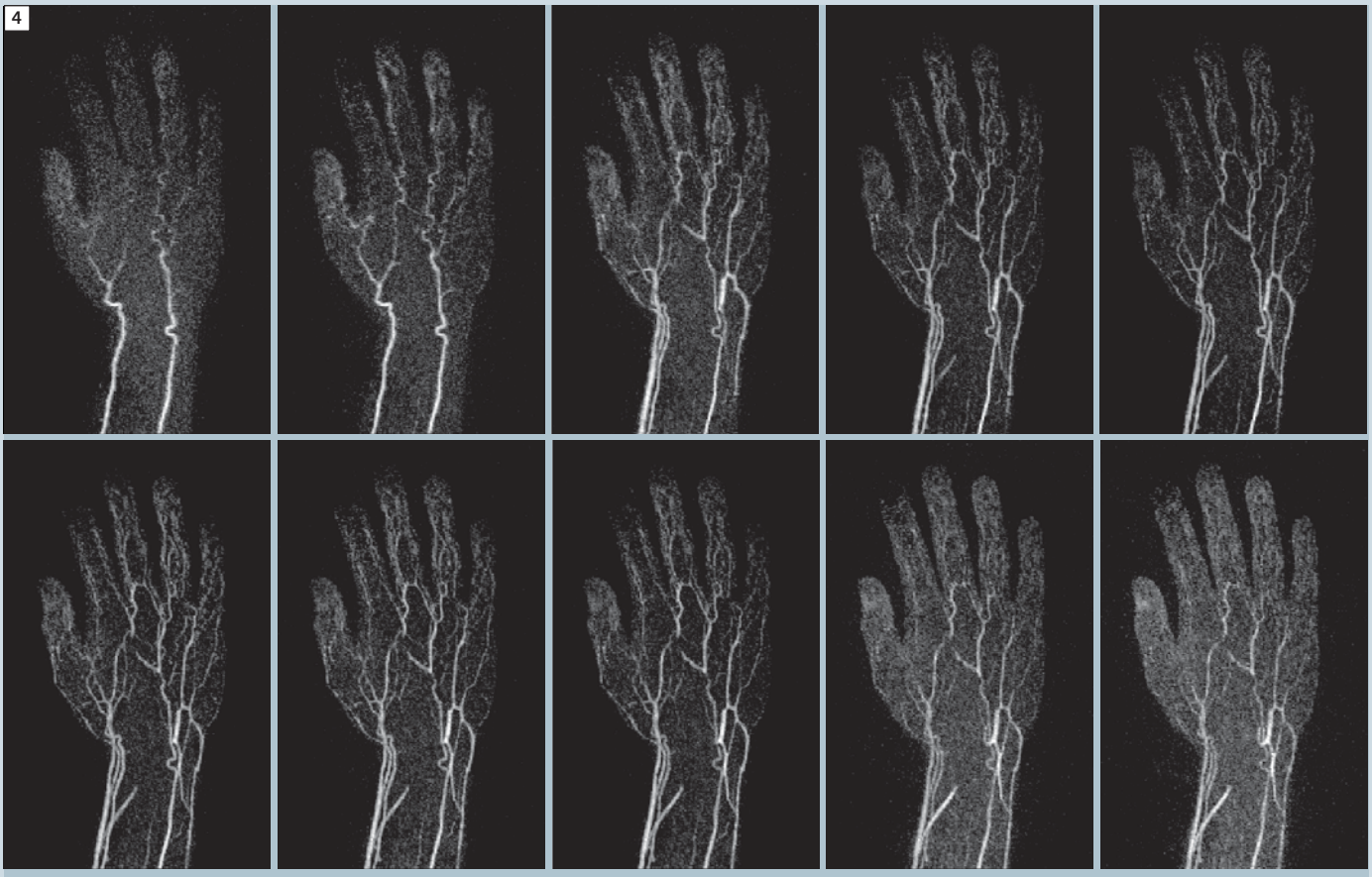

4 *syngo* TWIST dynamic MRA of the right hand for a 47-year-old female patient with functionally incomplete deep and superficial palmar arch. It shows extremely sparse contrasting of the vessels in the thumb (D1) and index finger (D2). 10 of 28 acquired contrast phases are shown.

results in a non-interpolated spatial/temporal resolution of 0.7 mm/0.7 mm/0.7 mm/3.2 sec. These 29 measurements produce a total of 29 raw/source data sets, with 29 subtraction data sets and up to three MIP data sets (ax, cor, sag), which also offer the opportunity to temporally interpolate the dynamic data (Figs. 3 and 4). In total, more than 2000 individual images are reconstructed during this examination.

Conclusion

The use of temporal and spatial high-resolution 3D TWIST MRA in angiographic diagnostics of the hand enables a spatial display of vascular pathology comparable to that of conventional static 3D MRA, while at the same time generating additional dynamic information. This information was previously available only through invasive digital subtraction angiography (DSA) or intravascular ultrasound.

References

1 Brauck K, Maderwald S, Vogt FM, Zenge M, Barkhausen J, Herborn CU. Time-resolved contrast-enhanced magnetic resonance angiography of the hand with parallel imaging and view sharing: initial experience. Eur Radiol. 2007 Jan;17(1): 183–92.

2 Brauck K, Vogt FM, Maderwald S, Ladd SC, Kroeger K, Laub G, Kroeker R, Quick HH, Barkhausen J. Time-resolved MR-angiography (TWIST) of the hand in comparison to digital subtraction angiography (DSA). In Proc. International Society for Magnetic Resonance in Medicine (ISMRM), 19–25 May 2007, Berlin, p. 2491.

Contact
Anton S. Quinsten
Institute for Diagnostic und Interventional Radiology and Neuroradiology
University Hospital Essen
Hufelandstr. 55
D-45122 Essen
Germany
anton.quinsten@uni-due.de

The Impact of Tim Planning on Workflow Initial Experience

Mark Lourensz

St. Vincent's Hospital Melbourne, Fitzroy, Victoria, Australia

Introduction

MRI is the modality of choice for imaging many systemic and pathological conditions. In our practice it is becoming more and more common to see requests for whole body or multi-region exams to evaluate and monitor a number of disease processes. This is a challenge from a number of points of view. Although we are here primarily to provide a service to our referral base and patients, we also need to be able to integrate these cases into our daily practice in a timely manner. Examination times need to be kept short to maintain patient tolerance and aid in general workflow. The set up and planning of these studies also needs to be straight forward so image quality can be maintained over a wide range of patients and imaging technologists. In the past we have successfully carried out these examinations, but they have often been time consuming and in some cases involved several visits to the MRI centre. With the installation of our 1.5T Siemens MAGNETOM Avanto scanner, and the recent upgrade to software version *syngo* MR B13, a number of tools have become available to us that have allowed the easy integration of whole body scanning in our daily schedule and streamlining of our workflow.

Technical Considerations

The smooth integration of both hardware and software on the current Siemens Tim (Total imaging matrix) system has had an immediate impact on the planning and ease of implementation of a number of our whole body and multi-region scanning protocols. We have had access to the Tim system and the integrated Parallel Acquisition Techniques (iPAT) for a number of years, but the introduction of several new software packages has streamlined the implementation of this whole process.
The key elements include:

Tim Planning Suite

Set-n-Go protocols – this has allowed us to develop and save a number of streamlined protocols in a compressed protocol tree using the set-n-go function provided in this technique. Protocols range from whole spine to whole body exams and together with the Tim planning UI allows efficient planning of these studies.

Inline Composing: As the name suggests this automatically stitches together multiple images to provide an extended view of the scanned area. This is particularly useful for scout images where an overall view can be taken of the whole body or spine for example, and subsequent imaging can then be planned over the area of interest. This ensures the region of interest is always covered, and multiple areas can be scanned with the minimal number of sequences and table moves to perform the examination.

Coupled Graphics: This allows all graphic proscriptions – sat pulses and sequences,

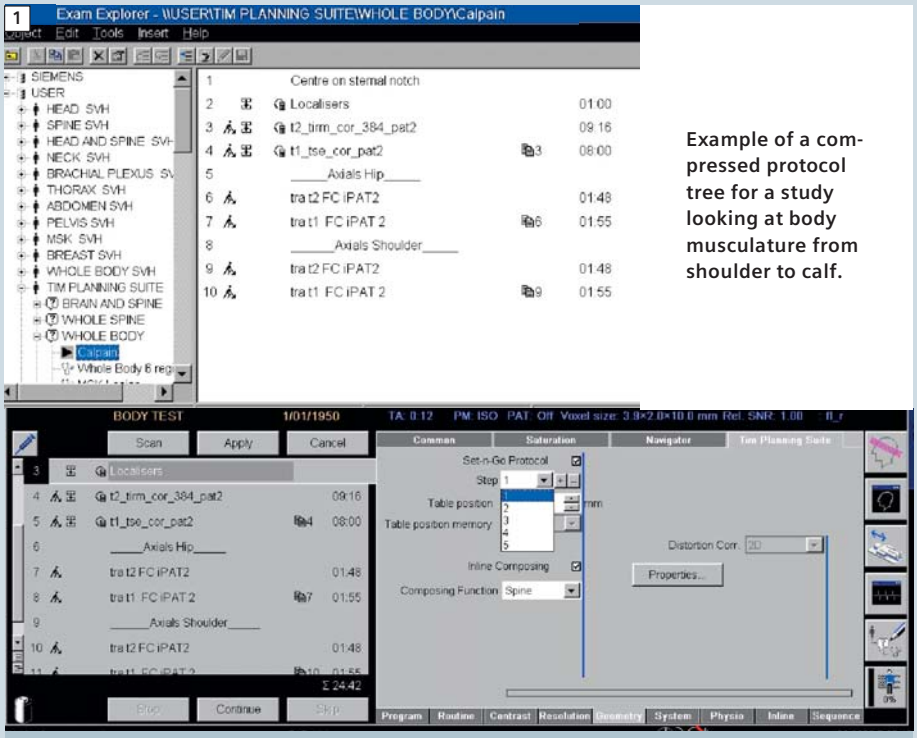

Example of a compressed protocol tree for a study looking at body musculature from shoulder to calf.

1 Localiser showing Set-n-Go protocol with 5 table positions.

to be grouped together and positioned and moved as a single unit. This is particularly useful for whole body scanning and multi-region angiography when we intend to display the end product as a composed image and maintain full coverage.

Scan at Center: This ensures all imaging is performed in the center of the bore, maximising homogeneity and shim for fat saturation techniques. This is especially important for large field of view studies and where multiple transverse sequences are required for our body and spine work. The above techniques have allowed us to develop and implement a number of multi-region imaging protocols into our daily practice. We believe the resulting protocols are efficient, provide good diagnostic results, and are able to be applied consistently by a number of technologists with varying skill levels. What has been in the past a time consuming and complex set of examinations has been greatly streamlined with a concomitant improvement in workflow and ease of application. The exams in which this technique has found constant use are:

1. Whole body screening for
- metastatic disease
- systemic disease

2. Neuro axis screening for
- primary investigation of pathology
- tumor staging / recurrence
- monitoring of disease progress e.g. MS
- primary investigation of idiopathic conditions

3. Multi area exams for
- multi-organ / system problems
- patients with multiple disease processes
- extensive MSK lesions

The Tim Planning Suite is now an integral part of all our multi-region examinations and provides both a technologist and patient friendly platform. We are now able to integrate these exams into our daily workflow in a time and cost efficient manner.

Contact
mark.lourensz@svhm.org.au

2

2 Tim Planning user interface (UI) showing composed scout image, coupled graphics, Auto-Coil Select, and scan@center all in use.

→ Application Tip

Planning of sagital slices can be problematic on patients with degenerative spinal disease, scoliosis and kyphosis. In these cases we find a further scout image consisting of a single coronal HASTE slice, 50–70 mm thick, positioned over the spine at each level, yields a very nice myelographic image to allow the accurate planning of sagital slices.

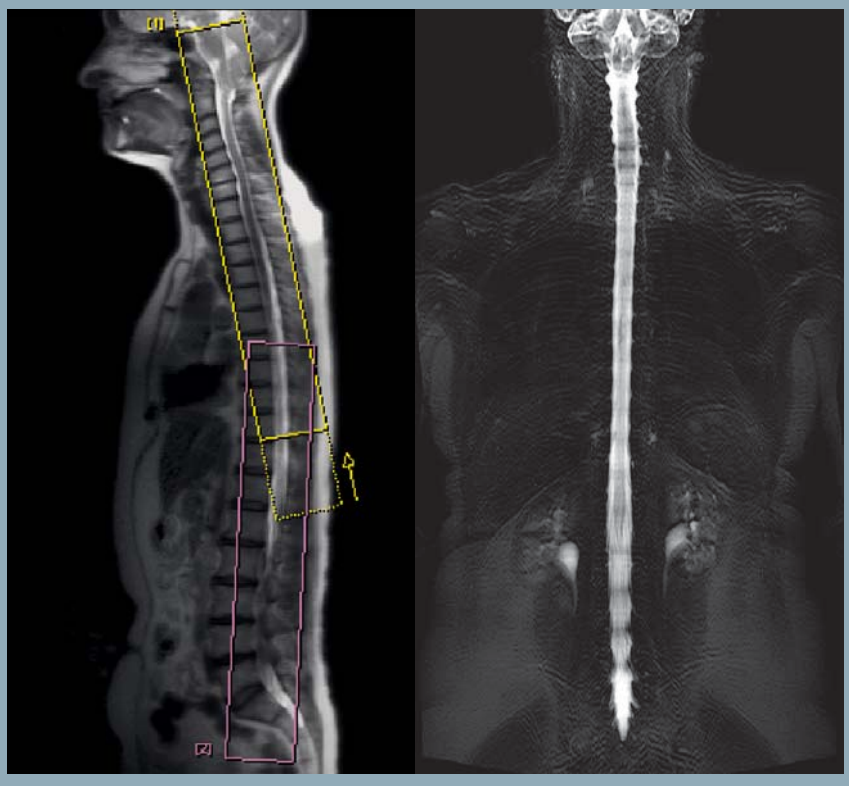

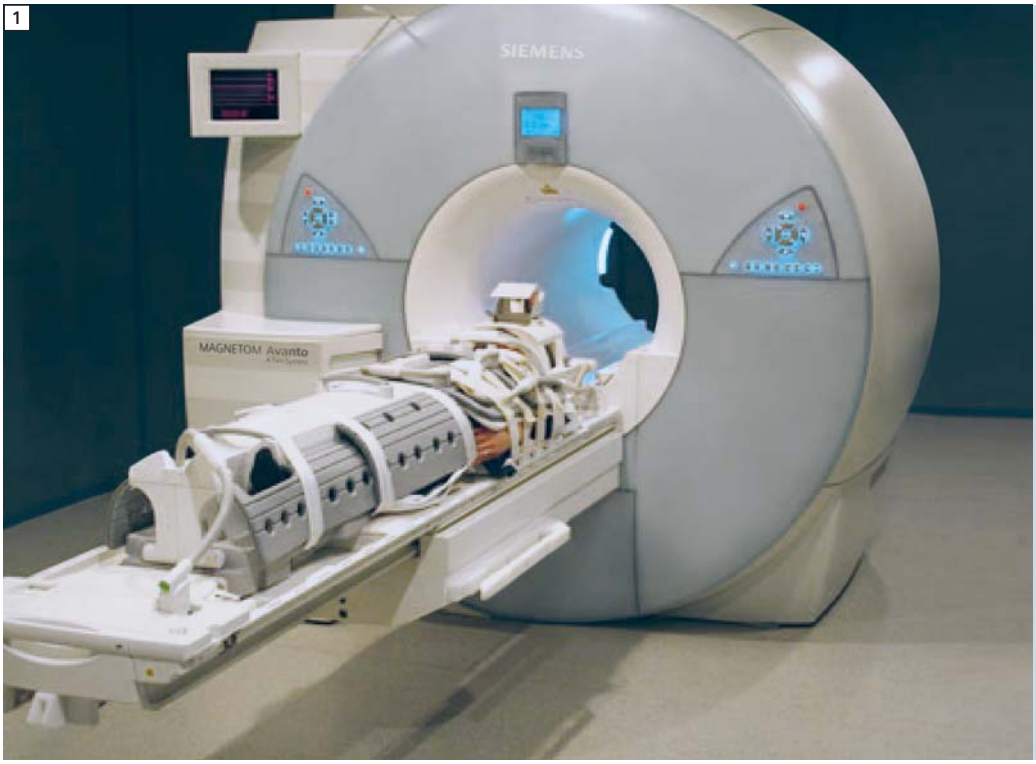

1 Patient with multiple coils applied in preparation for a whole body study.

Whole Body MRI – Recent Applications

M. Seale, M.D.; M. Lourensz; N. Trost, M.D.; Prof. O. Hennessy, M.D.

St. Vincent's Hospital Melbourne, Fitzroy, Victoria, Australia

Background

Whole body Magnetic Resonance Imaging (MRI) has been established in the imaging literature as a legitimate staging technique and realistic alternative to multimodality conventional staging methods (e.g. Computed Tomography (CT), bone scan) for patients with known malignancy where presence and location of metastases may affect treatment and prognosis [1, 2, 3]. However, MRI examination of the whole body or a large portion of it may also be useful in evaluating non-neoplastic conditions. Distribution of extensive local lesions and of multi-organ systemic disease may be assessed and monitored, providing useful clinical information.
High soft tissue contrast, high spatial resolution, multiplanar capability and lack of ionizing radiation make MRI a suitable modality for examining large areas of the body, particularly in patients who may need numerous follow-up studies in their lifetime. Recent technological advances in MR hardware and software have allowed decreased scan times, without compromising image quality.

Technical innovations enabling whole body MRI

Hardware

Moving table: No repositioning of patient is required during the scan, with 205 cm z-axis coverage on our 1.5T MAGNETOM Avanto.

Integrated coil system: With Tim – the Total imaging matrix – multiple phased array coils are applied simultaneously avoiding the need to change coils mid-exam.

Continued on page 80

Renal Cell Carcinoma

Case 1

68-year-old male with known right renal mass, and increased uptake in right humerus, right intertrochanteric region and left femoral shaft on bone scan **(Fig. 2)**.
Whole body STIR coronal MRI demonstrates the renal mass & confirms the metastases seen on bone scan **(Figs. 3–5)**. Numerous additional bone metastases were identified – in the right ischium, left acetabulum and intertrochanteric regions and left glenoid **(Figs. 4, 6, 7)**.

2

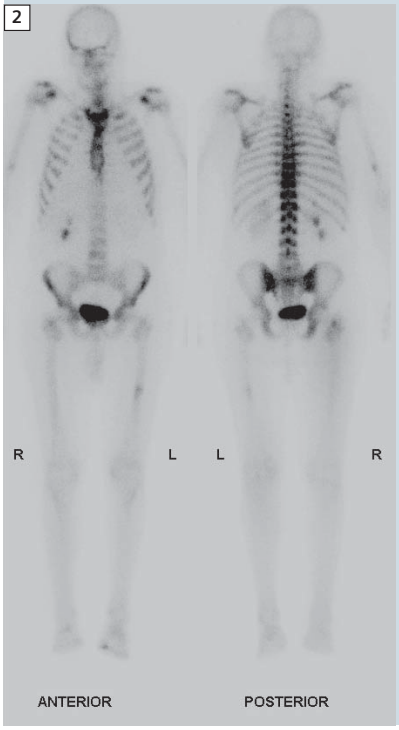

3

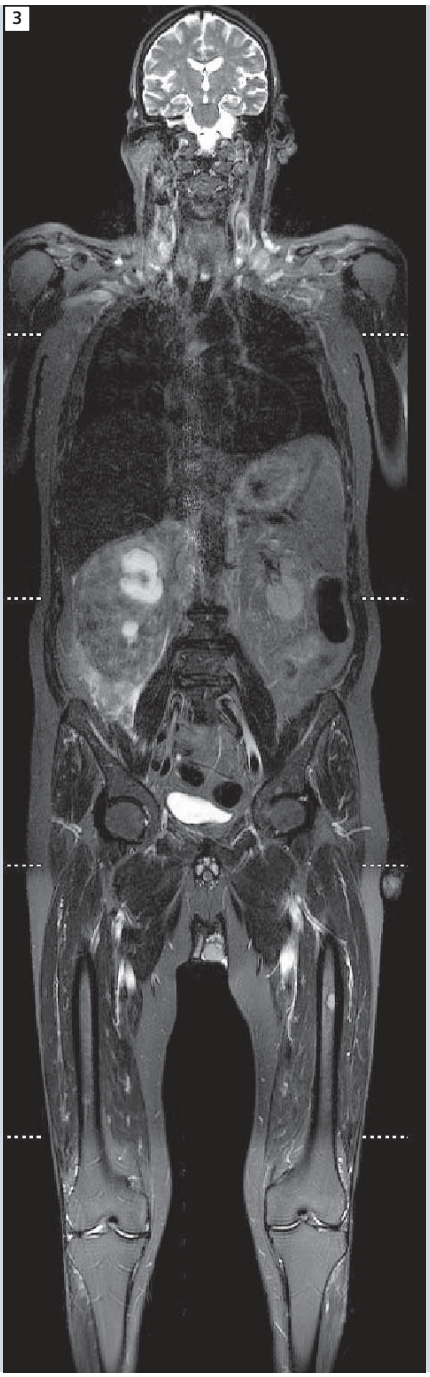

4

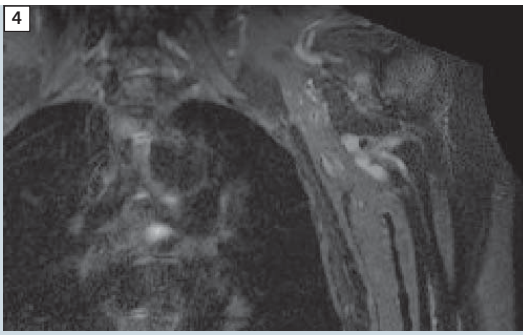

5

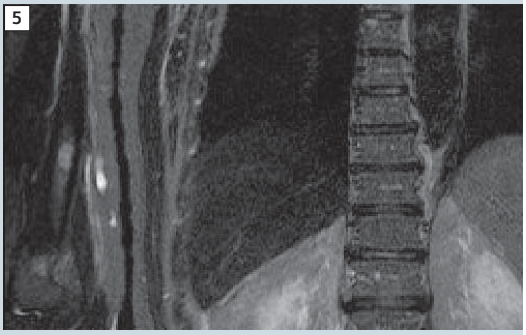

6

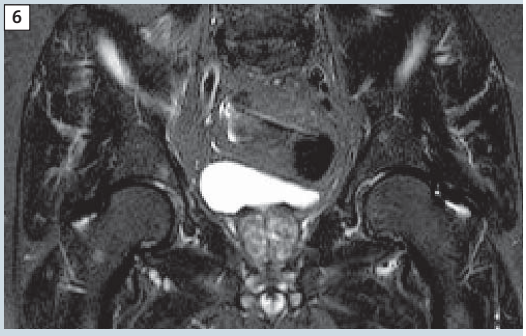

7

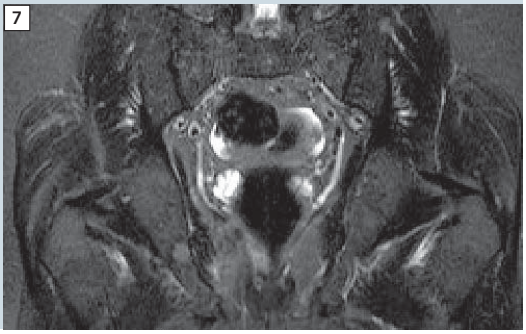

Case 2

50-year-old male presented with previous renal cell carcinoma and right scapular mass. Whole body coronal T1 and STIR sequences were performed to screen for other lesions, revealing a right temporal lobe lesion, left posterior rib metastasis and bone infarcts in the distal femora **(Figs. 8, 9, 10, 12)**, the latter thought due to previous chemotherapy. Axial sequences helped characterise the scapular mass **(Fig. 11)**.

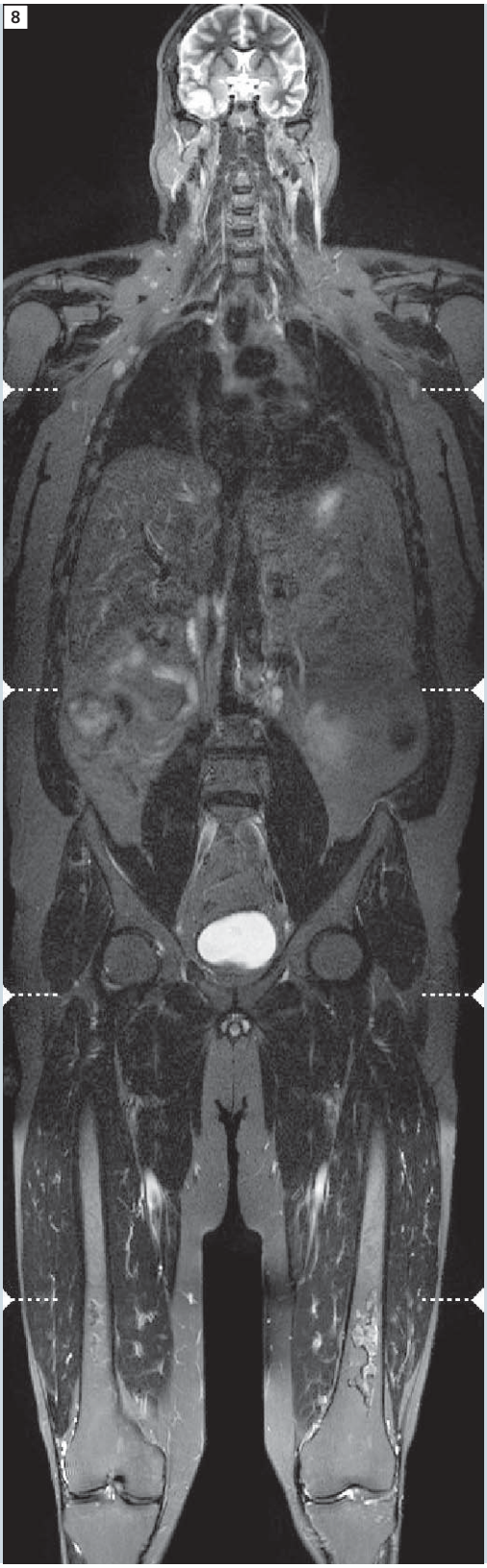

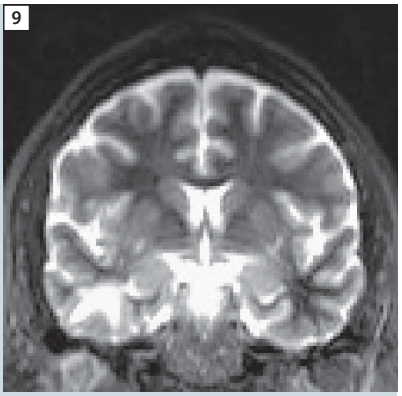

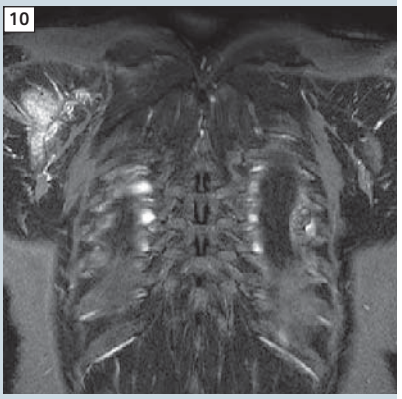

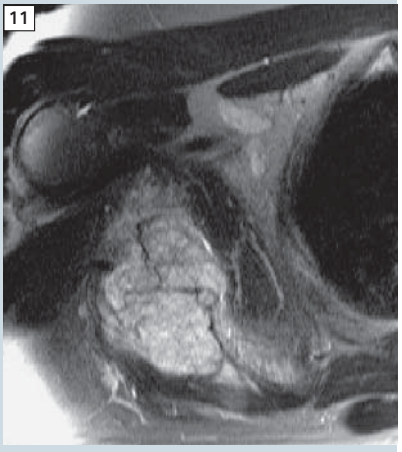

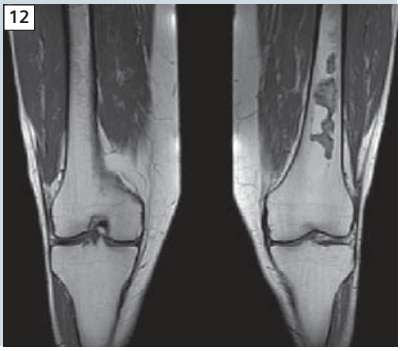

Malignant Melanoma

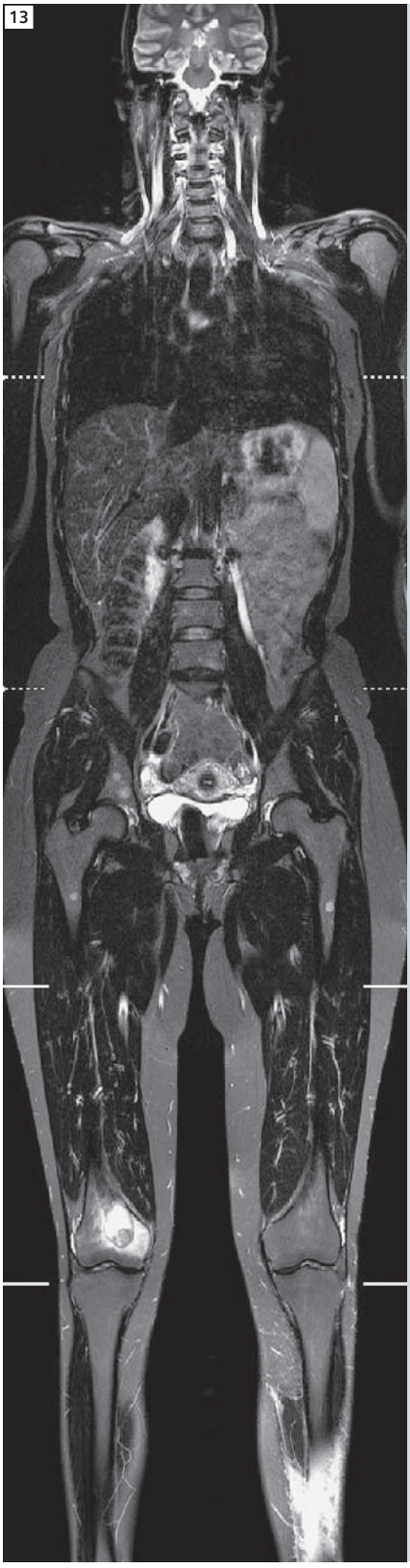
13

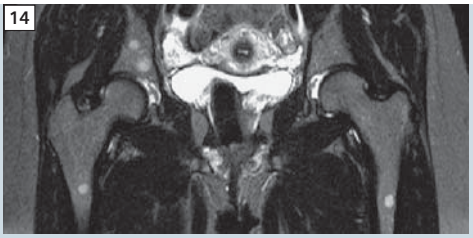
14

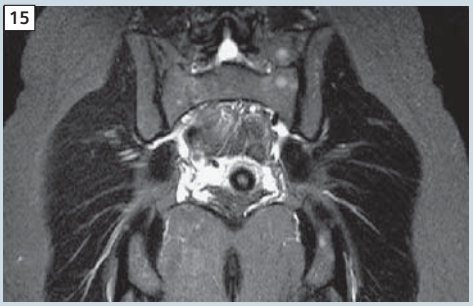
15

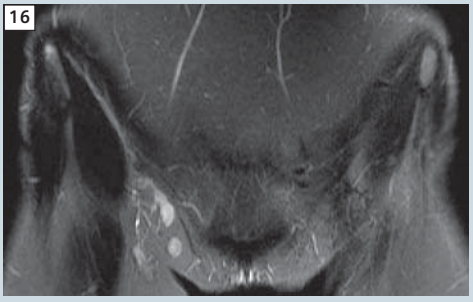
16

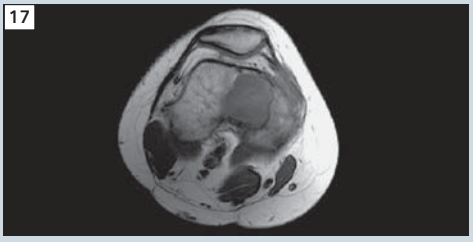
17

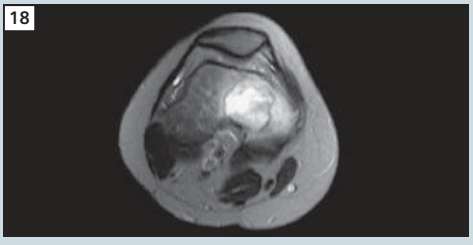
18

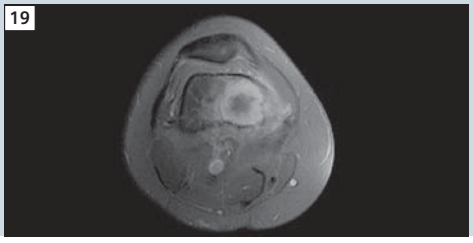
19

Case 3

42-year-old female with past history of melanoma, and known lesion in the distal right femoral metaphysis **(Fig. 13)**. At whole body MRI, 4 other right femoral, 1 left femoral, bilateral acetabular and sacral lesions **(Figs. 14, 15)** and right inguinal lymphadenopathy **(Fig. 16)** were demonstrated. This precluded radical curative resection of the distal femoral lesion (**Figs. 17–20**. T1, T2, and fat-saturated post contrast T1 axial and coronal images of the femoral lesion).

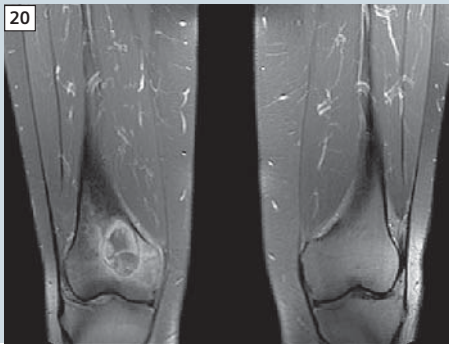
20

Lymphatic / vascular malformations

Case 4

32-year-old male presented with large lymphatic malformation of the right leg. T1 and STIR coronal sequences **(Figs. 21, 22)** show an extensive, predominantly subcutaneous malformation involving the leg, thigh, groin/buttock and abdominal wall. Fat saturated T2-weighted axial images **(Figs. 23–26)** give further anatomical information – the malformation involves the plane between gluteus maximus and the bony pelvis, and also extends into the true pelvis.

Surgical excision is the method of choice for local lymphatic malformations, but complete removal of the epithelium of the lesion is required for success. This is not practical in diffuse disease such as this case, where multiple complex surgical and percutaneous therapies may be required. Accurate anatomic detail is obviously essential prior to considering treatment options [4].

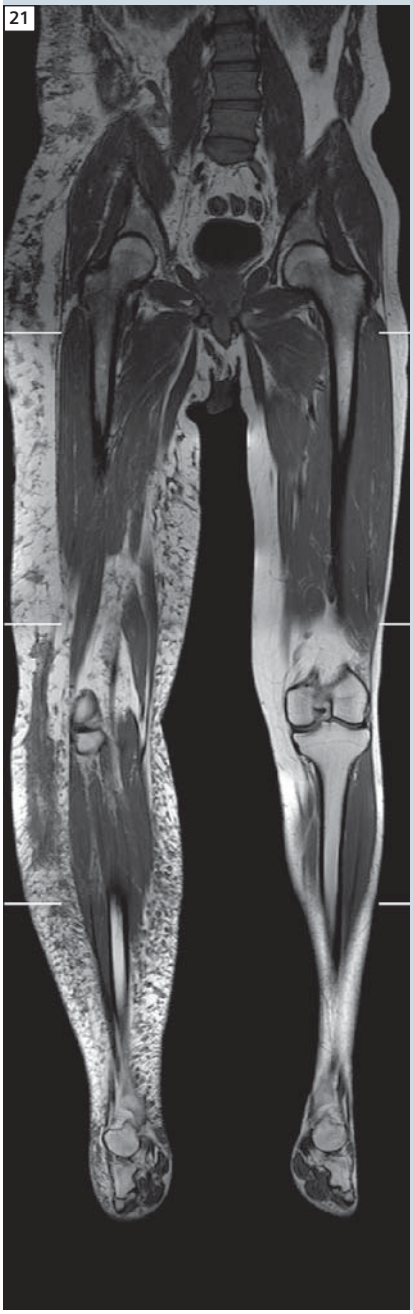

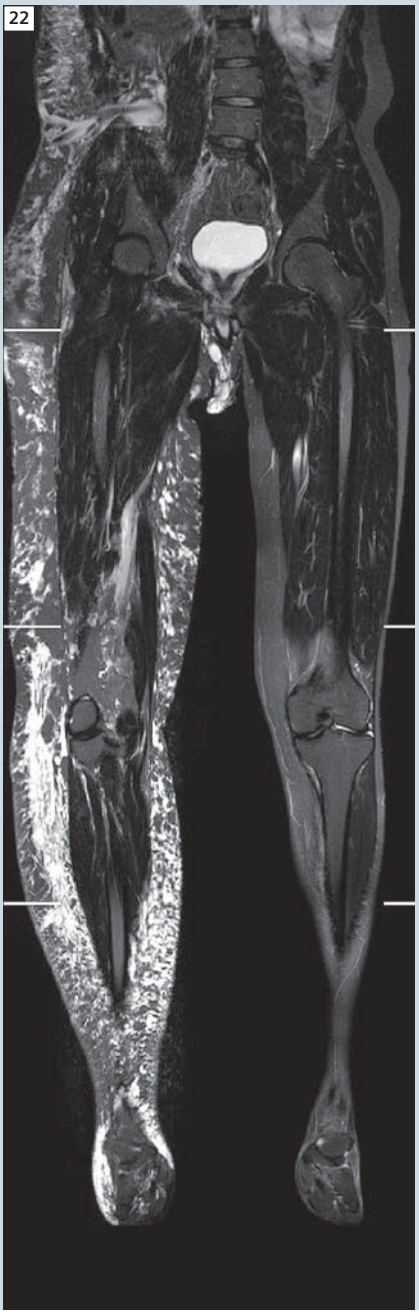

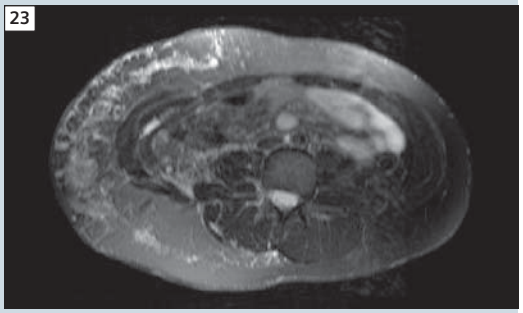

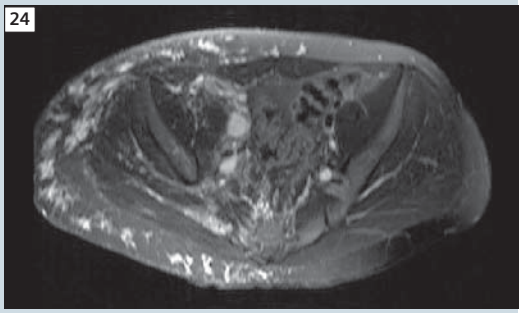

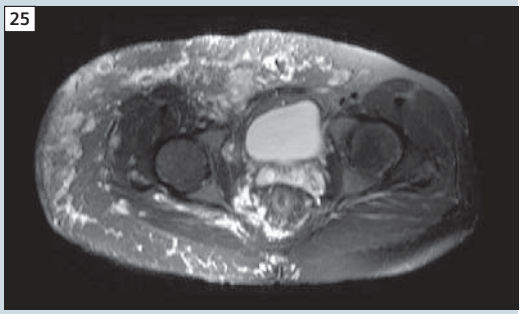

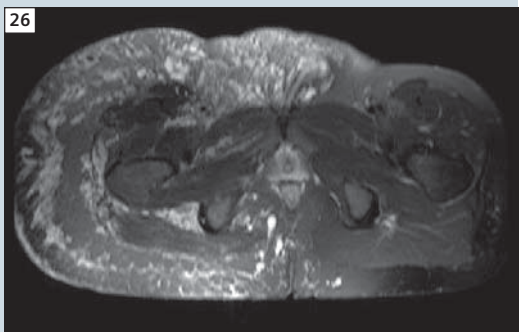

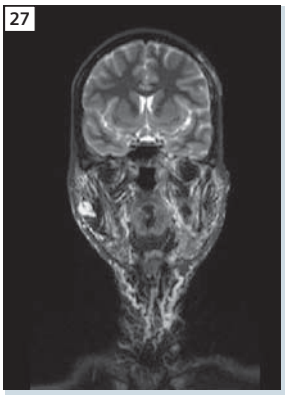

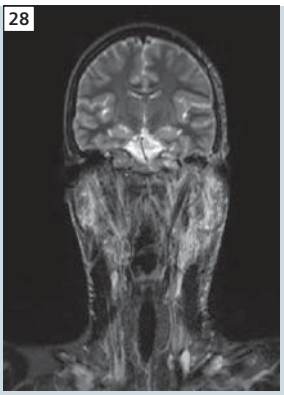

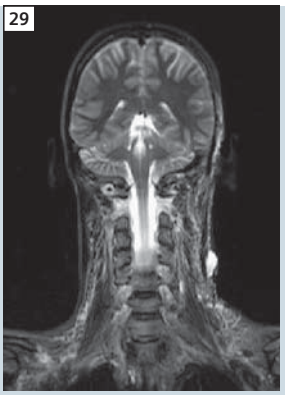

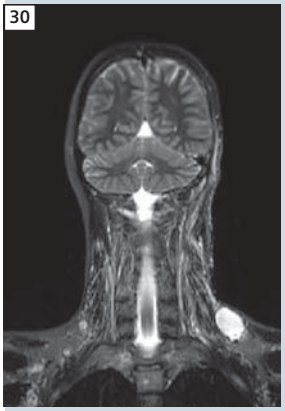

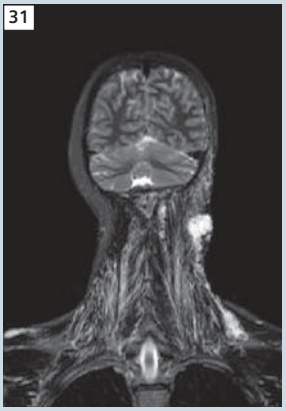

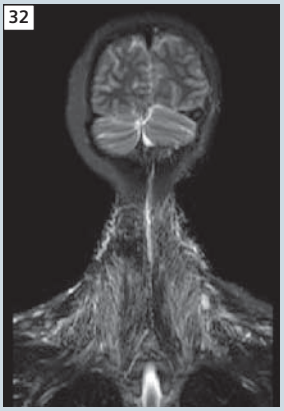

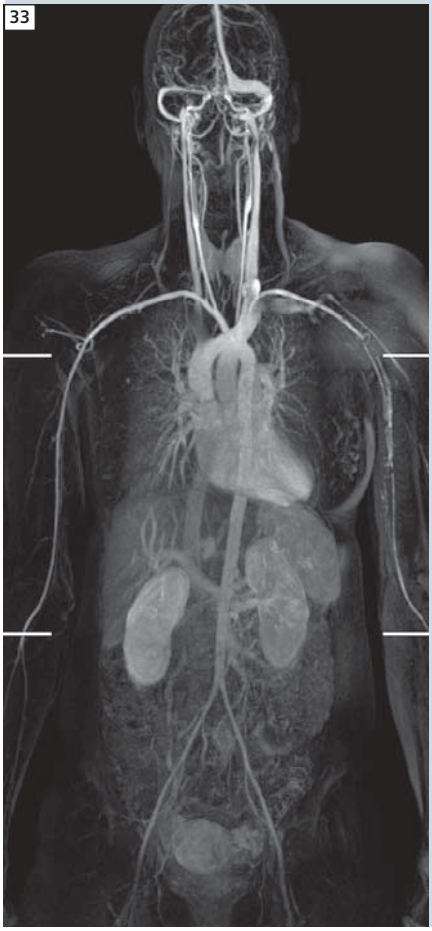

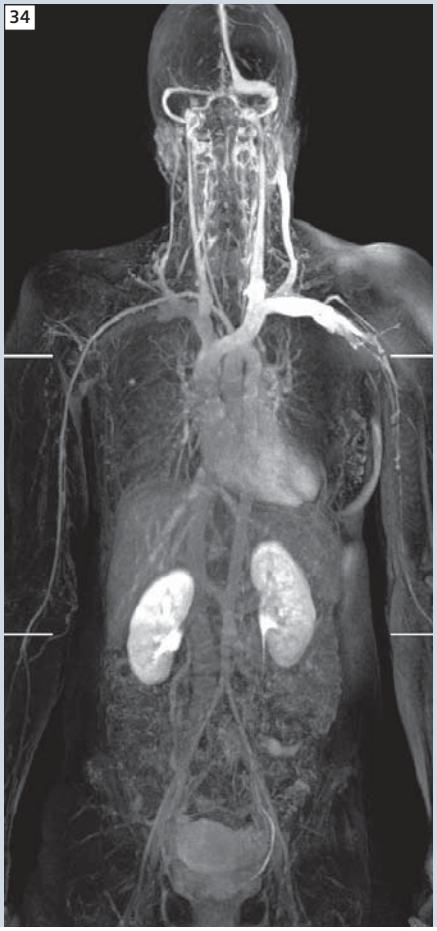

Case 5

32-year-old male presented with large vascular malformation of the neck. Coronal STIR images **(Figs. 27–32)** show the extent of the lesion, which involves the superficial neck, lower face and left scalp, right masseter and posterior cervical muscles. Arterial phase of post contrast MRA **(Fig. 33)** demonstrates normal arterial architecture of the neck and upper arms, without early venous filling, indicating a slow flow vascular malformation. The malformation is starting to fill on the venous phase of the dynamic study **(Fig. 34)**.

The two major roles of MRI in adult vascular malformation assessment are to delineate the anatomy of the lesion, and to differentiate slow from high flow vascular malformations. The latter is critical in determining appropriate management – high flow lesions may be treated with embolization, low flow lesions with sclerotherapy [4].

35

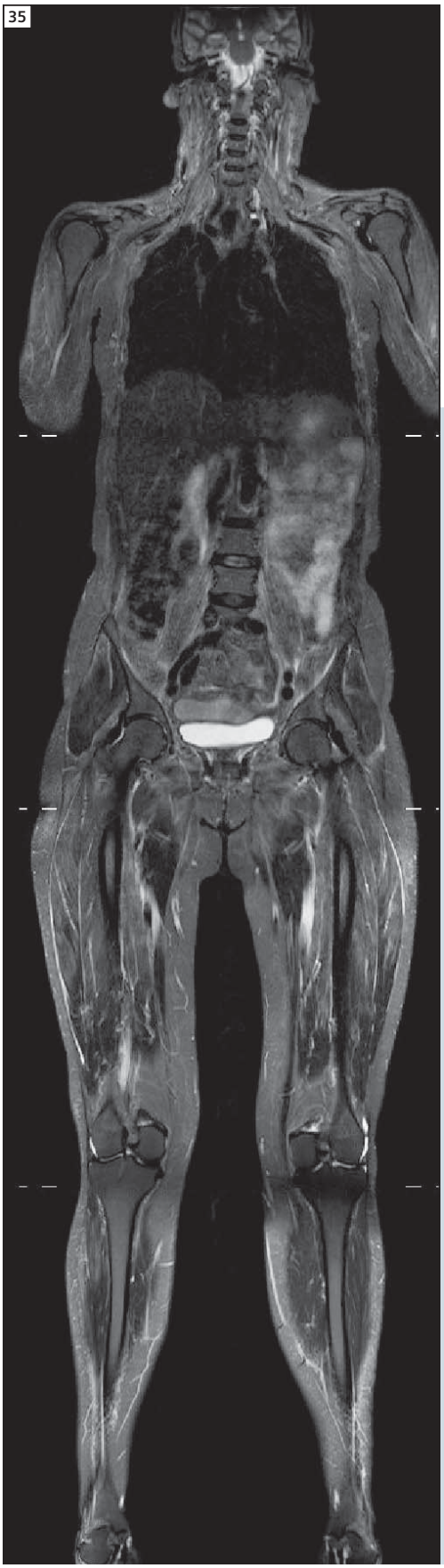

Muscle disorders

MRI is being used increasingly in assessment of inherited neuromuscular disorders including muscular dystrophies and mitochondrial disorders, and in acquired myopathies/myositis. Abnormal muscle signal, atrophy and fatty or fibrotic infiltration is well depicted. Distribution of disease can help direct appropriate genetic and biochemical investigations, and help target diagnostic muscle biopsy [5].

36

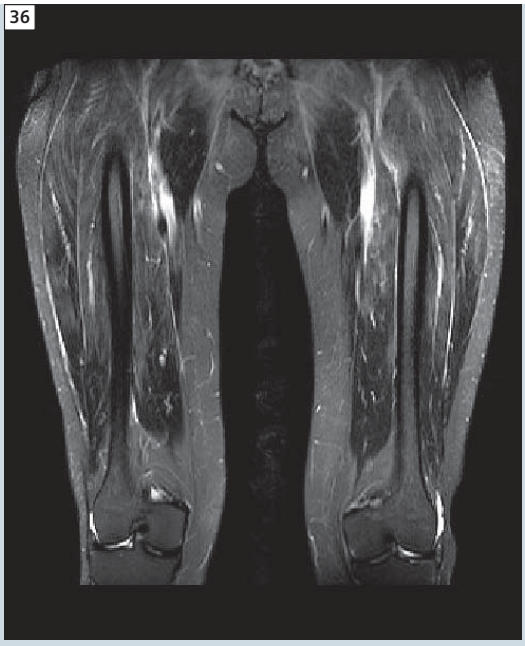

37

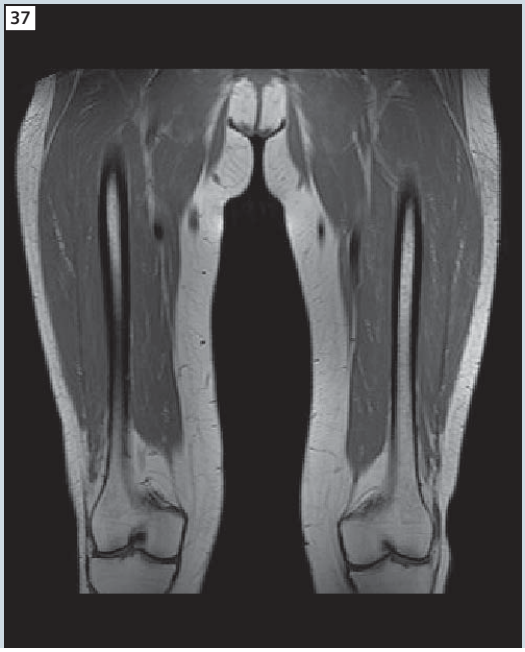

Case 6

54-year-old female presented with proximal limb weakness. Abnormally high signal in quadriceps muscles bilaterally were seen on STIR **(Figs. 35, 36)**, without fatty infiltration on T1-weighted images **(Fig. 37)**. This helped guide muscle biopsy, with subsequent diagnosis of dermatomyositis.

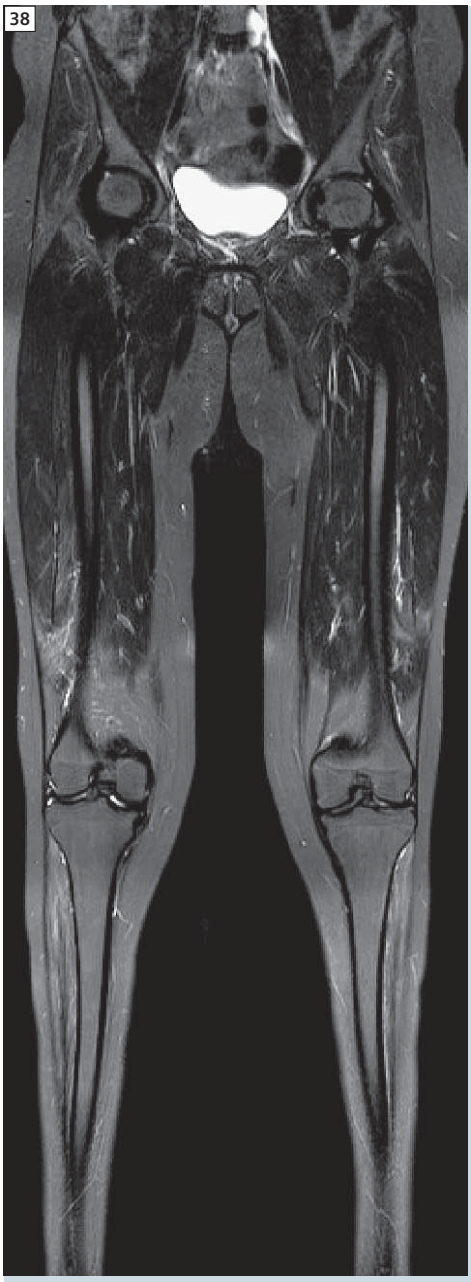

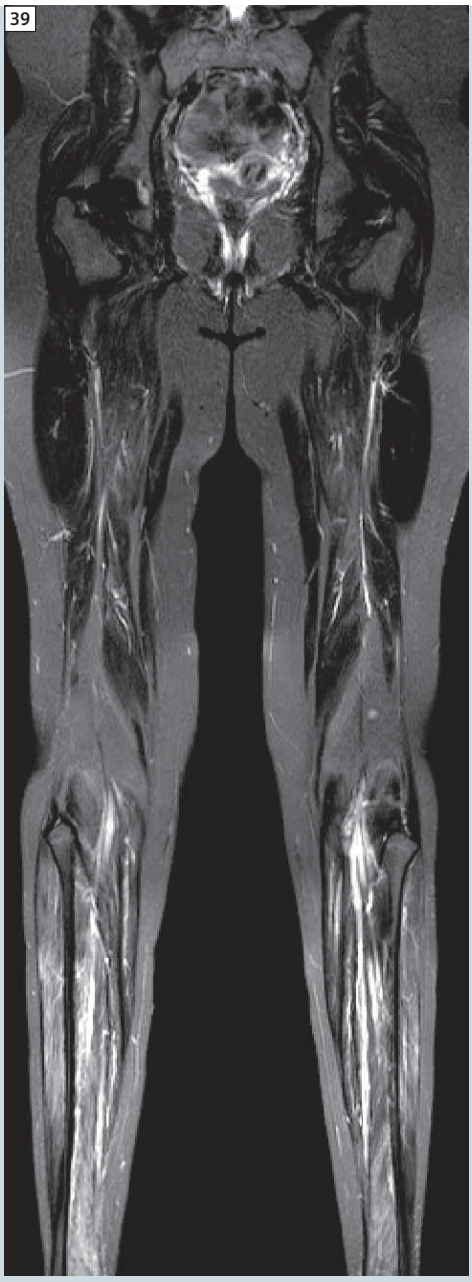

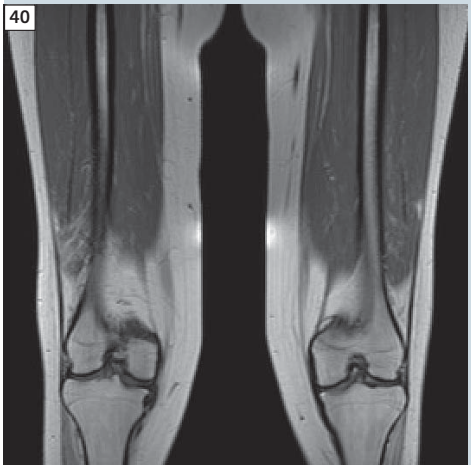

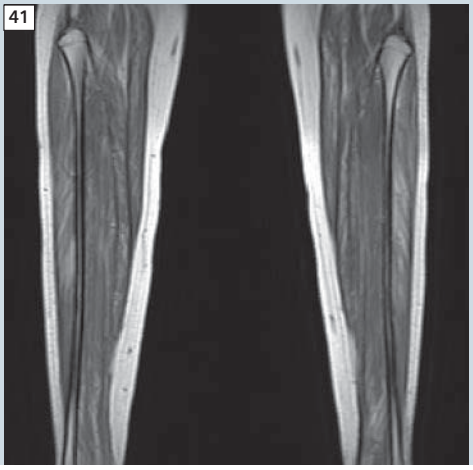

Case 7

14-year-old female presented with known hereditary myopathy, of uncertain type. The distribution of involved msucles is demonstrated, with abnormal signal on STIR **(Figs. 38, 39)** and fatty infiltration on T1-weighted images **(Figs. 40, 41)** in the distal vastus lateralis, and marked atrophy of the calf muscles bilaterally.

Bone disease

Extended portions of the skeletal system may be covered with MRI.

Case 8

This 83-year-old male with known Paget's disease presented with increasing left hip and thigh pain. Coronal T1-weighted and STIR sequences **(Figs. 43, 44)** demonstrate changes of Paget's, without oedema, frank fracture or aggressive bone lesion identified. Note previous open reduction and internal fixation (ORIF), right femur. Following initial image acquisition, coronal and sagittal curved MPR's of the bowed left femur were reconstructed to better evaluate the entrire length of bone in continuity **(Figs. 42, 45)**.

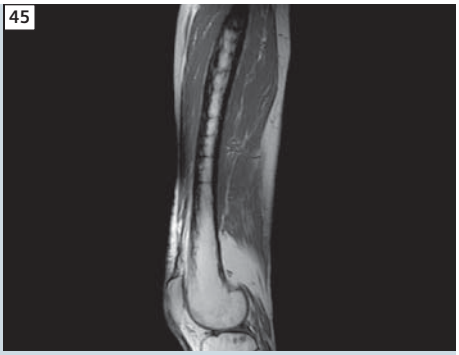

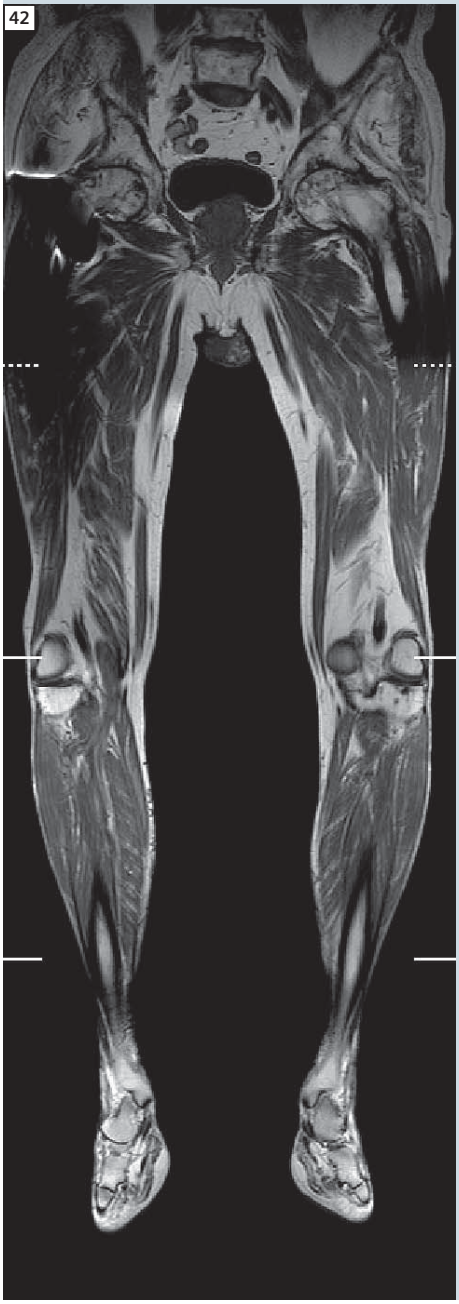

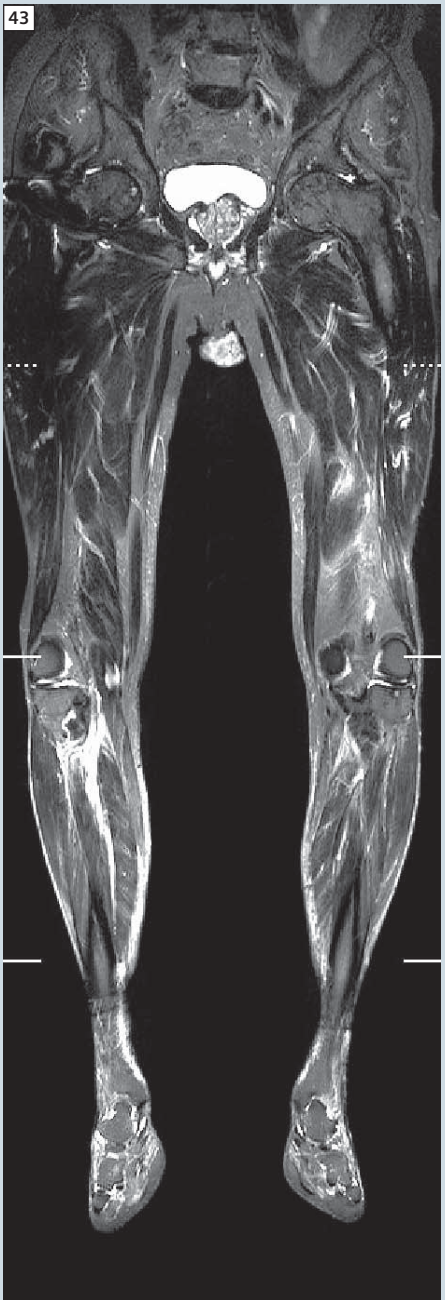

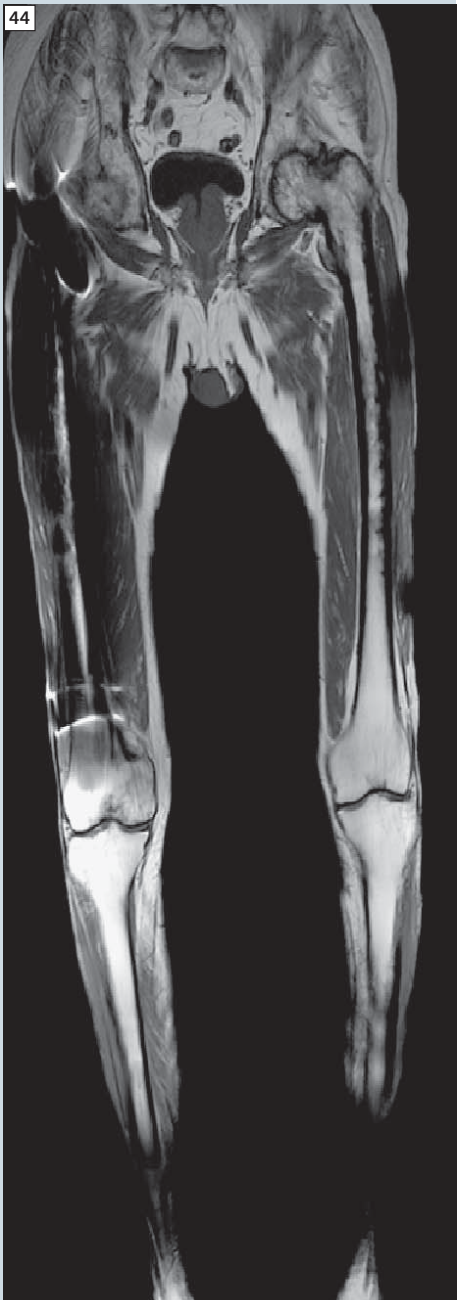

Neurofibromatosis

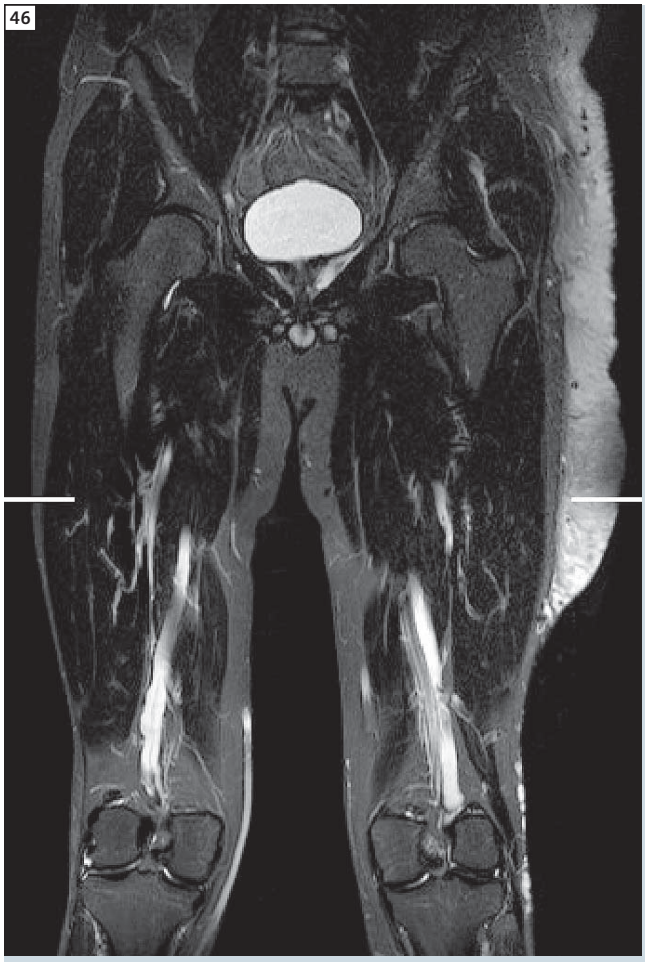

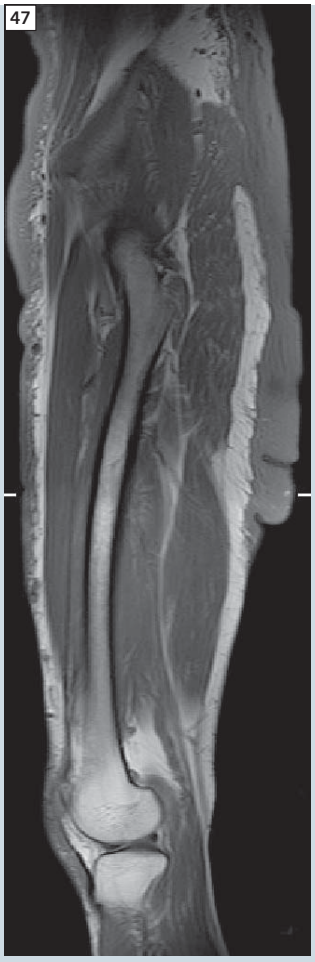

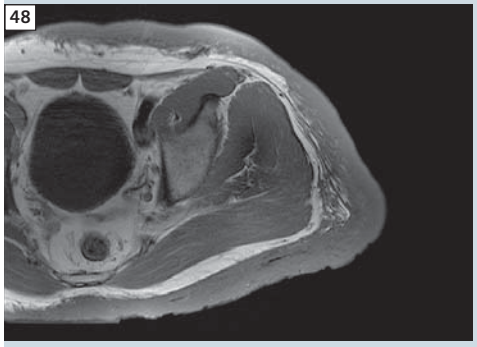

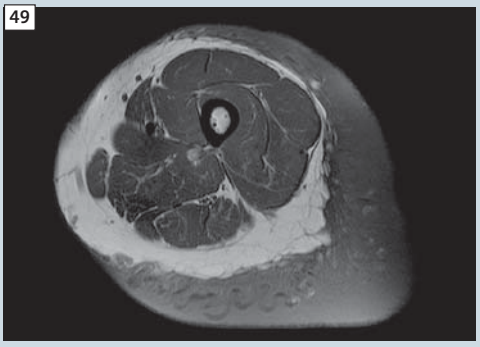

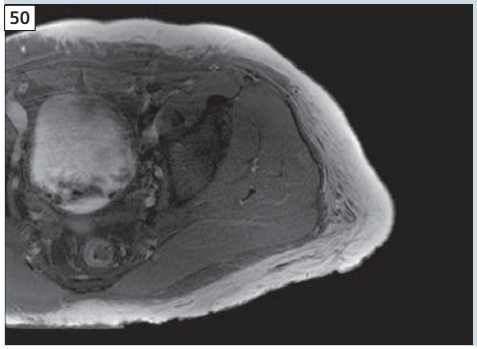

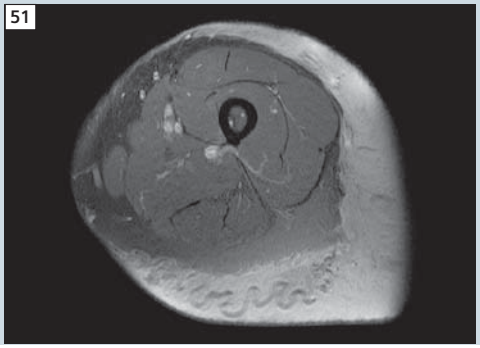

Case 9

35-year-old male with large plexiform neurofibroma of left buttock and thigh. These lesions are frequently disfiguring, disabling and if large, are prone to spontaneous haemorrhage. This was a pre-operative study prior to debulking, following numerous previous episodes of haemorrhage.

Coronal STIR and saggital T1-weighted sequences from above pelvis to below knee show an extensive but superficial lesion, confined to skin and subcutaneous tissue **(Figs. 46, 47)**.

Axial T1-weighted pre and post gadolinium images show vivid enhancement of the tumor. Large vessels are evident within the lesion **(Figs. 48–51)**.

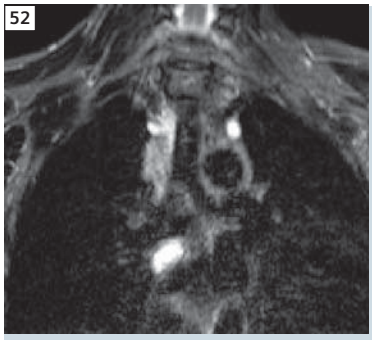

Case 10

17-year-old female with type 1 neurofibromatosis, prior to debulking of left pelvic / thigh plexiform neurofibroma. The study was performed to evaluate the anatomy and extent of the tumor, and to screen for other lesions. The extensive lobulated plexiform lesion involves the left pelvic side wall, adductor and extensor compartments of the thigh, and extends along the neurovascular bundle down to the popliteal fossa **(Figs. 53–58)**. Prior ultrasound had suggested a left adnexal mass – MRI showed no other lesion in the pelvis apart form the large neurofibroma. Small mediastinal neurofibromas are also evident **(Fig. 52)**. No other lesions were identified.

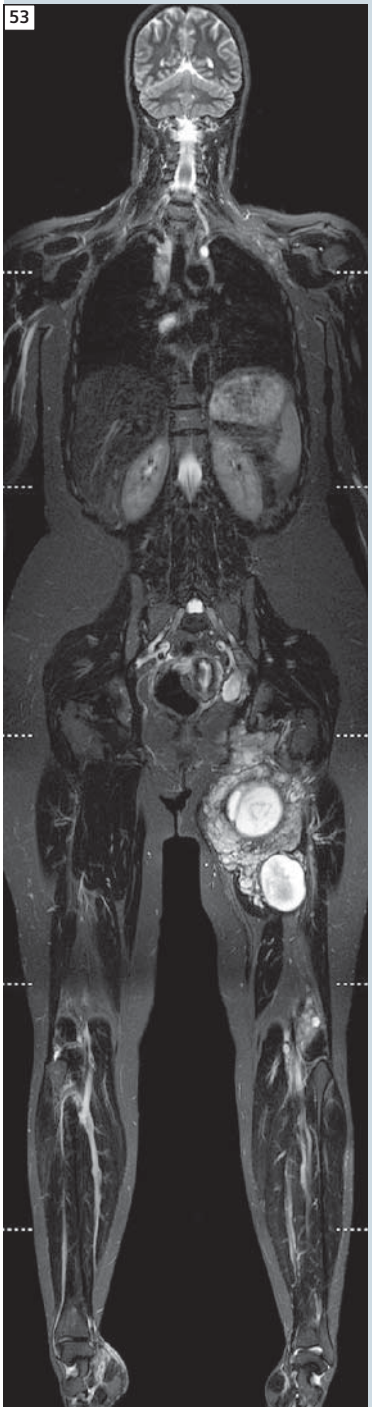

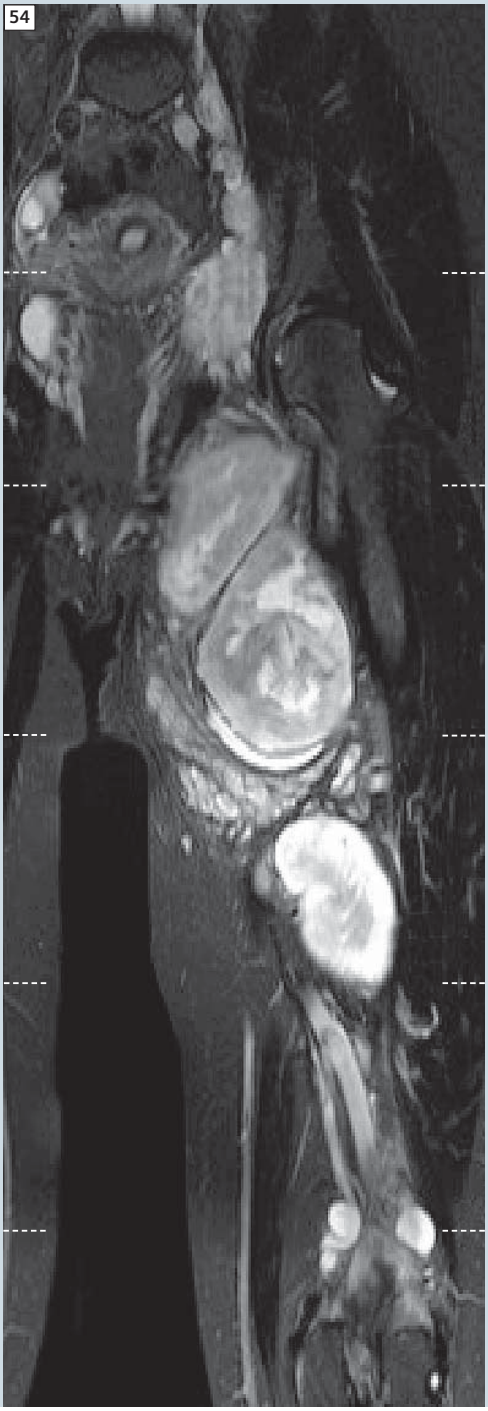

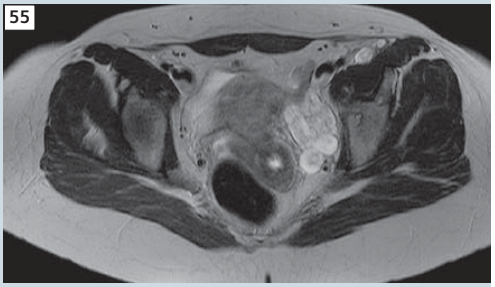

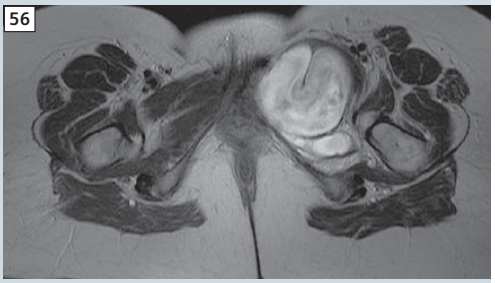

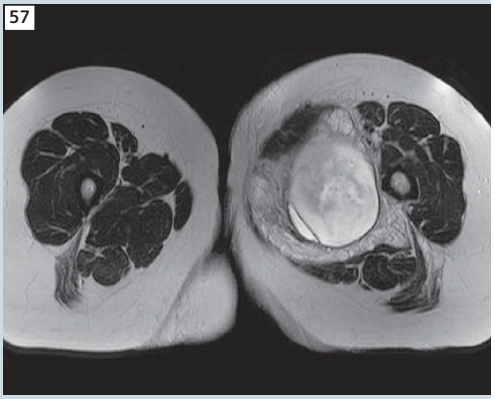

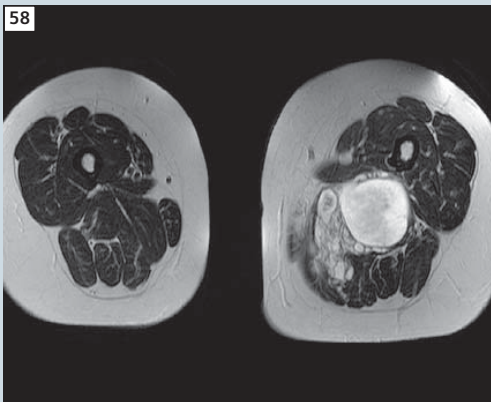

Gaucher's disease

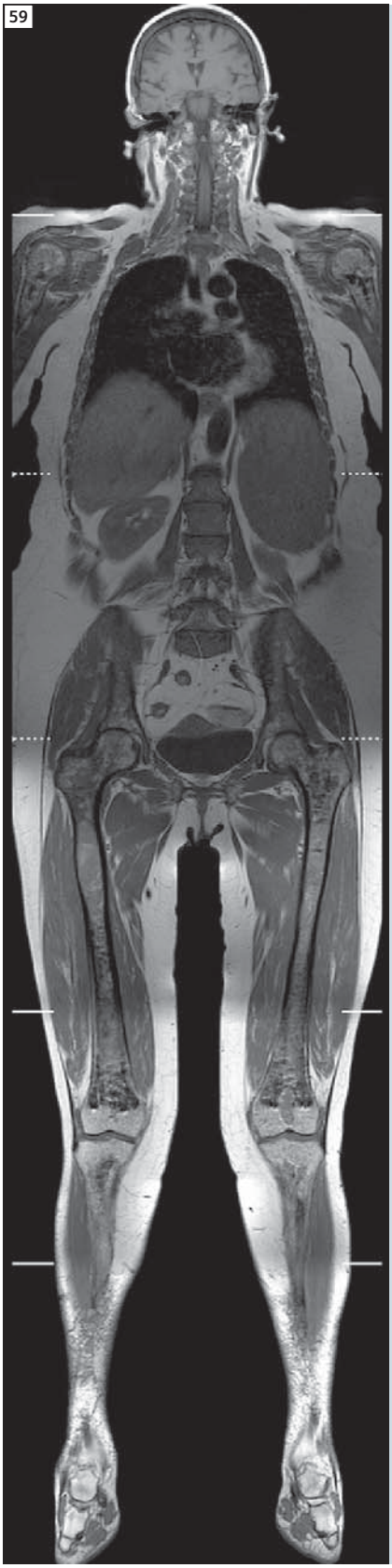

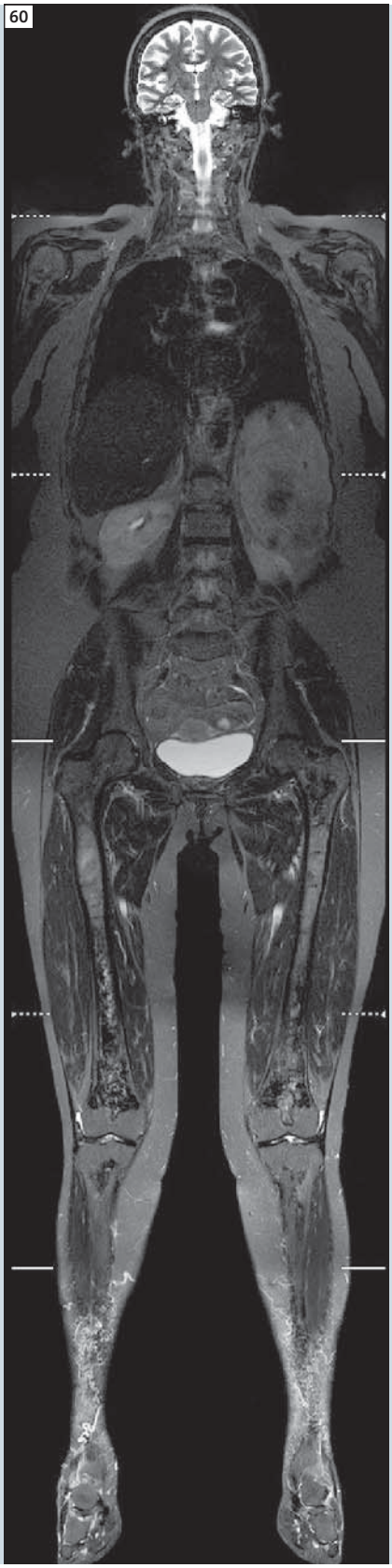

Case 11

69-year-old female with Gaucher's disease, a lysosomal storage disease due to deficiency of the enzyme glucocerebrosidase, leading to accumulation of glucocerebroside in liver, spleen, bone marrow and rarely, the lungs and brain. Complications of the commonest, non-neuronopathic form of the disease may include hepatomegaly, splenomegaly, hypersplensim, bone pain, bone infarcts and fractures due to osteopaenia and cortical thinning.
Radiologic findings include hepatosplenomegaly, osteopaenia, osteonecrosis, bone infarcts and bone deformity such as Erlenmeyer flask deformity. Radiologic assessment is useful in determining pattern of disease, and monitoring response to enzyme replacement therapy [6].
T1 and STIR coronal sequences of the whole body demonstrate marrow infiltration and bone infarcts in both femora, and hepatosplenomegaly **(Figs. 59, 60)**.
The focal splenic lesions seen best on T1-weighted axial and coronal TrueFISP sequences **(Figs. 61, 62)** are thought to be clusters of Gaucher cells – monocyte/macrophages laden with glucocerebroside [7].

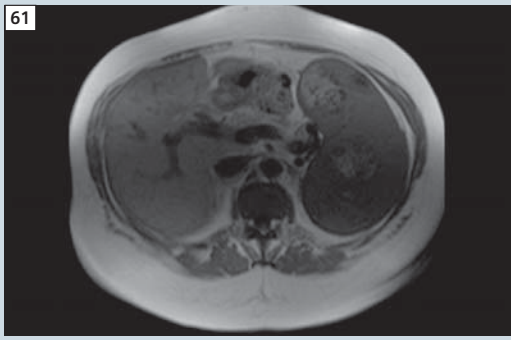

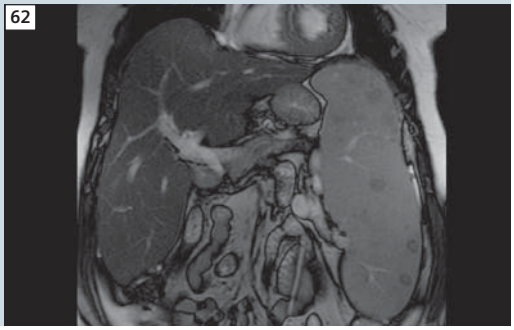

Continued from page 68

Multiple input channels: Allow simultaneous signal reception from multiple coils, reducing exam time.
Improved magnet design: Short bore, quieter machines improve patient comfort.

Software

Sequences: Turbo Spin Echo (TSE) techniques.
Parallel acquisition technique: iPAT decreases exam time, as spatial information from multiple receiver coils is used to reconstruct a single image.
Improved user interface and post processing: For example automatic composing software.

Imaging protocol

Advised protocols vary between authors and institutions. Most published material relates to imaging for metastases or vascular disease.
At our institution, we tailor our study depending on the primary pathology under investigation. Coronal T1 and STIR sequences are used predominantly, with additional sequences as required, for example:

- T1 and T2 axial sequences of the primary area of pathology are often performed for anatomic detail.
- When screening for metastases, dynamic post contrast liver, post contrast T1-weighted coronal sequences of the whole body and FLAIR sequences of the brain are added.
- When characterizing vascular malformations, MR Angiography (MRA) is added.

Total examination time is usually 30–45 minutes.
The shown cases are some examples of the use of whole body MRI, beginning with staging studies of patients with known malignancy, followed by other examples of the use of the technique.

Limitations of whole body MRI

- **Usual contraindications to MRI**
  For example pacemaker, claustrophobia, large body size, patients over 550 lbs
- **Availability of current generation scanner**
- **Lymph node evaluation**
  Differentiating reactive nodes from malignant nodes remains problematic.
- **Post-operative evaluation**
  Differentiating post-operative changes from residual or recurrent tumor can be difficult.
- **Organ-specific problems in detecting metastases or synchronous disease:**
  Bone – scintigraphy may be more sensitive in rib, scapula and skull metastases [1].
  Lung – CT is more sensitive in detecting nodules < 6 mm [1].
  Colon – MR is not sensitive in detecting neoplasms unless MR colonography is performed.
- **Follow-up requirements**
  If a lesion is detected during screening for metastases, a patient may need to return for dedicated diagnostic study of the lesion.

Conclusion

Due to ongoing technical advances, MRI has become a practical method of rapidly and accurately assessing the whole body or large body areas. Ongoing evaluation will be required to determine the diagnostic performance and cost-effectiveness of whole body MRI in cancer patients, but it offers a promising single-modality screening method for metastatic disease. In non-neoplastic conditions, whole body MRI may be the imaging test of choice due to lack of ionizing radiation, excellent soft tissue contrast and multiplanar capability.

Contact
Melanie Seale, M.D.
St. Vincent's Hospital Melbourne
41 Victoria Parade Fitzroy Victoria 3065
Australia
melanie.seale@svhm.org.au

References

1 Lauenstein TC, Semelka RC Emerging Techniques: Whole Body Screening and Staging with MRI. J. Magn. Reson. Imaging 2006:24:489–498.
2 Lauenstein TC, Goehde SC, Herborn CU et al. Whole Body MR Imaging: Evaluation of Patients for metastases. Radiology 2004; 233:139–148.
3 Schmidt GP, Haug AR, Schoenberg SO, Reiser MF. Whole-body MRI and PET-CT in the management of cancer patients. European Radiology 2006 16:1216–1225.
4 Ohgiya Y, Hashimoto T, Gokan T et al. Dynamic MRI for Distinguishing High-Flow from Low-Flow Peripheral Vascular Malformations. AJR 2005; 185:1131–1137
5 Mercuri E, Pichiecchio A, Allsop J et al. Muscle MRI in inherited neuromuscular disorders: Past, present, and future. J.Magn Reson Imaging 2007 25(2) 433–440.
6 Charrow J, Esplin JA, Gribble TJ et al. Gaucher disease: recommendations on diagnosis, evaluation, and monitoring. Arch. Intern Med 1998; 158(16):1754–60.
7 Poll LW, Koch JA, vom Dahl S et al. Gaucher disease of the spleen: CT and MR findings. Abdominal Imaging 2000 25(3):286–289.

Integration of the Tim Planning in Protocol Development for Multi-Region Scanning

Mark Lourensz; Valery Tay; Ravi Padmanabhan; Nicholas Trost

St. Vincent's Hospital Melbourne, Fitzroy, Victoria, Australia

Introduction

The advent of the Total imaging matrix (Tim) system, integrated Parallel Acquisition Techniques, and more recently the *syngo* Tim Planning Suite and Inline Composing has had a significant impact on the ease of use and workflow in cases where multiple body areas need to be examined in a single sitting. The Tim Planning Suite and Inline Composing in particular have allowed us to simplify and streamline our protocols for a number of exams, ranging from simple spinal cord compression cases to more complex whole body screening procedures. The Tim Planning user interface (UI) is of great benefit in planning multi area and whole body exams as the full extent of coverage can be seen in a single composed scout image and protocols can be adjusted and planned to minimize patient examination time as well as ensuring full coverage of the area under examination. This is particularly true in spinal cases where the whole spinal cord can be quickly scouted and the composed image displayed for accurate protocol planning. This is also of great benefit in patients with extensive MSK tumors where tumor extent can be readily seen on the scout images and subsequent imaging can be easily planned. More recently we have used the *syngo* Tim Planning Suite to develop an efficient protocol for evaluation of patients with limb girdle muscular dystrophies.

Background [1]

The Limb Girdle Muscular Dystrophies (LGMDs) are a heterogenous group of 16 genetic conditions, first described in the 1960s. Accurate diagnosis of the individual LGMD is important, as each LGMD may have different genetic implications and prognostic outcomes, including the presence of associated cardiac and respiratory complications.

LGMD-2A, the most common of the LGMDs, is caused by a deficiency of Calpain-3 – a muscle specific protease. Diagnosis of a LGMD-2A can be difficult and is based on recognising the clinical phenotype and demonstrating a calpain abnormality. A calpain abnormality is identified on Western Blot analysis, as a reduced or absent protein band. Calpain abnormalities, however, can occur as a secondary phenomenon in other muscle disorders as well.

To confirm the diagnosis of a LGMD-2A, a genetic abnormality in Calpain should be demonstrated with molecular sequencing of the gene. Molecular sequencing of Calpain is an expensive and time-consuming technique, currently performed only in limited centres in Australia. Accurate identification of potential LGMD-2A patients is therefore important, to aid in quicker diagnosis and selection of patients for molecular sequencing. The muscular dystrophies typically have selective involvement of particular muscle groups. Magnetic resonance imaging (MRI) can be used to accurately highlight the muscle groups affected. The neuroimaging profile obtained may be a useful tool to facilitate more accurate and rapid diagnosis.

Technical considerations

All examinations were performed on a 1.5T MAGNETOM Avanto 76 x 32 machine. The MRI protocol was designed not only to primarily demonstrate muscle changes in the hip and shoulder girdles, but also to demonstrate paraspinal, thigh, and calf muscles. The protocol needed to have a high degree of patient tolerance and accommodate a large range of body types. It also needed to be easily

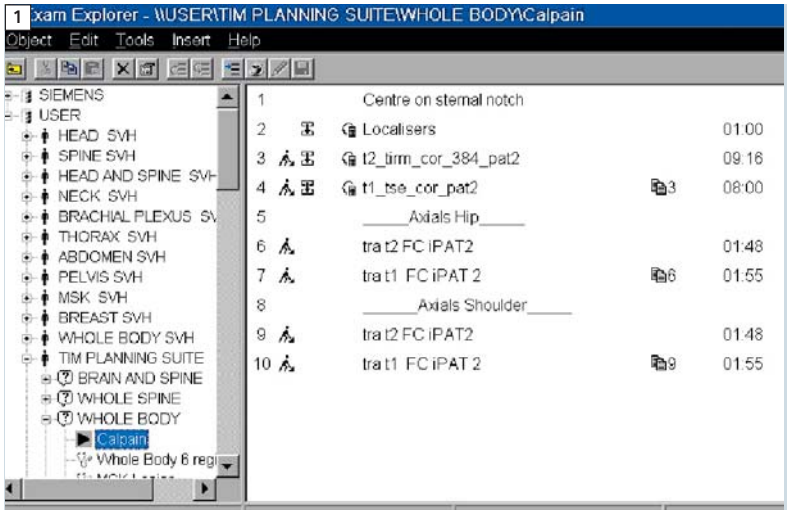

1 Saved Calpain protocol in the protocol tree.

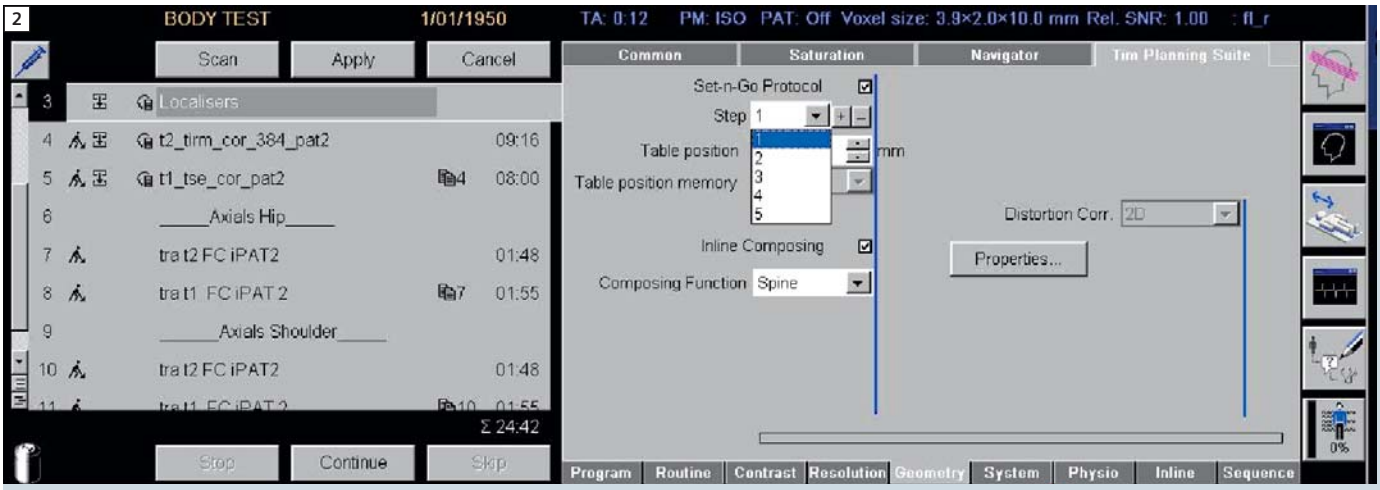

2 Localiser showing Set-n-Go protocol with 5 table positions.

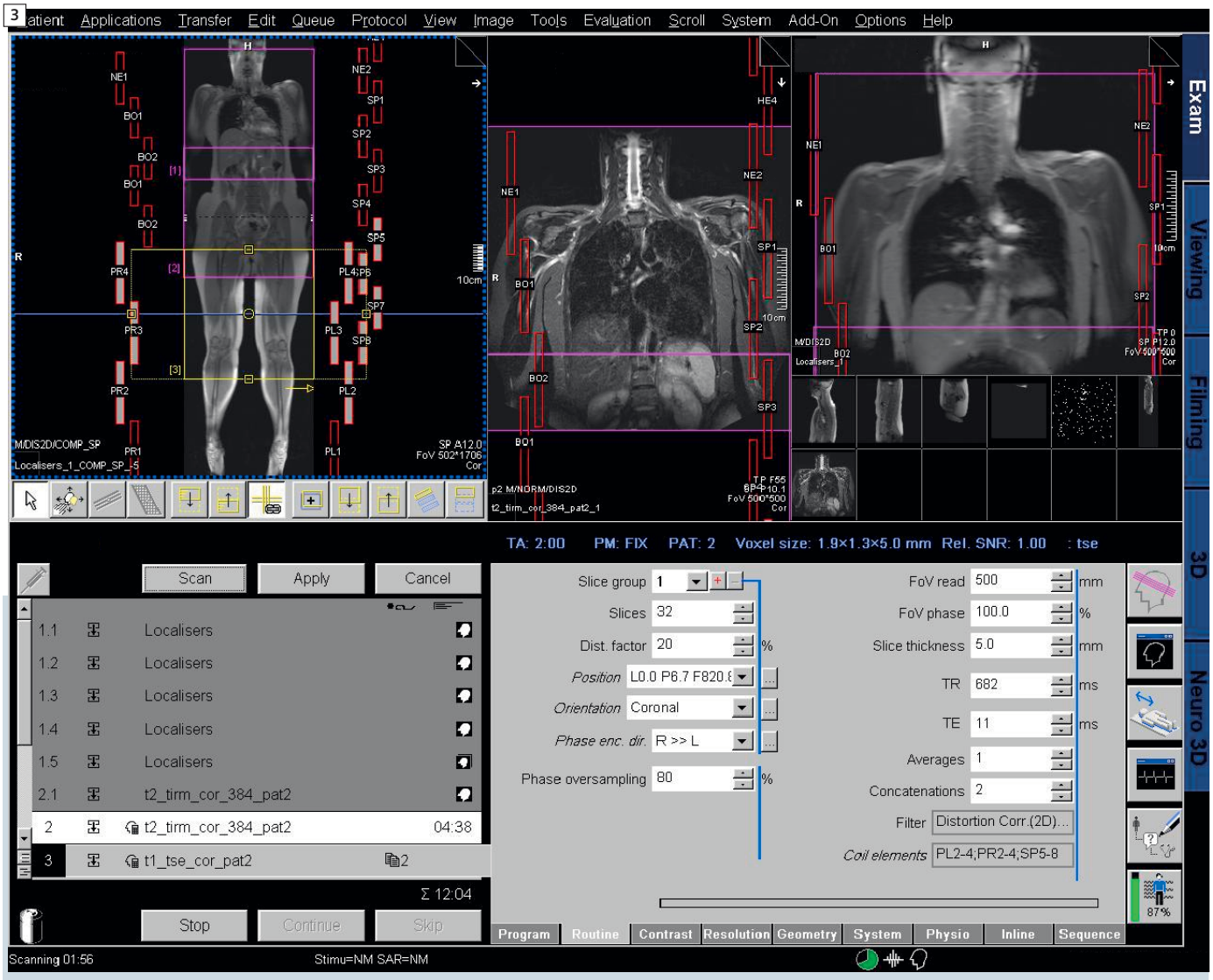

3 Localiser showing positioning of coronal T1. Coupled graphics and AutoCoil Select are turned on.

implemented by our technological staff and not compromise the workflow in our busy department.

Patient set-up: After completing a standard MRI safety questionnaire, patients were given a full explanation of the procedure. They were positioned head first on the MRI table, with shoulders comfortably against the Neck Matrix coil. Coils were positioned from the feet towards the head and all patients were given hearing protection and instructed in the use of the emergency call system

Coils: As well as the posterior elements of the Head, Neck, and Spine Matrix, both Body Matrix and the Peripheral Angio Matrix coils where used. The anterior Neck Matrix coil was used in all bar one case, where the patients' size and body habitus precluded its use. The anterior Head Matrix coil was not used, and this aided greatly in patient comfort. The short bore magnet ensured that the patients head was outside the bore for over 50% of the imaging time. The sternal notch was used as a common centring point for all patients.

Sequences: The Tim Set-n-Go protocol facility was used to provide a simplified protocol tree which could be easily implemented in the Tim Planning UI (Fig. 1). A whole body scout is performed using Inline composing to cover from the neck to the ankle (Fig. 2). This is then used to proscribe coronal STIR and T1-weighted sequences to cover the whole shoulder

Study methods / results [1]

14 patients with a muscular dystrophy or inherited myopathy were included in this study. Nine patients have likely LGMD-2A. Five patients, with confirmed diagnoses of other muscular dystrophies or inherited myopathies, were included. Two patients have facioscapulohumeral muscular dystrophy (FSH), with clinical similarities to a typical LGMD phenotype. Three patients with a distal presentation were included, to observe the differences in distal pattern seen.

PATIENT (MF, AGE)	CLINICAL PHENOTYPE	WESTERN BLOT	DIAGNOSIS				
				SHOULDER GIRDLE And ARM	TRUNK	PELVIC GIRDLE AndTHIGH	CALF MUSCLES
1 M24	LGMD Shoulder & Pelvic	Reduced Calpain	Calpainopathy -LGMD	Biceps, Rotator Cuff, Serratus Anterior,	Erector Spinae	Gluteus Maximus, Adductors, Hamstrings	Posterior Compartment-Medial Gastroc, Soleus
2 M58	LGMD Shoulder & Pelvic	Reduced Calpain	Calpainopathy -LGMD	Rotator Cuff, Serratus Anterior,	Erector Spinae	Gluteus Maximus, Adductors, Hamstrings	Posterior Compartment-Medial Gastroc
3 M72	LGMD Shoulder & Pelvic	Reduced Calpain	Calpainopathy -LGMD	Rotator Cuff, SerrAnt Trapezius, Lat Dorsi	Erector Spinae	Gluteus Maximus, Adductors, Hamstrings	Posterior Compartment-Soleus
4 F 76	LGMD Shoulder & Pelvic	Reduced Calpain	Calpainopathy -LGMD	Latissimus Dorsi		Gluteus Maximus, Hamstrings	Posteriot Compartment-Medial Gastroc, Soleus
5 M29	LGMD Pelvic Girdle	Reduced Calpain	Calpainopathy -LGMD	Latissimus Dorsi		Gluteus Maximus, Adductors, Hamstrings	Posterior Compartment-Medial Gastroc
6 M34	LGMD Pelvic Girdle	Reduced Calpain	Calpainopathy -LGMD			Gluteus Maximus, Hamstrings	Posterior Compartment-Medial Gastroc, Soleus
7 F42	LGMD Pelvic Girdle	Reduced Calpain	Calpainopathy -LGMD			Gluteus Maximus, Adductors, Hamstrings	Posterior Compartment-Medial Gastroc
8 M44	LGMD Pelvic Girdle	Reduced Calpain	Calpainopathy -LGMD			Gluteus Maximus, Hamstrings	Posterior Compartment-Medial Gastroc, Soleus
9 F58	LGMD Pelvic Girdle	Reduced Calpain	Calpainopathy -LGMD		Erector Spinae		Posterior Compartment-Medial Gastroc
10 M64	FSH		Facioscapulo-humeral dystrophy	Rotator Cuff, Serr Ant, Trapezius, Pectoralis, Biceps, Triceps		Hamstrings	Anterior Compartment-Tibialis Anterior
11 M65	FSH		Facioscapulo-humeral dystrophy	Biceps, Rotator Cuff, Pectoralis, LatDorsi			Anterior Compartment-Tibalis Ant, Peroneals
12 M29	Distal Leg Weakness	Absent Dysferlin	Dysferlinopathy -Miyoshi myopathy			Adducotrs, Abductors, Quadriceps	Posterior Compartment-Medial/Lat Gastroc, Sol, Anterior Compartment
13 F15	Distal Leg Weakness		Hereditary Inclusion Body Myopathy			Gluteus Maximus, Hamstrings	Anterior and Posterior Compartment
14 M40	Distal Leg Weakness		Hereditary Inclusion Body Myopathy			Adductors, Hamstrings	Anterior and Posterior Compartment

and hip girdle, thigh, and calf if necessary (Fig. 3). Thirty-two 5 mm slices are used for each table position to ensure consistent composing throughout the whole body, and 3 or 4 table positions are used to cover the regions of interest. These could be easily identified and planned on the UI to keep exam time to a minimum. Transverse T1 and T2 images are then obtained of both shoulder and hip girdles. The history function is used for both coronal and axial slices, so sequence set up time is kept to a minimum. After the initial coronal STIR set up on the scout image, scanning is continuous, except for table moves. This keeps total exam time down to approximately 30 minutes.

Technical outcomes

The imaging objectives of this study have been achieved and the scanning protocol has been very well tolerated by this group of patients. The short exam time and consistent high quality of the MR images has been made possible by the use of the Tim planning suite, Set-n-Go protocols, Inline Composing, integrated matrix coils, and integrated Parallel Acquisition Techniques (iPAT). These tools have made it possible to efficiently integrate what would have been in the past a cumbersome and time consuming exam, into our daily schedule.

Postero-medial compartment of proximal thigh and posterior compartment of the leg

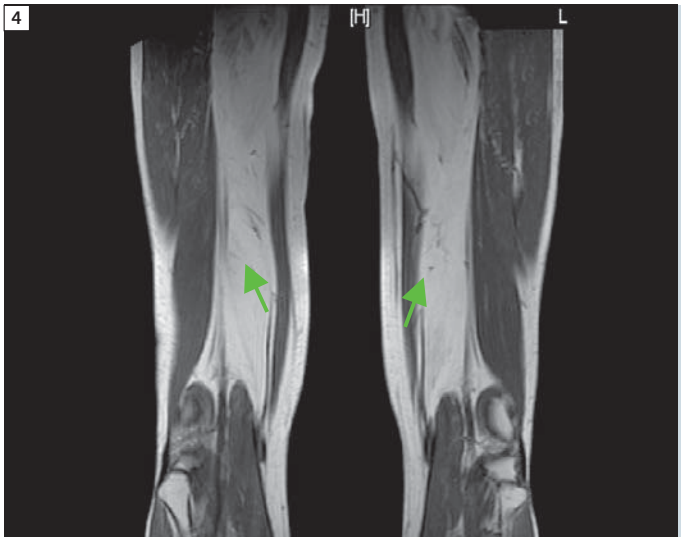

4 Coronal T1-weighted image of the posterior thigh of Patient 3 (LGMD). There is gross fatty replacement of the semimembranosus and semitendinosus muscles, with relative sparing of the biceps femoris.

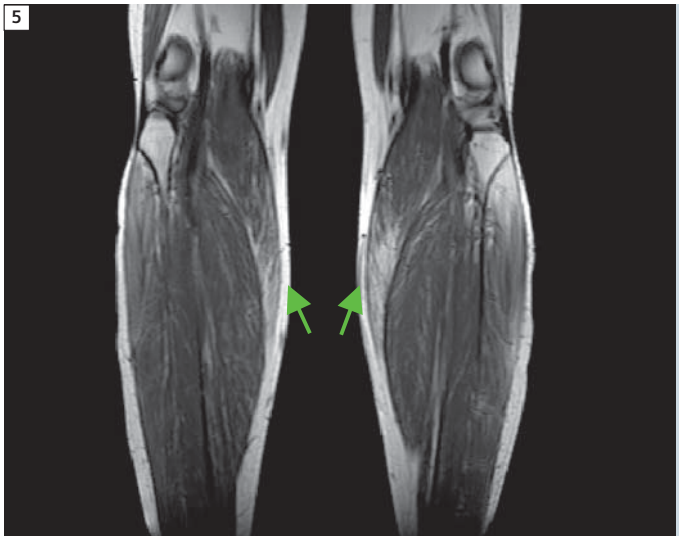

5 Coronal T1-weighted image of the lower leg of Patient 5 (LGMD). There is early preferential focal atrophy and fatty replacement of medial gastrocnemius.

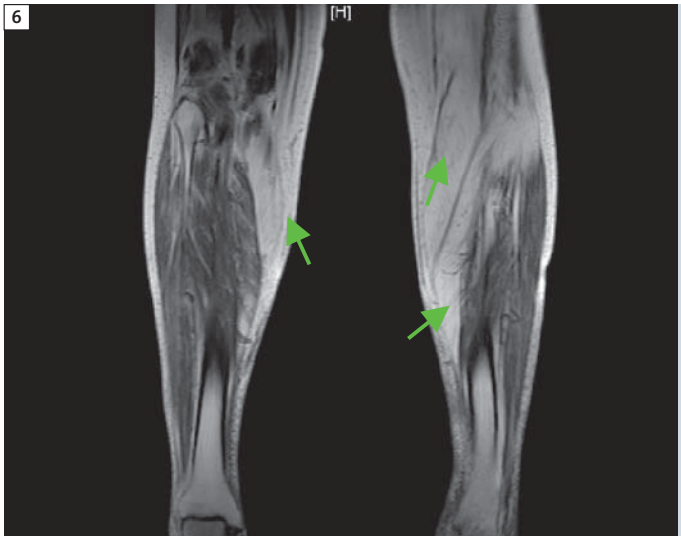

6 Coronal T1-weighted image of the lower leg of Patient 4 (LGMD). There is preferential focal atrophy of medial gastrocnemius, with sparing of lateral gastrocnemius.

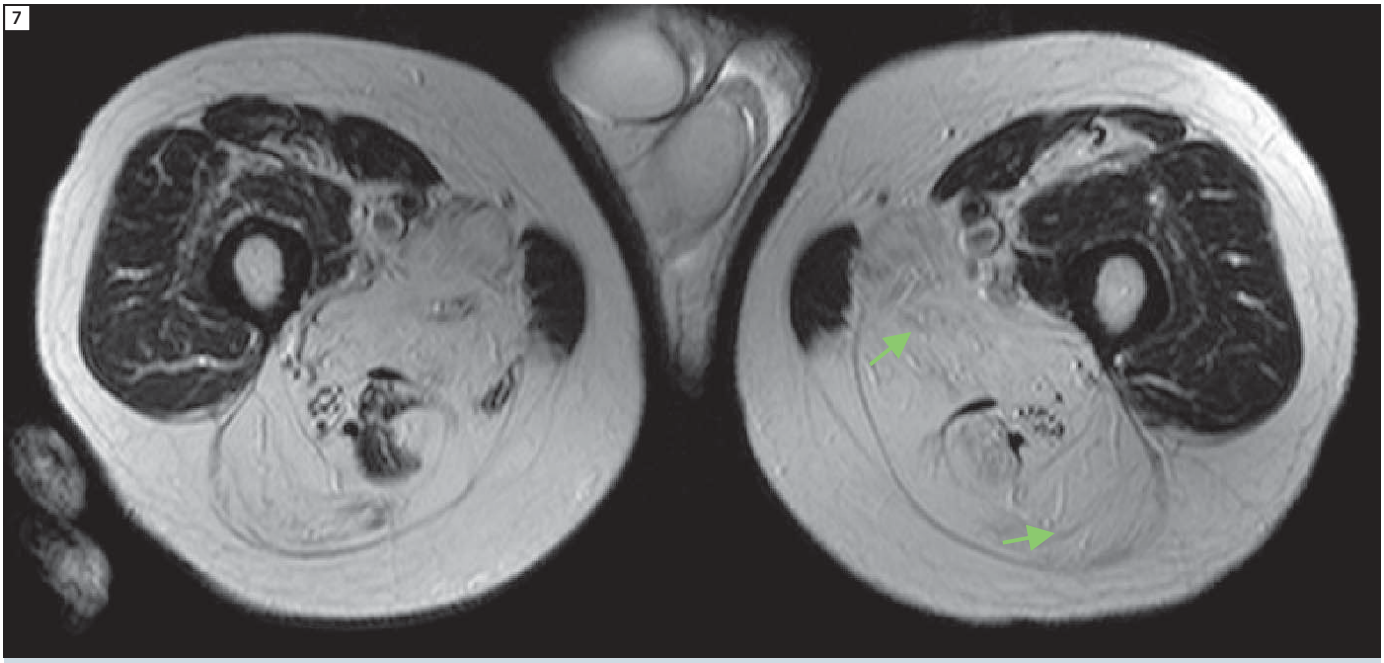

7 Axial T2-weighted image of the proximal thigh of Patient 3 (LGMD). There is gross fatty replacement of the gluteus maximus and the adductor muscles.

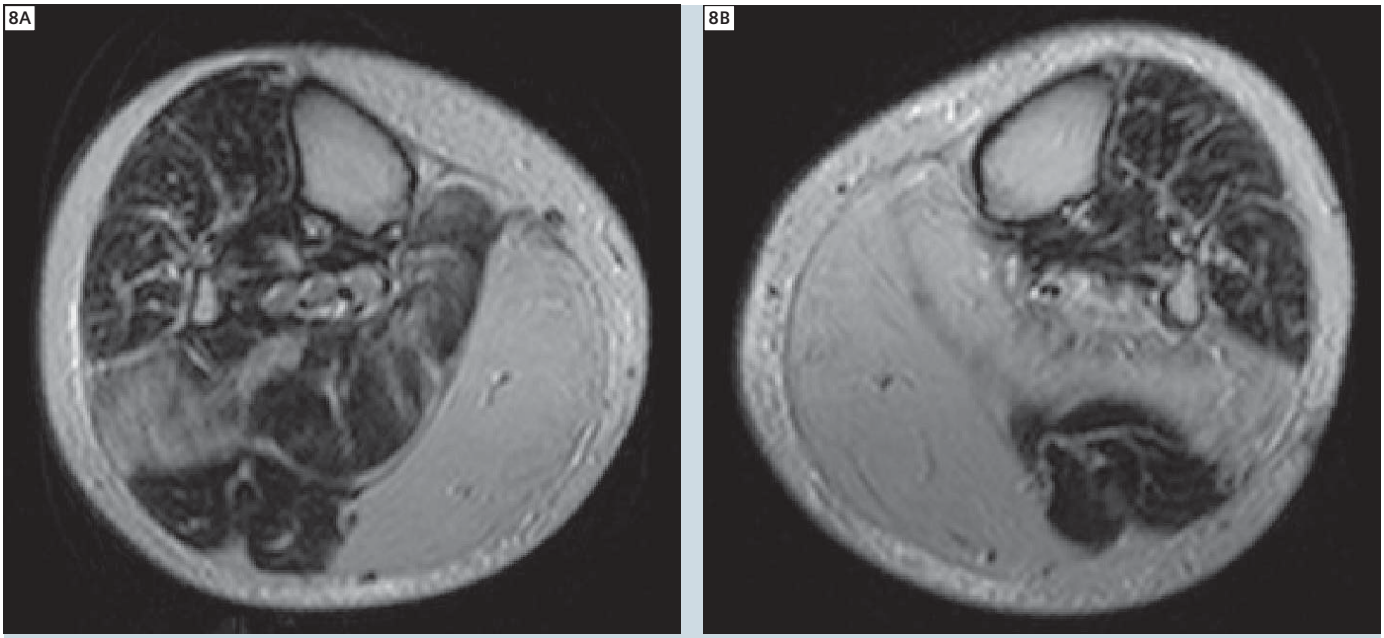

8 Axial T2-weighted image of the lower leg of Patient 4 (LGMD). There is fatty replacement of the medial gastrocnemius muscles bilaterally and the left soleus muscle.

Conclusions [1]

MRI can be used to obtain an accurate neuroimaging profile of the specific muscle groups affected in muscular dystrophies.
The muscles preferentially affected in the calpain-related LGMD are:
Pelvic Girdle: Hip adductors and hip extensors.
Hamstrings: Especially semimembranosus and semitendinosus muscles.
Posterior compartment: Especially medial gastrocnemius.
Upper Limb: Latissimus dorsi, rotator cuff muscles and serratus anterior.
The neuroimaging profile on MRI is a useful technique to aid in accurate diagnosis and differentiation of the individual muscular dystrophies.

Anterior compartment of the leg

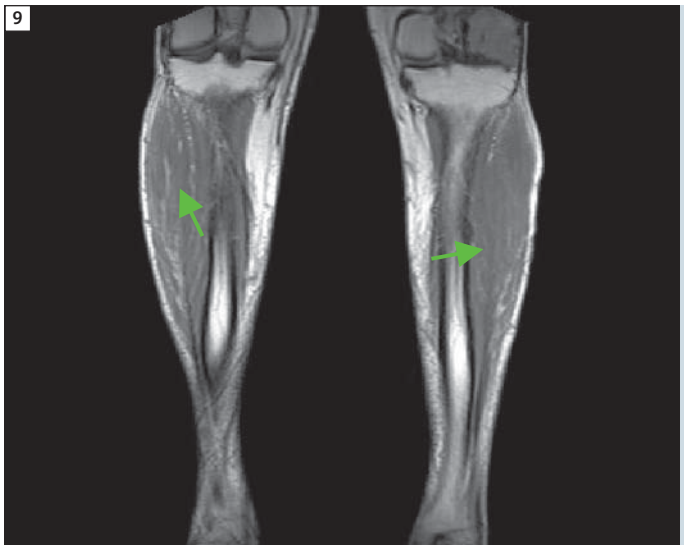

9 Coronal T1-weighted image of the lower leg of Patient 2 (LGMD). There is preservation of anterior compartment muscles.

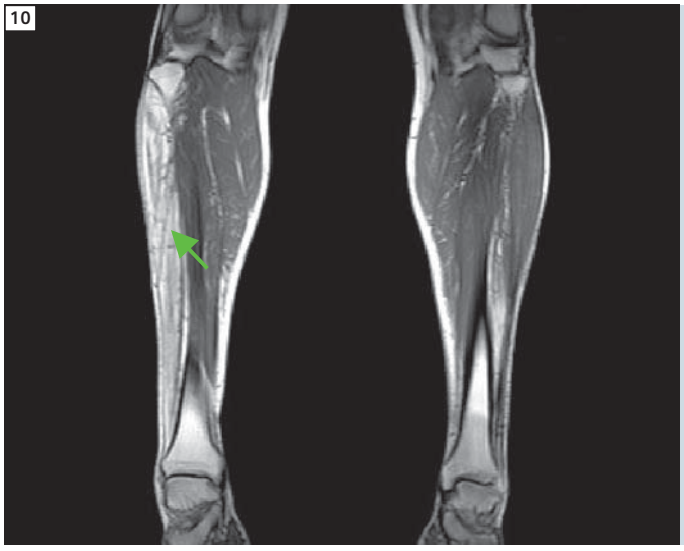

10 Coronal T1-weighted image of the lower leg of Patient 11 (FSH). There is atrophy and fatty replacement of the right anterior compartment.

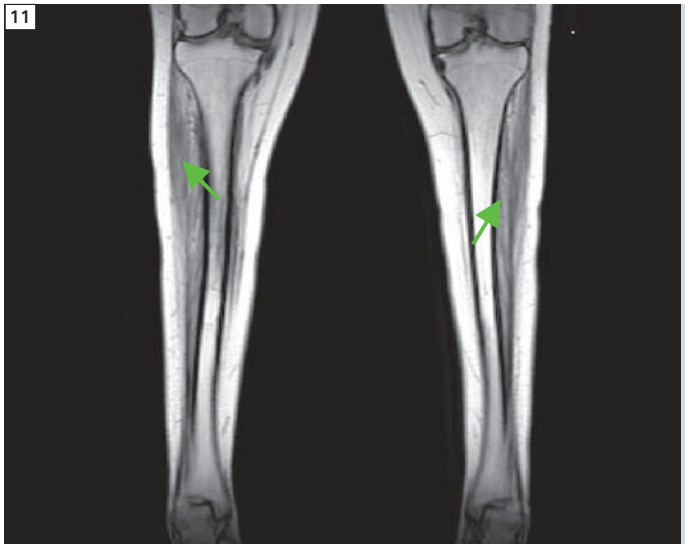

11 Coronal T1-weighted image of the lower leg of Patient 13 (hIBM). There is gross atrophy of the anterior compartments bilaterally.

Paraspinal muscles

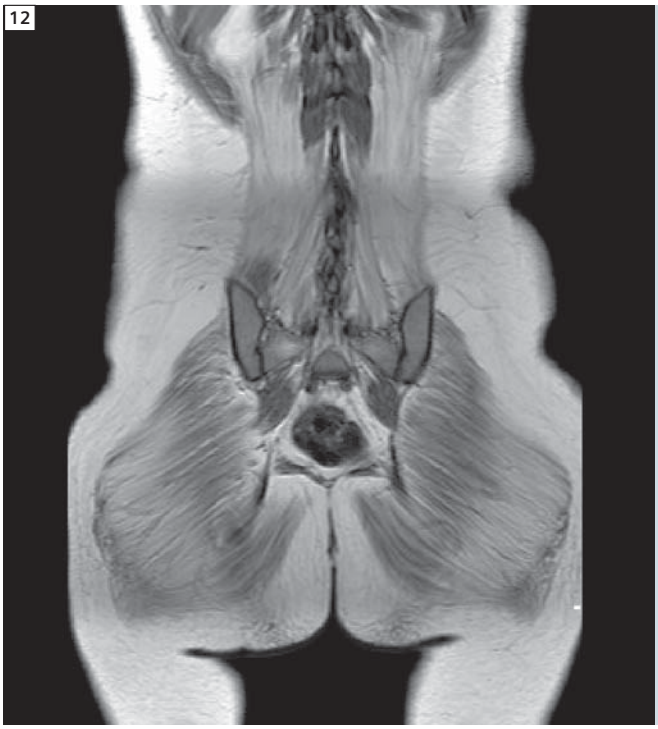

12 Coronal T1-weighted image of the posterior back of Patient 1 (LGMD). There is atrophy and fatty replacement of the lumbar paraspinal muscles and the gluteal muscles.

Contact
Mark Lourensz
St. Vincent's Hospital Melbourne
41 Victoria Parade Fitzroy Victoria 3065
Australia
mark.lourensz@svhm.org.au

References

1 Neuroimaging profile in the Muscular Dystrophies: Role of Magnetic Resonance Imaging
Valerie Tay[1,2], Maria Chiotis[3], Mark Lourensz[4], Ravi Padmanabhan[4], Katrina Reardon[1], Mark Cook[1]
[1] *Department of Neurology, St Vincent's Hospital, Melbourne, Australia*
[2] *Department of Medicine, The University of Melbourne, Australia*
[3] *National Muscular Dystrophy Research Centre*
[4] *Department of Radiology, St. Vincent's Hospital, Melbourne, Australia*

Upper limb muscles

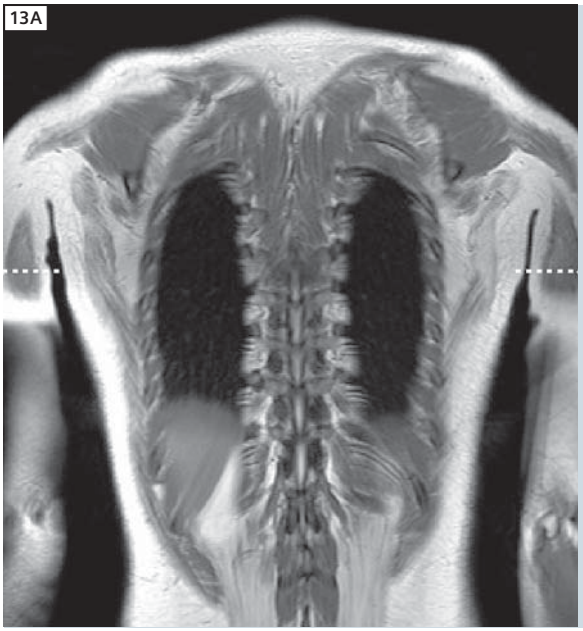

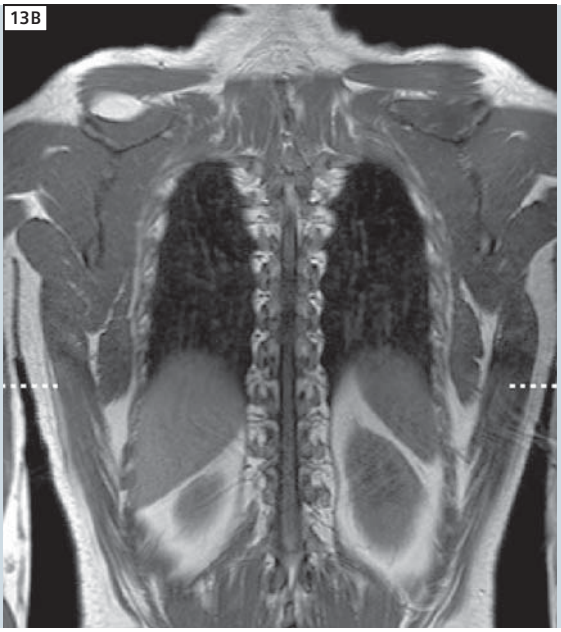

13 Coronal T2-weighted images of the posterior thoracic wall of Patient 1(LGMD), on the left (A), showing atrophy of the latissimus dorsi. A normal appearance is shown on the right. (B)

Case Report: Metastatic Liposarcoma

Nicholas Trost, M.D.; Mark Lourensz

MRI Centre, Medical Imaging Department, St. Vincent's Hospital Melbourne, Fitzroy, Victoria, Australia

Patient history

42-year-old female. Metastatic Liposarcoma. Primary in thigh treated 2 years prior. Regional pelvic metastases detected on routine follow-up MR. PET negative. Whole Body MRI performed to identify more distant secondary lesions.

Protocol

Standard Siemens imaging sequences were used. Coronal T1 and STIR of the whole body, 5 mm slice thickness. Transverse T2 and T1 through identified lesions, 8 mm slice thickness.
Post contrast coronal and transverse FatSat T1 to match the pre contrast T1-weighted images.

Image findings

Numerous lesions are demonstrated throughout the body. Small cervical lymph nodes appear benign. A 1 cm lesion in the left thyroid is most likely a primary thyroid nodule or cyst. High T2 intensity structure in the central mediastinum could represent a small pocket of pericardial fluid. It does not appear to enhance although post contrast sections are marred by pulsation artefact (Figs. 1, 2).
Numerous high signal foci in the supraclavicular regions bilaterally (Fig. 3), are due to venous structures and small nodes. Small soft tissue lesions in the axillary tails of the breasts may also represent small nodes. A 13 x 8 mm lesion that is of higher T2 intensity than nodes, lying in the left axilla deep to pectoralis minor is likely to be a metastasis (Figs. 4, 5).
There is a large metastasis that wraps around the medial border of the right scapula. The deeper locule measures 23 x 14 x 20 mm and invades the medial fibres of subscapularis.

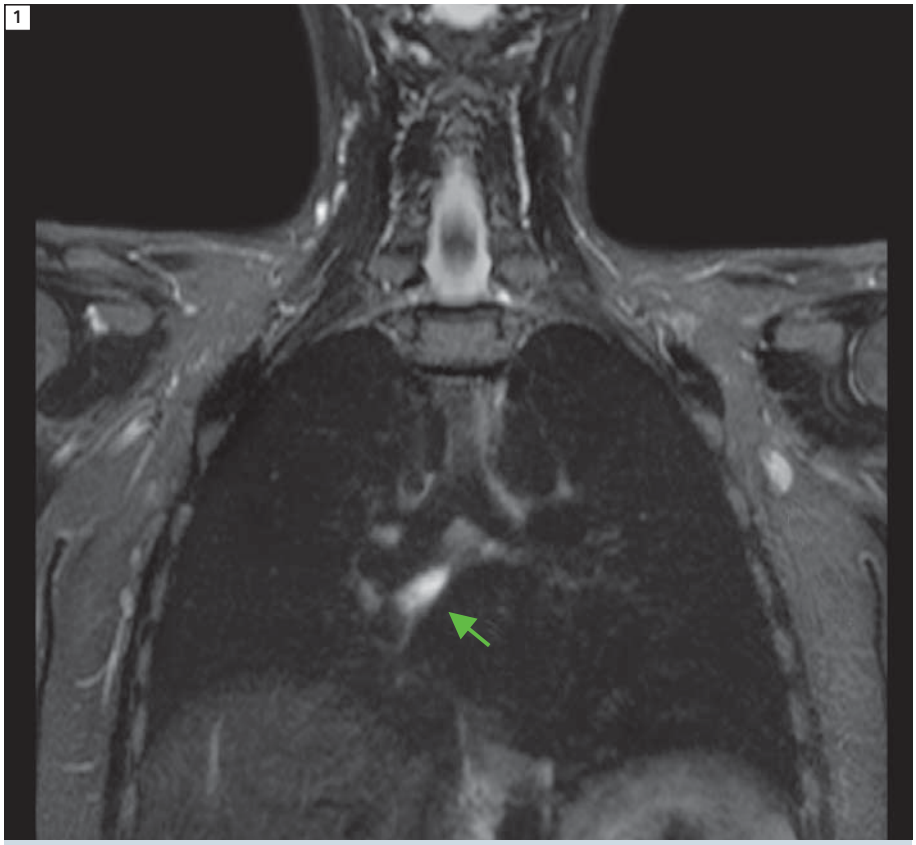

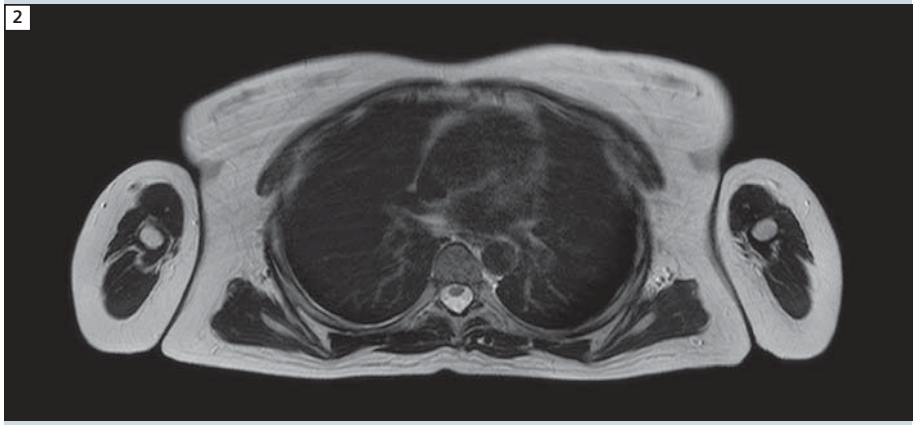

1 **2** High signal intensity non-contrast-enhancing lesion is present in the central mediastinum above the left atrium, that could represent a pocket of pericardial fluid. A definitive anatomical correlation on non-ECG gated transversal images, however, was not possible because of pulsation artifacts.

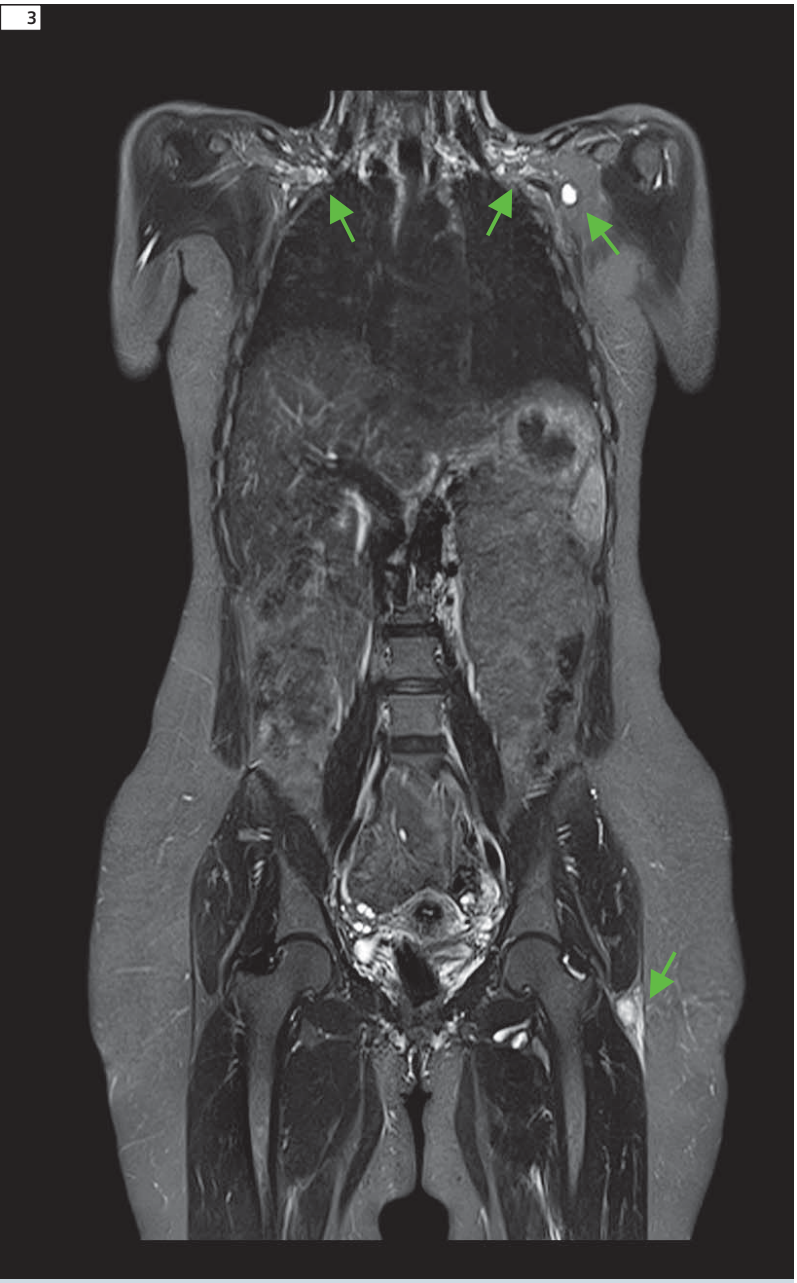

3 A small nodular lesion is well demonstrated in the left axilla, suspicious of a metastasis (see also Figs. 1 and 5). Another noticeable soft tissue lesion can be identified close to the left greater trochanter major within the muscle. Additionally, numerous lesions in the supraclavicular region can be identified, but based on this examination, it is difficult to differentiate between venous structures and small nodules.

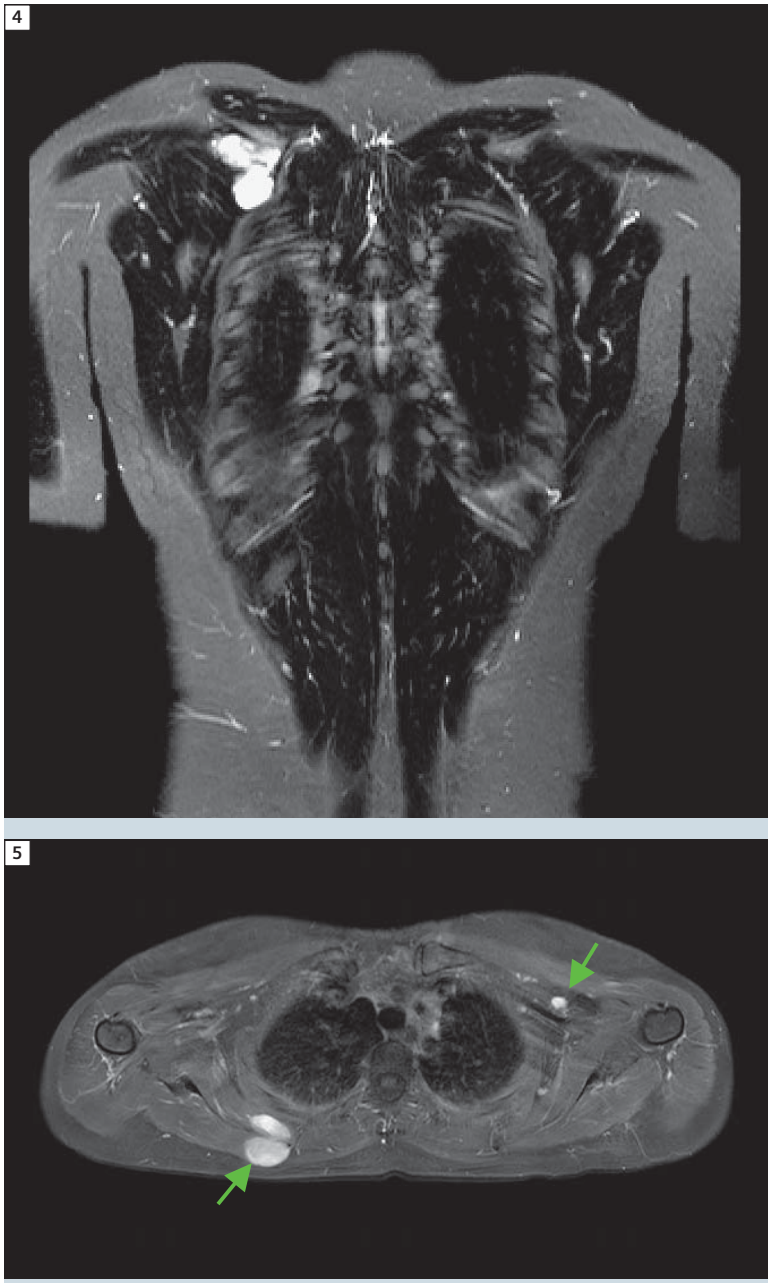

4 **5** Large lesion wrapping around the medial border of the right scapula, suspicious of metastatic spread of the liposarcoma.

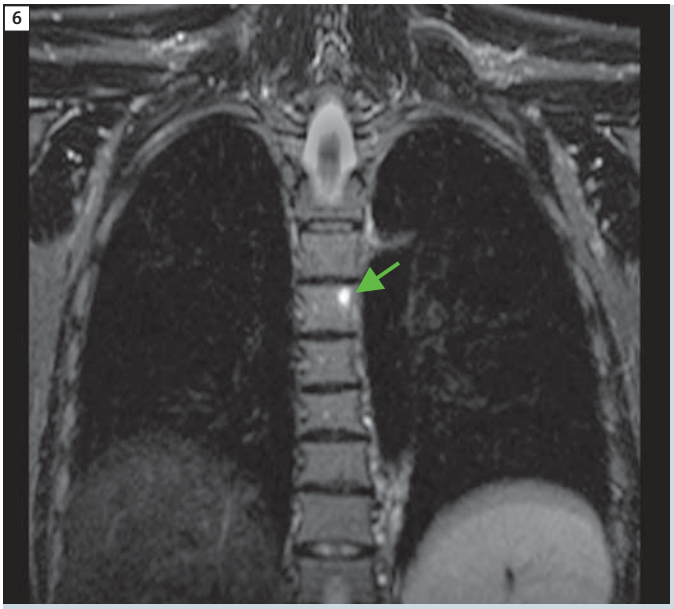

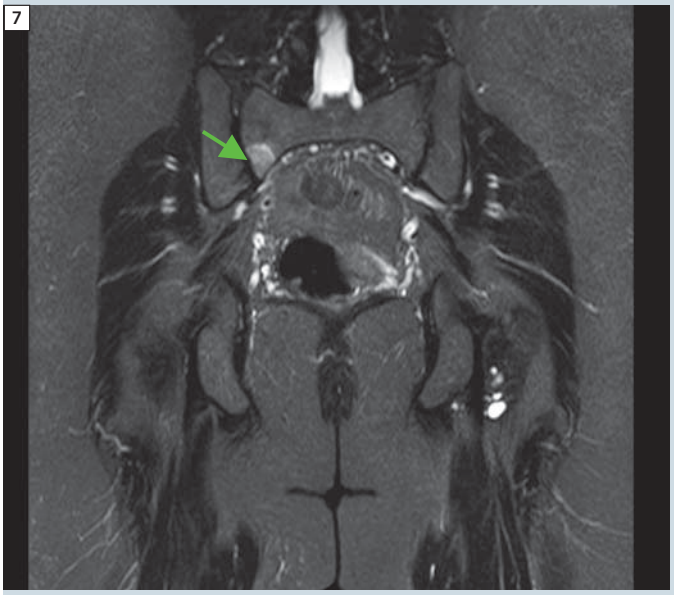

6 **7** Bone involvement of the pelvis and the 5th thoracic vertebra is shown in figures 6 and 7.

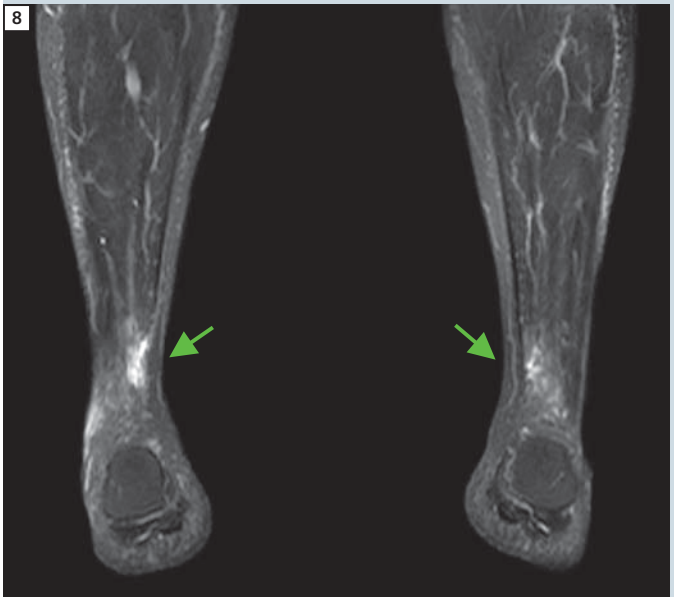

8 The signal alteration of the Achilles tendons as demonstrated in figure 8, however, is consistent with inflammation not metastatic spread of the liposarcoma.

The more superficial component measures 2.6 x 1.8 x 2.1 cm and invades the infraspinatus.
There is a small T2 hyperintense lesion in the T5 vertebral body (Fig. 6).
The pelvic lesions, in the soft tissues around the left hip and in the bones of the right sacrum and left ilium, were demonstrated on a targeted study 11 days prior and have not changed (Fig. 7).
The non-enhancing areas of high T2 signal adjacent to the musculo-tendinous junctions of the achilles tendons are likely inflammatory or degenerative in origin (Fig. 8).

Summary

The whole body MRI study demonstrates multiple lesions , consistent with metastases, in the bones and soft tissue of the pelvis, shoulder regions and T5 vertebrum. These were not demonstrated on a PET study. There may be other small metastatic lesions but these would be difficult to differentiate from normal structures such as small lymph nodes and veins.
Image acquisition was performed with a 1.5T MAGNETOM Avanto system, using Tim (Total imaging matrix) and the 12-channel Head Matrix coil, Neck Matrix coil, 2 Body Matrix coils and the Peripheral Angio Matrix coil.

Contact
Mark Lourensz, Chief MRI Technologist
MRI Centre
Medical Imaging Department
St Vincent's Hospital Melbourne
Fitzroy 3065,
Australia
mark.lourensz@svhm.org.au

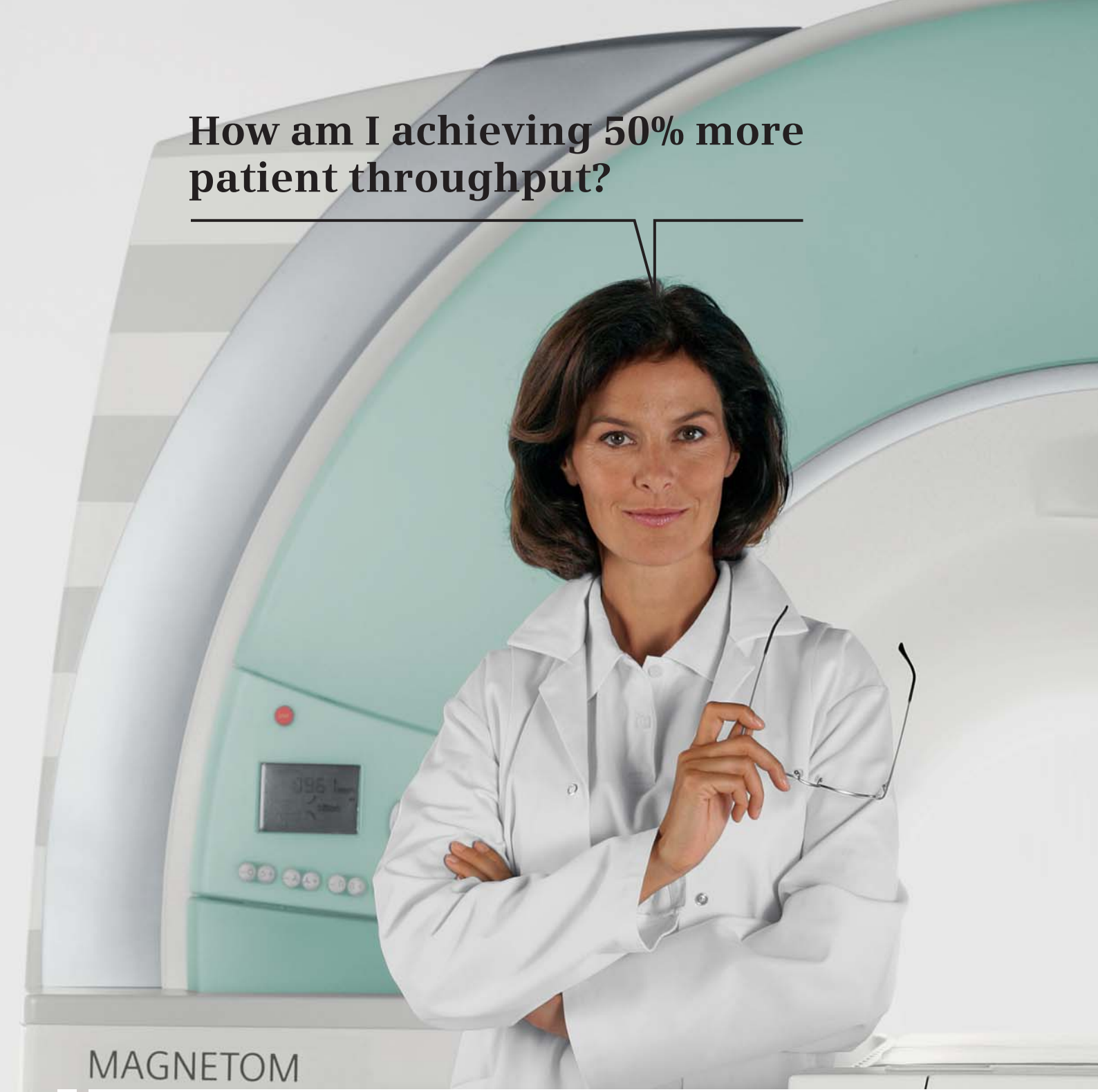

Siemens Tim technology enables multi-organ exams in one single patient setup.

By combining coils in any way, Tim® (Total Imaging Matrix) technology helps you to reduce your examination times by up to 50%. Around the world, Tim has become a standard in MRI. With thousands of installations, this is proven every day. Tim is providing incredible flexibility, accuracy, and speed for high-quality patient care while simultaneously lowering costs.
www.siemens.com/healthcare +49 69 797 6420

Answers for life.

SIEMENS

MR-Z1092-2-7600

Case Report: MRI Whole Body Bone Scan

Christine S. Lo[1]; Dr. Bill Wong; Dr. George T. J. Au; Gladys Goh Lo, M.D.[2]

[1]Li Ka Shing Faculty of Medicine, The University of Hong Kong, Hong Kong
[2]Department of Diagnostic & Interventional Radiology, Hong Kong Sanatorium & Hospital, Hong Kong

This 27-year-old-female was first told she had a small retroperitoneal tumor on routine pregnancy ultrasound. She was further advised to treat the tumor after her pregnancy. Thereafter, she presented to the urologist with a huge retroperitoneal mass measuring 11 x 9.5 x 10.5 cm (transverse x AP x cephalocaudal dimension) (Fig. 1). This mass displaced the right kidney downwards and also invaded it. The inferior vena cava (IVC) could not be seen and the left renal vein was intact and stretched over the mass. Enbloc resection of the tumor, right kidney and partial IVC resection performed. Pathology showed leiomyosarcoma of the IVC. Her oncologist ordered a whole body MRI bone scan a year later. This scan showed widespread metastases to the cervical spine, thoracic spine, lumbar spine and sacrum without extradural mass (Fig. 2). There was extensive metastasis to both breasts, the lungs, the liver and subcutaneous tissues. A recurrent tumor was also seen in the operative bed (Figs. 2, 3).

The MRI whole body bone scan protocol we use at our institution takes approximately 30 minutes. It is a non-contrast examination and consists of the following: coronal whole body STIR, sagittal T1 whole spine, sagittal STIR whole spine, axial STIR through the thorax, axial STIR through the pelvis (see table 1). This is a modification of the protocol proposed by Eustace S. et al. [1], the addition of sagittal T1 spine increases the specificity of spinal metastases. Metastatic lesions are low signal on T1-weighted images and high signal on STIR images whereas haemangiomas are high signal on both T1 and STIR images. The addition of axial STIR through the thorax and pelvis increases the sensitivity of detecting small rib and pelvic metastases. The MRI whole body scan is attractive because it is non-invasive. There is no ionizing radiation and there is no contrast injection. Sensitivity is 96.5%, specificity is 100% and 52% of patients had additional soft tissue abnormalities [1]. This is clearly exemplified by our case. In other cases, spinal cord compressions from extradural masses are easily and accurately shown. Significant oedema in muscles and soft tissues often surround bony metastases explaining the painful symptoms that the patients' experience. Occasionally unsuspected brain metastases are detected because of surrounding oedema seen in the brain on coronal STIR images.

MR whole body scan is playing an increasing role in our institution and this scan can be teamed up with MR whole body scan with contrast as well as MR whole body diffusion to increase the sensitivity and specificity of detecting M stage disease in oncologic patients.

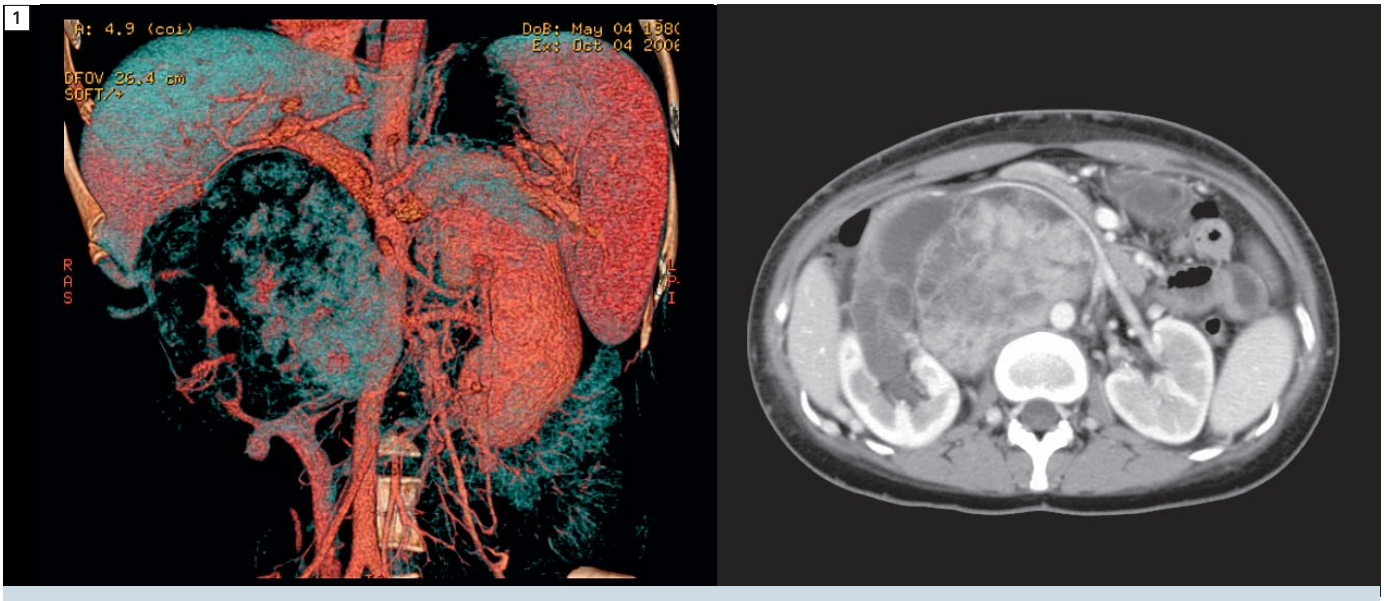

1 Large right retroperitoneal mass.

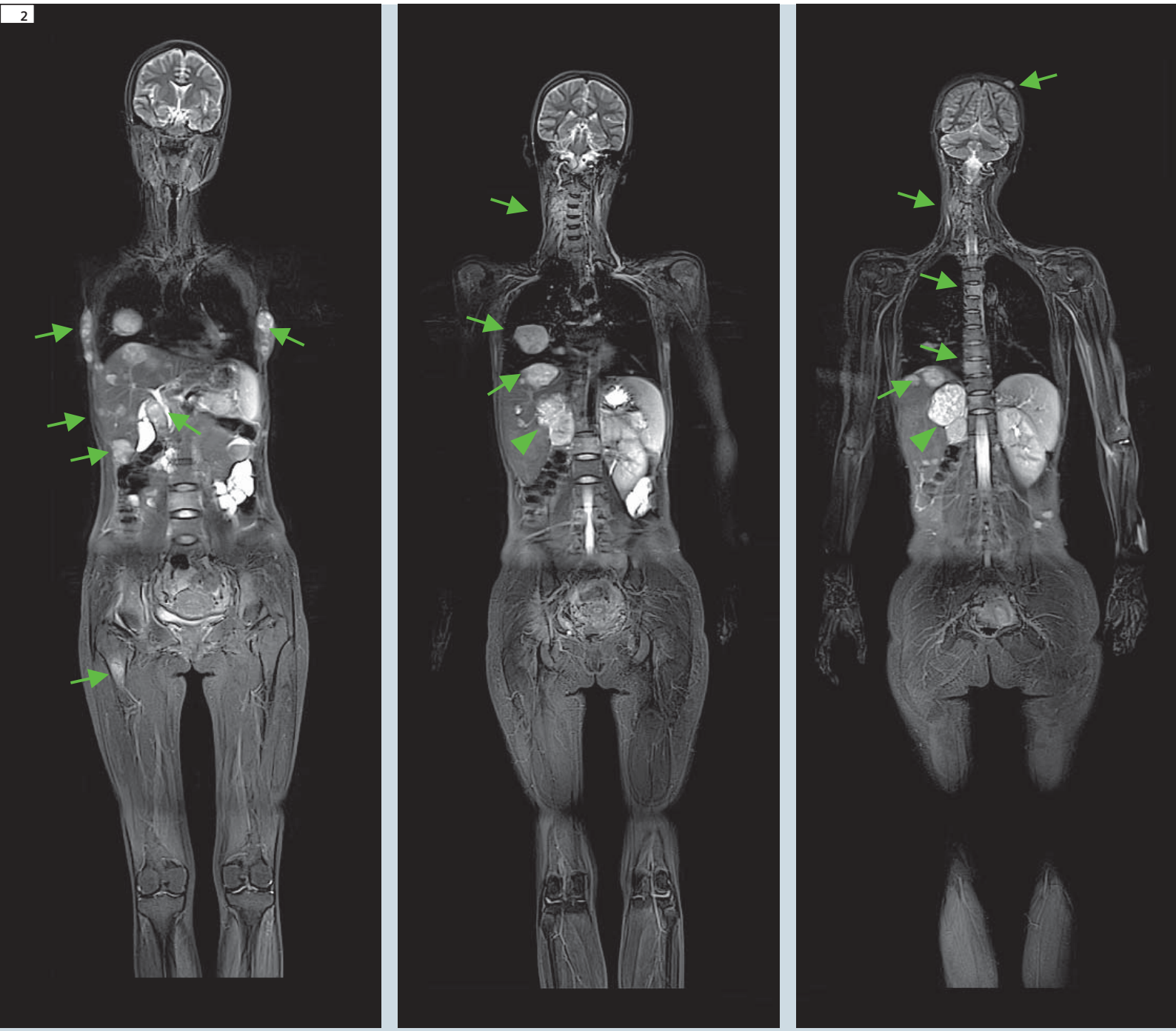

2 Metastases to both breasts, the lung, the liver and subcutaneous tissues (arrows). Recurrent tumor in operative bed (arrow head).

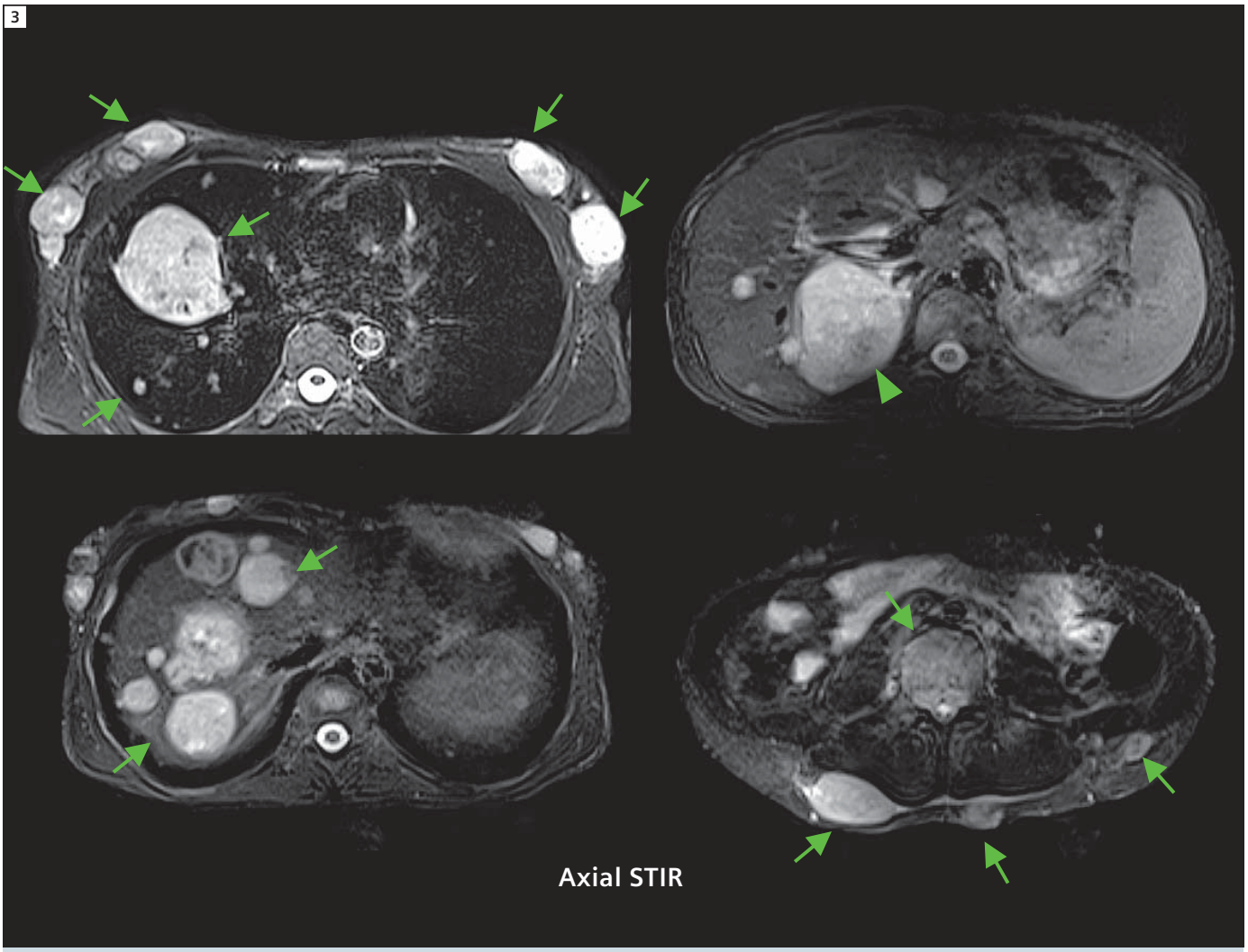

3 Metastases to the lung, the liver and subcutaneous tissues (arrows). Recurrent tumor in operative bed (arrow head).

Table 1: Our MRI bone scan protocol is as follows: (Total examination time is 30 minutes).

Sequence	Resolution (FOV, matrix, slice thickness)	Time
Coronal STIR (4 stations)	500 mm/ 314 x 448/ 10 mm	5'41"
Sagittal STIR whole spine (2 stations)	480 mm/ 311 x 448/ 5 mm	6'04"
Sagittal T1 whole spine (2 stations)	480 mm/ 358 x 512/ 5 mm	3'22"
Axial STIR (Thorax & pelvis, 2 stations)	380 mm/ 173 x 320/ 8 mm	2'30"

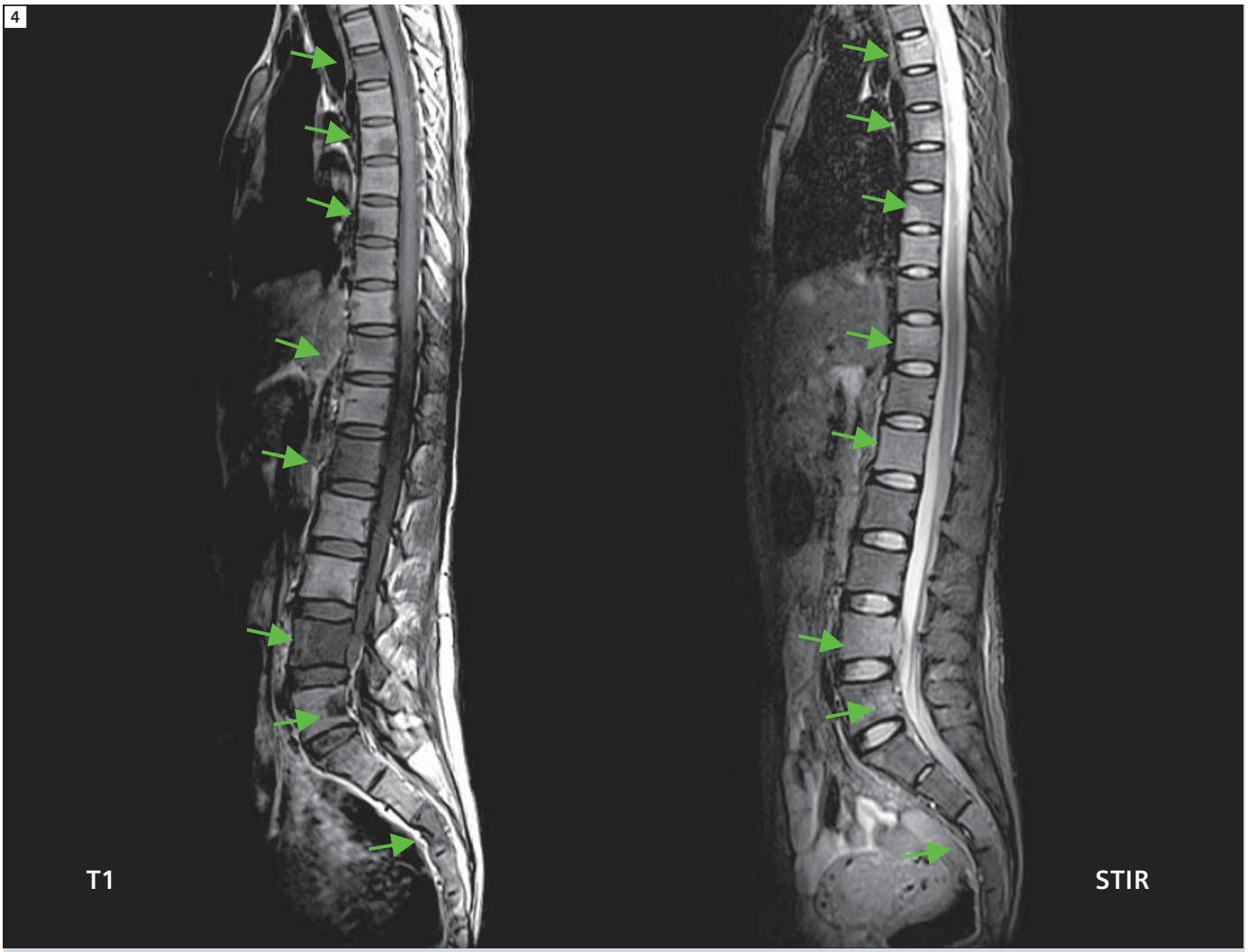

4 Metastases to cervical, thoracic, lumbar spine and sacrum.

References

1 Eustace S, Tello R, Decarvalho V, et al. A comparison of whole-body turbo short tau inversion recovery MR imaging and plan technetium 99m methylene diphosphonate scintigraphy in the evaluation of patients with suspected skeletal metastases. AJR 1997; 169:1655–61.

Contact
Gladys Lo, M.D.
Hong Kong Sanatorium & Hospital
2-4 Valley Road, Happy Valley
Hong Kong
drgl@hksh.com

Clinical Application of delayed Gadolinium Enhanded MRI of Cartilage (dGEMRIC)

Young-Jo Kim, M.D., Ph.D.[1]; Tallal Charles Mamisch, M.D.[2]

[1]Children's Hospital-Boston, Harvard Medical School, Boston, MA, USA
[2]University of Bern, Switzerland

Introduction

Joint preservation surgery of the hip for young patients with early osteoarthritis (OA) is increasingly recognized as an important therapeutic option. One of the underlying conditions that leads to joint injury is femoroacetabular impingement (FAI) due to decreased head-neck offset. In this condition, the aspherical femoral head causes mechanical damage to the articular cartilage, leading to pain and stiffness, and eventual osteoarthritis. Various surgical treatments exist to successfully treat the underlying bony abnormality of this condition. However, in all cases, the ultimate outcome is highly dependent on the amount of pre-existing articular cartilage damage [1].
Advances in MRI techniques for cartilage imaging have occurred in recent years. Hip imaging is particularly demanding because of the spherical nature of joint, deep anatomical position and the thin articular cartilage. However, advances in coil design and incorporation of parallel imaging has allowed practical application of not only high-resolution morphologic imaging but also some of the newer biochemical imaging techniques for early osteoarthritis.
Due to the importance of the extent of

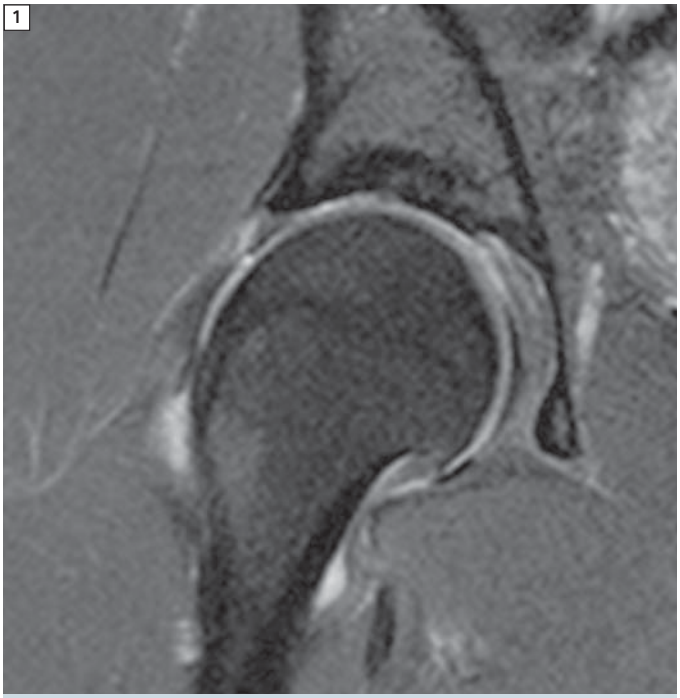

1 Clinical example of the routinely used T1-weighted 2D coronal Turbo Spin Echo acquisition; images were acquired with the standard surface coil. Resulting voxel size is 0.3 x 0.3 x 3.0 mm³.

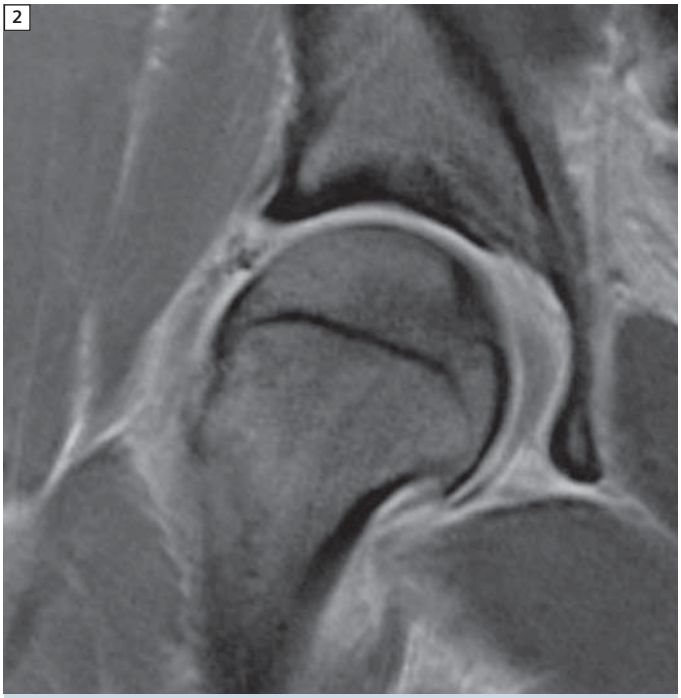

2 In this figure, the corresponding image to figure 1 of one of the two corresponding T1-weighted VIBE measurements is shown; this sequence is used for the dual flip angle fast T1 mapping. Resulting voxel size is 0.6 x 0.6 x 4.0 mm³.

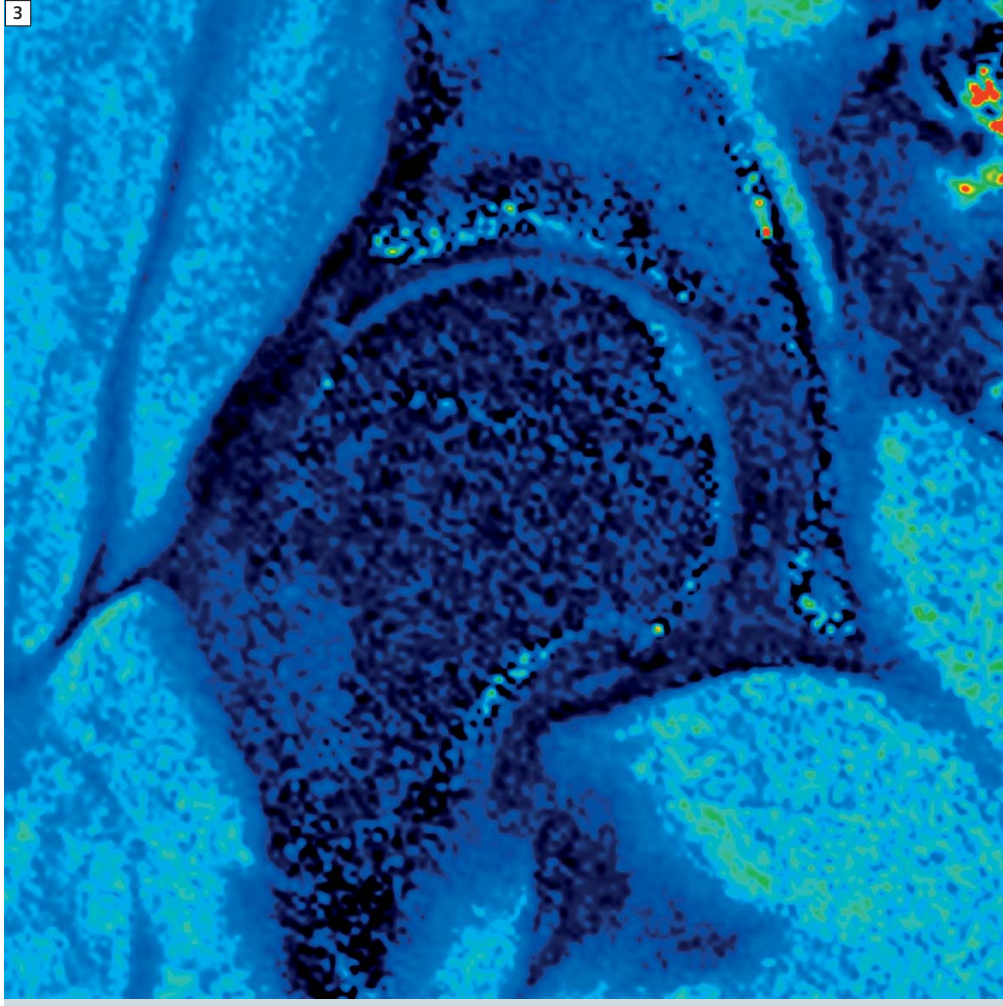

3 The resulting T1 map for the dGEMRIC imaging is shown in this figure. This map is calculated Inline using *syngo* Mapit. The blue color code shows different T1-times (the darker blue the color, the shorter the T1-time). The cartilage is well delineated and structural changes can be easily obviated or visualized.

the pre-existing articular cartilage damage in our clinical outcome after joint preserving procedures, we have incorporated the delayed Gadolinium Enhanced MRI of Cartilage (dGEMRIC) technique [2, 3] into our routine clinical imaging protocol. We have previously shown that dGEMRIC technique for the hip correlates with clinical symptoms [4] and is the best predictor of outcome after joint preservation surgery [5]. This technique takes advantage of the fact that in early OA, the negatively charged extracellular matrix is lost [6]. Using the dGEMRIC technique, the charge density is measured by the change in T1 relaxation times of the articular cartilage after penetration of gadopentetate-DTPA(2-) into the tissue. Intravenous injection of gadolinium allows the most rapid penetration of contrast agent into the articular cartilage due to penetration both from the synovial fluid as well as the subchondral bone. The patient needs to move the joint after injection and the dGEMRIC imaging needs to occur within a 30–100 minute time window after injection for a reliable biochemical assessment of the articular cartilage [7, 8].

Clinical imaging protocol

In our current clinical routine scan, we use a 1.5T Siemens MAGNETOM Avanto scanner with a surface coil for hip imaging. The patients are injected with Gadopentetate dimeglumine (Magnevist; Berlex Laboratories, Wayne, NJ). They are then asked to walk for 15 minutes. The imaging is started 30 min after contrast injection and the imaging protocol includes sequences for morphologic and biochemical imaging. The intra-venous gadolinium injection provides an indirect arthrogram and is much better tolerated by the patients than a direct injection arthography, which in many centers is the standard. Our imaging protocol consists of the following sequences:

1) coronal and sagittal oblique Turbo Spin Echo (TSE) acquisition with fat saturation (Fig 1.) (TR 530 msec, TE 11 msec, FOV 160 mm, matrix 512 x 512, slice thickness 3 mm),
2) 3D isotropic TrueFISP acquisition with water excitation (TR 12.6 msec, TE 5.5 msec, flip angle 30, FOV 160 mm, matrix 256 x 256 x 256, 0.63 mm voxel size),
3) Dual flip angle fast T1 mapping using two VIBE acquisitions for dGEMRIC imaging (Fig 2.), (TR 20 msec, TE 4.8 msec, flip angle 4.8/26.9, FOV 160 mm, matrix 256 x 256, slice thickness 4 mm).

The total scan time for this protocol is under 30 minutes and the *syngo* MapIt software performs the Inline T1 map calculations for the dGEMRIC imaging obviating the need for post-processing of imaging data (Fig. 3). Additionally, the 3D isotropic TrueFISP imaging data set is reconstructed in a rotating imaging plane around the femoral neck axis for accurate femoral head-neck junction and articular cartilage and labral characterization.

In order to obtain an accurate and reliable dGEMRIC imaging, the need for the patient to move the joint and delay the imaging for the appropriate amount of time is critical since the imaging technique relies on penetration of the contrast agent into the articular cartilage. Additionally, it is the anionic form of gadolinium that provides specificity to the imaging technique, hence, care must be taken to use the appropriate contrast agent. The dual flip angle fast T1 mapping technique with Inline map calculation makes this technique practical by decreasing the imaging time to practical levels and eliminating the

need for post-processing of the imaging data. The dual flip angle technique has been validated against the traditional inversion recovery technique. With this gradient echo based technique, it is important to center the hip in the middle of the imaging matrix since the T1 mapping data is inaccurate at the periphery of the imaging matrix. Additionally, the choice of flip angles are critical for this fast T1 mapping technique since the range of T1 in which this technique will be accurate is limited [9].

Clinical case example

The utility of this technique is illustrated in this case of a 19-year-old college hockey player suffering severe right hip pain that initially limited her playing. Eventually, the pain increased to the point where even every day activity became limited. The plain radiographs show intact joint space with no obvious evidence of osteoarthritis (Fig. 4). The lateral radiograph shows the prominence in the anterior head-neck junction consistent with a Cam type femoroacetabular impingement (Fig. 5). The surgical treatment options range from a limited anterior open arthrotomy and osteochondroplasty to a full surgical dislocation with trimming of the damaged acetabular rim and femoral head-neck junction osteochondroplasty. Advanced imaging is critical in proper patient selection for each surgical technique as well as predicting the prognosis of this patient after surgery.

The standard morphologic imaging shows some heterogeneity in the acetabular articular cartilage (Fig. 6 A). The femoral head cartilage appeared intact and the labrum appeared intact. However, on the dGEMRIC scan, the entire acetabular cartilage showed markedly lower T1 values, demonstrating increased enhancement of the extracellular matrix by the gadopentetate-DTPA(2-), suggesting lower inherent negative charge in the matrix and hence significant articular cartilage damage in the acetabulum (Fig. 6 B). Based on this information, the patient was scheduled for an open surgical dislocation and osteoplasty rather than the more limited surgery. At time of surgery, the extent of articular cartilage damage in the acetabulum is verified (Fig. 6 C). The addition of the dGEMRIC imaging technique to our clinical hip imaging protocol allows us to improve patient selection and therefore improve the ultimate outcome of our surgical procedure. It also allows us to avoid unnecessary surgery with improved staging of the articular cartilage damage at time of initial assessment. Additionally, the indirect arthrogram is much better tolerated by the patients than a direct injection arthography and the imaging technique is sufficiently fast and easy to use to allow the full complement of diagnostic imaging sequences to run within a 30 min scan time as part of a routine clinical imaging protocol.

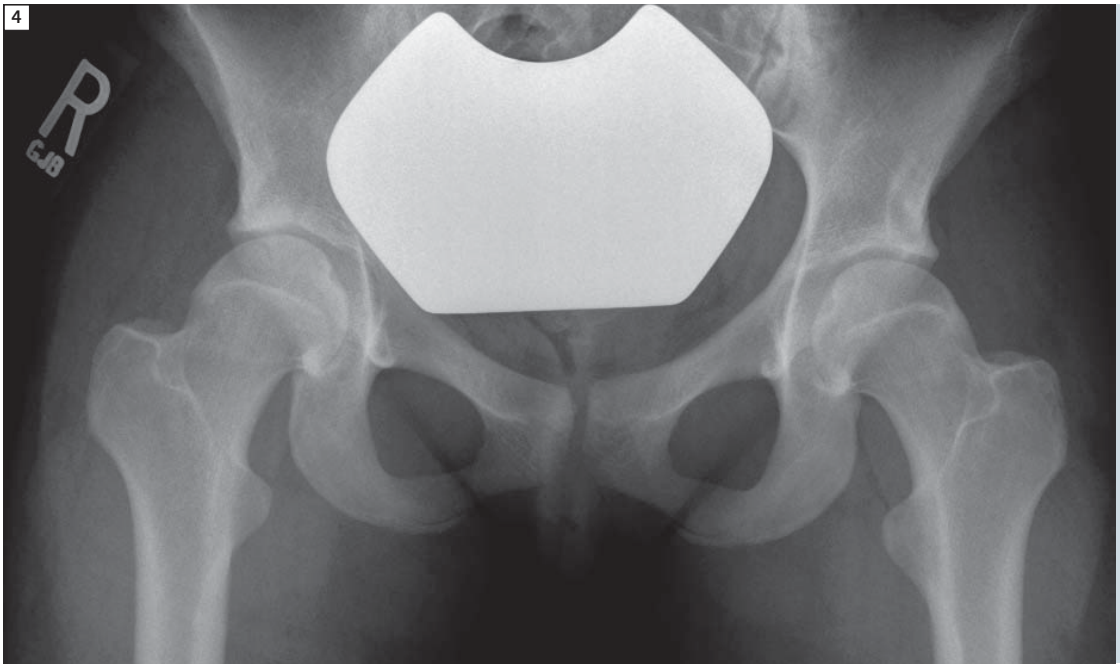

4 Pelvic radiograph of a 19-year-old woman with right hip pain. Minimal radiograph evidence of osteoarthritis is present. Some asphericity of femoral head suggesting possible impingement.

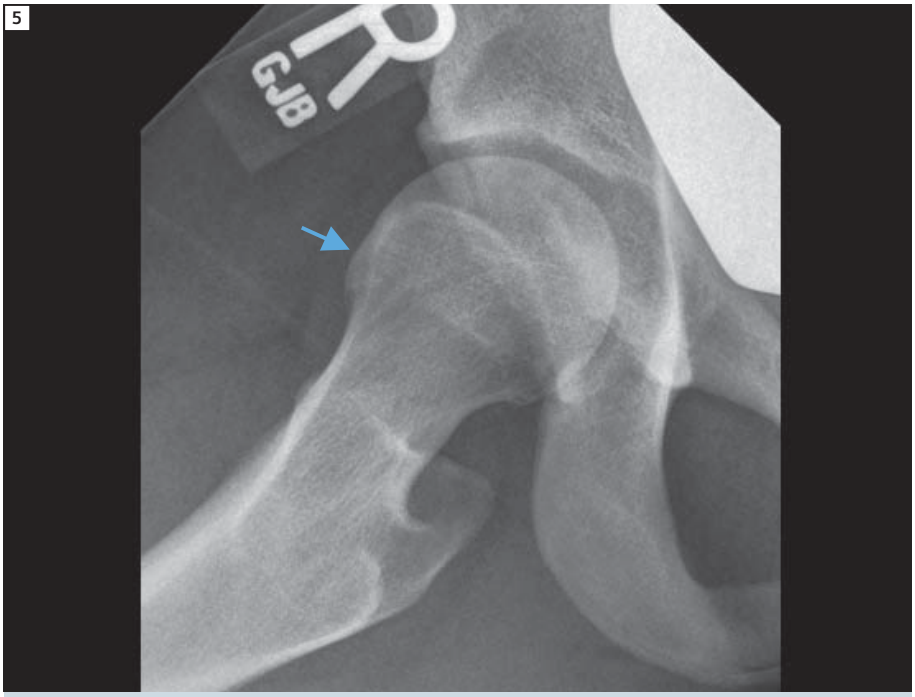

5 Lateral radiograph of the right hip shows a prominence in the anterior head-neck junction which could lead to Cam type femoroacetabular impingement.

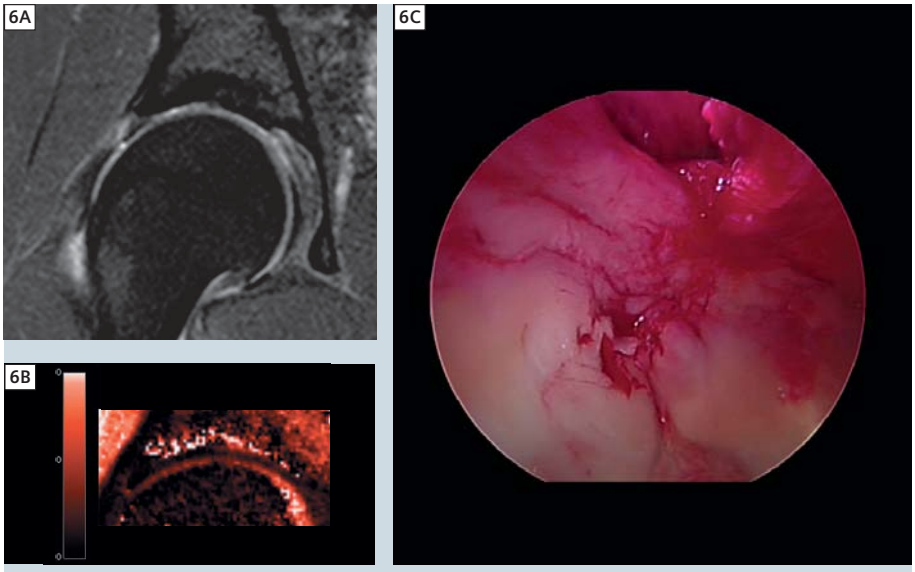

6A Coronal TSE image shows some focal signal change in the acetabular articular cartilage. **6B** The corresponding section on the dGEMRIC scan shows extensive articular cartilage change in the acetabular side but the femoral head cartilage appears intact. The lower T1 values (dark red and black areas) on the dGEMRIC scan corresponds to more cartilage degeneration. **6C** The intraoperative view shows intact labrum but deep fissuring of the acetabular articular cartilage.

References

1 Kim, Y.J., et al., Hip joint-preserving surgery: beyond the classic osteotomy. Instr Course Lect, 2006. 55: p. 145–58.
2 Bashir, A., et al., Glycosaminoglycan in articular cartilage: in vivo assessment with delayed Gd(DTPA)(2-)-enhanced MR imaging. Radiology, 1997. 205(2): p. 551–558.
3 Bashir, A., et al., Nondestructive imaging of human cartilage glycosaminoglycan concentration by MRI. Magn Reson Med, 1999. 41(5): p. 857–65.
4 Kim, Y.J., et al., Assessment of early osteoarthritis in hip dysplasia with delayed gadolinium-enhanced magnetic resonance imaging of cartilage. J Bone Joint Surg Am, 2003. 85–A(10): p. 1987–92.
5 Cunningham, T., et al., Delayed gadolinium-enhanced magnetic resonance imaging of cartilage to predict early failure of Bernese periacetabular osteotomy for hip dysplasia. J Bone Joint Surg Am, 2006. 88(7): p. 1540–8.
6 Venn, M. and A. Maroudas, Chemical composition and swelling of normal and osteoarthrotic femoral head cartilage. I. Chemical composition. Ann Rheum Dis, 1977. 36(2): p. 121–9.
7 Burstein, D., et al., Protocol issues for delayed Gd(DTPA)(2-)-enhanced MRI (dGEMRIC) for clinical evaluation of articular cartilage. Magn Reson Med, 2001. 45(1): p. 36–41.
8 Tiderius, C.J., et al., Hip dGEMRIC in asymptomatic volunteers and patients with early osteoarthritis: the influence of timing after contrast injection. Magn Reson Med, 2007. 57(4): p. 803–5.
9 Mamisch, T., et al., Comparison of delayed Gadolinium Enhanced MRI of Cartilage (dGEMRIC) using Inversion Recovery and Fast T1 Mapping Sequences. Mag Res Med, 2008. in press.

Contact
Young-Jo Kim, M.D., Ph.D.
Children's Hospital-Boston
300 Longwood Avenue
Boston, MA 02115
USA
young-jo.kim@childrens.harvard.edu

Questions & Answers on Hardware Topics

Jörg Stapf; Rolf Heinrichs; Matthias Nittka, Ph.D.

Siemens Healthcare, Erlangen, Germany

Q: What is the principle of "Zero-Helium Boil Off"?

A: Super-conducting magnets require built-in overdimensional thermos flasks for maintaining super-conductivity in cryostats (Fig. 1).
To ensure that the liquid helium used as coolant does not boil off too quickly, the helium dewar has to be very well insulated to reduce, for example, heat conduction and radiation. For this purpose, the helium vessel is suspended by materials that are poor heat conductors, such as GFK or reinforced carbon fiber materials. Furthermore, heat bridges are reduced as much as possible. The housing is evacuated to prevent convection currents. Irradiation on the helium vessel is reduced by Kelvin shields and super-insulating foils.
If the helium boiling off re-condenses via a 4K cold head, at least statically the magnet no longer boils off or consumes helium. The second stage extends into a volume connected to the helium vessel where it cools and re-liquifies the gas.
Since it is not easy to regulate the performance of the cold head, the excess refrigeration capacity is compensated for by a heater so that the working pressure in the helium vessel remains constant.
Eddy currents caused by gradient activity lead to additional heat transfer into the helium vessel.
If the sum of heat transferred is less than that of the refrigeration capacity of the cold head, a "zero boil off" system is obtained.
To maintain this state, the cold head has to be in continuous operation, and the line voltage as well as the chilled water supply should not fail, at all, or at worst, only briefly.
Normally, liquid helium is lost only within the framework of service activities, such as ramping or replacing cold heads. Unfortunately, liquid helium will also boil off when both the line voltage and chilled water supply fail for more than 3 hours.

1

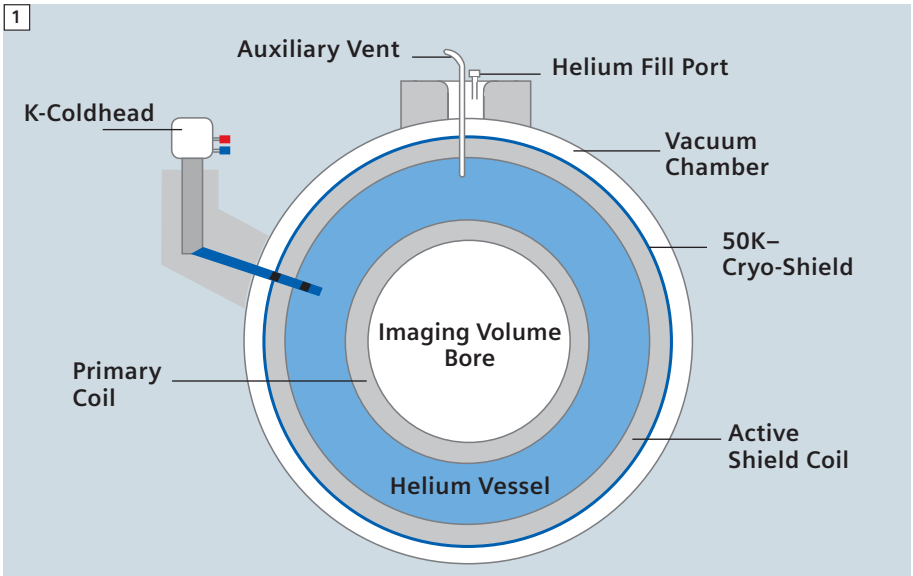

1 MR system.

Q: What is the difference between the different RF pulse types?

A: The RF pulse types are pure sequence parameters. This means they are not allocated to a hardware feature. By comparison, the Matrix Mode, for example, actually affects the surface coils (modes: CP, Dual, Triple depending on the coil).
The RF pulse types allow flexible control of the RF pulses (radio frequency pulses) of the sequences, for exciting or refocusing the MR signals and for various other applications:

- The "Normal" mode is optimized to cover a broad sequence application range providing for a well-defined slice profile.
- The "Fast" mode is implemented for time-critical protocols when rather short echo times are required. For this reason, it uses very short RF pulses.

A disadvantage of the "Fast" mode is that shorter RF pulses are normally accompanied by increased RF exposure for the patient (increase in the specific absorption rate).

- The "Low SAR" mode addresses high-performance protocols that may exceed the allowed SAR threshold. Usually, longer RF pulses are used, i.e., the RF-power output decreases.

One of the resulting disadvantages is that longer RF pulses increase the minimal timing of fast sequences. However, this is not required for all applications. It is important that every sequence defines the actual pulses that stand behind the RF pulse types and is able to change them at any time depending on other parameters.

Try them out on your system!

Trial Licenses for most of the applications featured in this issue of MAGNETOM Flash are available free of charge for a period of 90 days: Please contact your local Siemens representative for system requirements and ordering details.

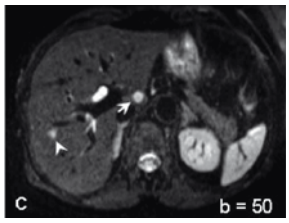

***syngo* DWI**

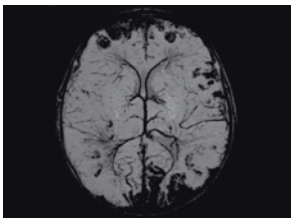

***syngo* SWI**

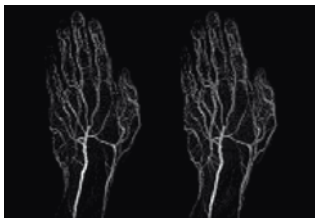

***syngo* TWIST**

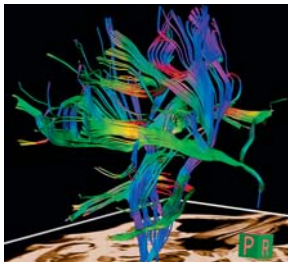

***syngo* DTI Tractography**

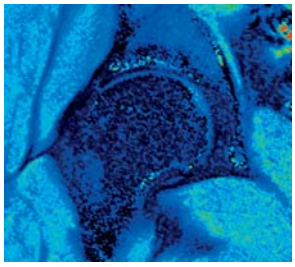

***syngo* MapIt**

Tim Planning Suite

MAGNETOM Flash – Imprint

Publisher:
Siemens AG
Medical Solutions
Business Unit Magnetic Resonance,
Karl-Schall-Straße 6, D-91052 Erlangen,
Germany

Editor in Chief: Antje Hellwich
(antje.hellwich@siemens.com)

Editorial Board: Dagmar Thomsik-Schröpfer, Ph.D.; Okan Ekinci, M.D.; Heike Weh; Bernhard Baden; Peter Kreisler, Ph.D.; Wellesley Were; Milind Dhamankar, M.D.; Kathleen Giannini; Gary R. McNeal; Sunil Kumar S.L., M.D.

Production: Norbert Moser, Siemens AG, Medical Solutions

Layout: independent Medien-Design
Widenmayerstrasse 16, D-80538 Munich

Printers: Farbendruck Hofmann, Gewerbestraße 5, D-90579 Langenzenn, Printed in Germany

MAGNETOM Flash is also available on the internet:
www.siemens.com/magnetom-world

German Federal Data Protection Law: Despatch is made using an address file which is maintained with the aid of an automated data processing system.
MAGNETOM Flash with a total circulation of 20,000 copies is sent free of charge to Siemens MR customers, qualified physicians, technologists, physicists and radiology departments throughout the world. It includes reports in the English language on magnetic resonance: diagnostic and therapeutic methods and their application as well as results and experience gained with corresponding systems and solutions. It introduces from case to case new principles and procedures and discusses their clinical potential.
The statements and views of the authors in the individual contributions do not necessarily reflect the opinion of the publisher.
The information presented in these articles and case reports is for illustration only and is not intended to be relied upon by the reader for instruction as to the practice of medicine. Any health care practitioner reading this information is reminded that they must use their own learning, training and expertise in dealing with their individual patients. This material does not substitute for that duty and is not intended by Siemens Medical Solutions to be used for any purpose in that regard. The drugs and doses mentioned herein are consistent with the approval labeling for uses and/or indications of the drug. The treating physician bears the sole responsibility for the diagnosis and treatment of patients, including drugs and doses prescribed in connection with such use. The Operating Instructions must always be strictly followed when operating the MR system. The sources for the technical data are the corresponding data sheets. Results may vary.
Partial reproduction in printed form of individual contributions is permitted, provided the customary bibliographical data such as author's name and title of the contribution as well as year, issue number and pages of MAGNETOM Flash are named, but the editors request that two copies be sent to them. The written consent of the authors and publisher is required for the complete reprinting of an article.
We welcome your questions and comments about the editorial content of MAGNETOM Flash. Please contact us at magnetomworld.med@siemens.com. Manuscripts as well as suggestions, proposals and information are always welcome; they are carefully examined and submitted to the editorial board for attention. MAGNETOM Flash is not responsible for loss, damage, or any other injury to unsolicited manuscripts or other materials. We reserve the right to edit for clarity, accuracy, and space. Include your name, address, and phone number and send to the editors, address above.

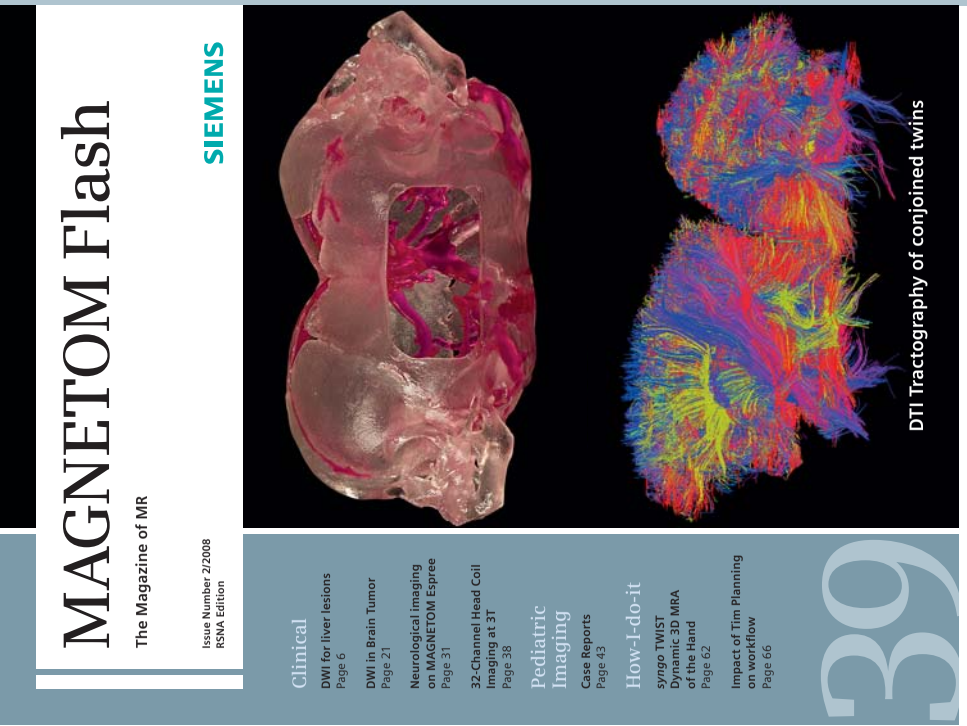

Subscription

Please enter your business address

Institution

Department

Function

Title

Name

Street

Postal Code

City

State

Country

MR system used

Please include me in your mailing list for the following Siemens Healthcare customer magazine(s):

- ☐ Medical Solutions
- ☐ MAGNETOM Flash
- ☐ SOMATOM Sessions
- ☐ AXIOM Innovations

Stay up to date with the latest information Register for:

- ☐ the monthly e-Newsletter

E-mail

- ☐ Yes, I consent to the above information being used for future contact regarding product updates and other important news from Siemens.
- ☐ unsubscribe from info service

Please print clearly!

SUBSCRIBE NOW!

– and get your free copy of future MAGNETOM Flash! Interesting information from the world of magnetic resonance – gratis to your desk. Send us this postcard, or subscribe online at **www.siemens.com/MAGNETOM-World**

MAGNETOM Flash

Siemens AG
Medical Solutions
Magnetic Resonance
Antje Hellwich - Marketing
P.O. Box 32 60
D-91050 Erlangen
Germany

Global Siemens Headquarters

Siemens AG
Wittelsbacherplatz 2
80333 Muenchen
Germany

Global Siemens Healthcare Headquarters

Siemens AG
Healthcare Sector
Henkestr. 127
91052 Erlangen
Germany
Phone: +49 9131 84-0
www.siemens.com/healthcare

www.siemens.com/healthcare-magazine

Order No. A91MR-1000-55C-7600 | Printed in Germany | CC MR 01000 ZS 110825. | © 11.08, Siemens AG

On account of certain regional limitations of sales rights and service availability, we cannot guarantee that all products included in this brochure are available through the Siemens sales organization worldwide. Availability and packaging may vary by country and is subject to change without prior notice. Some/All of the features and products described herein may not be available in the United States.

The information in this document contains general technical descriptions of specifications and options as well as standard and optional features which do not always have to be present in individual cases.

Siemens reserves the right to modify the design, packaging, specifications and options described herein without prior notice.
Please contact your local Siemens sales representative for the most current information.

Note: Any technical data contained in this document may vary within defined tolerances. Original images always lose a certain amount of detail when reproduced.

Global Business Unit

Siemens AG
Medical Solutions
Magnetic Resonance
Henkestr. 127
91052 Erlangen
Germany
Phone: +49 9131 84-0
www.siemens.com/healthcare

Local Contact Information

In Asia
Siemens Pte Ltd
The Siemens Center
60 MacPherson Road
Singapore 348615
Phone: +65 6490-8096

In Canada
Siemens Canada Limited
Medical Solutions
2185 Derry Road West
Mississauga ON L5N 7A6
Canada
Phone: +1 905 819-5800

Europe/Africa/Middle East
Siemens AG
Medical Solutions
Henkestr. 127
91052 Erlangen
Germany
Phone: +49 9131 84-0

Latin America
Siemens S.A.
Medical Solutions
Avenida de Pte. Julio A. Roca No 516,
Piso 7
C1067ABN Buenos Aires
Argentina
Phone: +54 11 4340-8400

USA:
Siemens Medical Solutions U.S.A., Inc.
51 Valley Stream Parkway
Malvern, PA 19355-1406
USA
Phone: +1-888-826-9702